CYLINDRICAL SHELL HYBRID FINITE ELEMENTS

Gordon Edwards, B.Sc.

Thesis submitted to the University of Nottingham for the degree of Doctor of Philosophy

May 1974

CONTENTS

	Page
ABSTRACT	1
1. INTRODUCTION	2
1.1 Thin Shells	2
1.2 The Finite Element Method for the Analysis of Shells	2
1.3 The Choice of a Suitable Shell Theory for the Construction of Finite Elements	4
1.4 The Work of this Thesis	7
2. VARIATIONAL PRINCIPLES AND THE HYBRID METHOD FOR THE CONSTRUCTION OF FINITE ELEMENTS	10
2.1 Introduction	10
2.2 Variational Principles	12
2.2.1 The Functionals	12
2.2.2 Application to Finite Element Analysis	14
2.2.3 Treatment of a Dynamic Problem	17
2.3 Points Arising from this Analysis	20
2.3.1 The Element Stiffness Matrix	20
2.3.2 The Mass Matrix	20
2.3.3 The Effect of a Non-Equilibrating Stress Assumption	20
2.3.4 Loading Vectors	21
2.3.5 The Length of the Stress Assumption	22
2.3.6 The Evaluation of Stresses	23
2.3.7 Equilibrium, Hybrid and Conforming Displacement Assumption Elements	23
3. A TRIANGULAR HYBRID PLATE BENDING ELEMENT	25
3.1 Existing Plate Bending Elements	25

Page

3.2 The Present Work 27

3.3 The Formulation of the Triangular Hybrid Bending Element 27

3.3.1 Introduction 27

3.3.2 The Boundary Displacement Assumptions 28

3.3.3 The Stress Assumption 29

3.3.4 The Evaluation of Edge Work and Complementary Strain Energy 31

3.3.5 The Calculation of Stresses 32

3.3.6 The Addition of a Mass Matrix 33

3.4 Results Obtained using the Triangular Hybrid Bending Element 34

3.4.1 Simply Supported Square Plate under a Central Point Load 34

3.4.2 Clamped Square Plate with Central Point Load 35

3.4.3 Clamped Square Plate under Uniform Loading 36

3.4.4 Natural Frequencies of the Clamped Square Plate 37

3.5 The Performance of the Hybrid Triangle 39

3.5.1 The Simply Supported Plate with Central Point Load 39

3.5.2 The Clamped Square Plate with Central Point Load 40

3.5.3 The Clamped Square Plate under Uniform Loading 40

3.5.4 Natural Frequencies of Clamped Square Plate 41

4. A FLAT TRIANGULAR HYBRID ELEMENT FOR THE ANALYSIS OF SHELLS 48

4.1 Introduction 48

4.2 The Combination of Bending and Membrane Effects 49

4.3 The Evaluation of a Hybrid In-Plane Stiffness Matrix 51

4.4 The Calculation of Stresses 52

Page

4.5 An In-Plane Displacement Assumption Stiffness Matrix for use with the Tocher Triangle 52

4.6 Problems Analysed 54

4.6.1 The Pinched Cylindrical Shell 54

4.6.2 A Simply Supported Panel Under Pressure Loading 55

4.7 Conclusions 56

5. A THIN HYBRID CYLINDRICAL SHELL ELEMENT OF RECTANGULAR PLANFORM 80

5.1 Introduction 80

5.2 Unsatisfactory Features of the Existing Element 81

5.2.1 Edge Displacement Assumptions 81

5.2.2 The Stress Assumption 82

5.2.3 The Stress-Strain Relationship 83

5.2.4 The Nodal Degrees of Freedom 83

5.3 The Formulation of the New Element 84

5.3.1 Element Geometry 84

5.3.2 Edge Displacement Assumptions 84

5.3.2.1 The Straight Sides 12 and 34 84

5.3.2.2 The Curved Sides 13 and 24 86

5.3.3 Equilibrium Equations 87

5.3.4 The Stress Assumptions 88

5.3.5 The Stress-Strain Relationship 90

5.3.6 The Evaluation of the Stiffness Matrix 92

5.3.7 The Calculation of Stresses 93

5.4 Problems Analysed 94

5.4.1 The Pinched Cylindrical Shell 94

5.4.2 The Simply Supported Panel under Pressure Loading 96

5.4.3 The Cylindrical Shell Roof Problem 96

5.5 Conclusions 98

5.5.1 The Stress Assumptions 98

	Page
5.5.2 The Boundary Displacement Assumptions	98
5.5.3 The Convergence of Stresses	100
5.5.4 Comparison with other Finite Element Results	101
5.5.5 Interpretation of Results in Future Problems	103
6. A THIN HYBRID CYLINDRICAL SHELL ELEMENT OF TRIANGULAR PLANFORM	138
6.1 Introduction	138
6.1.1 The Uses of the Element	138
6.1.2 Early Versions of the Element	138
6.1.3 Later Developments	139
6.2 The Formulation of the Element	140
6.2.1 Geometry and Degrees of Freedom	140
6.2.2 Edge Displacement Assumptions	141
6.2.2.1 Rigid Body Terms	141
6.2.2.2 Extra Variations	142
6.2.2.3 The Assumption in Terms of Nodal Variables	144
6.2.2.4 The Expression for the Distance along the Side	145
6.2.3 The Stress Assumption	146
6.2.4 The Evaluation of the Complementary Strain Energy	146
6.2.5 The Evaluation of Edge Work	148
6.2.6 Calculation of Results	149
6.3 Test Problems	149
6.3.1 Introduction	149
6.3.2 Tests Involving Negative Curvature	150
6.3.3 Tests on Changing the Position of the Fourth Node	151
6.3.4 The Simply Supported Panel under Pressure Loading	151
6.4 Discussion of Results	152
6.4.1 Tests Involving Negative Curvature	152
6.4.2 Changing the Position of the Fourth Node	152

Page

6.4.3 The Simply Supported Panel 153

6.4.3.1 Comparisons with the Previous Elements 153

6.4.3.2 The Effects of Distortion 154

7. A MITRED BEND IN A PIPE ANALYSED USING THE TWO HYBRID CYLINDRICAL SHELL ELEMENTS 178

7.1 Introduction 178

7.2 Details of the Mitred Bend and Previous Solutions 178

7.3 The Finite Element Idealization 180

7.4 Conversion of the Finite Element Stresses into the Form Necessary for Comparisons 181

7.5 Results Obtained 183

7.5.1 Change of Diameter at Section BB 183

7.5.2 Stresses at Section BB 183

7.5.3 Stresses at Section AA and the Intersection 183

7.6 Discussion of Results 185

7.6.1 Deflections 185

7.6.2 Stresses at Section BB 185

7.6.3 Stresses at Section AA 186

7.6.4 Stresses Predicted at the Intersection 186

7.6.5 The General Performance of the Elements 187

8. CONCLUSIONS, THOUGHTS AND SUGGESTIONS FOR FURTHER WORK 200

8.1 Conclusions from the Work 200

8.2 Thoughts on the Hybrid Method in General 201

8.3 Suggestions for Further Work 203

8.3.1 Work on Elements Developed in this Thesis 203

8.3.2 Further Applications of the Hybrid Method 204

8.3.2.1 A Doubly Curved Element 204

8.3.2.2 Thick Shell Elements 205

Page

Appendix 1 NOVOZHILOV'S STRAIN ENERGY EXPRESSION FOR THIN SHELLS AND THE STRESS-STRAIN RELATIONSHIP 206

A1.1 Introduction 206

A1.2 The Strain Energy Expression of Novozhilov 206

A1.3 The Forces at the Middle Surface 208

A1.4 The Relation between Forces, Moments and Strains 209

Appendix 2 THE EXACT SOLUTION FOR THE RECTANGULAR SIMPLY SUPPORTED PANEL UNDER PRESSURE LOADING 211

A2.1 The Panel 211

A2.2 Novozhilov's Shell Theory 211

A2.3 Displacement Assumptions 212

A2.4 Calculation of Results 213

Appendix 3 BIBLIOGRAPHY 215

ACKNOWLEDGEMENTS 220

Note: Figures relating to a particular chapter are to be found at the end of that chapter.

ABSTRACT

The work is concerned with the application of the hybrid finite element method to thin plate and cylindrical shell structures. One plate bending element and three shell elements are studied. The plate element is the same as one already appearing in the literature but it is also used here to form the basis of a flat triangular element for the analysis of shells.

The main effort, however, has been devoted to the development of two new hybrid cylindrical shell elements. One is of rectangular and the other of triangular planform. The aim has been to use fully compatible edge displacement assumptions (with exact representations of rigid body motions) together with stress assumptions consisting of complete polynomials. In assessing the performance of these elements the primary concern has been the quality of stress predictions.

The two elements are tested separately on a variety of problems and found to give good results which compare well, in some cases, with those obtained using more complicated displacement assumption elements. They are then used together to analyse a cylinder intersection problem - that of a mitred bend in a pipe subjected to an in-plane bending moment. Results comparing well with some available strain gauge readings are obtained.

As a result of the work some general conclusions on the hybrid method are drawn. More specific conclusions relating to these elements are also noted and suggestions for further work are made.

Chapter 1

INTRODUCTION

1.1 Thin Shells

This thesis is concerned with the development of hybrid finite elements for the analysis of thin cylindrical shells. Thin shells are used in many items of modern industrial equipment, for instance, in the aerospace, nuclear, marine and petrochemical industries.

A shell is a body bounded by two curved surfaces and is "thin" if the distance between these surfaces, the thickness, is small in comparison with the other dimensions. The other identifying features of a thin shell are its edges and its reference surface (the locus of points lying midway between the two bounding surfaces). Novozhilov(1) defines thin shells as having a ratio of thickness/(radius of curvature of reference surface) of less than 1/20.

Within the framework of all thin shell theories the reference surface is the most significant feature since (a) it defines the shape and (b) its behaviour governs the behaviour of the shell. (see Appendix 1).

1.2 The Finite Element Method for the Analysis of Shells

The Finite Element Method considers a structure to be made up of a number of discrete elements, the behaviour in the interior of each being dependent upon the behaviour of "nodes" situated on its surface. Elements are joined to other elements only at nodes. A set of linear equations relates (usually) the forces and displacements at the nodes of the structure. With the application of suitable boundary conditions and forces, the displacements of the structure can be found by inversion of the matrix.

Early finite element analyses of shells used closed rings or s[illegible] conical elements to deal with shells of revolution. More generally shaped shells were first analysed by means of a number of flat elements (usually of either triangular or rectangular shape) based on the common displacement assumption formulation. Bending and membrane effects within each element are uncoupled (thus misrepresenting the true state of stress in a curved shell) but coupling is introduced when elements are joined together at angles to model the structure.

There are also two other deficiencies inherent in this method. Firstly, the geometry of the shell is always mis-represented and secondly, there is usually displacement incompatibility between elements, since bending and membrane displacements are of different orders of approximation. These deficiencies are explained in greater detail in Chapter 4. Often large numbers of elements are needed to obtain accurate answers but because of the relative simplicity of the elements the method is used quite extensively.

Attempts to reduce the number of elements necessary for accurate results led initially to the development of curved displacement assumption models capable of representing geometry exactly. At first these tended to be designed for a particular shape e.g. cylindrical shell elements; but later, elements for the analysis of doubly curved shells were produced.

Curved elements were found to be an improvement upon the flat elements but at the expense of (a) being more complicated to construct and (b) often using high order derivatives i.e. non-geometric freedoms at nodes. (A "geometric" freedom is considered to be a simple displacement or rotation.) Non-geometric freedoms are

difficult to accommodate in the analysis of a practical shell structure which may use various element types and have changes in thickness between elements.

As an alternative to the common displacement assumption form, the use of so called "hybrid" models has been proposed. These make use of a stress-assumption over the body of the element with a displacement assumption only around the boundaries (Chapter 2). So far, results for the displacements and natural frequencies of plates and shells have indicated the excellent possibilities of this approach.

An aspect of the performance of hybrid elements which has, so far, received relatively little attention, however, is their capability for predicting stress distributions. It was decided during the early part of this work to concentrate on this aspect since, also, it would give the best insight into their physical behaviour. An element having satisfactory performance in terms of stress predictions is likely to give good estimates of deflections and natural frequencies.

1.3 The Choice of a Suitable Shell Theory for the Construction of Finite Elements

If standard works on shell theory, e.g. those of Love(8,9), Timoshenko(3), Novozhilov(1) or Flügge(2) are studied it is found that each theory gives slightly different sets of equations relating to a particular shell problem. Warburton(56), among others, has made a study of the merits of shell theories when used for the construction of finite elements. He considers solutions to dynamic problems but the findings are valuable when considering static stress analysis.

Generally, for a shell which is deformed under the action of a set of loads, four sets of independent equations can be formulated.

(i) The relationships between stress resultants and stresses - the stress resultants are formed by the integration of stresses through the thickness of the shell.

(ii) The equilibrium equations for an infinitesimal element of the shell - these relate stress resultants, body forces and (in dynamic problems) inertia forces acting on the element.

(iii) The relationship (usually linear) between stress resultants and strains.

(iv) The strain-displacement relationships. These equations express the strains and curvatures as derivatives of the three displacements u, v and w in the plane of and perpendicular to the shell surface.

Warburton, for the dynamic case, considers the two basic methods of solving shell problems (a) by substituting directly into the equilibrium equations and (b) the energy method. Method (a) consists of substituting from equations (iii) and (iv) above into (ii) - resulting in three equations in the three unknown displacements u, v and w. The solution of the problem requires the determination of u, v and w in terms of the shell coordinates and, in the dynamic case, the time t.

Method (b) uses relations (iii) and (iv) again but instead of formulating the equilibrium equations, expressions for the strain and kinetic energies of an element of the shell are constructed and integrated over the whole volume. If appropriate functions for displacements are used it forms an alternative

method of obtaining exact solutions to problems. The final equations are obtained by applying Lagrange's equation or Hamilton's principle.

Warburton states three requirements for an acceptable finite element shell theory.

(i) From an engineering viewpoint - the simplest theory giving results of acceptable accuracy is required.

(ii) If the two methods of solution outlined above are applied to the same problem - then the final set of equations in each case should be identical (not an essential condition but advantageous).

(iii) If rigid body displacements are imposed upon a shell element there should be no resulting strains or curvatures from the strain-displacement relationship.

The above points have all been studied by various workers but only for specific cases. Cantin(68) shows that for cylindrical shells most theories do not satisfy criterion (iii) above. Three theories which do, however, are those of Novozhilov(1), Naghdi(69) and Sanders(70).

Considering criterion (ii), that of consistency, Novozhilov's theory gives exactly the same results for the vibrations of a cylindrical shell using both approaches. The theories of Love(9) and Timoshenko(3) are not satisfactory in this respect. The complete theory of Flügge(2) also gives the same results using the two methods - but not the same results as the theory of Novozhilov.

From the point of view of simplicity and accuracy of various theories Warburton uses the natural frequencies of uniform

cylindrical shells with simply supported ends as a relative measure. Using the complete theories, with no simplifications (Warburton outlines some of the simplications which can be made) the theories of Novozhilov, Flügge and Sanders give differences in the first natural frequency of a particular shell of the order of 0.3%. However, much larger differences can be found if the approximate forms of these theories are used.

The conclusion is therefore reached, on the basis of this and other examples, that no advantage is to be gained, from the point of view of accuracy, in using one theory in preference to the others. However, considering simplicity and the criteria involving rigid body motions and consistency outlined above, the theory of Novozhilov is considered the most suitable for use in a general shell finite element.

These findings led previous workers (53,55) to adopt the Novozhilov theory for the construction of a hybrid shell element which gave excellent deflection and natural frequency predictions. It was therefore decided, on the basis of the above evidence, to use the Novozhilov theory exclusively for all elements in this thesis.

1.4 The Work of this Thesis

Initially flat elements are used to solve various problems and a three-noded hybrid bending triangle is programmed and shown to give good stress and natural frequency predictions on flat plate problems. Membrane effects are then introduced and the element is used to analyse a test shell problem by approximating the geometry by a series of flat triangles. The results obtained are compared

with those using one of the most common displacement assumption flat triangles and found to be superior.

The work is mainly concerned, however, with the development and testing of two hybrid thin cylindrical shell elements. The first is of rectangular planform and has five simple geometric degrees of freedom at each of the four corner nodes. It was constructed after some investigations were made of an existing hybrid element of the same shape due to Henshell et al.(53). During the course of these, several unsatisfactory features were discovered and as a result a new element was constructed. It is particularly suitable, when used with other elements, for the stress analysis of ring and axially stiffened cylindrical shells.

The element is tested on a standard problem to determine the convergence of its stress predictions and is then applied to several other problems to enable comparisons to be made with other elements. It is found to give excellent stresses and to compare favourably with other, often more complex elements.

To extend the application of the rectangular element, one of triangular planform is then developed and tested. This again has four nodes, uses the same geometric freedoms and can be used in conjunction with the first to analyse cutouts and intersection regions in cylindrical shells. It is roughly equivalent in shape to half of the rectangular element after being cut along a diagonal - the shape of the "cut" being defined by the position of the fourth node. The element is tested in its own right on the same standard problem used for the rectangle and is found to give stress predictions of similar accuracy for the same mesh sizes.

As a conclusion to the work a cylinder-cylinder intersection problem is then treated using the two elements. The problem is a mitred bend in a pipe subjected to an in-plane bending moment. Stress distributions are obtained which are found to be in good agreement with some available strain gauge values.

In the whole of this work the suite of routines comprising the PAFEC 70+ finite element scheme was used extensively to compute the results.

Chapter 2

VARIATIONAL PRINCIPLES AND THE HYBRID METHOD FOR THE CONSTRUCTION OF FINITE ELEMENTS

2.1 Introduction

The classical variational principles used in the small deflection theory of elasticity are the Principle of Minimum Potential Energy and the Principle of Minimum Complementary Energy. These contain, respectively, the displacements and stresses as variables.

Traditional approximate solutions using variational principles e.g. the Ritz method involve making assumptions for the variables in the functionals. These assumptions should be continuous and possess derivatives which are also continuous up to the order contained in the corresponding Euler differential equations.

The Euler equation, essentially, is a necessary condition for the functional in the variational principle to exhibit a minimum. It can be shown that if the functional contains derivatives up to the nth order then the Euler equation is a differential equation of order 2n. For example in a plate bending problem the functional in the Principle of Minimum Potential Energy contains an expression for the strain energy of the plate and includes terms of the form $\partial^2 w/\partial x^2$, $\partial^2 w/\partial y^2$, $\partial^2 w/\partial x \partial y$ (where w is the lateral deflection and x and y are the coordinates of a point on the plate). The Euler equation for this problem is therefore a fourth order differential equation containing terms such as $\partial^4 w/\partial x^4$. In the Ritz method, continuous functions are assumed which are often infinite series and therefore satisfy the above continuity requirement automatically.

The finite element method is a variation of the Ritz procedure which treats the problem in a piecewise manner by splitting it up into elements. The unknowns are represented by functions which need satisfy the above continuity condition only within each element. However, if the value of the functional for the whole structure is to be represented accurately by the sum of the values for each individual element, then additional inter-element continuity requirements must be satisfied. These ensure that terms such as $\partial^2 w/\partial x^2$ in the functional of the plate bending problem quoted earlier remain finite in the small region between adjoining elements. For this, it can be proved necessary for the variable and its derivatives to exhibit inter-element continuity up to one order less than the order of the derivatives appearing in the functional of the variational principle. Thus for the plate bending problem continuity of w and normal slope is necessary.

If the above continuity conditions are maintained then the functional in the variational principle is accurately represented by the sum of its values within each element. The two classical variational principles are in this case directly applicable. Examples are the compatible (conforming) displacement assumption model frequently used in finite element analysis and the dual formulation of the equilibrium model in which inter-element stress continuity is maintained.

It is possible, however, to apply the finite element method where the above inter-element continuity conditions do not exist. Variational principles can be constructed to describe this process by relaxing continuity requirements in the basic forms. Such relaxations are introduced into the functionals as conditions of

constraint using the method of Lagrangian Multipliers. The multipliers can later be identified as physical quantities in the problem e.g. boundary tractions or stresses (see later).

In addition to the two basic principles mentioned earlier (containing respectively displacements and stresses as variables) there are other, more general principles derived from these which are more useful to consider in the present context. These are the Hu-Washizu and Hellinger-Reissner Principles which contain combinations of displacements, stresses and strains in their functionals. Pian(71) gives a particularly good description of how modified forms of these can be obtained in which the continuity requirements are relaxed.

It is proposed in this chapter to indicate how the Hu-Washizu and Hellinger-Reissner Principles can be derived from the Principle of Minimum Potential Energy and how the latter of these can be converted into the Principle of Minimum Complementary Energy. A modified Hellinger-Reissner Principle will then be constructed to account for the relaxation of inter-element continuity and the Modified Complementary Energy Principle which is the basis of "hybrid" elements will be derived. Finally, to demonstrate the application of these principles to the construction of hybrid elements a general dynamic problem is treated and stiffness, mass and consistent loading vectors for an element are derived.

2.2 Variational Principles

2.2.1 The Functionals

The Principle of Minimum Potential Energy, on which assumed displacement finite elements are based, states that a quantity

known as the total potential energy (P) of the structure is a minimum when the structure deflects under load.

The total potential energy is given by

$$P = \int_{VOL.} \left[\tfrac{1}{2} \epsilon_{ij} \sigma_{ij} - \bar{F}_i u_i \right] d(VOL) - \int_{S_\sigma} \bar{T}_i u_i \, dS \qquad (2.1)$$

where repeated suffices are summed following the usual convention and

ϵ_{ij} - are the strains

σ_{ij} - are the stresses

u_i - displacements of structure

$\bar{F}_i$ - the prescribed body forces

$\bar{T}_i$ - the prescribed surface traction

S_σ - is the portion of the boundary of the structure over which the surface tractions are prescribed.

If we now wish to introduce the strains as an additional field variable we must make use of the strain-displacement relations as a constraint and use the method of Lagrange multipliers. If this is done and the variation of the functional so obtained is equated to zero, it can be shown that the Lagrange multipliers are equal to the stresses.

Hence if the strain-displacement relations are expressed in the form

$$\epsilon_{ij} = \tfrac{1}{2}\left(u_{i,j} + u_{j,i} \right) \qquad (2.2)$$

(where , denotes differentiation) a functional Π_i can be derived from (2.1) which includes the strains

$$\Pi_i = \int_{VOL} \left\{ \tfrac{1}{2} \epsilon_{ij} \sigma_{ij} + \sigma_{ij} \left[\tfrac{1}{2}\left(u_{i,j} + u_{j,i} \right) - \epsilon_{ij} \right] - \bar{F}_i u_i \right\} d(VOL) - \int_{S_\sigma} \bar{T}_i u_i \, dS \qquad (2.3)$$

and where the constraint is included in the volume integral. Simplifying (2.3) gives

$$\Pi_i = \int_{VOL} \left\{ -\tfrac{1}{2} \epsilon_{ij} \sigma_{ij} + \sigma_{ij} \cdot \tfrac{1}{2} \left(u_{i,j} + u_{j,i} \right) - \bar{F}_i u_i \right\} d(VOL) - \int_{S_\sigma} \bar{T}_i u_i \, dS \qquad (2.4)$$

Equation (2.4) gives the functional of the Hu-Washizu Principle containing strains, displacements and stresses as field variables.

If the strains are eliminated from (2.4) by the introduction of the stress-strain relationship (S_{ijkl} being the compliance matrix) the functional of the Hellinger-Reissner Principle is obtained

$$\Pi_R = \int_{VOL} \left\{ -\tfrac{1}{2} S_{ijkl} \sigma_{ij} \sigma_{kl} + \sigma_{ij} \cdot \tfrac{1}{2} \left(u_{i,j} + u_{j,i} \right) - \bar{F}_i u_i \right\} d(VOL) - \int_{S_\sigma} \bar{T}_i u_i \, dS \qquad (2.5)$$

which contains only the displacements and stresses as variables.

Finally, if the stress-equilibrium equations are introduced into (2.5) after the second term in the volume integral has been integrated by parts, the functional of the Principle of Minimum Complementary Energy is obtained. This contains only the stresses as field variables

$$\Pi_C = \int_{VOL} \left\{ -\tfrac{1}{2} S_{ijkl} \sigma_{ij} \sigma_{kl} \right\} d(VOL) + \int_{S_u} T_i \bar{u}_i \, dS \qquad (2.5a)$$

where S_u is the portion of the boundary where displacements are prescribed. (The whole boundary $S = S_\sigma + S_u + S_\sigma$ where S_σ is the part of the boundary where neither surface traction nor displacement are prescribed.)

2.2.2 Application to Finite Element Analysis

If the Hellinger-Reissner Principle is applied to a finite

element idealization the functional of (2.5) becomes

$$\pi_R = \sum_n \left\{ \int_{V_n} \left[-\tfrac{1}{2} S_{ijkl}\,\sigma_{ij}\,\sigma_{kl} + \tfrac{1}{2}\sigma_{ij}\left(u_{i,j}+u_{j,i}\right) - \bar{F}_i u_i \right] d(\text{VOL}) - \int_{S_{un}} T_i\left(u_i - \bar{u}_i\right) dS - \int_{S_{\sigma n}} \bar{T}_i u_i\, dS \right\} \qquad (2.6)$$

where V_n is the volume of the n'th element and S_{un} is the portion of the boundary of the element where the displacements $\bar{u}_i$ are prescribed. The integral around S_{un} in the above functional imposes the constraint that along this part of the boundary of the element $u_i \equiv \bar{u}_i$. In this case the corresponding Lagrange multipliers can be shown to be T_i the boundary tractions.

In the above functional stresses and displacements are assumed separately for individual elements. In this case the inter-element continuity requirements involve continuity of displacements but not stresses.

A possible way of relaxing these displacement continuity requirements is to use separate functions for the displacement field u_i within the element and the displacements $\tilde{u}_i$ along the boundaries. The boundary displacements can be chosen to satisfy inter-element compatibility and the constraint between u_i and $\tilde{u}_i$ introduced as in (2.6). The boundary tractions (Lagrangian multipliers) of adjacent elements are independent and the condition of constraint imposes the compatibility of the two sets of displacements at the element boundary. In this case the constraint integral must be performed around the entire boundary of each element, ∂V_n .

The functional can be written as

$$\pi_{mR1} = \sum_n \left\{ \int_{V_n} \left[-\tfrac{1}{2} S_{ijkl}\,\sigma_{ij}\,\sigma_{kl} + \tfrac{1}{2}\sigma_{ij}\left(u_{i,j}+u_{j,i}\right) - \bar{F}_i u_i \right] d(\text{VOL}) - \int_{\partial V_n} T_i\left(u_i - \tilde{u}_i\right) dS - \int_{S_{\sigma n}} \bar{T}_i \tilde{u}_i\, dS \right\} \qquad (2.7)$$

In the above functional σ_{ij} , u_i , T_i , and $\tilde{u}_i$ can all, in principle be independent. One of the equations obtained by setting the variation of (2.7) to zero, however, is

$$T_i = \sigma_{ij} \nu_j \tag{2.8}$$

where ν_j is the unit normal.

If this condition is satisfied Π_{mR1} will contain only three field variables i.e. σ_{ij} and u_i in the interior of the element and $\tilde{u}_i$ along the element boundary.

Integrating the second term in the volume integral in (2.7) by parts gives

$$\Pi_{mR2} = \sum_n \left\{ \int_{V_n} \left[-\tfrac{1}{2} S_{ijkl}\, \sigma_{ij} \sigma_{kl} - \sigma_{ij,j}\, u_i - \bar{F}_i u_i \right] d(\text{VOL}) + \int_{\partial V_n} T_i \tilde{u}_i \, dS - \int_{S_{\sigma_n}} \bar{T}_i \tilde{u}_i \, dS \right\} \tag{2.9}$$

If, in addition, the assumed stresses within each element are chosen to satisfy the equilibrium equation

$$\sigma_{ij,j} + \bar{F}_i = 0 \tag{2.10}$$

then the second two terms in the volume integral of (2.9) disappear and the displacements u_i no longer appear in the volume integral. The only displacements then involved in the functional are those along the element boundary. Only two variables are present and the functional is that of the Modified Complementary Energy Principle which is the basis of both the Equilibrium and Hybrid Stress Assumption finite element models.

$$\Pi_{mc} = \sum_n \left\{ \int_{V_n} \left[-\tfrac{1}{2} S_{ijkl}\, \sigma_{ij} \sigma_{kl} \right] d(\text{VOL}) + \int_{\partial V_n} T_i u_i \, dS - \int_{S_{\sigma_n}} \bar{T}_i u_i \, dS \right\} \tag{2.11}$$

In simple static problems it is usually relatively easy to satisfy (2.10) - so the modified Hellinger-Reissner Principle of (2.9) is seldom used. However, in dynamic and initial stress problems it is useful.

2.2.3 Treatment of a Dynamic Problem

As an illustration of the use of the Hellinger-Reissner Principle outlined above, a typical dynamic problem will be treated in finite element terms and element matrices will be derived. Such a problem could, for instance, be the small vibrations of a flat plate.

A Hellinger-Reissner variational functional can be obtained corresponding to (2.7) by adding a kinetic energy term

$$\Pi_{mR_1} = \int_{t_1}^{t_2} \sum_n \left\{ \iint_{V_n} \left[-\tfrac{1}{2} S_{ijkl}\,\sigma_{ij}\sigma_{kl} + \tfrac{1}{2}\sigma_{ij}\left(u_{i,j}+u_{j,i}\right) - \bar{F}_i u_i - \tfrac{1}{2}\rho \dot{u}_i^2 \right] d(VOL) \right.$$
$$\left. - \int_{\partial V_n} T_i\left(u_i - \tilde{u}_i\right) dS - \int_{S_{\sigma_n}} \bar{T}_i\,\tilde{u}_i\, dS \right\} dt \qquad (2.12)$$

where ρ is the density of the material under question.

Earlier (equations (2.9) and (2.10)) the stress-equilibrium equations only involved the body forces and were easy to satisfy in the stress assumption. In the present dynamic case, however, the equations contain the unknown displacements u_i and it is not possible to assume element stress distributions to satisfy these. Also, if a stress assumption is made and (2.8) used to evaluate boundary tractions, these are not likely to be accurate approximation of the true values. In addition, then, to there being some freedom in the choice of stress assumptions, the choice of edge displacements $\tilde{u}_i$ need not be compatible with the interior displacements u_i . There are therefore many possible finite element formulations, each having different assumptions. An important feature, however, is that in all cases the resulting matrix equations will only have the nodal displacements as unknowns if displacement assumptions are made in terms of these.

Corresponding to equation (2.9) the expanded version of (2.12) becomes

$$\Pi_{mR_2} \approx \int_{t_1}^{t_2} \sum_n \left\{ \left[-\tfrac{1}{2} S_{ijkl}\,\sigma_{ij}\,\sigma_{kl} - \sigma_{ij,j}\,u_i - \bar{F}_i u_i - \tfrac{1}{2}\rho \dot{u}_i^2 \right] d(vol) + \int_{\delta V_n} \sigma_{ij}\,\nu_j\,\tilde{u}_i\,dS - \int_{S\sigma_n} \bar{T}_i\,\tilde{u}_i\,dS \right\} dt \qquad (2.13)$$

In the finite element approach the stresses within each element are approximated by a finite number of parameters $\{\beta\}$

$$\{\sigma\} = [P]\{\beta\} \qquad (2.14)$$

and the term representing Ti along each boundary $(\sigma_{ij}\,\nu_j)$ can be expressed also in terms of $\{\beta\}$

$$\{\sigma_\nu\} = [R]\{\beta\} \qquad (2.15)$$

Next, the boundary displacements $\tilde{u}_i$ common to two adjacent elements are interpolated from the nodal values common to the two elements

$$\{\tilde{u}\} = [L]\{q\} \qquad (2.16)$$

The displacements u_i in the interior can, in principle, be independent of $\tilde{u}_i$, but normally these too are interpolated in terms of the same set of nodal variables

$$\{u\} = [N]\{q\} \qquad (2.17)$$

Since u_i and $\tilde{u}_i$ are independent, $\tilde{u}_i$ can easily be chosen to satisfy inter-element continuity, whereas it is not necessary for u_i to do this.

The derivative of σ_{ij} may be written as

$$\{\sigma\}' = [P]'\{\beta\} \qquad (2.18)$$

and substituting equations (2.14) → (2.18) into (2.13) gives the variational functional as

$$\Pi_{mR_2} = \int_{t_1}^{t_2} \sum_n \left[-\tfrac{1}{2}\{\beta\}^T[H]\{\beta\} - \{\beta\}^T[D]\{q\} - \{q\}^T[\bar{Q}] - \tfrac{1}{2}\{\dot{q}\}^T[M]\{\dot{q}\} + \{\beta\}^T[G]\{q\} - \{q\}^T[\bar{Q}_2] \right] dt \qquad (2.19)$$

where :—

$$[H] = \int_{V_n} [P]^T [S][P]\, d(VOL) \qquad [M] = \int_{V_n} \rho [N]^T [N]\, d(VOL)$$

$$[D] = \int_{V_n} [P]'^T [N]\, d(VOL) \qquad [G] = \int_{\partial V_n} [R]^T [L]\, dS \qquad (2.20)$$

$$[Q]_1 = \int_{V_n} [N]^T [F]\, d(VOL) \qquad [Q]_2 = \int_{\partial V_n} [L]^T [\bar{T}]\, dS$$

Setting the variation of Π_{mR_2} with respect to $\{\beta\}$ in (2.19) to zero gives

$$-[H]\{\beta\} + \{[G] - [D]\}\{q\} = 0 \qquad (2.21)$$

Solving for $\{\beta\}$ from (2.21) and using this expression in (2.19) gives

$$\Pi_{mR_2} = \int_{t_1}^{t_2} \sum_n \left(\tfrac{1}{2}\{q\}^T [K]\{q\} + \tfrac{1}{2}\{\dot{q}\}^T [M]\{\dot{q}\} - \{q\}[Q] \right) dt \qquad (2.22)$$

where

$$[K] = \{[G] - [D]\}^T [H]^{-1} \{[G] - [D]\} \qquad (2.23)$$

is the element stiffness matrix.

$[M]$ = the element mass matrix

$[Q] = [Q]_1 + [Q]_2$ = generalized forces

If the element matrices are assembled to form the respective global matrices $[K^*]$, $[M^*]$ and $[Q^*]$ variation of (2.19) with respect to the unrestrained nodal displacements will yield the dynamic equation

$$[M^*].\{\ddot{q}\} + [K^*]\{q\} = [Q^*] \qquad (2.24)$$

2.3 Points arising from this Analysis

2.3.1 The Element Stiffness Matrix

In the above example the stress assumption does not have to satisfy the equilibrium equations and two displacement assumptions are made which may be incompatible along the element boundaries.

If the assumed stresses are made to satisfy the homogeneous equilibrium equations, however, ($\sigma_{ij,j} = 0$) then the matrix $[D]$ of (2.20) disappears and the stiffness matrix $[K]$ is in fact the same as that which would be obtained using the Modified Complementary Energy Principle (2.11).

2.3.2 The Mass Matrix

Successful dynamic results using the above approach have been demonstrated by Dungar, Severn & Taylor(33) and are also included later in this thesis. If the interior displacements u_i do not have to be compatible with the edge assumptions $\tilde{u}_i$ then a good deal of freedom of choice is involved. However, since in (33) the stresses are only chosen to satisfy the homogeneous equations of equilibrium and not the dynamic ones, the solutions are strictly an application of the Hellinger-Reissner principle, and not that of Minimum Complementary Energy, although for the reasons pointed out in (2.3.1) the two stiffness matrices are identical.

2.3.3 The Effect of a Non-Equilibrating Stress Assumption

If in (2.13) the assumed stresses satisfy the homogeneous equilibrium equations (without body forces) or the non-homogeneous set (with body forces) then the term involving $\sigma_{ij,j} u_i$ in the volume integral is no longer present. This approach is adopted with all the hybrid elements in this thesis.

Pian(71) has investigated the effect, however, of using stress assumptions which do not satisfy either of the equilibrium equations, such that the term $\sigma_{ij,j}\, u_i$ still appears. From preliminary studies on the vibration analysis of a simple beam it appears that when the internal displacements u_i match those at the boundary of the element $\tilde{u}_i$, the extra terms have no effect. However, when u_i and $\tilde{u}_i$ do not coincide then the effect of the $\sigma_{ij,j}\, u_i$ term in some cases produces non-convergent solutions.

Pian concludes that it is best to choose the assumed stresses to satisfy the homogeneous equilibrium equations so that the terms do not appear. It seems that there must be a certain matching condition between the assumed u_i and $\tilde{u}_i$ which must be satisfied, otherwise, to guarantee the convergence of the finite element solution.

2.3.4 Loading Vectors

The matrix $[Q]_1$ of (2.20) indicates how the prescribed body force $\bar{F}_i$ can be lumped using the assumed displacements u_i. If, however, the stress assumption is chosen to satisfy the equilibrium equations with body forces present, then the term $\bar{F}_i u_i$ in (2.13) does not appear and $[Q]_1$ vanishes. It may therefore be regarded as an inconsistent loading vector.

If the equilibrating stress assumption is made in two parts, however, then consistent nodal loads can be obtained.

Let $\{\sigma\} = [P]\{\beta\} + [P]_F\{\beta\}_F$ where $[P]_F\{\beta\}_F$ is a (2.25)

particular solution of the equilibrium equations with the prescribed body force and $[P]\{\beta\}$ as before satisfies the homogeneous equilibrium equations. If (2.25) is used in (2.13) instead of (2.14), then the consistent loading vector turns out to be

$$[\bar{Q}] = [G]^T [H]^{-1} [H]_F \{\beta\}_F + [S] \tag{2.26}$$

where $$[S]^T = -\{\beta\}_F [G]_F + \int_{S_{\sigma_n}} [\bar{T}][L]\, ds$$

where $[R]_F^T$ performs a similar function to $[R]$ in (2.15)

$$[G]_F = \int_{\partial V_n} [R]_F^T [L]\, ds \qquad [H]_F = \int_{V_n} [P]^T [S] [P]\, d(VOL) \tag{2.27}$$

and other quantities have been defined earlier.

Strictly speaking, this is only a consistent loading vector if all the columns in $[P]_F$ are included in $[P]$. Therefore, if the body force is a high order function of the coordinates, then a large number of assumed stress modes must be used in $[P]$ to evaluate the stiffness matrix. In practice it is found, certainly for the elements described later in this thesis, that if some higher order terms are used in $[P]_F$, reasonable loading vectors are still obtained.

2.3.5 The Length of the Stress Assumption

Theoretically, in equation (2.14) there is no limit to the number of undetermined coefficients $\{\beta\}$ which can be used. The quality of results obtained, however, depends upon the number of terms and, as will be shown later, best results are not obtained with large numbers of terms. There is, however, a theoretical minimum length for the assumption.

If the variational of the functional of (2.19) is taken with respect to $\{q\}$, the displacements, then it can be shown that if N, the total number of assumed stress modes of all elements is smaller than M, the total number of degrees of freedom on the structure, then there will, in general, be no solution for the β's. It can be proved, however, that if in each individual

element (where m is the number of stress terms, k is the number of degrees of freedom and l is the number of rigid body modes) the inequality $m \geqslant k-l$ is satisfied, then a solution for $\{\beta\}$ is guaranteed. If too few stress terms are used it is possible for spurious rigid body motions to appear in the stiffness matrix i.e. deformations producing no stresses.

2.3.6 The Evaluation of Stresses

The relationship (2.21) enables the coefficients of the stress assumption to be expressed in terms of the element displacements. If, as is usual, the assumption is chosen to satisfy equilibrium and the matrix $[D]$ in (2.21) ceases to exist, then the equation can be re-written as

$$\{\beta\} = [H]^{-1}[G]\{q\}$$

The computation of the $[H]^{-1}$ and $[G]$ matrices is an intrinsic part of the element routine and these can be put on to backing store at this stage. When it is required to evaluate stresses from the displacements they can be recalled and the above relationship used to compute $\{\beta\}$.

2.3.7 Equilibrium, Hybrid and Conforming Displacement Assumption Elements

Both the assumed stress hybrid model and the Equilibrium model used by de Veubeke(36,37) are based on the Modified Complementary Energy Principle, (2.11). In a somewhat similar manner to the conforming displacement assumption model (where displacements are continuous between elements), the equilibrium approach ensures continuity of boundary tractions.

De Veubeke has used the method of dual finite element analysis by conforming displacement assumption and equilibrium models extensively. These analyses yield bounds to the strain energy content of the structure. Since the direct flexibility influence coefficient (generalized displacement due to corresponding generalized force of unit magnitude) is equal to the strain energy, its upper and lower bounds can also be established.

The direct influence coefficient using a hybrid element, however, may be either an upper or lower bound. It can be proved, however, always to lie between that of the conforming displacement assumption model with the same boundary displacements and that of the equilibrium model using the same interior stresses.

The boundary displacements of the hybrid model can be considered as constraints on the structure - but only along certain lines (the element boundaries). A conforming displacement assumption model, however, imposes constraints over the whole of the structure and can be proved always to underestimate the strain energy content giving a stiff solution.

The use of a finite number of stress terms in the hybrid model (with the same edge displacements), introduces flexibility which offsets the stiffness of the assumed displacements to some extent. Increasing the number of stress modes, however, makes the stresses more and more compatible with the edge displacements and in the limit the solution would approach that of the conforming displacement assumption element.

Chapter 3

A TRIANGULAR HYBRID PLATE BENDING ELEMENT

3.1 Existing Plate Bending Elements

Excellent accounts of much of the early work on plate bending finite elements are given by Clough and Tocher(19) and Zienkiewicz (14,15). Workers concentrated mainly on the production of elements of rectangular or triangular shape based upon the assumed displacement (Minimum Potential Energy) approach. The majority of these used non-conforming displacement assumptions. Lateral displacements between elements were usually compatible, but normal slopes were often discontinuous.

Two of the more successful rectangular elements of this type were constructed by Dawe(16) and Melosh(17). The first uses a displacement assumption of twelve terms in x and y (the coordinates of a point on the element). The element of Melosh was developed purely on the basis of physical reasoning. The element is assumed to distort along its edges with shapes defined by beam functions and these are assumed to decrease linearly towards the opposite edge.

Two typical non-conforming triangles were those of Adini(20) and Tocher(21). These were similar to the Dawe element in that simple polynomial expressions for the displacements were used but generally they were not so successful. In the case of the Tocher triangle, which will be used later, the displacement assumption for the lateral deflection w consists of nine terms

$$w = \left[1, x, y, xy, x^2, y^2, x^3, y^3, xy(x+y)\right] \cdot \begin{Bmatrix} \alpha_1 \\ \vdots \\ \alpha_9 \end{Bmatrix}$$

A later development has been the production of general quadrilateral non-conforming elements. These include midside nodes which enable the sides to be curved to analyse, for instance, circular plates.

It was thought necessary, however, in an attempt to improve results, to develop conforming elements having both displacement and normal slope continuity. Two of the best rectangles were (a) that attributed variously to Bogner, Fox and Schmit(22), Butlin and Leckie(23) and Mason(24), and (b) that of Clough and Felippa (18) (which can, in fact, take the form of a general quadrilateral). Triangular conforming elements were produced by Clough and Tocher(19), Bazeley et al.(25), Butlin and Ford(26) and Cowper et al.(27). These conforming elements either use high order derivatives as nodal freedoms in order to assure conformity (the disadvantages of this method are outlined in Chapter 1) or are complicated in some other way such as being composed of sub-elements e.g. the Clough-Tocher triangle(19) and the Clough-Felippa quadrilateral(18) (which uses Clough-Tocher triangles as sub-elements). Separate displacement assumptions are made in each sub-element and these are matched at nodes on the interior sub-element boundaries. In this way conformity between master elements can be obtained.

The use of an alternative variational principle to construct hybrid assumed stress elements (see Chapter 2) has also received attention. The method was originally introduced by Pian(28,29) to produce a rectangular in-plane element but later Severn and Taylor(32) constructed rectangular and triangular bending elements which proved successful for vibration analysis(33). Hybrid plate bending elements of various shapes were later investigated by Allwood and Cornes(34) and Neale et al.(35).

3.2 The Present Work

In this chapter the programming and testing of a hybrid plate bending triangle are described. Results for stresses, deflections and natural frequencies are compared with those obtained using other hybrids and comparable displacement assumption forms. The Tocher element(21) described in the previous section is programmed for comparison purposes. The results demonstrate well the degree of improvement possible using the hybrid approach.

The present hybrid element is similar in many ways to that of Severn and Taylor(32) and was subsequently found to be identical to a particular form of the general polygonal element of Allwood and Cornes(34). The detail of its formulation differs from these, however, in that assumptions for stress resultants are made instead of stresses.

The element was programmed as a result of the work of Henshell et al.(53) and Neale(55) who introduced the concept of an "optimized" stress assumption in which the length and form of the assumption are carefully selected. Stress distributions obtained are demonstrated to be of good accuracy and generally the static results confirm those of Allwood and Cornes in that the shorter stress assumptions give the best results.

To enable the element to be used on dynamic problems a displacement assumption is made and a mass matrix derived as described in Chapter 2. Good natural frequency results are obtained.

3.3 The Formulation of the Triangular Hybrid Bending Element

3.3.1 Introduction

The construction of hybrid elements is described in detail

in the previous chapter. For the evaluation of the stiffness matrix it is necessary to make assumptions for stresses within the element and displacements along the boundary. For the construction of a mass matrix a displacement assumption must also be made within the element.

3.3.2 The Boundary Displacement Assumptions

The geometry of the element and nodal degrees of freedom are shown in Fig.(3.1). The freedoms at each node consist of the displacement normal to the element and the two rotations about the element x and y axes. These simple freedoms allow the definition of cubic normal displacement and linear normal slope along edges. Each edge is treated separately and for purposes of interpolation the nodal rotations are transformed into a rotation along (θ_s) and a rotation perpendicular (θ_n) to the edge under consideration.

Thus, along the edge joining nodes 2 and 3 in Fig.(3.1) which is at an angle ψ to the x axis as shown

$$\begin{Bmatrix} w \\ \theta_s \\ \theta_n \end{Bmatrix} = \begin{bmatrix} 1-3\left(\frac{s}{\ell}\right)^2+2\left(\frac{s}{\ell}\right)^3 & -\ell\left\{\left(\frac{s}{\ell}\right)-2\left(\frac{s}{\ell}\right)^2+\left(\frac{s}{\ell}\right)^3\right\} & \left\{2\left(\frac{s}{\ell}\right)^2-2\left(\frac{s}{\ell}\right)^3\right\} & \ell\left\{\left(\frac{s}{\ell}\right)^2-\left(\frac{s}{\ell}\right)^3\right\} \\ \left\{1-\left(\frac{s}{\ell}\right)\right\} & & & \left(\frac{s}{\ell}\right) \\ \frac{6}{\ell}\left\{\left(\frac{s}{\ell}\right)-\left(\frac{s}{\ell}\right)^2\right\} & \left\{1-4\left(\frac{s}{\ell}\right)+3\left(\frac{s}{\ell}\right)^2\right\} & -\frac{6}{\ell}\left\{\left(\frac{s}{\ell}\right)-\left(\frac{s}{\ell}\right)^2\right\} & -\left\{2\left(\frac{s}{\ell}\right)-3\left(\frac{s}{\ell}\right)^2\right\} \end{bmatrix} \begin{Bmatrix} w_2 \\ \theta_{s2} \\ \theta_{n2} \\ w_3 \\ \theta_{s3} \\ \theta_{n3} \end{Bmatrix} \quad (3.1)$$

Where s is the distance along the edge measured from node 2

ℓ is the length of the edge

w_i is the normal displacement at node i

θ_{si} is the rotation <u>along</u> the edge at node i (the normal slo

θ_{ni} is the rotation <u>perpendicular</u> to the edge at node i

The functions in (3.1) are standard Hermitian interpolation formulae expressing the cubic variation of w and linear variation of Θ_s . Θ_n is obtained by differentiating the expression for w with respect to s.

The rotations Θ_{si} and Θ_{ni} can be expressed in terms of the actual nodal variables on the side 2,3 i.e.

$$\Theta_{si} = \Theta_{yi} \sin\psi - \Theta_{xi} \cos\psi$$
$$\Theta_{ni} = \Theta_{yi} \cos\psi + \Theta_{xi} \sin\psi \qquad (3.2)$$

Therefore by substituting equations (3.2) into (3.1) the variation of w , Θ_s and Θ_n can be defined uniquely in terms of the nodal freedoms. Hence the displacements of an adjoining edge, with the same nodal displacements, will be compatible in every way.

This treatment is applied to all edges of the element.

3.3.3 The Stress Assumption

The stresses are considered to be integrated through the thickness of the plate to form stress resultants which act on the middle surface (Appendix 1). These are shown acting on an infinitesimal element of plate in Fig.(3.2).

Considering the equilibrium of the infinitesimal element under the action of the stress resultants it can be shown that the following three equations apply

$$\partial Q_y/\partial y + \partial Q_x/\partial x = 0$$
$$-\partial M_{xy}/\partial x + \partial M_y/\partial y = Q_y \qquad (3.3)$$
$$-\partial M_{yx}/\partial y + \partial M_x/\partial x = Q_x$$

where, in the case of flat plates, $M_{xy} = M_{yx}$.

Equations (3.3) are the equilibrium equations with no applied load or "homogeneous" equilibrium equations described in Chapter 2. Following the method outlined there, a stress assumption is made which satisfies (3.3). It is of polynomial form in the element coordinates x and y of Fig.(3.1).

$$\begin{Bmatrix} M_x \\ M_y \\ M_{xy} \\ Q_x \\ Q_y \end{Bmatrix} = \begin{bmatrix} 1 & x & y & & & & & & \\ & & & 1 & x & y & & & \\ & & & & & & 1 & x & y \\ & 1 & & & & & & & -1 \\ & & & & 1 & & & -1 & \end{bmatrix} \cdot \begin{Bmatrix} \beta_1 \\ \vdots \\ \beta_9 \end{Bmatrix} \qquad (3.4)$$

It can be seen that each column of (3.4) satisfies (3.3). This particular assumption was chosen after carefully considering the results and findings of other workers.

The assumption must involve at least a minimum number of parameters $\{\beta\}$, (see previous chapter) otherwise the stiffness matrix is likely to contain spurious rigid body motions. This is explained fully by Tong and Pian(30,31,29,28). In the present case this minimum length (given by the difference between the number of degrees of freedom and the number of rigid body motions) is 9-3 = 6.

Theoretically, there is no upper limit to the length of the assumption, but the work of Allwood and Cornes(34) and Severn and Taylor(32) has given a guide in the case of a triangular bending element involving the 9 simple freedoms used here. Allwood and Cornes, who make assumptions for stresses (not stress resultants) conclude that a nine-term assumption involving linear distributions is best. Longer assumptions involving quadratic terms give no improvement and generally cause the element to become too stiff. These findings coincide with those of Neale(55) who found for both

a hybrid rectangular cylindrical shell and a rectangular plate bending element that an assumption close to the minimum possible length is usually the best.

Pian(30) demonstrates, in fact, that by using higher and higher order stress functions one is only approximating more closely the solution using compatible displacement assumption elements (having the same edge displacements as the hybrid). These always give a stiff solution. (See Section 2.3.7 of Chapter 2)

It was, then, with these findings in mind that the assumption (3.4) was chosen. There are 9 undetermined parameters $\{\beta\}$, three more than the necessary minimum.

3.3.4 The Evaluation of Edge Work and Complementary Strain Energy

Following the method outlined in Chapter 2 the calculation of a stiffness matrix involves the evaluation of (i) the work done by the stresses on the edge displacements, and (ii) the complementary strain energy of the element.

For the evaluation of edge work the stress resultants along an edge must be transformed into forces in the direction of the displacements i.e. a transverse force and moments parallel and perpendicular to the edge.

For example along edge 1,2 in Fig.(3.1)

$$\begin{Bmatrix} F_w \\ F_{\theta x} \\ F_{\theta y} \end{Bmatrix} = \begin{bmatrix} 0 & 0 & 0 & 0 & 1 \\ 0 & -1 & 0 & 0 & 0 \\ 0 & 0 & -1 & 0 & 0 \end{bmatrix} \cdot \begin{Bmatrix} M_x \\ M_y \\ M_{xy} \\ Q_x \\ Q_y \end{Bmatrix} \qquad (3.5)$$

The same principle holds for the other two edges but the expressions become more involved. By then substituting for the moments in terms of $\{\beta\}$ it is possible to express the forces for each edge in the form of Chapter 2

$$\{\sigma_v\} = [R].\{\beta\} \tag{3.6}$$

For the calculation of the complementary strain energy the linear relationship between stress-resultants and strains used is

$$\begin{Bmatrix} M_x \\ M_y \\ M_{xy} \end{Bmatrix} = \frac{Et^3}{12(1-\nu^2)} \begin{bmatrix} 1 & \nu & 0 \\ \nu & 1 & 0 \\ 0 & 0 & \frac{(1-\nu)}{2} \end{bmatrix} \cdot \begin{Bmatrix} -\partial^2 w/\partial x^2 \\ -\partial^2 w/\partial y^2 \\ 2\partial^2 w/\partial x \partial y \end{Bmatrix} \tag{3.7}$$

where ν = Poisson's Ratio.

For the present element the integrals were carried out numerically using a Gauss Process of order 2. To evaluate the strain energy only the bending moments of (3.7) are involved but both the bending moments and the shear forces (3.5) are needed to evaluate the edge work.

3.3.5 The Calculation of Stresses

As with allelements in the PAFEC 70+ scheme the evaluation of stresses takes place in a stressing routine after the displacements of the structure have been found(11). The structural displacements relating to a particular element are identified and converted to displacements in element axes.

For hybrid elements the evaluation of stresses is particularly convenient because there is already an explicit expression for them. If, as in the present case, the stress assumption satisfies the equilibrium equations, then the matrix $[D]$ in equation (2.19) of Chapter 2 ceases to exist. Equation (2.21) becomes

$$\{\beta\} = [H]^{-1}[G]\{q\} \qquad (3.3)$$

where $\{q\}$ is the vector of nodal displacements of a particular element. The $[H]^{-1}[G]$ matrix, formed in the element routine, must be written to backing store and recalled to the stressing routine during the calculation of stresses for the particular element. When $\{\beta\}$ is known the stresses at any point in the element can be evaluated.

3.3.6 The Addition of a Mass Matrix

In the previous chapter the method of deriving a mass matrix for use with a hybrid element is described. This involves a displacement assumption being made over the whole of the element, which need not necessarily be consistent with the edge displacement assumptions. This can be justified, as explained earlier, in terms of a modified Hellinger-Reissner Principle. Nevertheless, a mass matrix derived by this method must be inconsistent, even if the two displacement assumptions are compatible, since the interior displacement assumption will not usually be compatible with the assumed stresses.

It was decided, in this case, to try various displacement assumptions. Initially one coinciding with the edge assumptions was used - that of Clough and Tocher(19). This involves splitting the element up into three sub-elements to make the lateral deflection vary cubically and the normal slope linearly along each edge. A great deal of computation is involved.

Simpler displacement assumptions such as that of Tocher(21) (given in Section 3.1) were then tried. This particular one was found to give answers almost as good as those using the Clough-

Tocher mass matrix and because of the simplicity of calculation was considered to be the most efficient formulation.

3.4 Results Obtained Using the Triangular Hybrid Bending Element

3.4.1 Simply Supported Square Plate under a Central Point Load

To investigate the performance of the element in statics a simply supported square plate with a central point load was analysed using various meshes. The plate is shown in Fig.(3.3) together with the properties of the material and a typical mesh used. Symmetry conditions allow $\frac{1}{4}$ of the plate to be analysed and the mesh shown is designated n = 3.

In Fig.(3.4) there is a plot (line labelled HT) of the non-dimensional central deflection coefficient $10^3 W_c D/PL^2$ (where $D = Et^3/12(1-\nu^2)$) against the mesh size n. Other curves are (i) that using the simple non-conforming Tocher triangular displacement assumption element(21) designated T, (ii) that of the conforming displacement assumption element of Clough and Tocher(19) designated HCT and (iii) that using the element of Adini(20) (labelled A) which is similar to the Tocher element except that the xy term is omitted from the complete cubic expansion $(x + y)^3$ in the displacement assumption.

The exact value for the central deflection coefficient of 11.6008 is quoted by Timoshenko(3). At all meshes the present element underestimates the central deflection behaving in a very similar manner to the conforming displacement assumption element HCT. The present results are always closer to the exact. The Tocher displacement assumption element (T) gives stiff solutions

at coarse meshes and "overshoots" the exact solution to converge on an answer which is too flexible. The element of Adini (A) is much too stiff at all meshes.

3.4.2 Clamped Square Plate with Central Point Load

To enable comparisons to be made between the present element and those of Severn and Taylor(32) and Allwood and Cornes(34) the plate of the previous section was next analysed with clamped edges. The idealizations used were different, however, and these are shown in Fig.(3.5). The hypotenuse of each element now points into the corner B. The deflection under the central load was again taken as a measure of the accuracy of the solutions and in Fig(3.6) the ratio of (finite element deflection)/(exact deflection) is plotted for various meshes on $\frac{1}{2}$ of the plate.

The present element again behaves in a similar way to the element of Clough and Tocher (HCT) and at all mesh sizes the results are again closer to the exact. Compared with the hybrid element of Severn and Taylor (ST) the present element gives slightly more accurate answers at meshes n = 2, 4 and 6 but is not as accurate at the coarsest mesh considered. For the two meshes (n = 2 and n = 4) for which comparisons are available results are, as expected, indistinguishable from those of the triangular version of the element of Allwood and Cornes(34).

All hybrid models in this problem are underestimating the central deflection, i.e. behaving in a similar way to a conforming displacement assumption model. Also shown in Fig.(3.6), however, is the curve using the equilibrium model (see Chapter 2) of de Veubeke and Sander(37). This converges to the exact from above

and in a similar way to the convergence of the conforming displacement model from below, this can always be proved to be the case.

3.4.3 Clamped Square Plate under Uniform Loading

This problem was considered to enable bending moments to be compared with exact distributions and with those obtained using other elements. One quarter of the plate of Fig.(3.5) was analysed with a 4 x 4 mesh and the uniform load was approximated by a series of point loads. Loads of 1 lbf. were applied at all interior nodes and $\frac{1}{2}$ lbf. at all edge nodes except at D where the load was $\frac{1}{4}$ lbf. This is equivalent to a distributed loading of 0.445 lbf./in^2 of plate surface.

The results are shown in Figs.(3.7) and (3.8). Severn and Taylor(32) present their results in the form shown in Fig.(3.7) - the exact solution is that given in (32) calculated by a finite difference procedure. At a particular node along DC there are in general three elements meeting - one of which has a right angle at the node. The value given by the element containing the right angle and the average given by the two other elements are considered separately. In both cases the present element gives values closer to the exact than those of Severn and Taylor.

In Fig.(3.8) the results are presented in a different way and are compared with solutions using the Tocher triangle(21). The distribution of bending moments within elements lying along CD is now plotted and compared with the exact. The hybrid is seen to give linear distributions which follow the exact curve closely with relatively small discontinuities between elements. The Tocher element, in contrast, gives stresses with large

discontinuities. The values given at mid-side positions are nevertheless seen to be close to the correct curve.

An interesting point is that the Tocher element gives slightly different answers along CD and AD (indicated in the Figure). This will be discussed later.

3.4.4 Natural Frequencies of the Clamped Square Plate

To test the performance of the hybrid element in the prediction of natural frequencies the same clamped square plate was analysed with elements again orientated as in Fig.(3.5). Only symmetric modes were considered and frequencies are expressed in terms of a non-dimensional frequency factor $\alpha = p/(DL^4\rho)^{\frac{1}{2}}$ where:

p = circular frequency = $2\pi f$

$D = Et^3/12(1-\nu^2)$

ρ = mass/unit area.

Table (3.1) compares the frequency factors, at two mesh sizes, for the first two doubly symmetric modes. Three elements are used - (i) the present hybrid HT, (ii) the element of Dungar, Severn and Taylor (DST) and (iii) the Tocher element (T). The DST element is the stiffness matrix of Severn and Taylor with a mass matrix derived by using the displacement assumption of Adini(20) described in Section 3.4.1. The mass matrix used with the present element is the one derived using the Tocher displacement assumption. The exact solutions are those given by Claassen and Thorne(72).

The results using the present hybrid element are generally closest to the correct answer. It will be noted that both hybrid elements give frequencies which are higher than the exact whilst the Tocher element always underestimates the frequencies of these two modes.

In Table (3.2) the effect of using different mass matrices with the present hybrid stiffness matrix is examined. The first 10 natural frequencies in symmetric/symmetric modes using a (4 x 4) mesh are given.

The mass matrices used are:

(i) that derived from the conforming Clough-Tocher displacement assumption (19)

(ii) that derived from the simple non-conforming Tocher assumption described in Section 3.1.

(iii) that derived from the displacement assumption used by Dungar, Severn and Taylor. This is also the Adini(20) assumption.

Also included are the frequencies using the Tocher stiffness and mass matrices. The exact values are those given by Claassen and Thorne(72) evaluated by the summation of a double Fourier sine series. Results for the first four frequencies only are available.

The various mass matrices give results which differ by very small amounts, certainly on the lower modes, when used with the hybrid stiffness matrix. On this basis it was therefore thought most efficient always to use the Tocher mass matrix since the computation is much simpler than when using the Clough-Tocher assumption.

A convergence test was then carried out on the first three symmetric frequencies using this form of the element. Table (3.3) shows the frequency factor for various meshes. Convergence to less than 1% is achieved on the fundamental frequency compared with the exact solutions of Claassen and Thorne.

3.5 The Performance of the Hybrid Triangle

3.5.1 The Simply Supported Plate with Central Point Load

These results are useful because they enable the hybrid element to be compared with displacement assumption elements of similar complexity. All elements in Fig.(3.4) make use of the same nine degrees of freedom.

The most interesting comparison is between the hybrid and the conforming displacement assumption element of Clough and Tocher (CST) which along its edges has the same displacements as the hybrid. Pian (30,31) and co-workers come to the conclusion that a hybrid element will give a more flexible solution (in terms of the displacement under a load) than a conforming displacement assumption model with the same edge displacements. This is demonstrated here.

Generally, however, although the conforming displacement assumption element can be proved to converge monotonically from below, the result using the hybrid can lie on either side of the exact and monotonic convergence is not guaranteed. In fact, on this problem, the present hybrid does exhibit monotonic convergence.

The curves for the Tocher element (T) and that of Adini (A) are typical of non-conforming displacement assumption models. Convergence, monotonic or otherwise, is not guaranteed and indeed the Adini element has not converged at the finest mesh considered. The excessive stiffness of this element is due to the omission of the xy term from the displacement assumption. Its absence means that the state of uniform twist ($\partial^2 w/\partial x \partial y$) cannot be represented.

The Tocher element has converged to an answer which is too flexible and convergence is non-monotonic.

3.5.2 The Clamped Square Plate with Central Point Load

Direct comparisons on this problem indicate the superiority of the present hybrid over that of Severn and Taylor at all but the very coarsest mesh considered. This is difficult to explain but must be due in some way to their more complicated stress assumption. In fact, using this mesh Severn and Taylor obtain their most accurate value for the bending moment at the edge of the plate. They consider this to be fortuitous.

At the two meshes $n = 2$ and $n = 4$ the present element gives the same values as the best triangular version of the general element of Allwood and Cornes(34). They make assumptions for stresses (rather than stress resultants) which are equivalent to the present ones. Since their edge displacement assumptions are also of the same form the two elements are identical.

3.5.3 The Clamped Square Plate under Uniform Loading

The present hybrid gives values for the bending moment along a line of symmetry of the plate which are very close to the exact curve both at nodes and within elements. The large discontinuities in stress using the Tocher element are due to the non-conforming nature of the displacement assumption. Slightly different bending moments are given, also, along the lines CD and AD in Fig.(3.5). If the displacement assumption

$$w = \left[1, x, y, x^2, xy, y^2, x^3, y^3, xy(x+y)\right] \cdot \begin{Bmatrix} \alpha_1 \\ \vdots \\ \alpha_9 \end{Bmatrix}$$

is examined it will be seen that since this is not a complete cubic expansion it is not invariant under a changes of axes. Therefore when elements are orientated in differnt ways along physically similar lines in the strucutre they will generally give different stresses. These slight differences are shown in Fig.(3.8).

3.5.4 Natural Frequencies of Clamped Square Plate

The results on this problem generally confirm the slight superiority of the present element over that of Severn and Taylor. It is evident, also, that the type of mass matrix used is of less importance than the type of stiffness matrix.

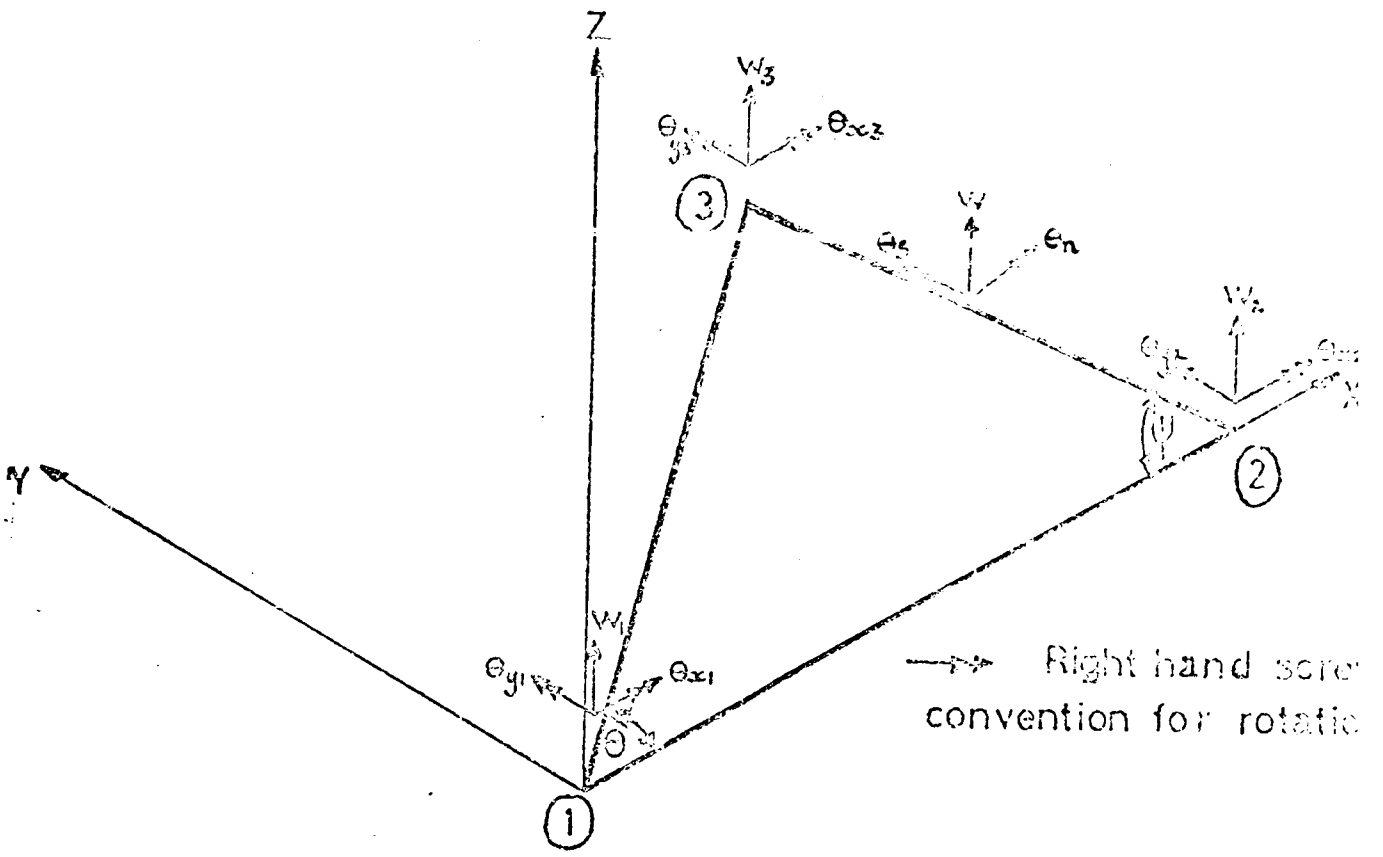

FIG. 3.1 TRIANGULAR BENDING ELEMENT.

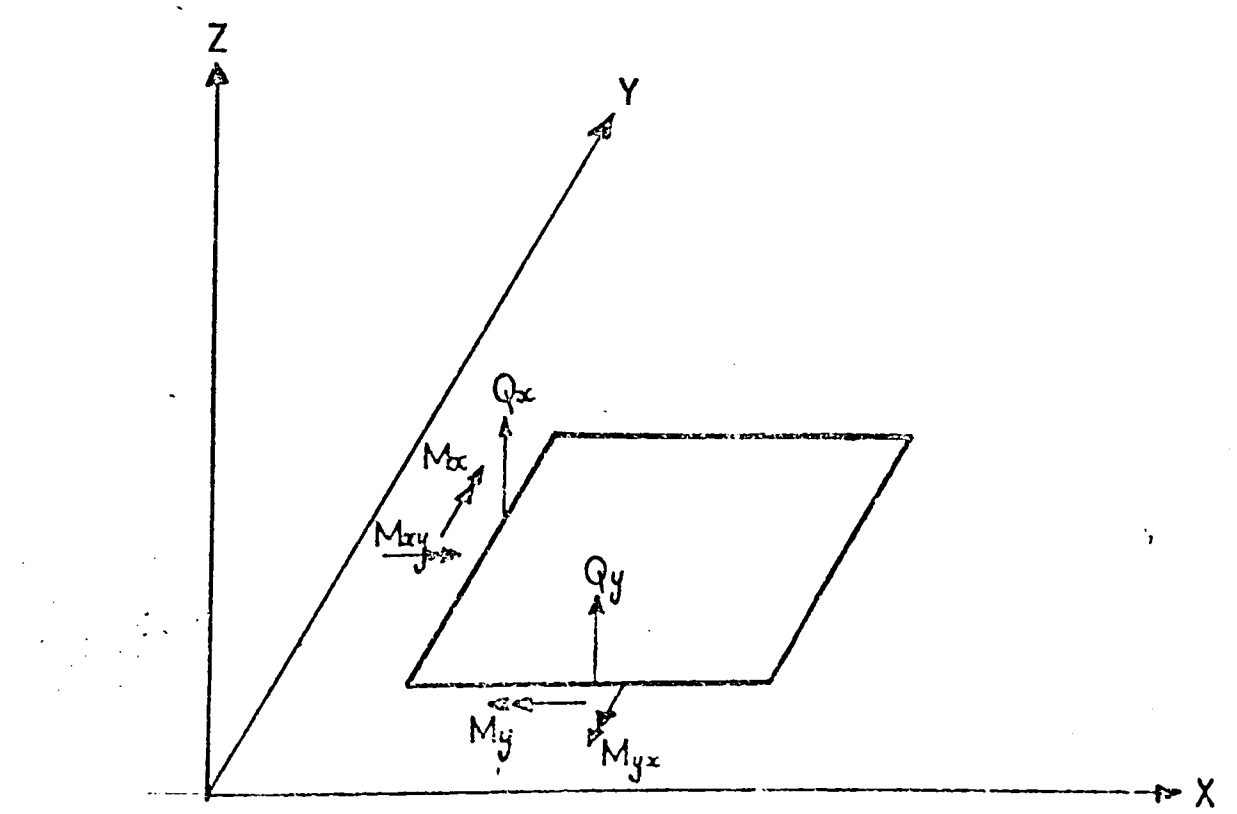

FIG. 3.2 STRESS RESULTANTS ON AN ELEMENT OF SHELL.

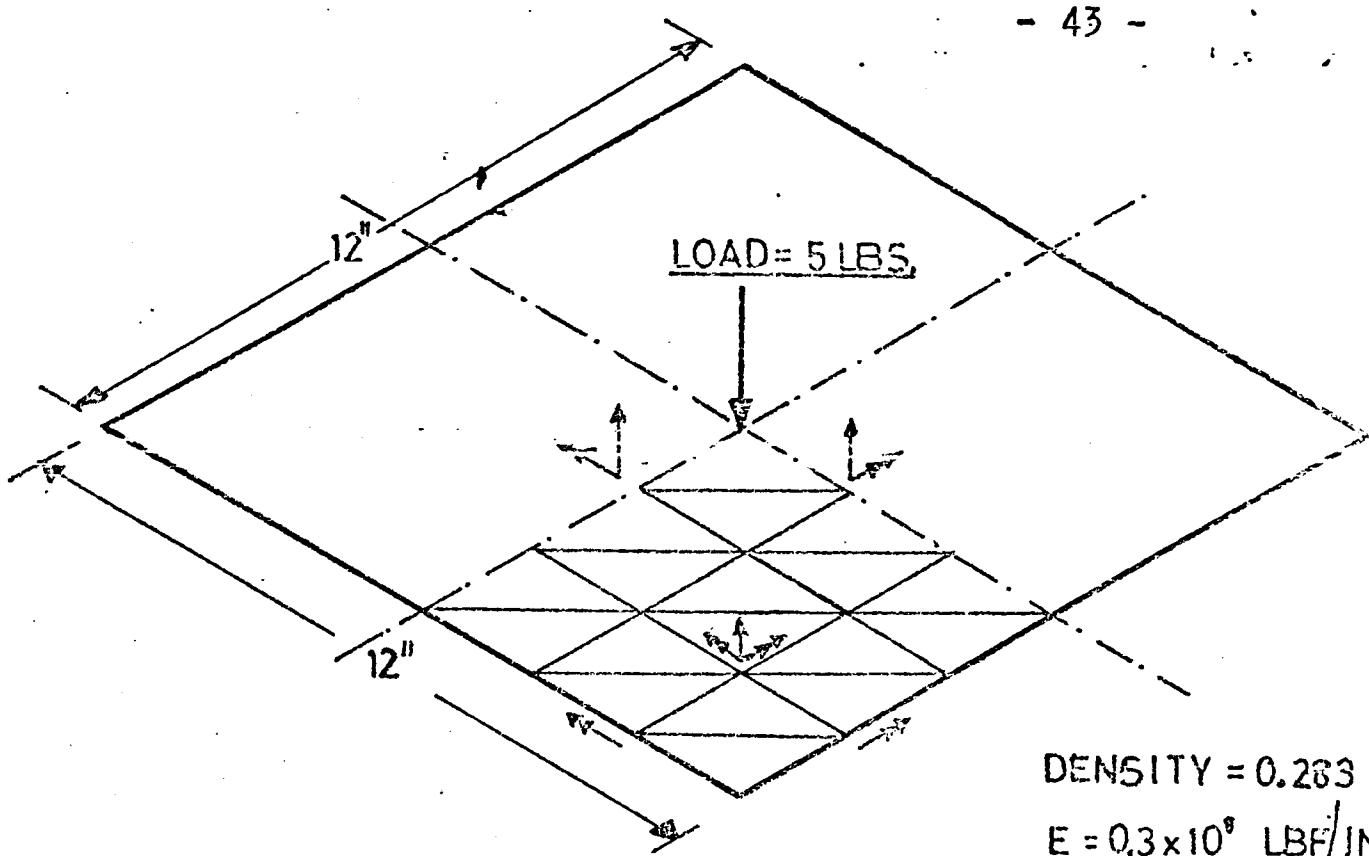

FIG 3.3 SIMPLY SUPPORTED SQUARE PLATE UNDER CENTRAL POINT LOAD

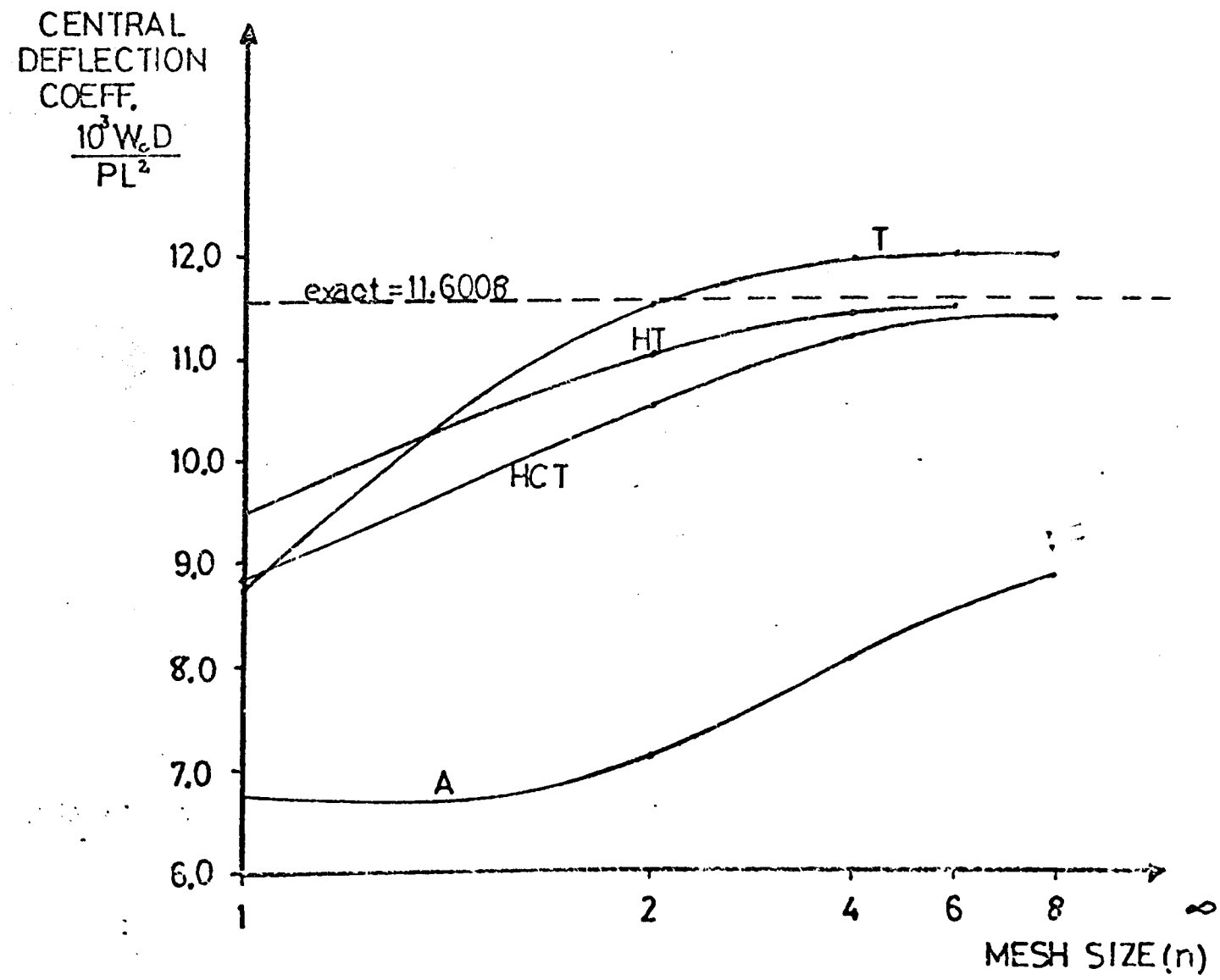

FIG. 3.4 CONVERGENCE OF TRIANGULAR ELEMENTS ON SIMPLY SUPPORTED SQUARE PLATE PROBLEM.

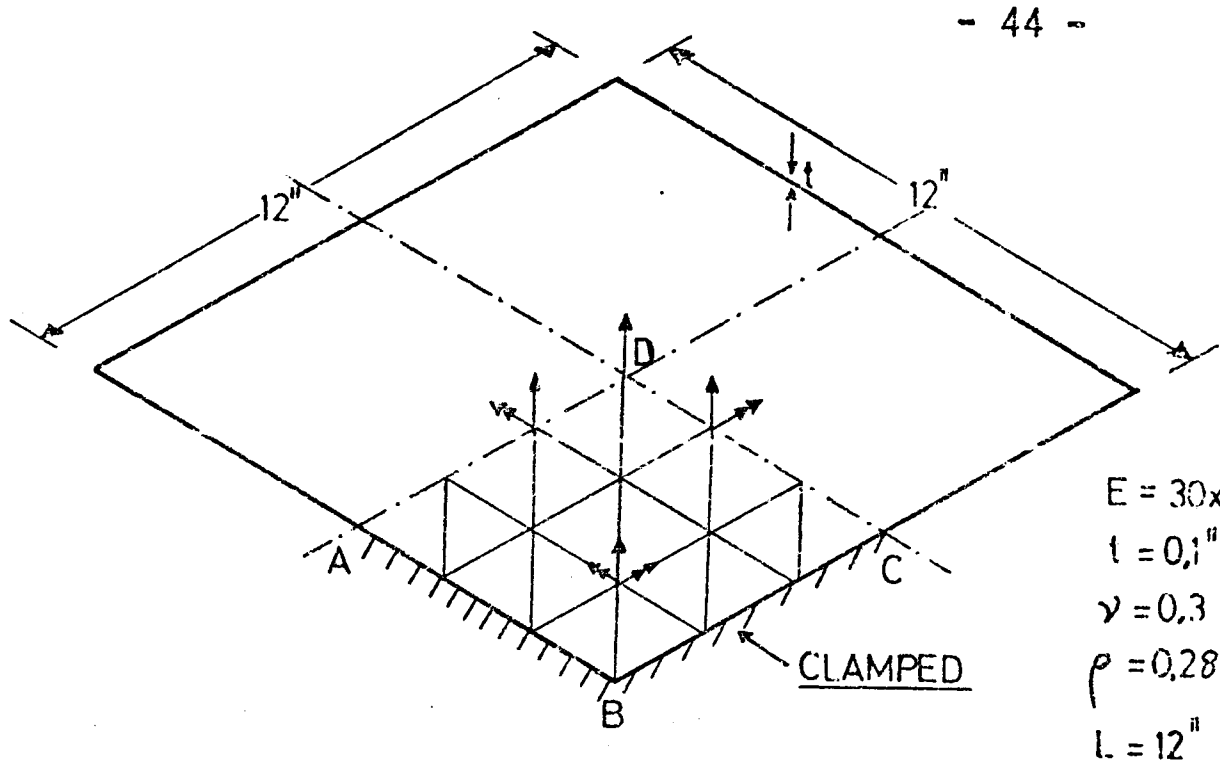

$E = 30 \times 10^6$ LBF/IN^2
$t = 0{,}1"$
$\nu = 0{,}3$
$\rho = 0{,}283$ LB/IN^3
$L = 12"$

FIG 3.5 CLAMPED SQUARE PLATE

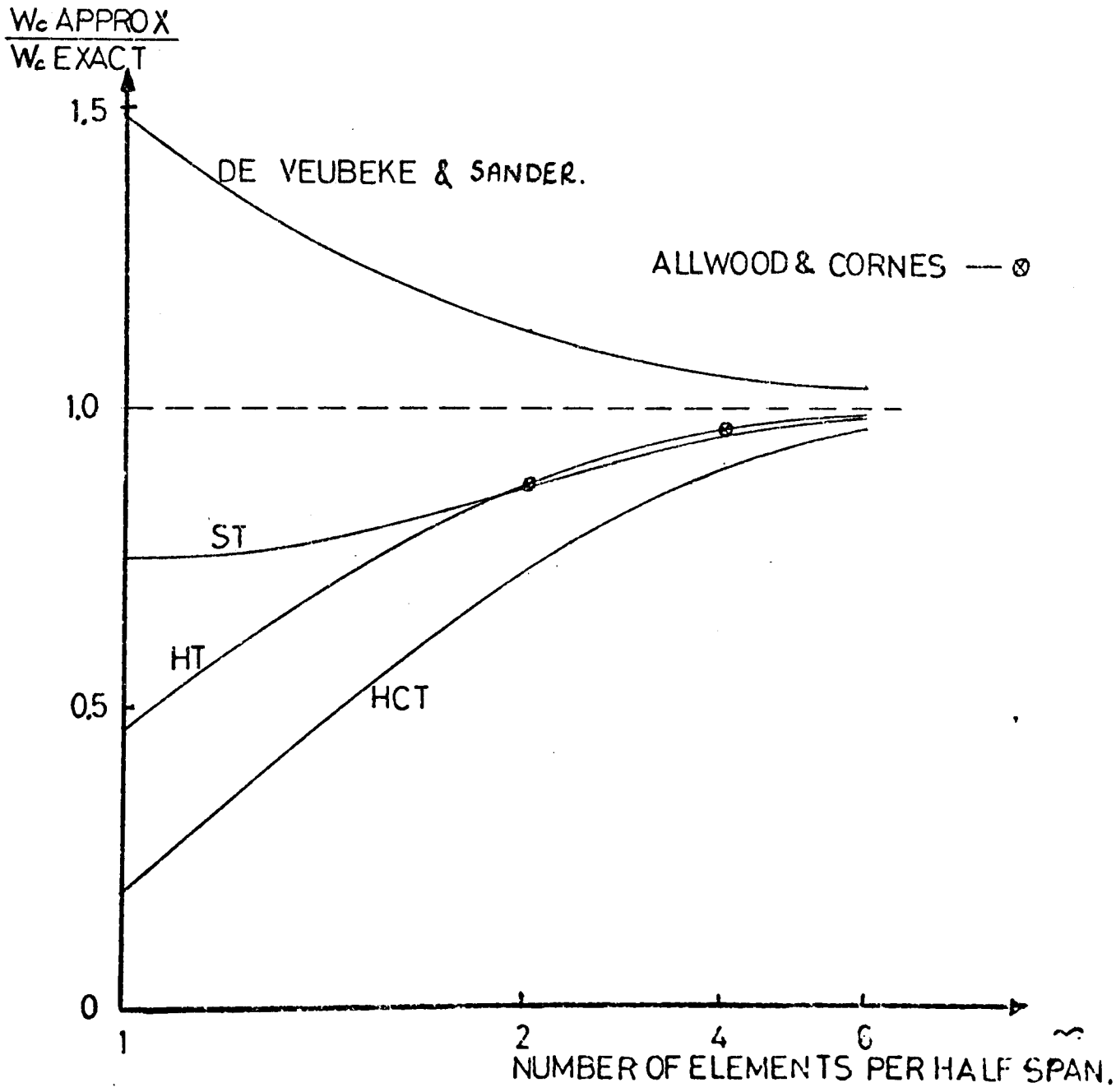

FIG 3.6 DEFLECTION OF CLAMPED SQUARE PLATE UNDER CENTRAL POINT LOAD

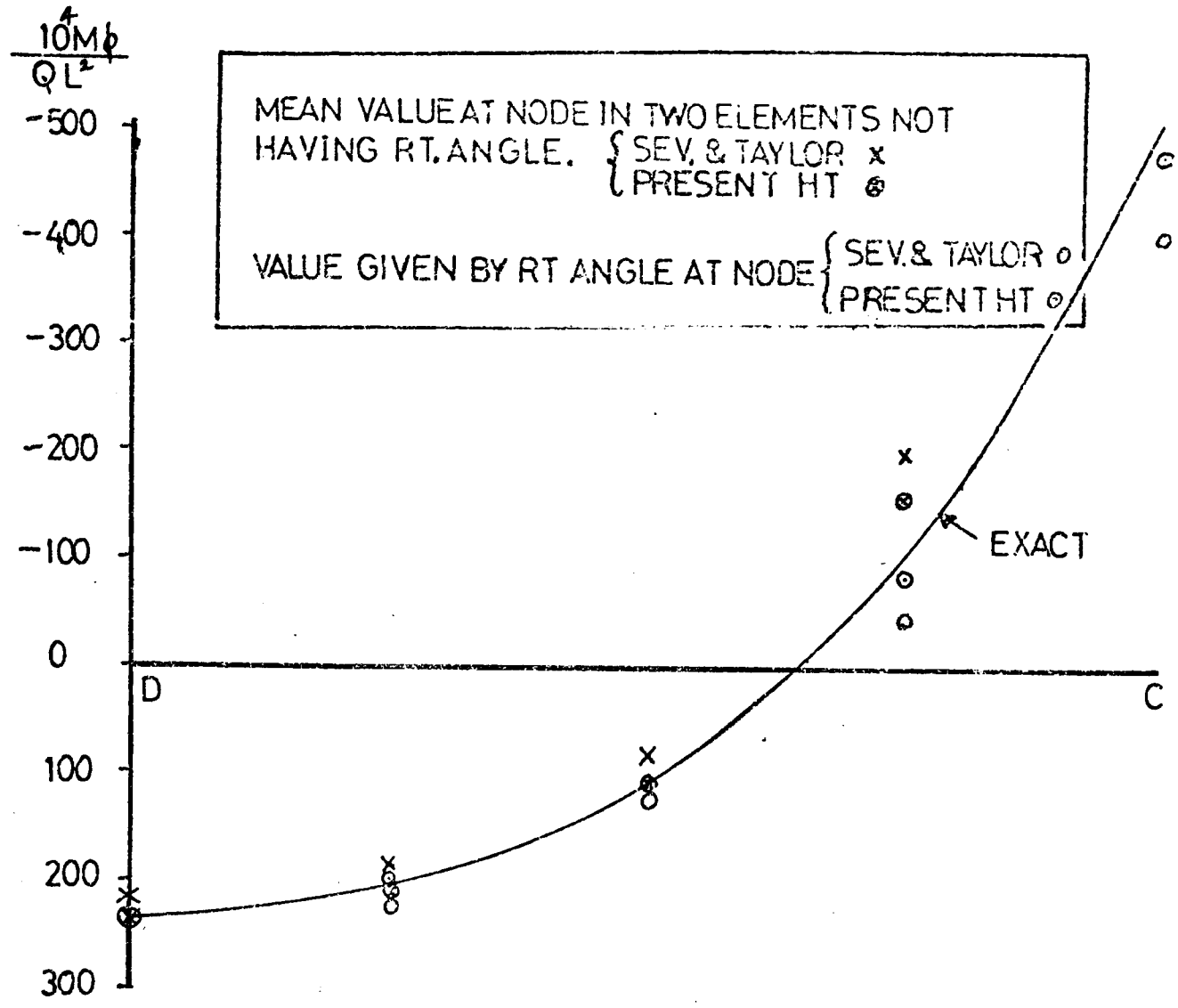

FIG 3.7 BENDING MOMENTS IN CLAMPED SQUARE PLATE UNDER UNIFORM LOADING (AV. VALUES AT NODES)

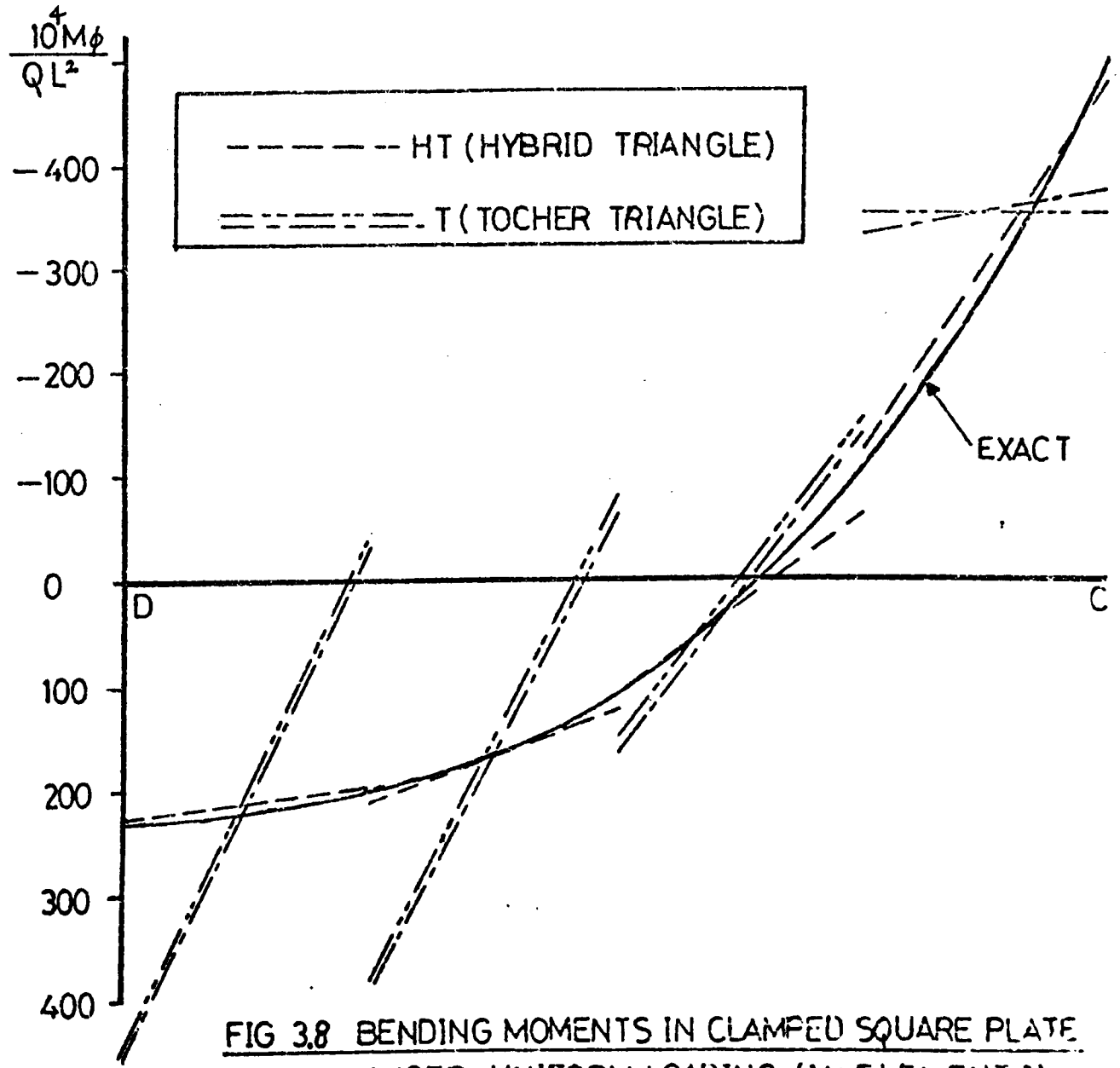

FIG 3.8 BENDING MOMENTS IN CLAMPED SQUARE PLATE UNDER UNIFORM LOADING (IN ELEMENTS)

TABLE 3.1 FREQUENCY FACTORS (α) FOR CLAMPED SQUARE PLATE

$\alpha = p/(DL^4\rho)^{\frac{1}{2}}$ $p = 2\pi f$ $D = Et^3/12(1-\nu^2)$ ρ = mass/unitarea

	Exact Solution	3 x 3 Mesh			4 x 4 Mesh		
		D.S.T.	T	HT	D.S.T.	T	HT
1st Doubly Symmetric Mode	35.985	36.80	34.10	36.43	36.41	34.47	36.21
2nd Doubly Symmetric Mode	132.204	146.85	122.73	145.90	139.27	124.43	138.89

TABLE 3.2 NATURAL FREQUENCIES (HERTZ) OF CLAMPED SQUARE PLATE USING VARIOUS MASS MATRICES (4 x 4 MESH)

Freq. No.	HT Stiffness + Clough-Tocher Mass	HT Stiffness + Tocher Mass	HT Stiffness + D.S.T. Mass	Tocher Triangle	Exact
1	245.11	245.12	245.50	233.35	242.83
2	932.54	932.40	936.77	841.26	887.92
3	940.33	940.16	938.63	842.25	892.13
4	1548.61	1550.48	1555.50	1374.51	1420.61
5	2359.54	2357.85	2359.24	1957.26	
6	2392.52	2389.56	2391.05	1967.12	
7	2856.36	2861.55	2914.27	2441.78	
8	2949.89	2960.17	2931.39	2458.69	
9	4170.33	4202.02	4258.58	3437.11	
10	5216.05	5180.24	5170.19	3572.95	

TABLE 3.3 CONVERGENCE OF FIRST THREE SYMETRIC FREQUENCIES OF CLAMPED SQUARE PLATE

		Frequency Factor (α) (Percentage Error)		
Degrees of Freedom	Mesh on $\frac{1}{4}$ Plate / Mode (M,n)	1,1	1,3-3,1	1,3+3,1
1	1 x 1	47.3287 (31.5226)		
8	2 x 2	37.1163 (3.1432)	171.1192 (30.0487)	182.0914 (37.7343)
21	3 x 3	36.4322 (1.4608)	143.6912 (9.2038)	145.9420 (10.3908)
40	4 x 4	36.2120 (0.7412)	137.4407 (4.4534)	138.8903 (5.0569)
65	5 x 5	36.1177 (0.3682)	135.2354 (2.777)	136.1326 (2.971)
EXACT FREQUENCY FACTOR		35.9852	131.5808	132.2048

Note: m,n are the numbers of half waves in the x and y coordinate directions respectively.

The nodal lines for the $1,3\pm3,1$ modes are as follows:

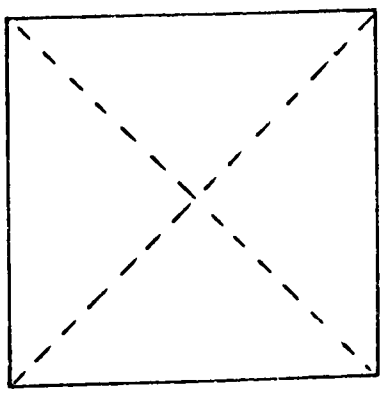

1,3 − 3,1

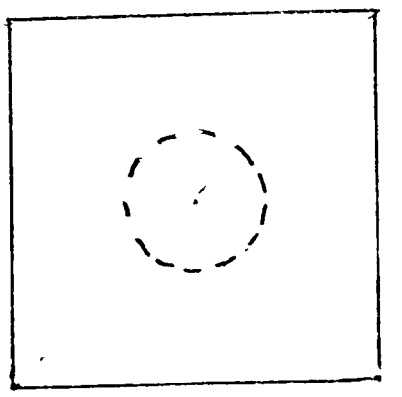

1,3 + 3,1

Chapter 4

A FLAT TRIANGULAR HYBRID ELEMENT FOR THE ANALYSIS OF SHELLS

4.1 Introduction

First approaches to the analysis of general shell structures used a number of flat elements containing both bending and membrane effects. In each separate element the effects are uncoupled; coupling is only introduced when elements are joined together at angles to model the shell. For instance, an in-plane force in one element will transmit both bending and membrane components to an adjoining element at an angle.

In addition to this there are two other deficiencies associated with the approach. Firstly, it is normal for bending and in-plane displacements to be of different orders of approximation so when two elements are joined at an angle a mis-match or incompatibility of displacements occurs. Hence it is possible for gaps to appear between elements. However, the effect tends to diminish with decreasing mesh size when elements become more and more co-planar.

The second deficiency is concerned with the misrepresentation of geometry which arises. The assembly of flat plates is only an approximation to the shape of the shell and does not satisfy the requirements of thin shell theories which deal with continuous middle surfaces.

Despite the above disadvantages the method is still used extensively. Often a large number of elements are needed to overcome geometric and incompatibility problems, but because the elements are relatively easy to program and they generally use smaller amounts of store and computer time, their use is often

preferred to that of more complex curved elements.

Some of the successful analyses which have appeared in the literature are those of Hrennikoff and Tezcan(41), Zienkiewicz and Cheung(44), Clough and Johnson(42) and Carr(43). These all used displacement assumption elements of various forms but an interesting analysis from the point of view of the present work is that of Dungar, Severn and Taylor(33) who, in addition to plate bending problems, consider the vibrations of a single curvature, constant thickness arch dam. Their element is based on a hybrid formulation, the plate bending portion being that mentioned in the previous chapter and the in-plane matrices being based on a linear assumption for the variation of stresses within the element.

It was decided here to construct a flat triangular hybrid shell element using the bending stiffness matrix of the previous chapter. Superimposed upon this is an in-plane matrix based upon an assumption of constant stresses. To compare results the same in-plane matrix was added to the Tocher displacement assumption element of the previous chapter.

4.2 The Combination of Bending and Membrane Effects

Fig.(4.1) shows a general three noded bending triangle with the degrees of freedom used before. Also shown is a membrane triangle whose effects are to be superimposed upon the first. This has two degrees of freedom at each of the nodes, displacements in the element x and y coordinate directions. The flat shell element formed by superposition of these two then has five degrees of freedom at each node.

The procedure for combining the two stiffness matrices and

two mass matrices is exactly the same. The bending stiffness matrix relates forces and displacements thus

$$\{F\}_e^b = [K_b]\{q\}_e^b \tag{4.1}$$

where $[K_b]$ is the (9 x 9) symmetric stiffness matrix,

$$\{q\}_e^b = \{w_1, \theta x_1, \theta y_1, w_2, \theta x_2, \theta y_2, w_3, \theta x_3, \theta y_3\}^T$$

and $\{F\}_e^b$ is a vector of forces and moments corresponding to $\{q\}_e^b$

Similarly for the membrane stiffness matrix

$$\{F\}_e^m = [K_m]\{q\}_e^m \tag{4.2}$$

where $[K_m]$ is the (6 x 6) stiffness matrix

$\{q\}_e^m$ is the vector of displacements $\{u_1\ v_1\ u_2\ v_2\ u_3\ v_3\}^T$

and $\{F\}_e^m$ the corresponding vector of in-plane forces.

The two stiffness matrices can now be combined to form one (15 x 15) matrix relating the displacements

$$\{u_1\ v_1\ w_1\ \theta x_1\ \theta y_1 \mid u_2\ v_2\ w_2\ \theta x_2\ \theta y_2 \mid u_3\ v_3\ w_3\ \theta x_3\ \theta y_3\}^T$$

to the corresponding vector of forces

$$\{Fu_1\ Fv_1\ Fw_1\ Fex_1\ Fey_1 \mid Fu_2\ Fv_2\ Fw_2\ Fex_2\ Fey_2 \mid Fu_3\ Fv_3\ Fw_3\ Fex_3\ Fey_3\}^T$$

This involves copying parts of the relevant rows and columns from the two component matrices into the correct positions in the total stiffness matrix.

In Fig.(4.1) the rotation perpendicular to the surface of the element is not included as a degree of freedom. When using thin plate or shell theory the displacements of the middle surface only are considered. The strains of the middle surface are defined uniquely by five degrees of freedom - the rotation normal to the surface does not enter into the expression for the strain energy.

However, when two flat elements are joined together to approximate a shell (Fig.(4.2)) there will be a contribution to a rotational stiffness perpendicular to the shell due to the components of in-plane rotational stiffness of both elements. If two elements become co-planar then it is important not to include the normal rotation as a degree of freedom in the idealization. When elements meet at angles, however, it is possible to (i) leave six general degrees of freedom at a node or (ii) declare local axes and have no rotation normal to the surface of the shell. Both approaches have been tried and little practical difference in the results has been found.

4.3 The Evaluation of a Hybrid in-plane Stiffness Matrix

To compute an in-plane stiffness matrix an assumption of constant in-plane stress was made. As before there is a minimum length for the stress assumption which in this case is equal to three (degrees of freedom - number of rigid body modes). A stress assumption with three unknown coefficients was therefore chosen to give the well known constant stress triangle.

The assumption can be stated in terms of stresses thus

$$\begin{Bmatrix} \sigma_x \\ \sigma_y \\ \tau_{xy} \end{Bmatrix} = \begin{bmatrix} 1 & 0 & 0 \\ 0 & 1 & 0 \\ 0 & 0 & 1 \end{bmatrix} \cdot \begin{Bmatrix} \beta_1 \\ \beta_2 \\ \beta_3 \end{Bmatrix} \qquad (4.3)$$

This assumption can be shown to satisfy the homogeneous equilibrium equations.

For the evaluation of the complementary strain energy the standard plane stress relationship for in-plane effects was used

$$\begin{Bmatrix} \epsilon_x \\ \epsilon_y \\ \epsilon_{xy} \end{Bmatrix} = \frac{1}{E} \begin{bmatrix} 1 & -\nu & 0 \\ -\nu & 1 & 0 \\ 0 & 0 & 2(1+\nu) \end{bmatrix} \cdot \begin{Bmatrix} \sigma_x \\ \sigma_y \\ \tau_{xy} \end{Bmatrix} \qquad (4.4)$$

It is possible, with the nodal degrees of freedom used for the in-plane triangle to make an assumption of linearly varying displacement over the whole of the element and to take values only along the edges for the calculation of edge work.

The displacement assumption used is therefore of the form

$$\begin{Bmatrix} u \\ v \end{Bmatrix} = \begin{bmatrix} 1 & x & y & 0 & 0 & 0 \\ 0 & 0 & 0 & 1 & x & y \end{bmatrix} \cdot \begin{Bmatrix} \alpha_1 \\ \vdots \\ \alpha_6 \end{Bmatrix} \qquad (4.5)$$

The coefficients $\{\alpha\}$ can then be related to the nodal quantities by substituting the coordinates of the nodes in the above expression. Since both the u and v displacements (Fig.(4.1)) only vary linearly along the side of an element, displacement continuity is maintained between adjacent co-planar elements.

To compute the matrices numerical integration with a second order Gauss process was again used.

4.4 The Calculation of Stresses

For the flat shell element two matrices (the $[H]^{-1}[G]$ matrix of Chapter 2) relating stresses to nodal displacements for bending and in-plane effects, are carried through on backing store into the stressing routine. The bending and in-plane displacements for a particular element are then separated in the stressing routine and the two sets of stresses evaluated independently.

4.5 An in-plane Displacement Assumption Stiffness Matrix for use with the Tocher Triangle

For comparison purposes it was necessary to add an in-plane matrix to the Tocher element of Chapter 3 to form another flat

shell element. This was evaluated by a displacement assumption approach using the assumption (4.5). This, in fact, gives the same in-plane stiffness matrix as obtained using the above hybrid method.

Normally the two assumptions for stresses and edge displacements made in hybrid elements are incompatible along the boundaries. However, in the case of the hybrid in-plane matrix described in Section 4.3 this is not the case. If the constant stress assumption (4.3) is inserted in (4.4) and the strains are expressed as derivatives of u and v, the following equation is obtained.

$$\begin{Bmatrix} \partial u/\partial x \\ \partial v/\partial y \\ \partial u/\partial y + \partial v/\partial x \end{Bmatrix} = \frac{1}{E} \begin{bmatrix} 1 & -\nu & 0 \\ -\nu & 1 & 0 \\ 0 & 0 & 2(1+\nu) \end{bmatrix} \cdot \begin{Bmatrix} \beta_1 \\ \beta_2 \\ \beta_3 \end{Bmatrix} \qquad (4.6)$$

It is apparent from (4.6) that the strains can be integrated to give an equivalent displacement assumption of the form

$$u = A_1 x + B_1 y + C_1$$
$$v = A_2 x + B_2 y + C_2 \qquad (4.7)$$

where the constants A_i, B_i are in terms of the β's , E and ν This is identical to (4.5).

Therefore an assumption for constant in-plane stresses[15] in this case equivalent to an assumption of linearly varying displacements and the stress and displacement assumptions along the edges of the element are entirely compatible.

If, then, the linear displacement field is used to evaluate a stiffness matrix using the Principle of Minimum Potential Energy, exactly the same assumption is made as when constructing the matrix using the Modified Complementary Energy Principle. The two are simply alternative methods of constructing the well known constant

stress in-plane stiffness matrix.

Therefore differences between the results using the two flat shell elements will be due to the differences in the bending stiffness matrices alone, since the in-plane matrices are identical.

It is evident that in the case of all hybrid elements, when a stress assumption is made a displacement distribution is implied by integration of equations equivalent to (4.6). Quite often, however, it is either impossible to integrate the stress assumption or displacements are given which are incompatible with the edge assumptions. The present example, then, is a very special case.

4.6 Problems Analysed

4.6.1 The Pinched Cylindrical Shell

The problem is shown diagramatically in Fig.(4.3). The shell is simply supported at each end and is subjected to two equal diametrically opposed point loads halfway along its length. This, a far more severe problem than the more usually quoted "Pinched Cylinder" in which there are no end supports, is used by Lindberg et al.(65) to test their triangular shell element. The exact results they quote are from a double fourier series solution of Flügge's equations using 80 terms in each direction.

Both the present hybrid and the assumed displacement element were used to predict the displacements of the cylinder. Symmetry allowed only $\frac{1}{8}$ of the problem to be treated using uniform (3 x 3), (4 x 4) and (6 x 6) meshes. These involved 52, 93 and 211 degrees of freedom after boundary conditions had been applied. The deflections along the top (DC) of the cylinder were compared with exact values to measure the convergence of the solutions.

Fig.(4.4) shows the normal displacements along DC using the two elements. At all three mesh sizes the assumed displacement element gives the more flexible answers, which in this case lie closer to the exact. With the finest mesh considered here the deflection under the point load is underestimated by 18½% and 30½% by the assumed displacement and assumed stress elements respectively. The severity of the problem is indicated by the fact that the (4 x 4) uniform mesh using the complex element of Lindberg et al.(65) gives an error of over 10% in this deflection.

4.6.2 A Simply Supported Panel under Pressure Loading

To provide a more comprehensive test of the elements it was necessary to deal with a problem for which exact values of all displacements and particularly, stresses are available. A simply supported, square, cylindrical panel under pressure loading (Fig. (4.5)) was chosen. The method used to evaluate the exact distributions is outlined in Appendix 2. With the particular geometry and dimensions chosen here, stresses due to bending and membrane actions are of the same order of magnitude.

In the finite element idealizations the pressure loading was approximated by a series of point loads normal to the surface. In Chapter 2 it is explained how "consistent" loading vectors can be derived for hybrid elements. It is also possible to derive these for displacement assumption models.

The experience of previous workers has been that these consistent vectors give loads which are very little different from those obtained if the force is simply distributed equally among the nodes. In view of this fact, but mainly because the geometrical misrepresentation would complicate matters, it was decided not to use this method. In later chapters of this thesis consistent

pressure loading vectors are obtained.

Both (4 x 4) and (8 x 8) meshes were used on $\frac{1}{4}$ of the panel. The arrangement of the elements for the (4 x 4) mesh is shown in Fig.(4.5) and also the positive convention for stress resultants is defined. The assumed stress bending element of the previous chapter was developed using a different convention for bending moments and this has been taken into account when interpreting results. The conventions used in Fig.(4.5) are those of Novozhilov(1) and will be used throughout the remainder of this work.

The results for displacements and stress resultants along lines of symmetry of the panel are shown for both meshes in Figs. (4.6) to (4.23). The stresses plotted are those given along edges of elements lying along the lines under consideration.

At the two mesh sizes the hybrid and assumed displacement elements give virtually the same displacements and in-plane stress resultants. The major difference is seen in the prediction of bending moments. The hybrid element shows small discontinuities between elements and also the distributions are closer to the exact curve. In contrast the bending moments given by the assumed displacement element show extremely large jumps between elements - this being especially noticeable in Mx and Mϕ. However, values given at midpoints of the sides under consideration lie close to the exact curve.

4.7 Conclusions

The general superiority of the hybrid element compared with the assumed displacement model, certainly in predicting stresses, is evident from these results. This is consistent with the findings

regarding the plate bending elements of the previous chapter. The hybrid shell element, on the present problems, tends to give stiffer results for displacements which means that in the case of the pinched cylindrical shell these lie further from the exact. In this problem it is obvious, however, that much finer meshes would be needed to give reasonable answers - possibly with the mesh being refined locally around the point of application of the load.

Since the edge displacement assumptions used for the hybrid element are compatible for elements in the same plane, they can be considered as being better approximations to compatible displacements when the elements are joined at angles, than those of the assumed displacement element. The excessive flexibility of the displacement element, noted for plate bending in the previous chapter, is thus the fortuitous reason for its better performance on this problem.

The difference between the deflections obtained on the simply supported panel is much less marked. The hybrid elements give marginally the smaller deflections at point D (the centre of the panel) but the difference is too small to be shown on the figure (4·17).

From this limited set of results it is difficult to generalize as to how stress outputs should be interpreted in other problems. The assumed displacement element does not perform satisfactorily and cannot be considered seriously as an element to be used for stress predictions. It is possible that with large numbers of elements reasonable answers could be obtained if values at mid-side positions or centroids of elements only are considered.

The hybrid appears, on this basis however, to be very useful. It will be apparent from later sections of this work that the results

using this are comparable with those using more complicated, curved hybrids which were developed subsequently. The geometry of these allows cylindrical shells to be modelled exactly, but these problems can also be treated using the present element. Furthermore, this element is also capable of analysing general shells with double curvature. It does, of course, suffer from the limitations of all flat shell elements (Section 4.1) but its performance on the problems considered here would seem to justify more extensive investigations on a variety of shell structures.

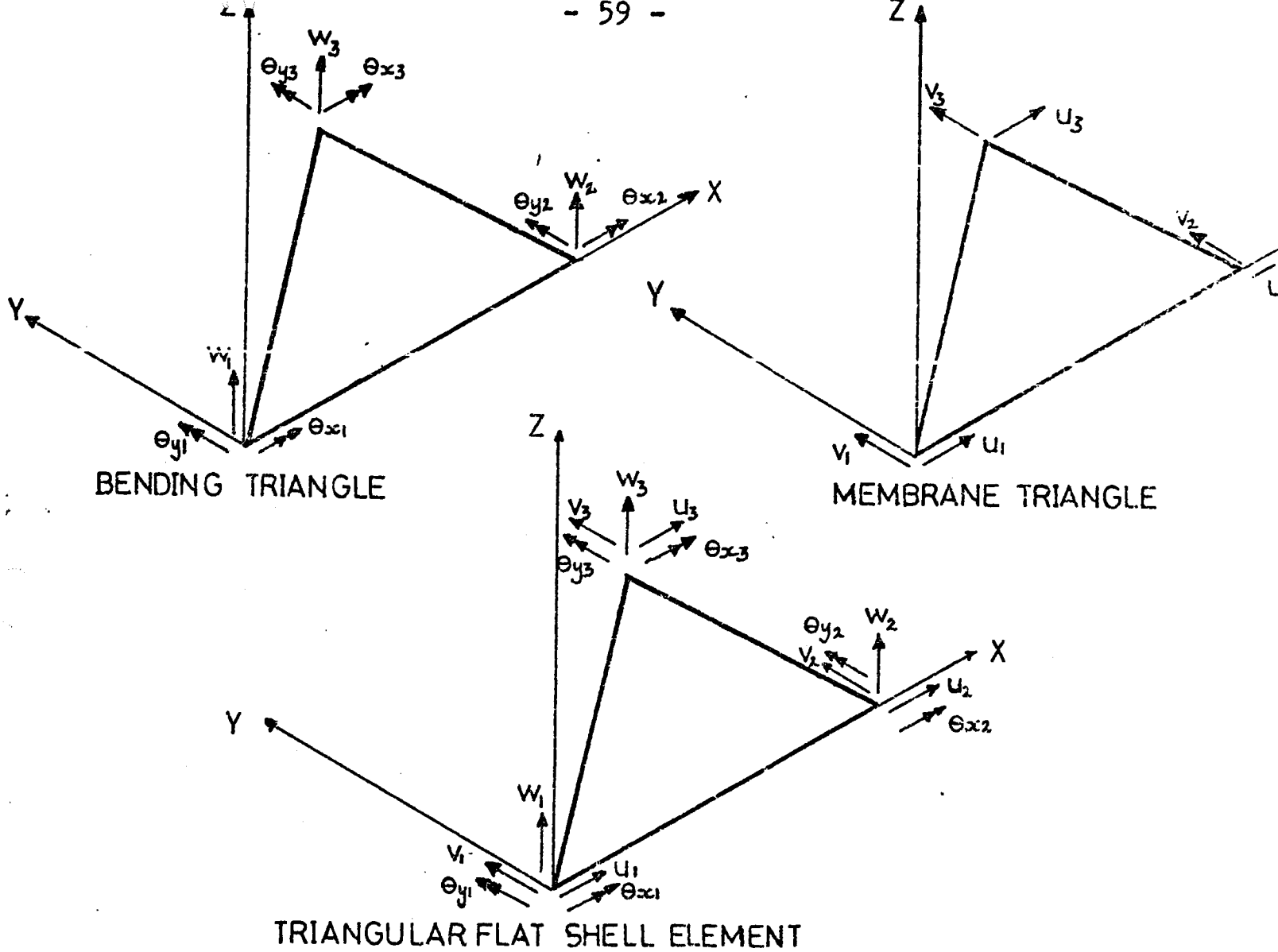

FIG 4.1 SUPERPOSITION OF BENDING AND MEMBRANE TRIANGLES.

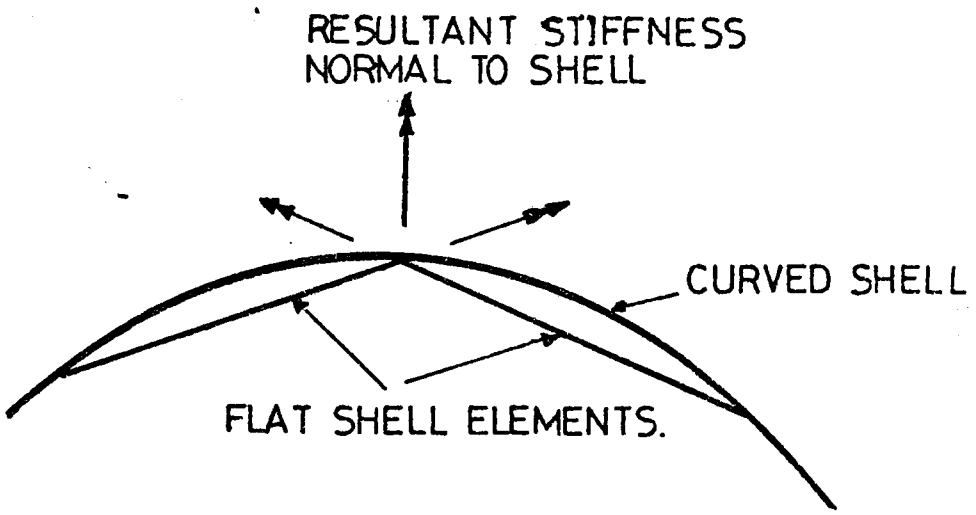

FIG 4.2 STIFFNESS OF A SHELL COMPOSED OF FLAT ELEMENTS

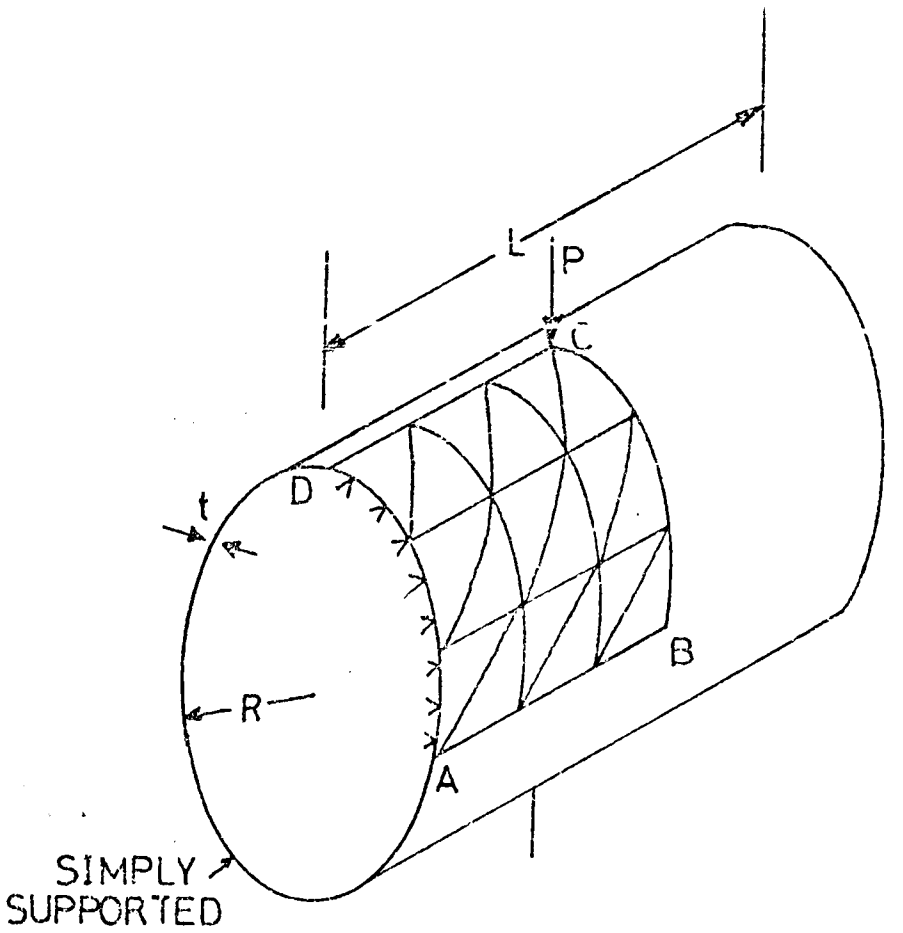

R = 2"
L = 4"
t = 0.02"
ν = 0.3
E = 3.0x10⁷ LBF/IN²
P = 5 LBF

FIG 4.3 PINCHED CYLINDRICAL SHELL PROBLEM

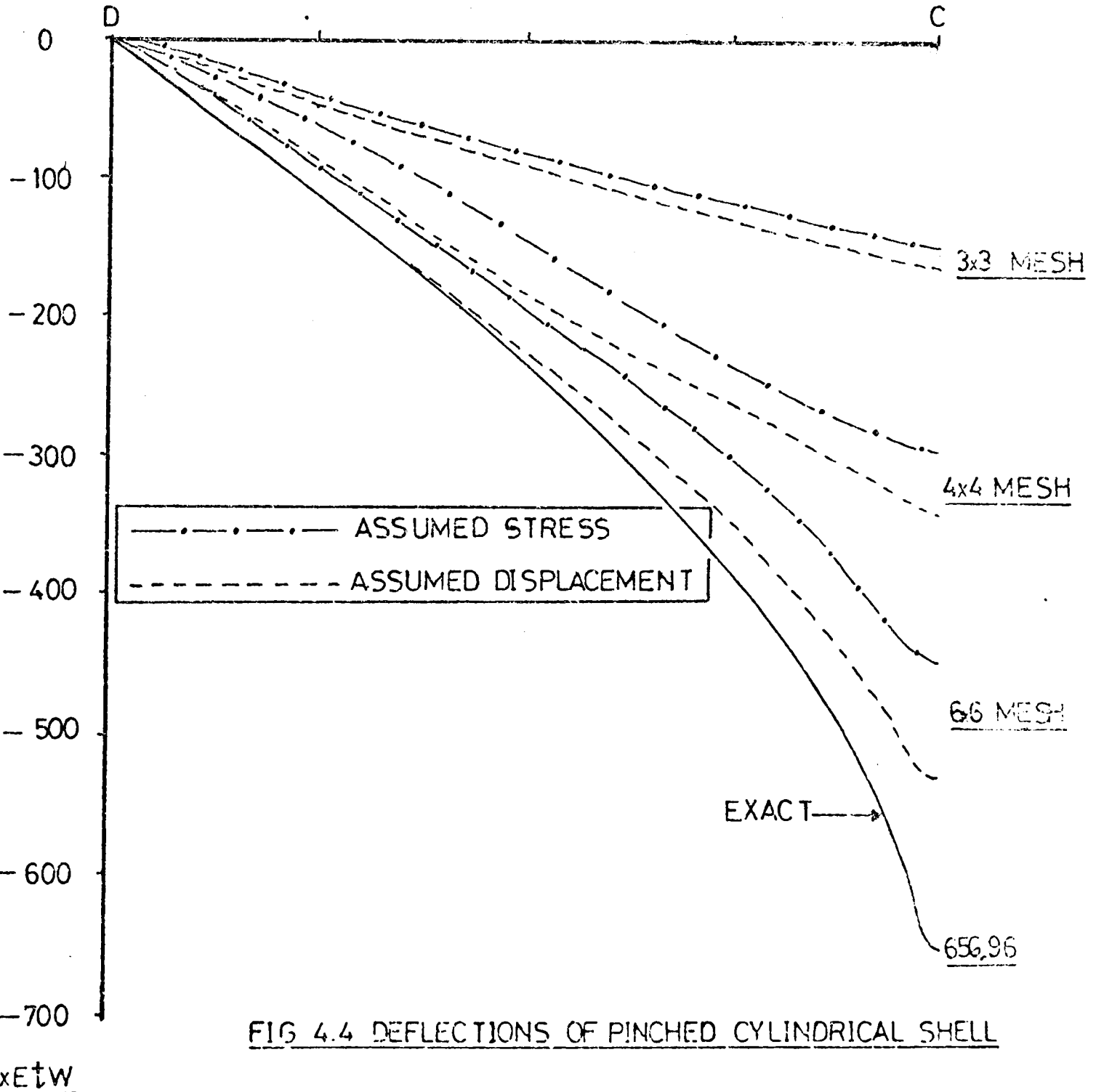

FIG 4.4 DEFLECTIONS OF PINCHED CYLINDRICAL SHELL

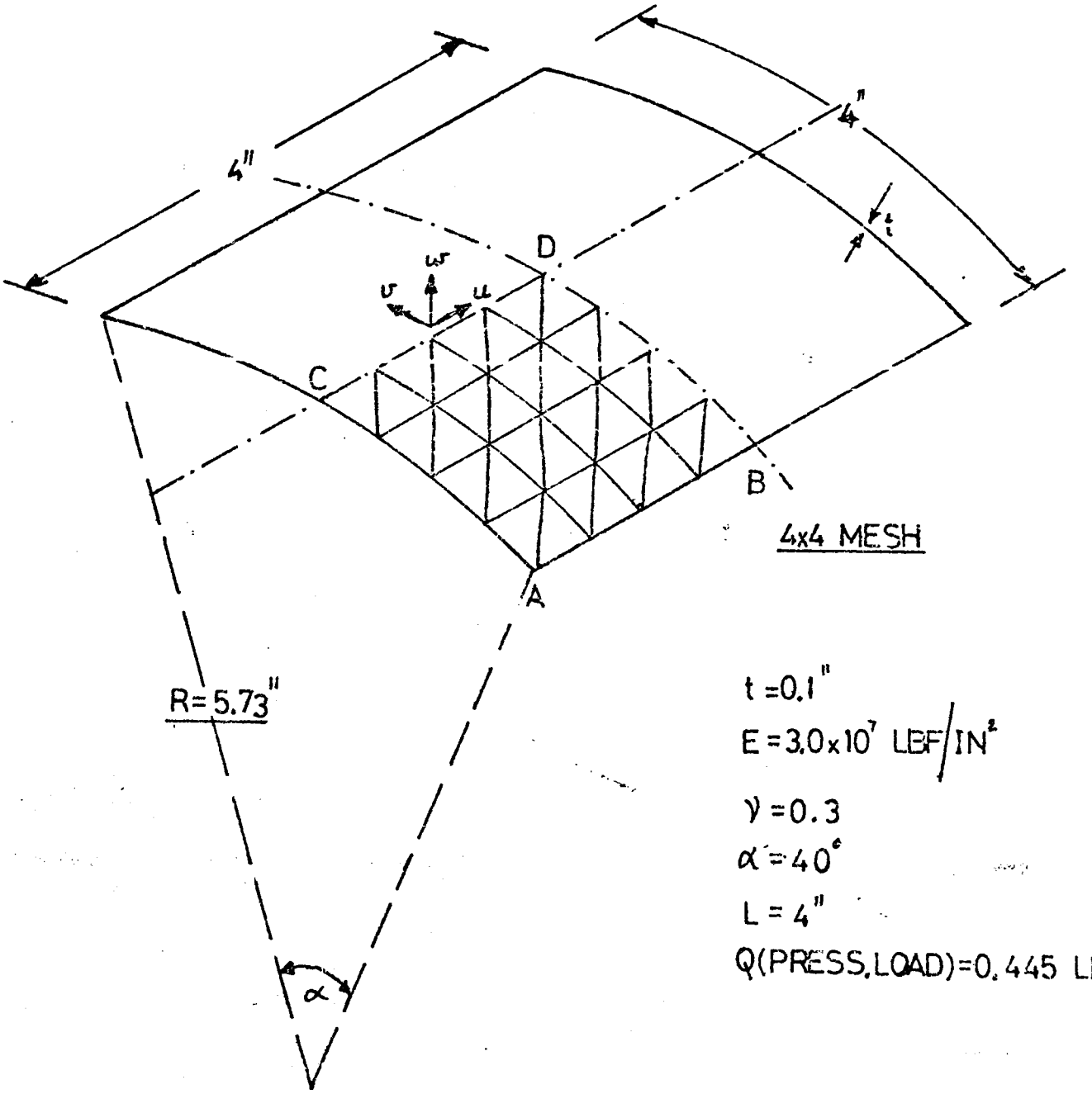

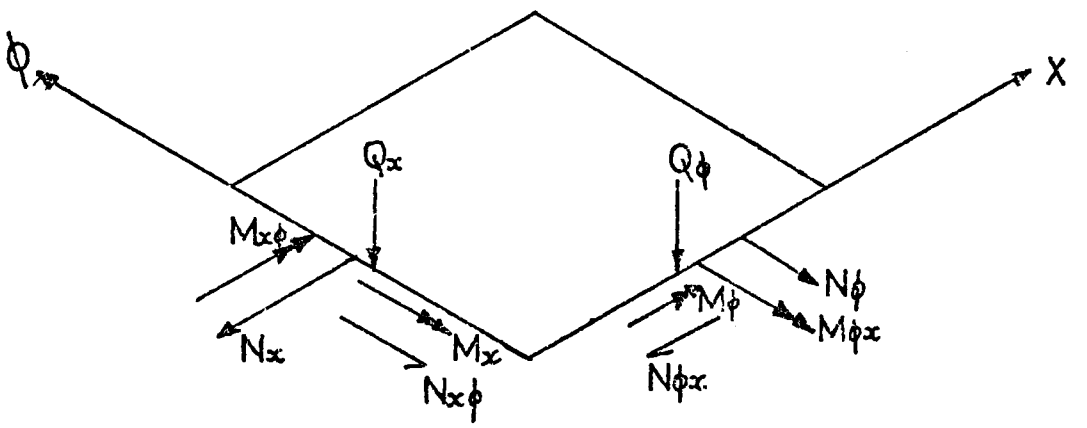

FIG 4.5 SIMPLY SUPPORTED PANEL USING FLAT ELEMENTS

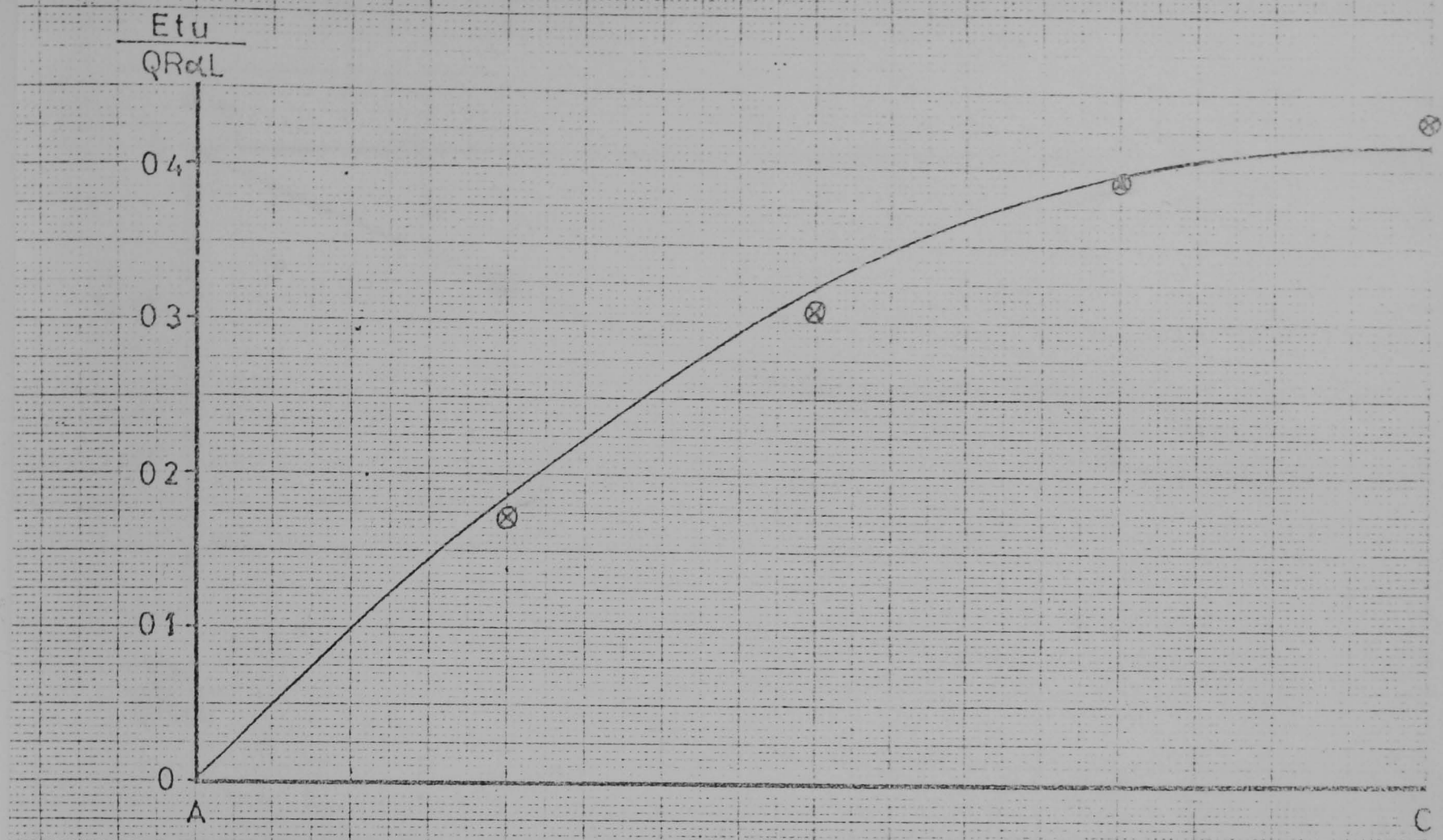

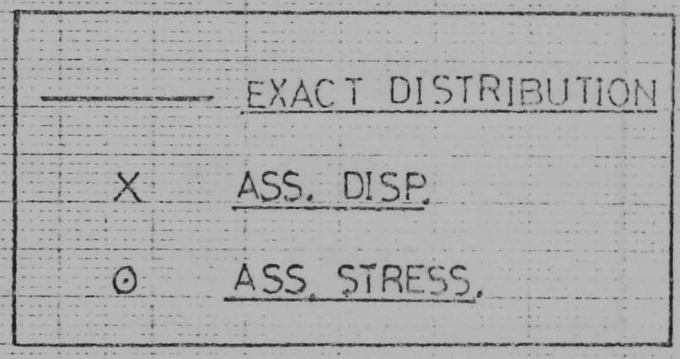

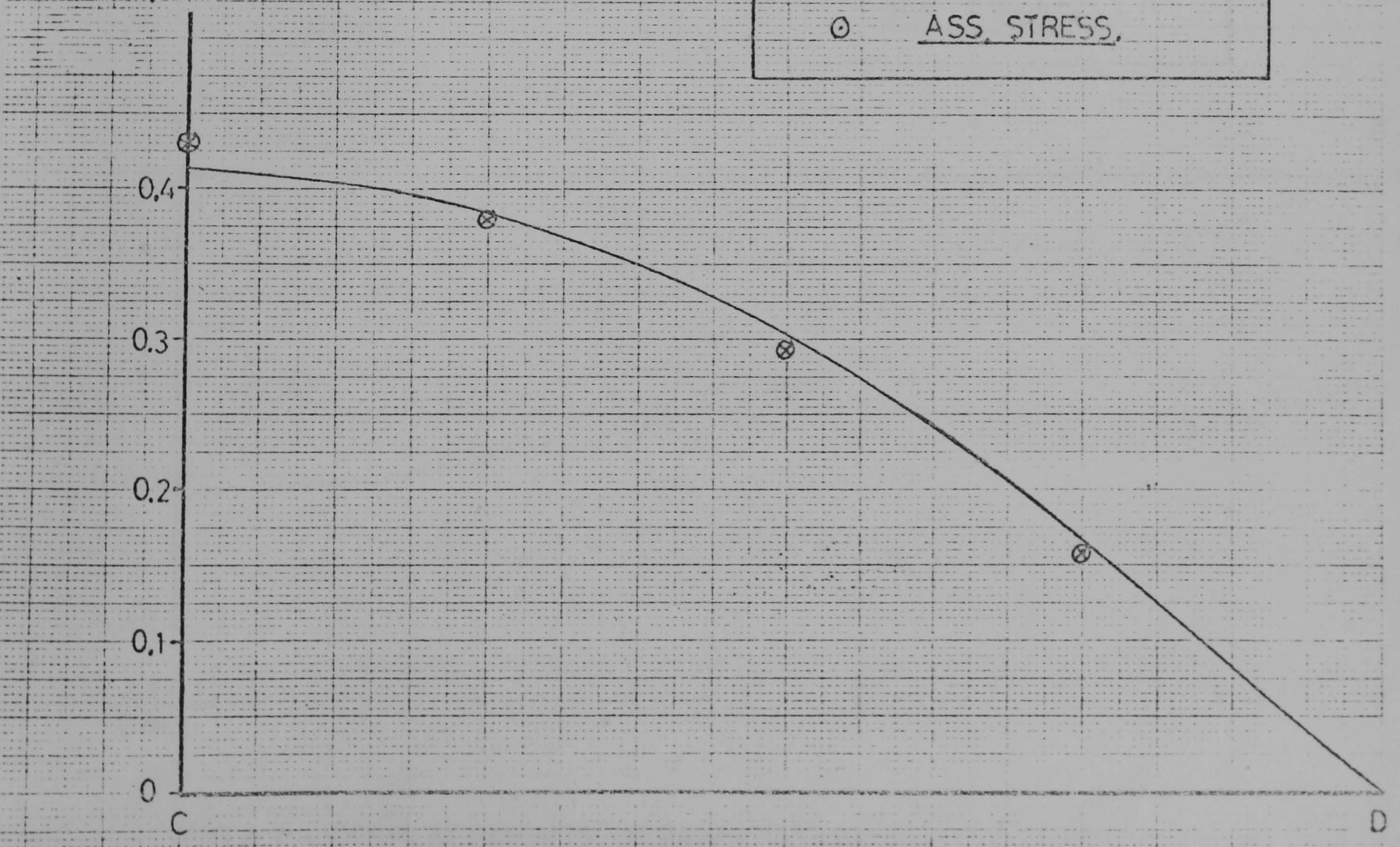

FIG 4.6 u DISPLACEMENTS OF PANEL USING 4x4 MESH OF TRIANGULAR FLAT ELEMENTS

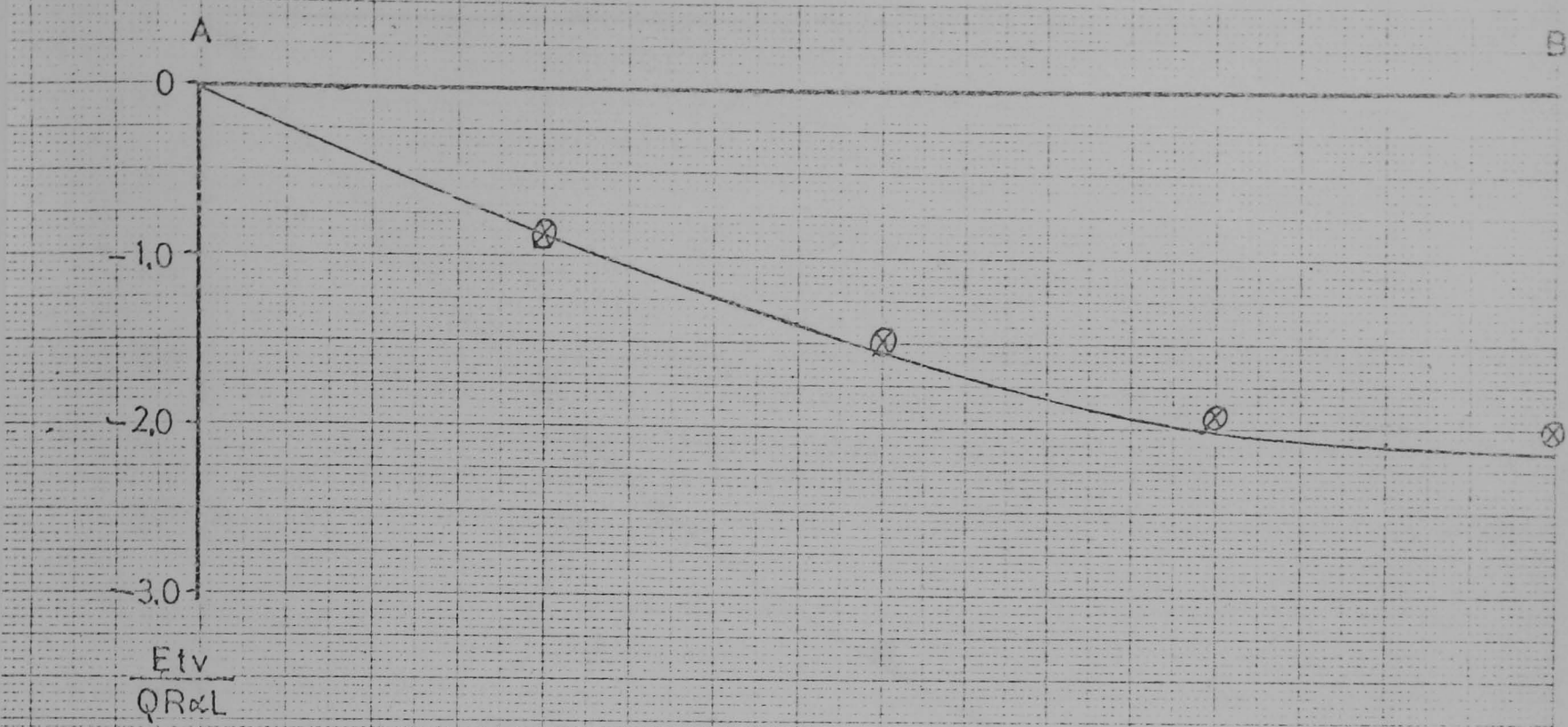

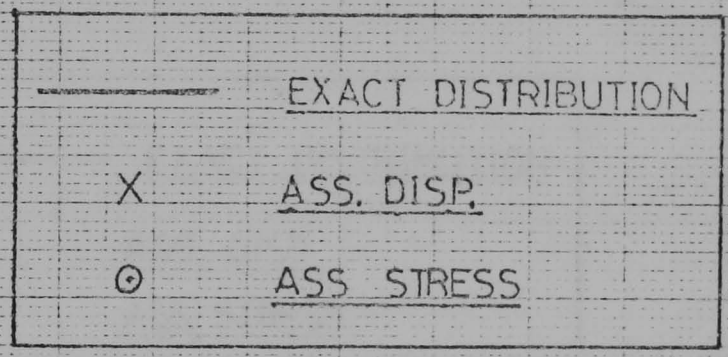

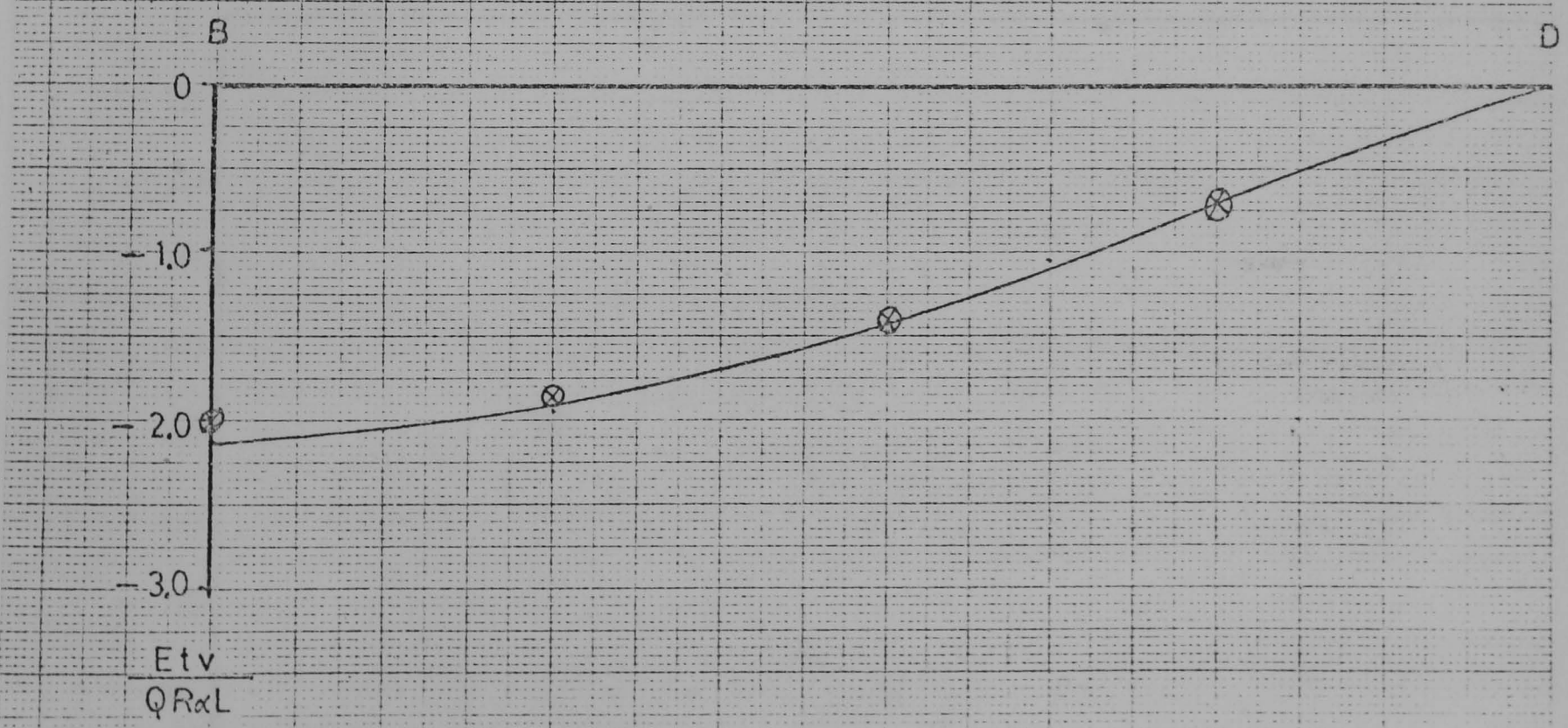

FIG 4.7 v DISPLACEMENTS OF PANEL USING 4x4 MESH OF TRIANGULAR FLAT ELEMENTS

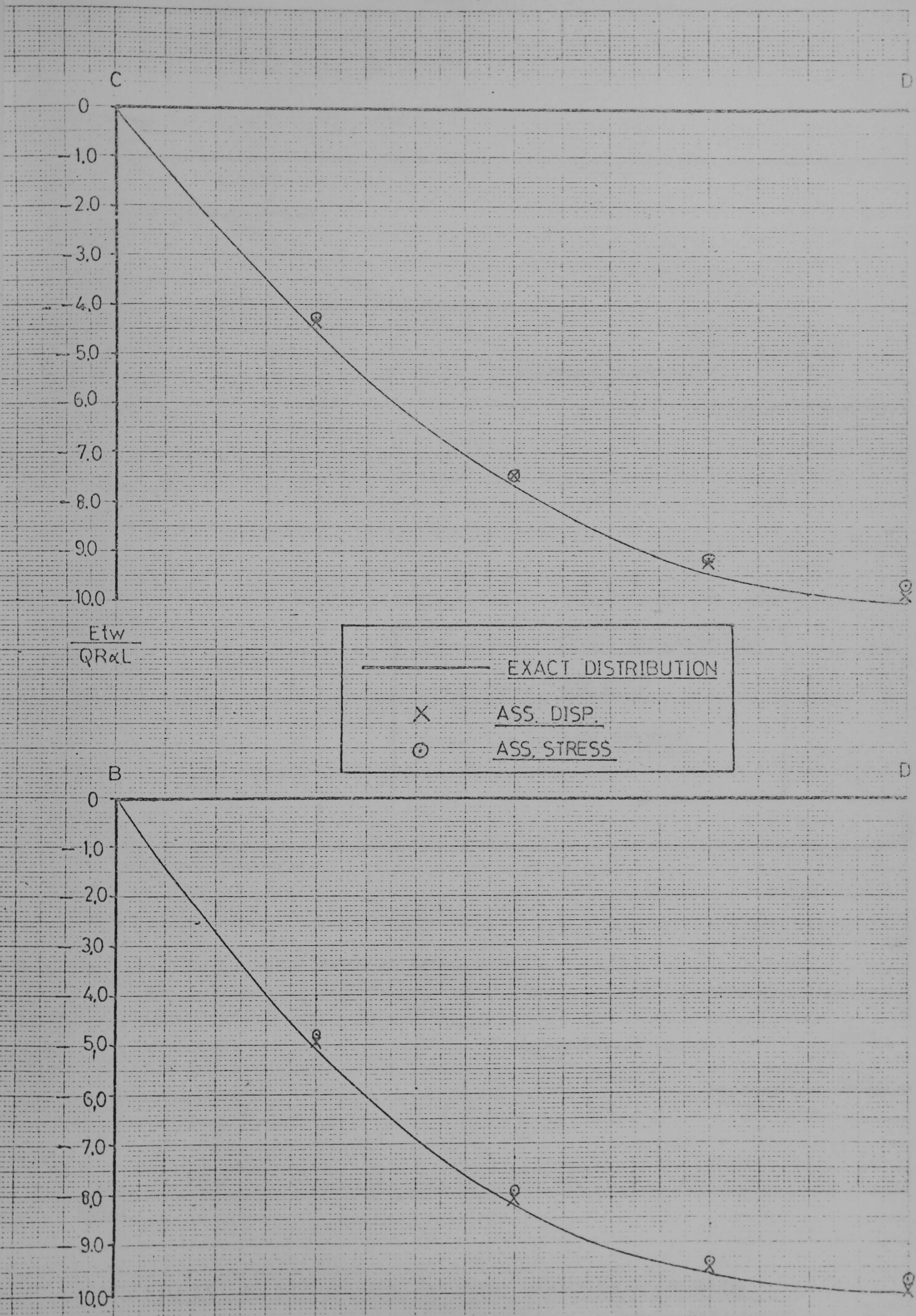

FIG 4.8 w DISPLACEMENTS OF PANEL USING 4x4 MESH OF TRIANGULAR FLAT ELEMENTS.

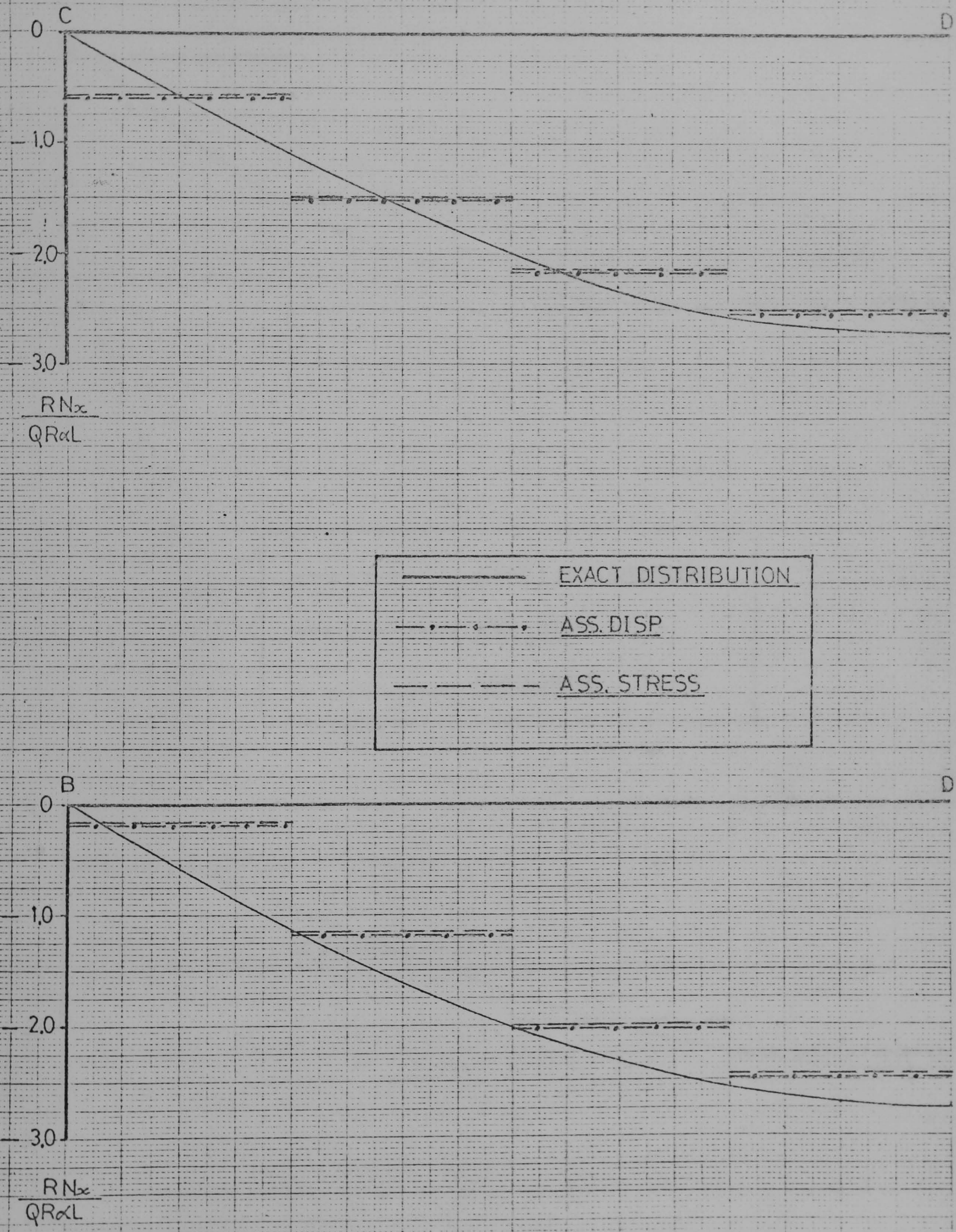

FIG 4.9 N_x STRESS RES. ON PANEL USING 4 X 4 MESH OF TRIANGULAR FLAT ELEMENTS.

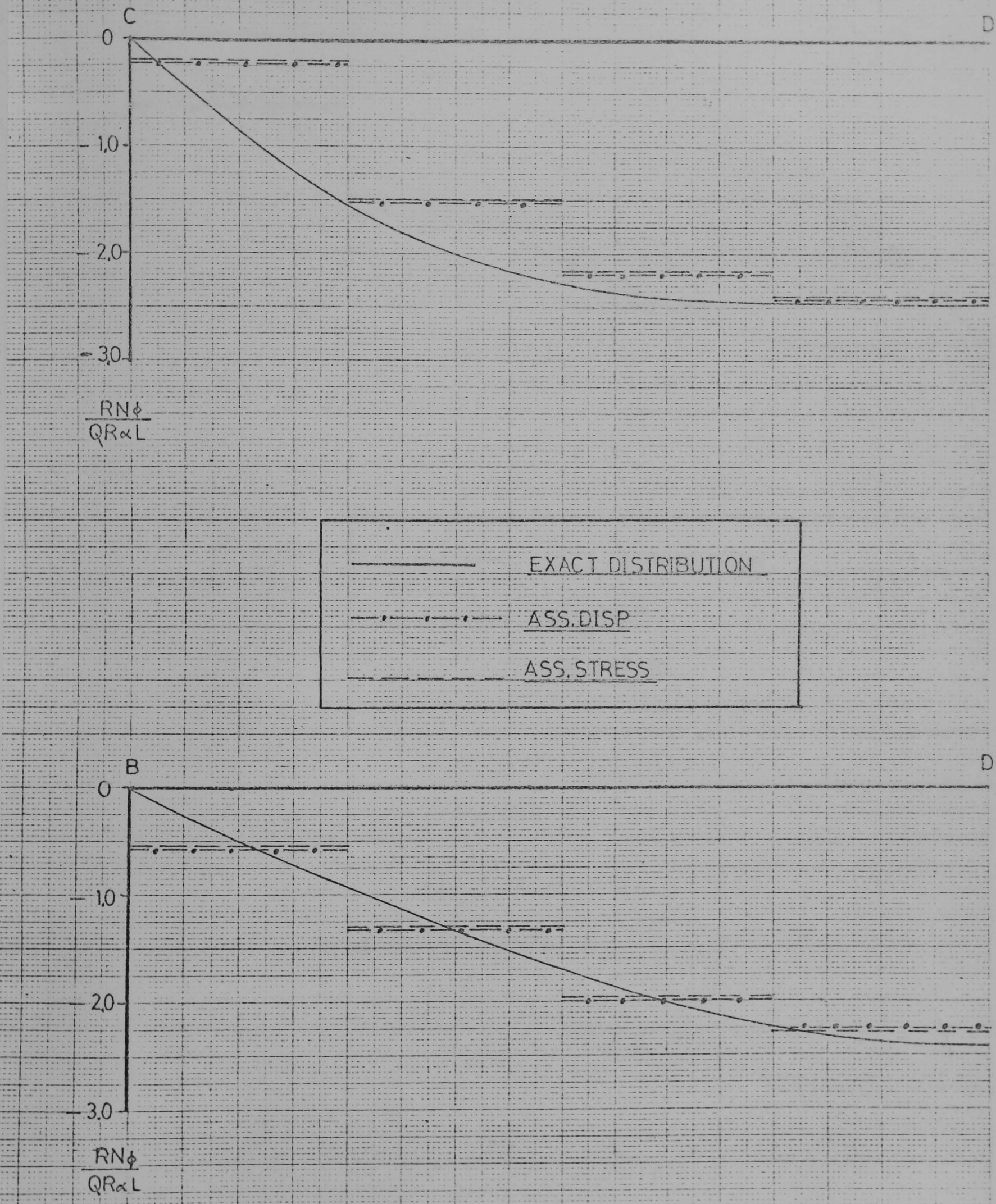

FIG 4.10 Nϕ STRESS RES. ON PANEL USING 4x4 MESH OF TRIANGULAR FLAT ELEMENTS

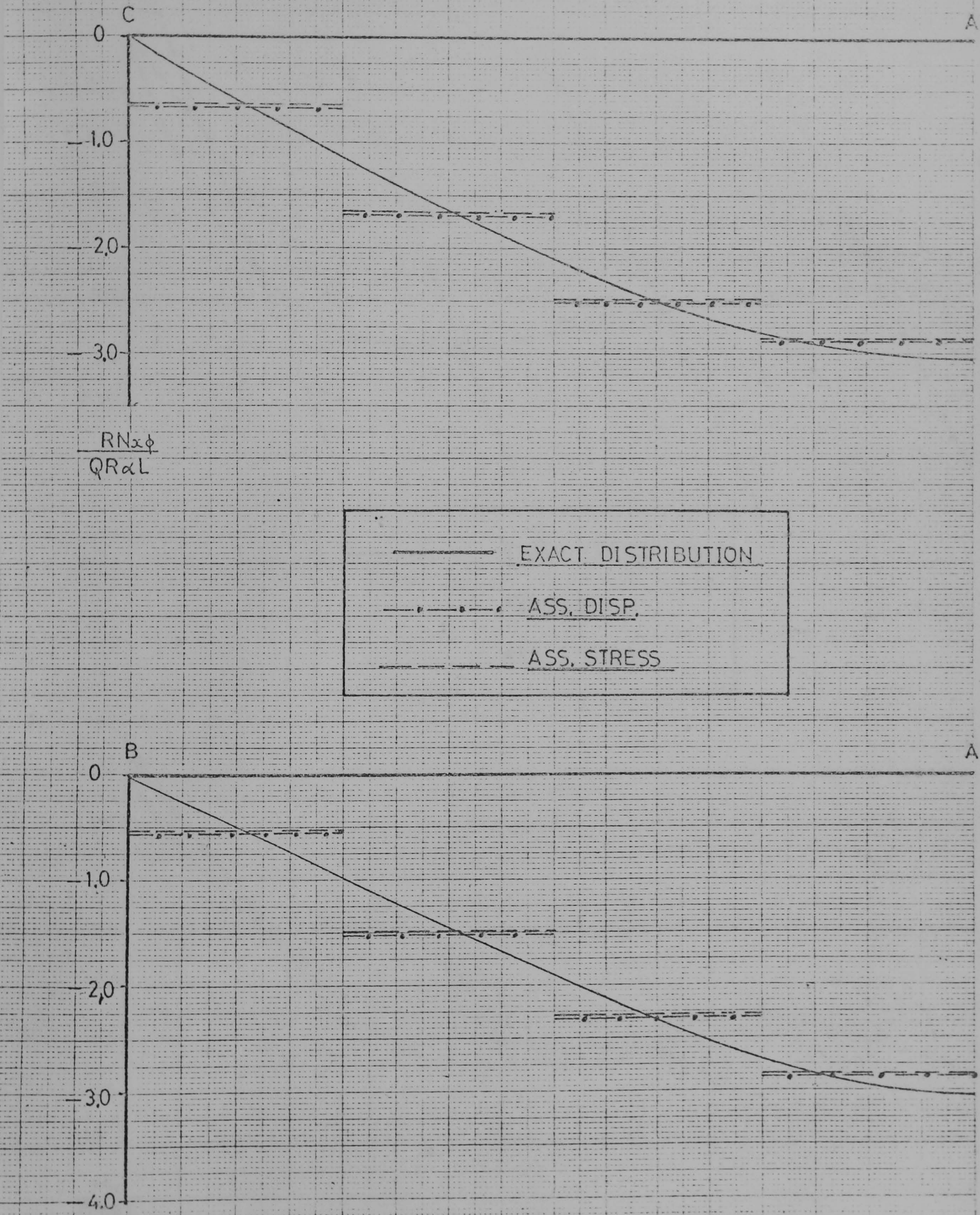

FIG 4.11 $N_{x\phi}$ STRESS RES. ON PANEL USING 4X4 MESH OF TRIANGULAR FLAT ELEMENTS.

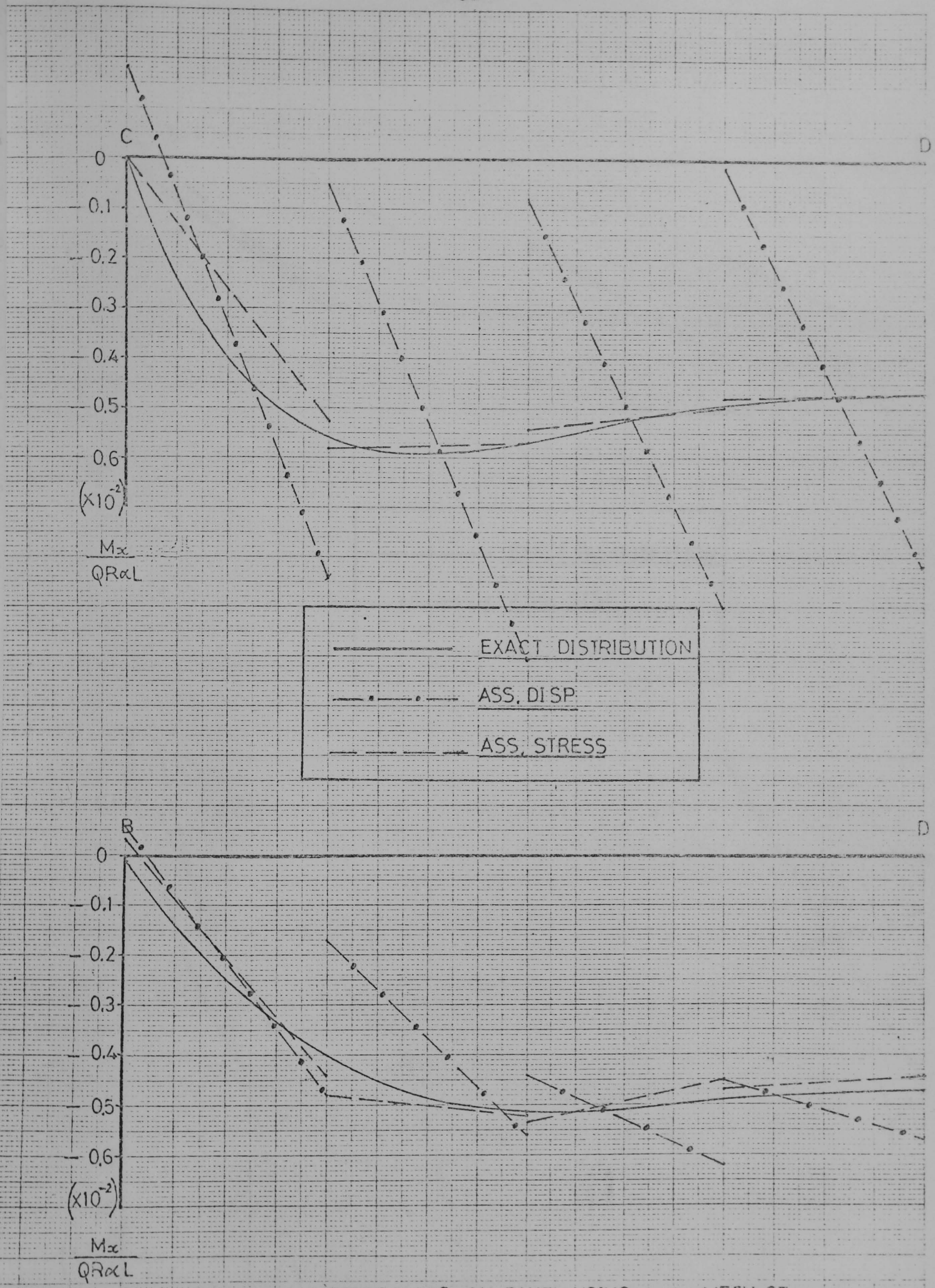

FIG 4.12 Mx STRESS RES. ON PANEL USING 4x4 MESH OF TRIANGULAR FLAT ELEMENTS

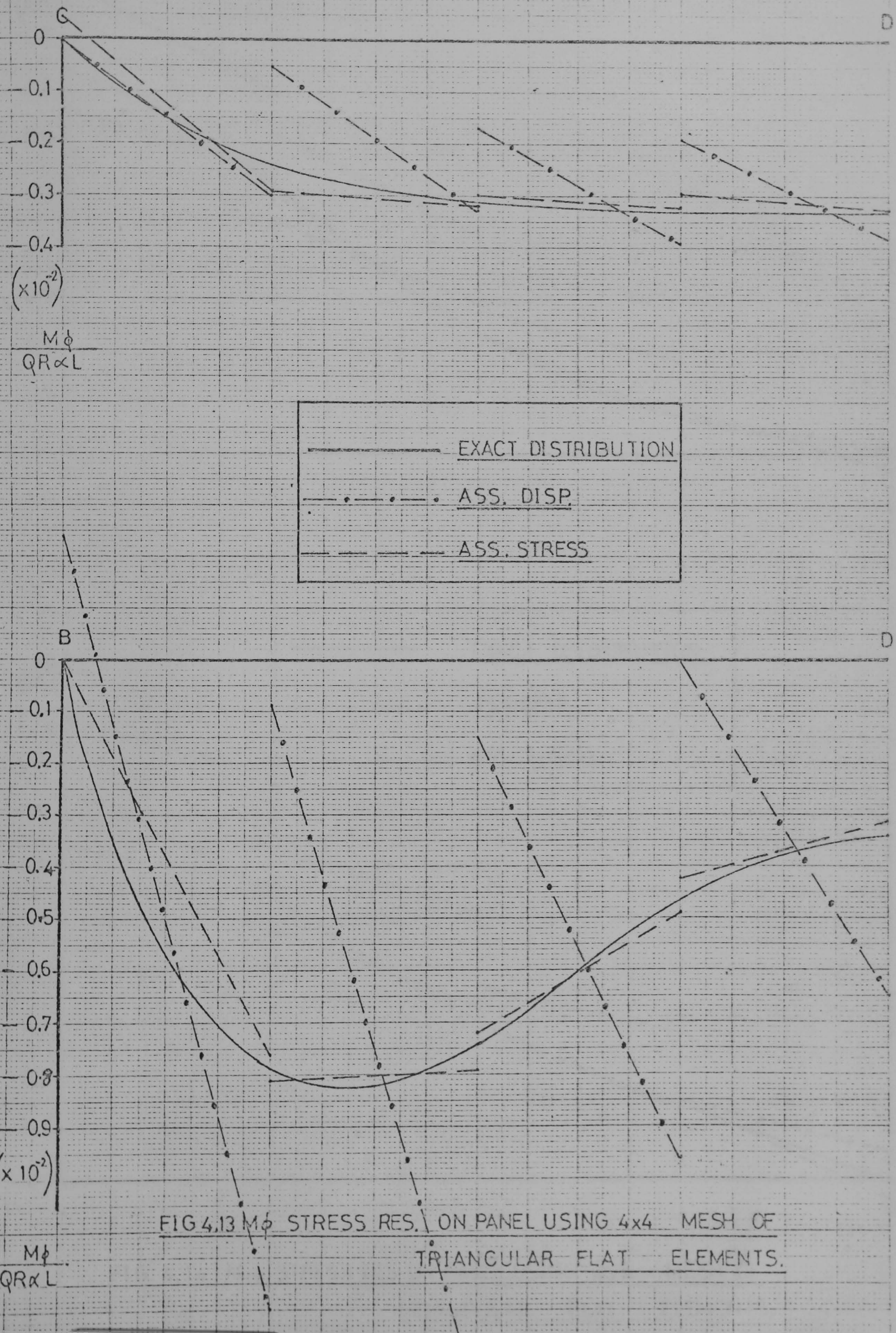

FIG 4.13 Mφ STRESS RES. ON PANEL USING 4x4 MESH OF TRIANCULAR FLAT ELEMENTS.

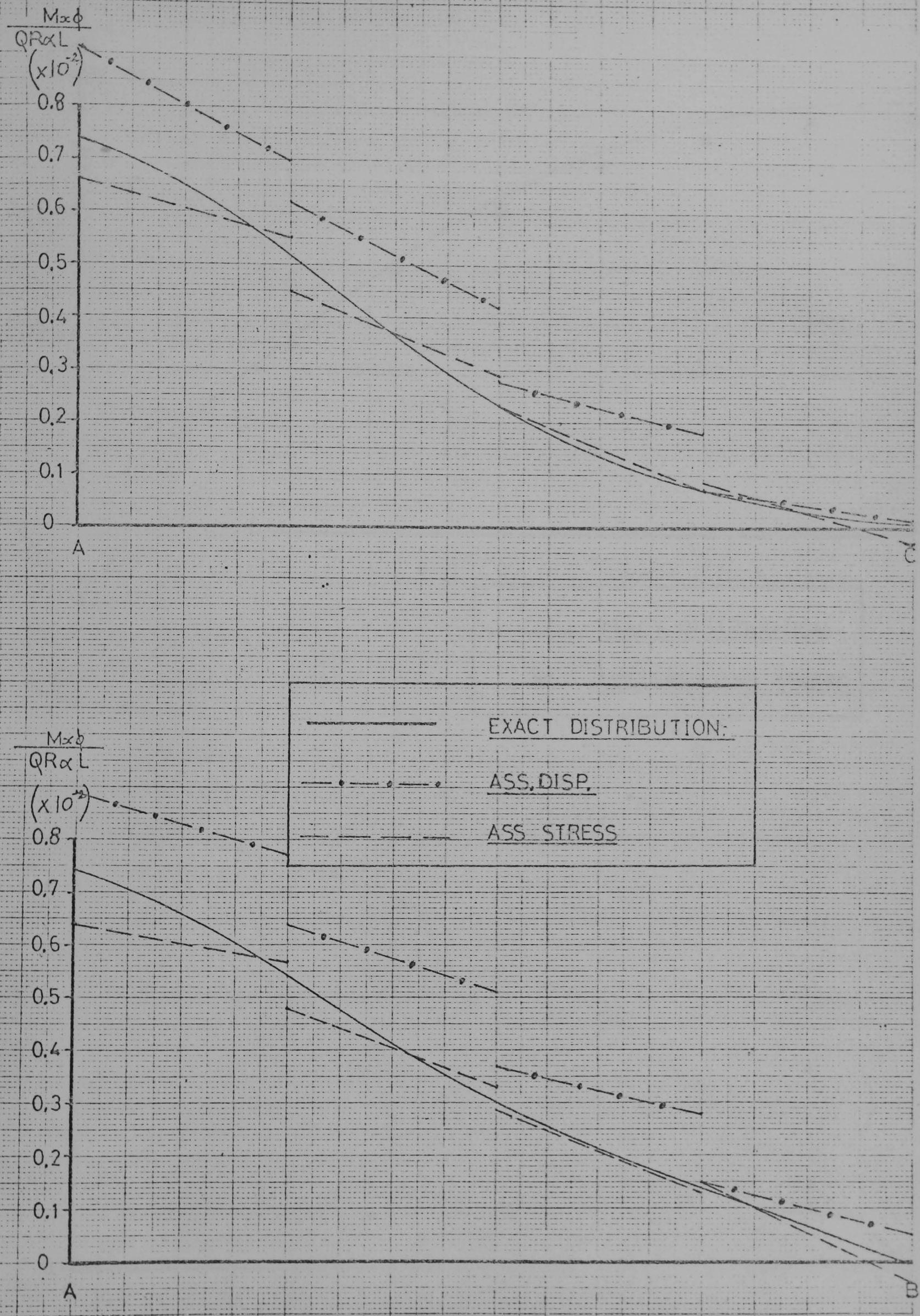

FIG 4.14 Mxφ STRESS RES. ON PANEL USING 4x4 MESH OF TRIANGULAR FLAT ELEMENTS.

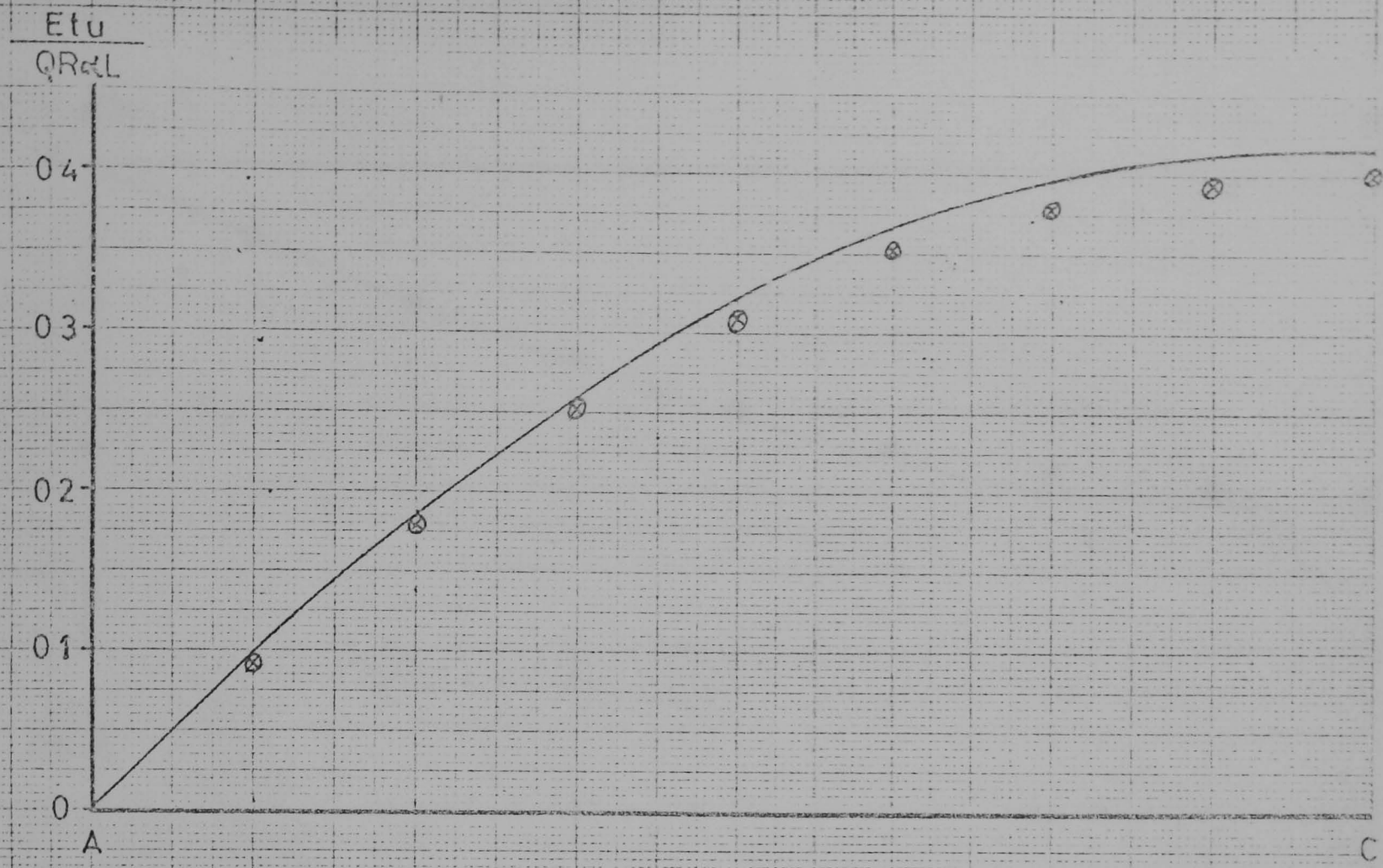

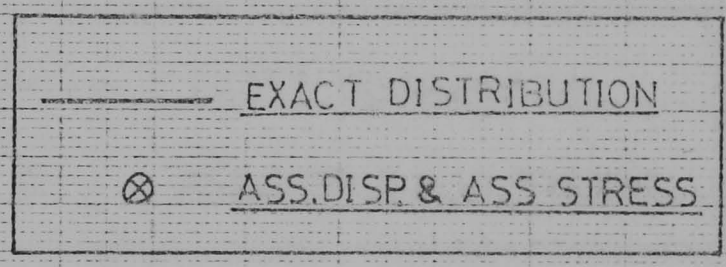

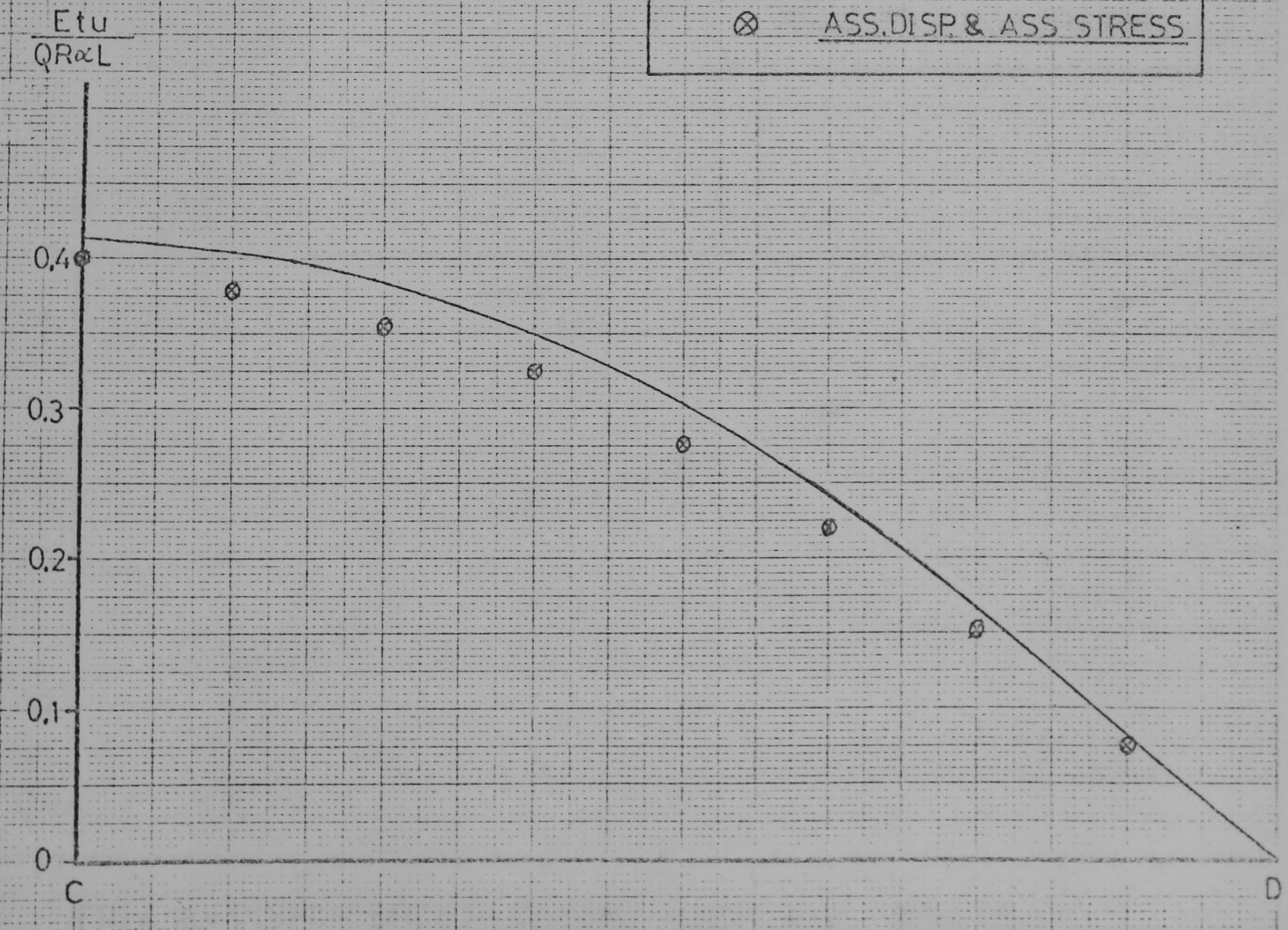

FIG 4.15 u DISPLACEMENTS OF PANEL USING 8×8 MESH OF TRIANGULAR FLAT ELEMENTS

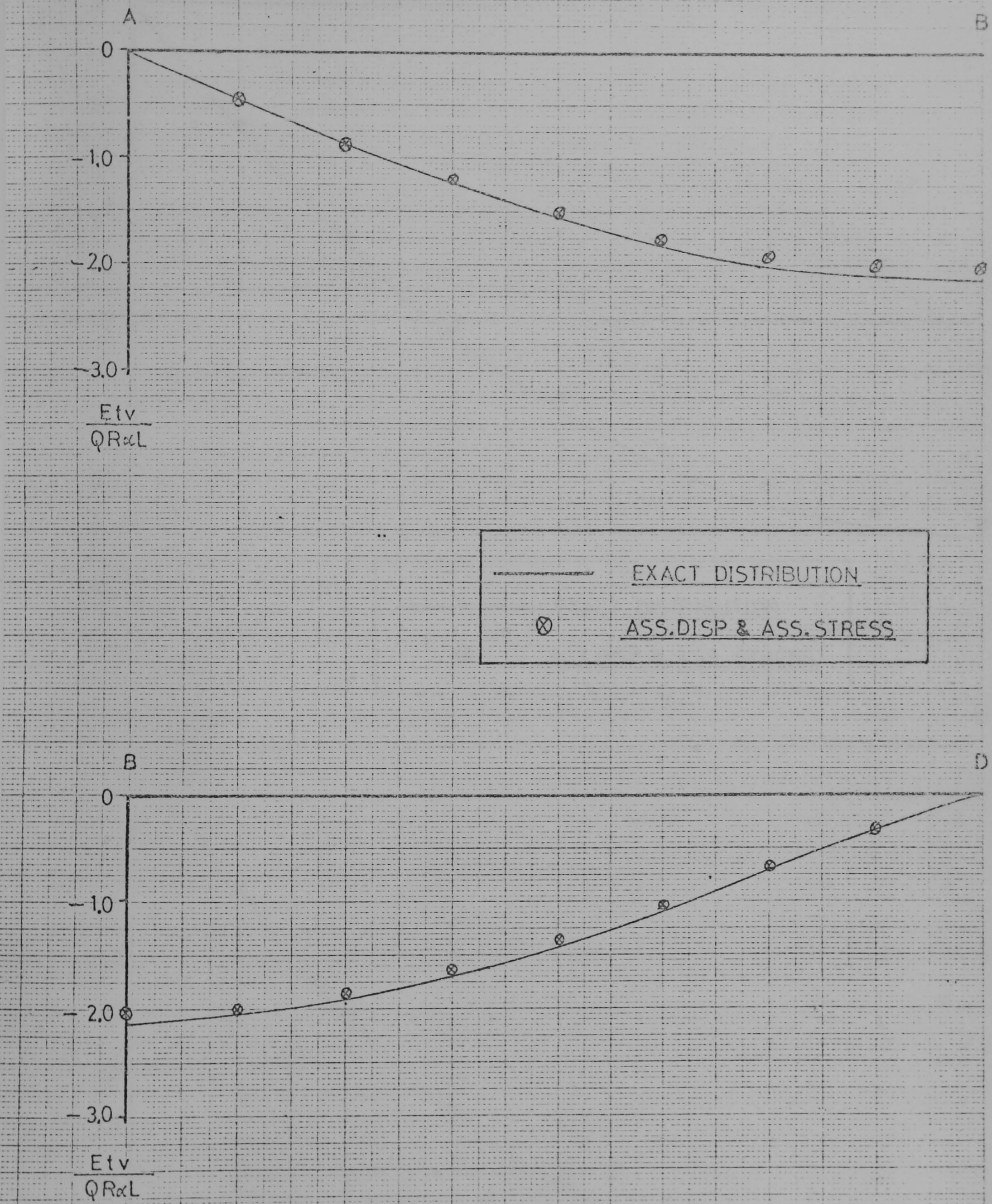

FIG 4.16 v DISPLACEMENTS OF PANEL USING 8x8 MESH OF TRIANGULAR FLAT ELEMENTS

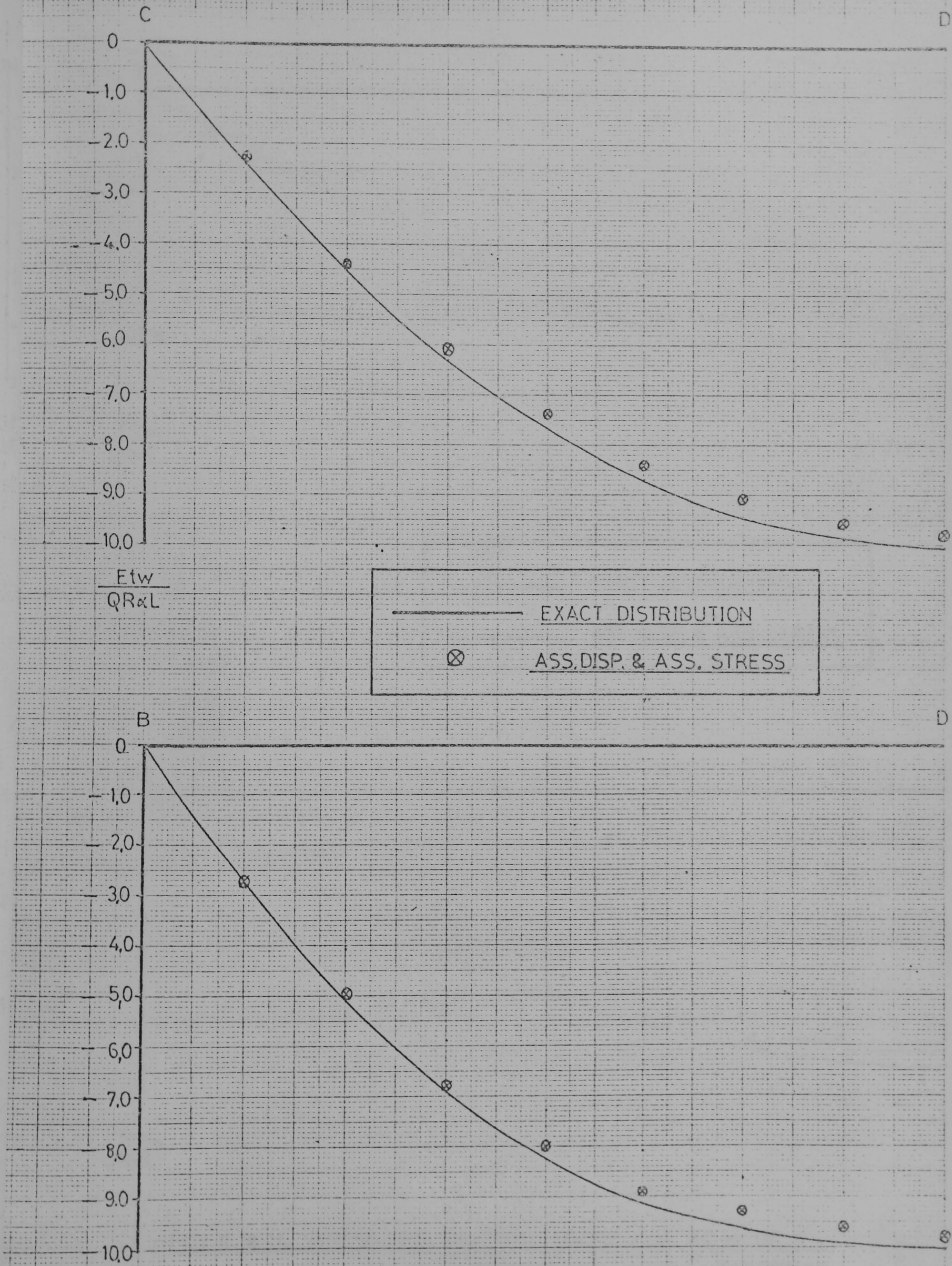

FIG 4.17 w DISPLACEMENTS OF PANEL USING 8x8 MESH OF TRIANGULAR FLAT ELEMENTS.

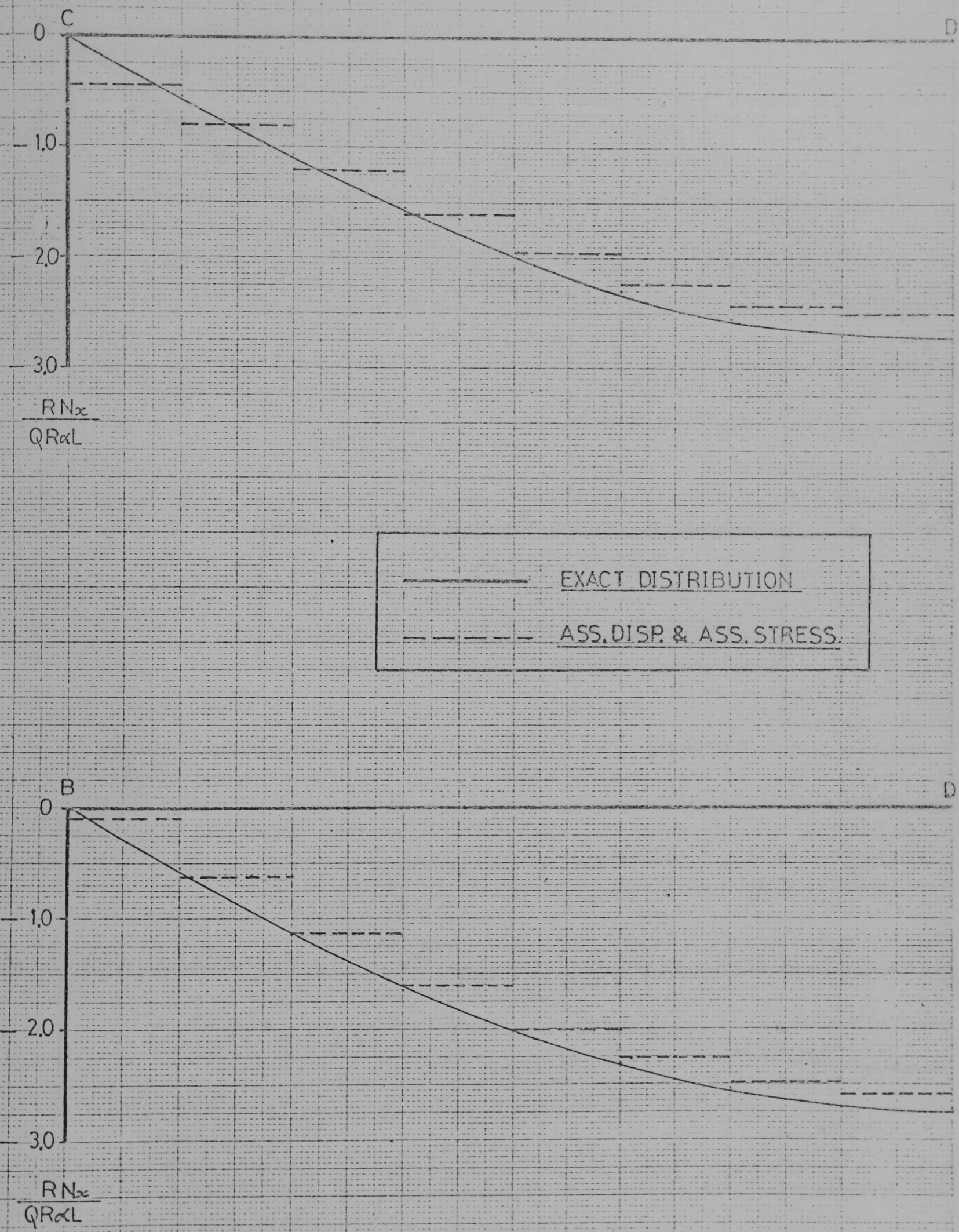

FIG 4.18 N_x STRESS RES. ON PANEL USING 8x8 MESH OF TRIANGULAR FLAT ELEMENTS.

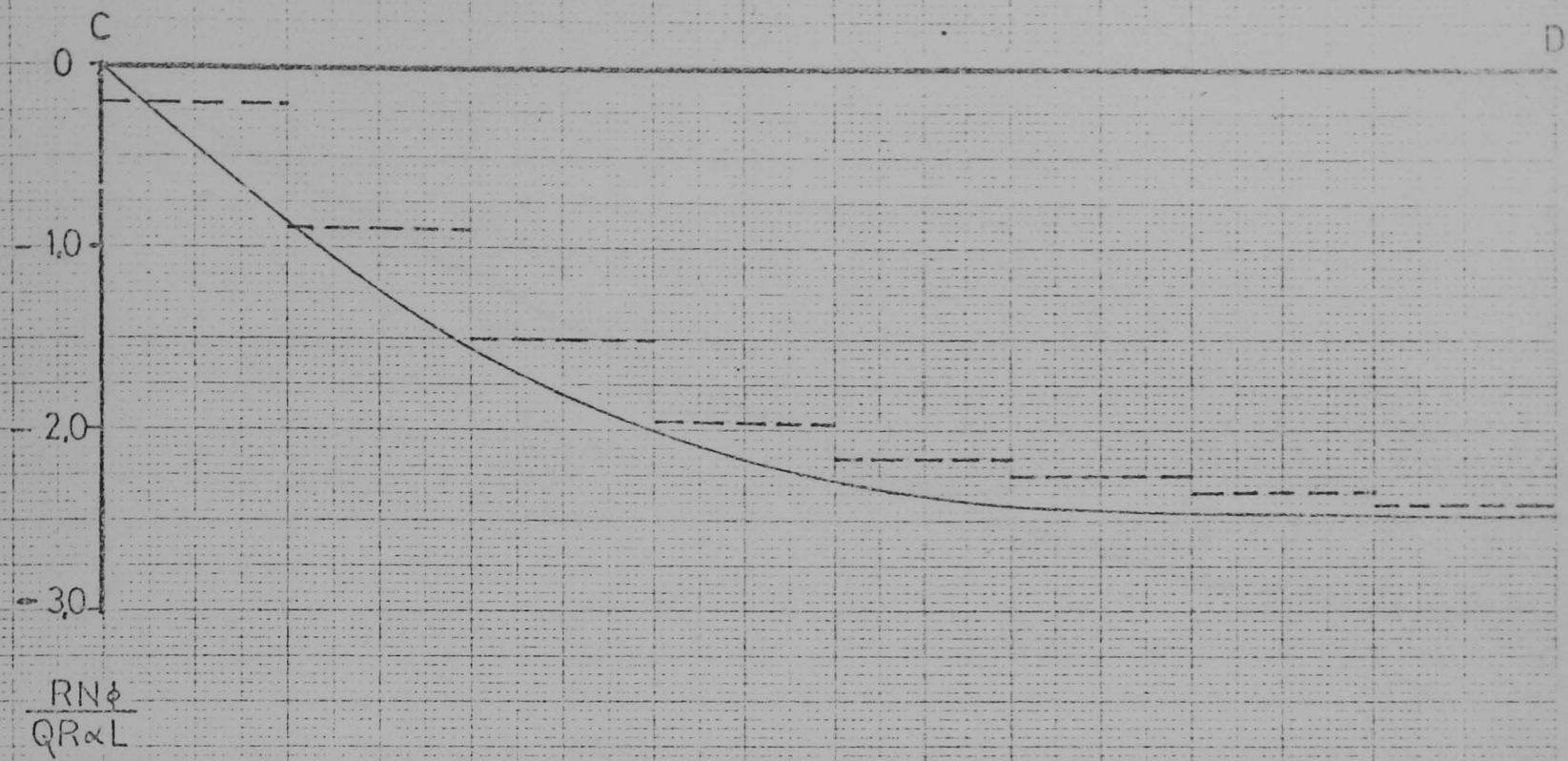

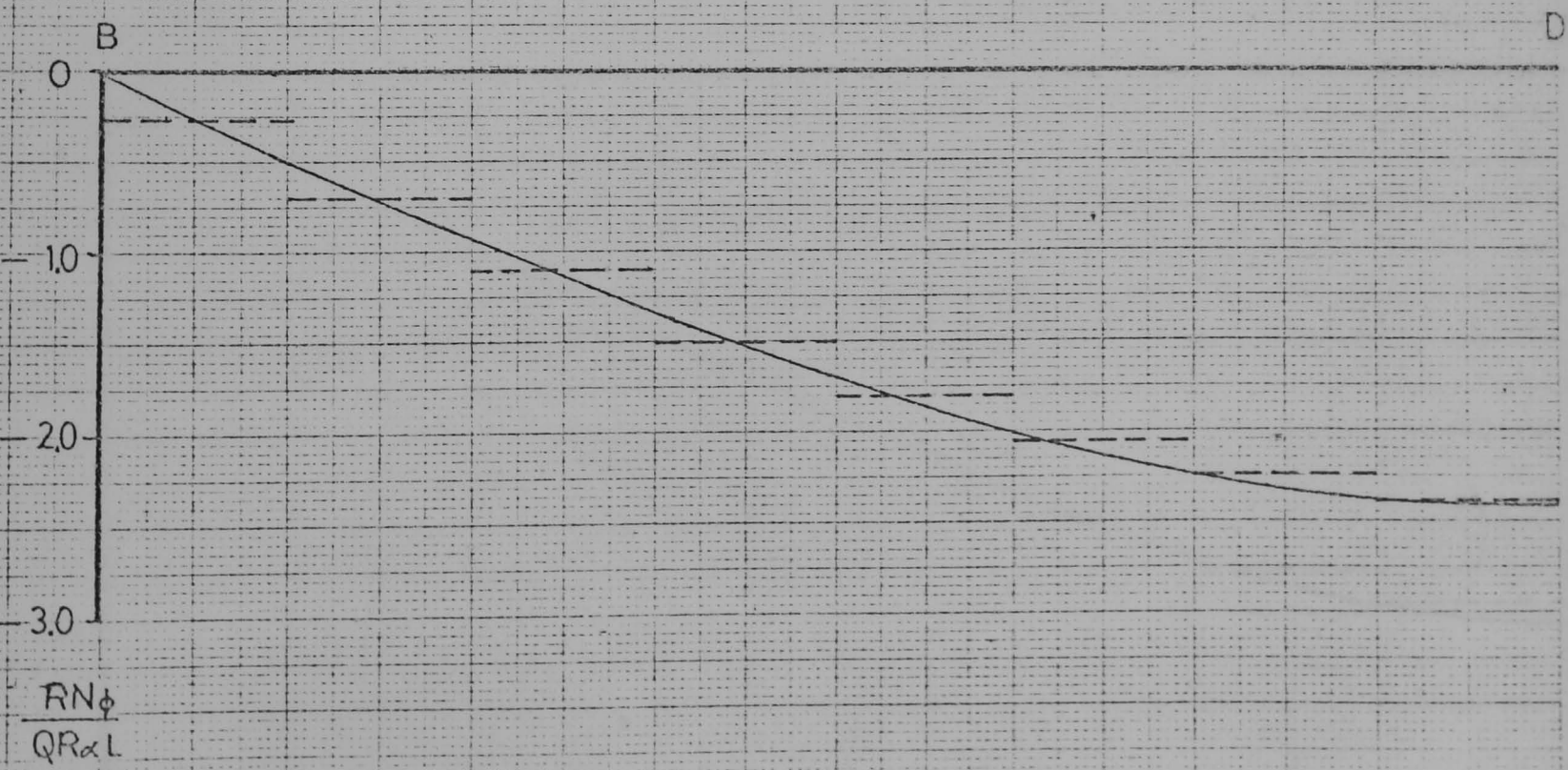

FIG 4.19 N_ϕ STRESS RES. ON PANEL USING 8x8 MESH OF TRIANGULAR FLAT ELEMENTS

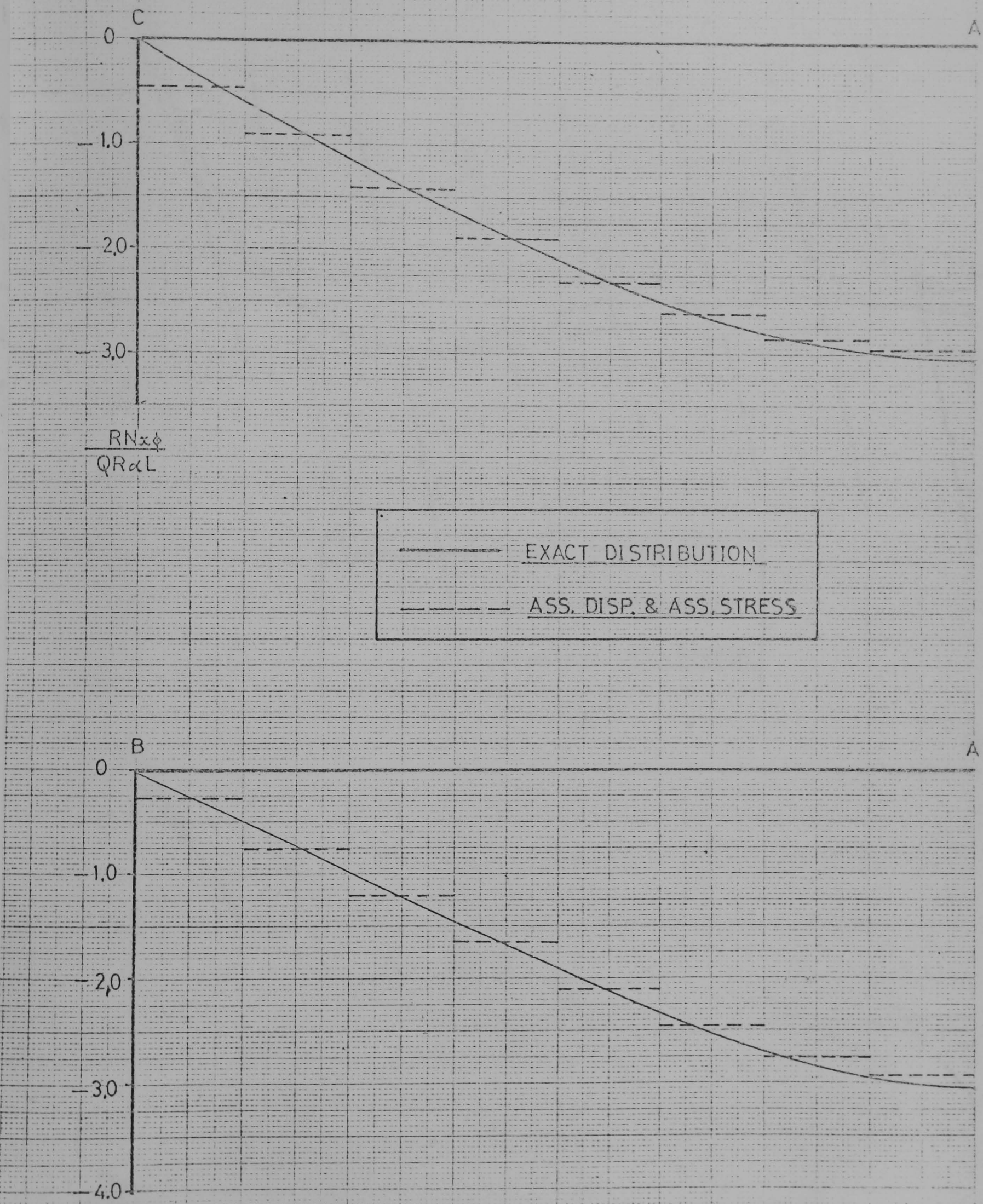

FIG 4.20 Nxφ STRESS RES. ON PANEL USING 8x8 MESH OF TRIANGULAR FLAT ELEMENTS.

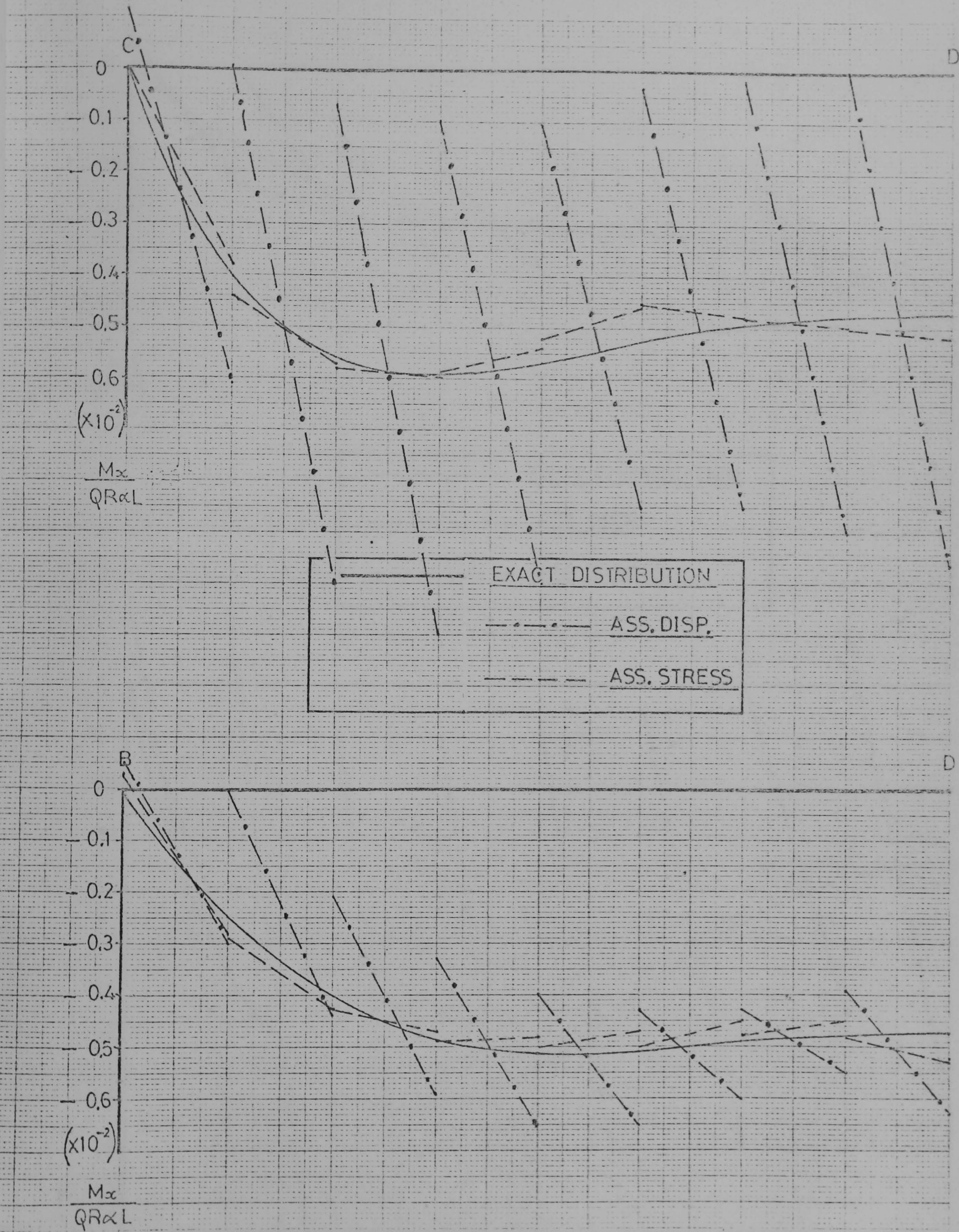

FIG 4.21 M_x STRESS RES. ON PANEL USING 8x8 MESH OF TRIANGULAR FLAT ELEMENTS

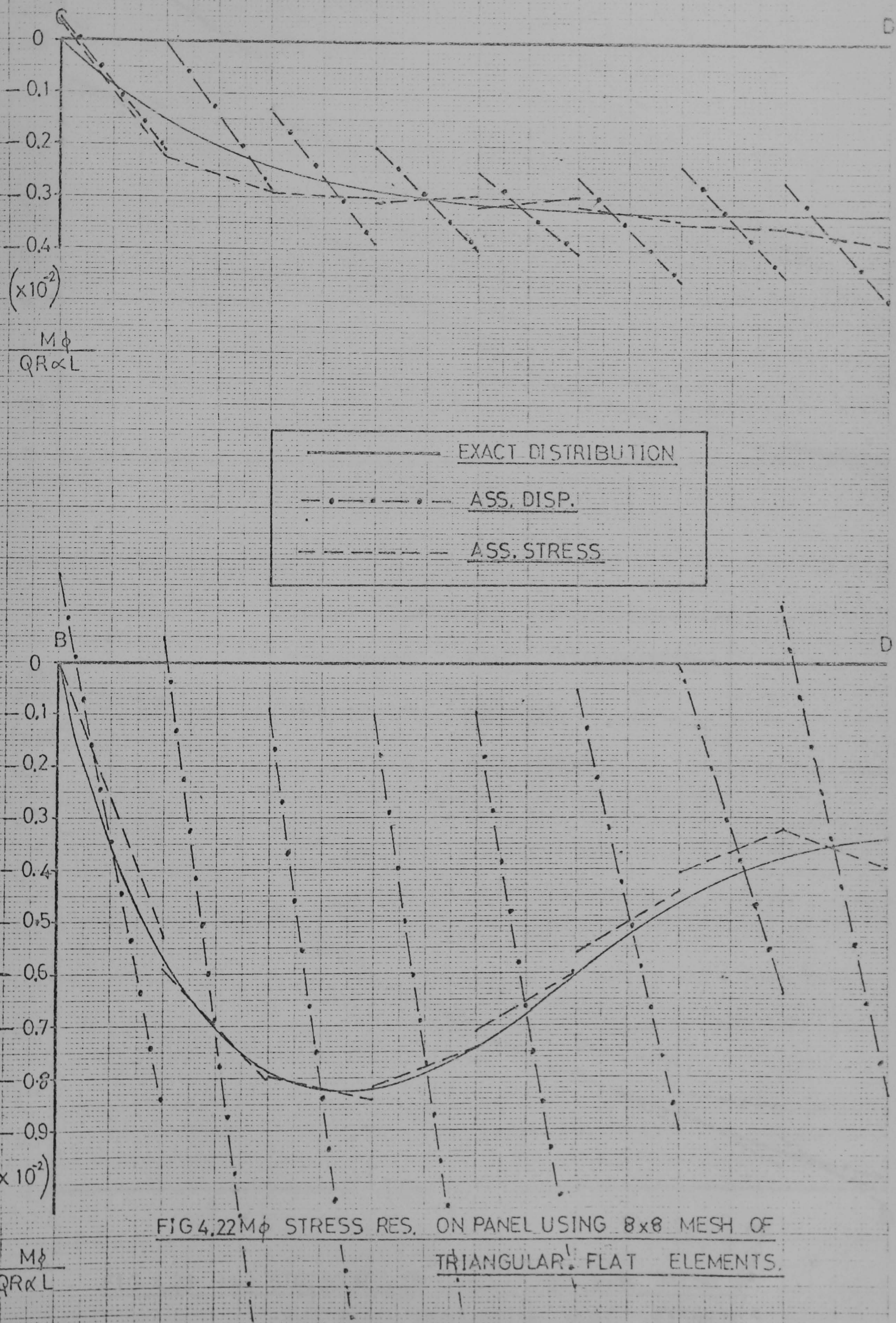

FIG 4.22 Mφ STRESS RES. ON PANEL USING 8x8 MESH OF TRIANGULAR FLAT ELEMENTS.

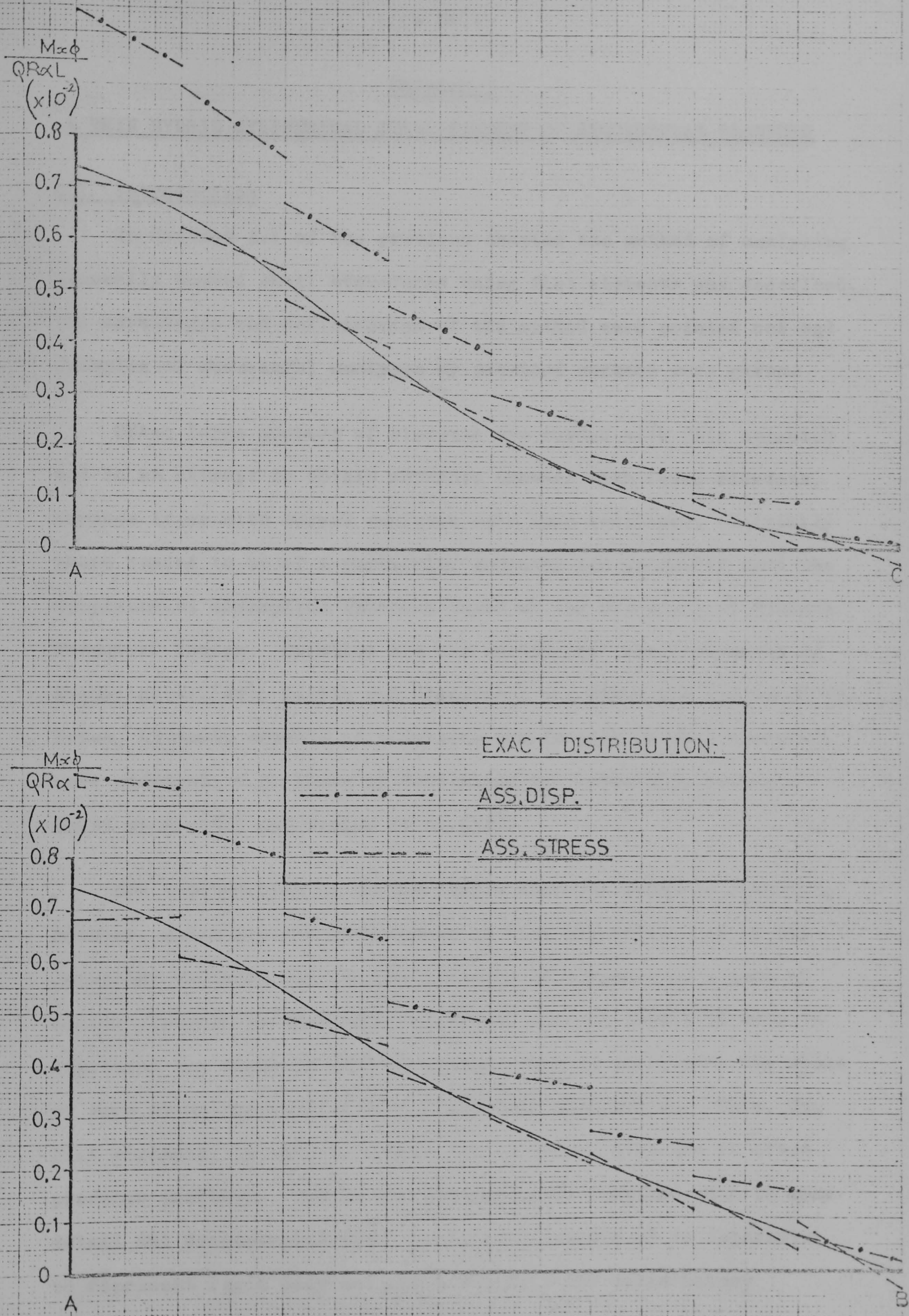

FIG 4.23 Mxφ STRESS RES. ON PANEL USING 8x8 MESH OF TRIANGULAR FLAT ELEMENTS.

Chapter 5

A THIN HYBRID CYLINDRICAL SHELL ELEMENT OF RECTANGULAR PLANFORM

5.1 Introduction

In Section 4.1 of the previous chapter the method of analysing generally shaped shell structures using flat elements was described. The advantages and deficiencies of the method were pointed out and examples of successful analyses by previous workers were given.

Often large numbers of elements are needed with this approach and in an attempt to obtain accurate answers with fewer elements, various types with curved surfaces were then developed. Initially these tended to be of a particular geometry and generally used the displacement assumption approach based on the Principle of Minimum Potential Energy. Examples are the cylindrical shell elements of Bogner et al.(44), Cantin and Clough(45) and Olsen and Lindberg(46). Later, elements capable of modelling shells with general curvature were produced, e.g. those of Strickland and Loden(50), Bonnes, Dhatt et al.(51) and Cowper et al.(52).

The construction of curved finite elements presents problems, however, which are not encountered in flat elements. One of the important criteria for the satisfactory convergence of a mesh of finite elements is that each individual element should be able to represent the state of uniform strain - and in particular the state of zero strain associated with rigid-body type motion. This, for flat elements, is easy to ensure but in curved elements it often presents problems. Cantin and Clough(54,55) examined this in some detail and demonstrated that in certain problems it is imperative to represent rigid body motions adequately for satisfactory convergence.

Also, many of the more complicated curved shell elements use degrees of freedom which are equivalent to strains. The disadvantages of these "non-geometric" freedoms were outlined in Chapter 1. An example of this type is the shallow shell triangle of Cowper et al.(52) using 36 degrees of freedom.

Recently Henshell et al.(53,55) have produced a hybrid cylindrical shell element which they demonstrated, in some applications, to be comparable with the element of Cowper et al. The element, shown in Fig.(5.1), is of rectangular planform and uses five simple geometric freedoms at each of the four nodes. It generally gives excellent static deflection and natural frequency predictions.

The element was, however, tested only on deflection and natural frequency problems and no investigations of stress predictions were made. During the present work some preliminary studies of this were undertaken and results were quite encouraging. However, the element included a number of features which were thought to be unsatisfactory but whose effect on results could not easily be predicted. It was therefore decided to construct a new element with the intention of eliminating these features and then to examine in detail the stress predictions obtained.

5.2 Unsatisfactory Features of the Existing Element

5.2.1 Edge Displacement Assumptions

To enable both mass and stiffness matrices to be evaluated a displacement assumption was made over the whole area of the element (Chapter 2). For reasons explained in (53) and (55) displacements in axes parallel and perpendicular to the base plane (Fig.(5.1))

were assumed and the edge values only were used to compute the boundary work necessary for the construction of the stiffness matrix. The polynomials used for the in-plane and transverse displacements were, however, of different orders and therefore when two elements were joined to form a smooth, cylindrical surface, displacements along the straight edges between elements were not continuous.

In the new element only edge assumptions are made in terms of the "natural" displacements in the tangent plane of and perpendicular to the shell surface. Continuity of displacements is then assured for adjoining elements forming part of a continuous surface.

5.2.2 The Stress Assumption

During the development of the existing element the concept of an "optimized" stress assumption was introduced. The terms were chosen carefully, keeping the same edge displacements, to give good answers on all problems. It was thought necessary, since the new element would use different edge displacement assumptions, to re-examine the form of the stress assumption.

A feature of the existing assumption was that all stress resultants were not represented to the same degree of accuracy in both directions. Particular resultants were, for instance, constrained to be constant in one direction whilst varying linearly in the other. It was thought possible that although an assumption such as this might give the best deflection and natural frequency predictions, it would not be the best to use for the prediction of stresses. It was therefore decided to consider stress assumptions with, as far as possible, uniform representations of stress in all directions. It was also intended to investigate assumptions of different lengths.

5.2.3 The Stress-Strain Relationship

To enable the stress assumption to satisfy all the equilibrium equations of the shell (given later in Section 5.3.3), Henshell et al. differentiated between the two in-plane shear stress resultants $N_{x\phi}$ and $N_{\phi x}$ and the two twisting moments $M_{x\phi}$ and $M_{\phi x}$ (Fig.(5.2)).

When these particular stress resultants were evaluated on sample problems they were found to be seriously in error. The shell theory of Novozhilov(1) was then studied and the conclusion reached that no distinction should be made between $M_{x\phi}$ and $M_{\phi x}$ but the equilibrium equations should be satisfied by allowing slight differences to exist between the assumptions for $N_{x\phi}$ and $N_{\phi x}$. This will be explained in detail later.

5.2.4 The Nodal Degrees of Freedom

As a consequence of the form of the displacement assumption the nodal degrees of freedom were, as in Fig.(5.1), parallel and perpendicular to the base plane. The rotational freedom normal to the base plane, considered as being approximately normal to the shell surface, was not used giving an element with 20 degrees of freedom - 5 at each node. In the new formulation (Fig.(5.3)), the natural deflections in the surface of the shell are considered as nodal freedoms. The rotation normal to the shell surface, being inapplicable to thin shell analysis, is not used - again giving 5 degrees of freedom at each node.

For the purpose of merging in the PAFEC 70+ scheme the stiffness matrix must be expressed in terms of degrees of freedom in the base-plane. This results in a (24 x 24) stiffness matrix (3 displacements and 3 rotations at each node).

5.3 The Formulation of the New Element

5.3.1 Element Geometry

The symbols used to specify the size and shape of the element are shown in Fig.(5.3). The stress-assumption (Section 5.3.4) is made in terms of the surface coordinates x and s. The length of the element is denoted by the parameter ℓ and the curved width by the parameter WID. The angle subtended by the curved side is 2β .

5.3.2 Edge Displacement Assumptions

As stated earlier, to ensure continuity it was decided to work in terms of natural shell displacements. For each of the sides, which are considered separately, it is necessary to express the displacements of a point along the side in terms of the nodal variables at the ends (Fig.(5.3)). Two separate formulations are used, one for the two straight sides and one for the two curved sides.

Since it is only necessary to make displacement assumptions along the edges of the element, the problems of representing accurately the rigid body motion are somewhat reduced. It is only necessary to represent accurately the rigid body motion of the sides when considered separately as curves in space. This will ensure adequate representation in the element as a whole.

5.3.2.1 The Straight Sides 12 and 34

The five displacements at each end of the straight sides allow linear interpolation of u and v displacements and cubic interpolation of w. Hermitian polynomials are used to express the displacements of a point directly in terms of the nodal variables. For example along side 12, if x is the distance measured along the side from node 1 towards node 2, and ℓ is the length of

the side then:

$$\begin{Bmatrix} u \\ v \\ w \\ \theta_x \\ \theta_s \end{Bmatrix} = \begin{bmatrix} 1-\left(\frac{x}{\ell}\right) & & & & \\ & 1-\left(\frac{x}{\ell}\right) & & & \\ & & 1-3\left(\frac{x}{\ell}\right)^2+2\left(\frac{x}{\ell}\right)^3 & & -\ell\left\{\left(\frac{x}{\ell}\right)-2\left(\frac{x}{\ell}\right)^2+\left(\frac{x}{\ell}\right)^3\right\} \\ & & & 1-\left(\frac{x}{\ell}\right) & \\ & & \frac{1}{\ell}\left\{6\left(\frac{x}{\ell}\right)-6\left(\frac{x}{\ell}\right)^2\right\} & & \ell\left\{\left(\frac{x}{\ell}\right)-\frac{4}{\ell}\left(\frac{x}{\ell}\right)+\frac{3}{\ell}\left(\frac{x}{\ell}\right)^2\right\} \end{bmatrix}$$

$$\begin{bmatrix} \left(\frac{x}{\ell}\right) & & & & \\ & \left(\frac{x}{\ell}\right) & & & \\ & & 3\left(\frac{x}{\ell}\right)^2-2\left(\frac{x}{\ell}\right)^3 & & \ell\left\{\left(\frac{x}{\ell}\right)^2-\left(\frac{x}{\ell}\right)^3\right\} \\ & & & \left(\frac{x}{\ell}\right) & \\ & & -\frac{1}{\ell}\left\{6\left(\frac{x}{\ell}\right)-6\left(\frac{x}{\ell}\right)^2\right\} & & -\ell\left\{\frac{2}{\ell}\left(\frac{x}{\ell}\right)-\frac{3}{\ell}\left(\frac{x}{\ell}\right)^2\right\} \end{bmatrix} \cdot \begin{Bmatrix} u_1 \\ v_1 \\ w_1 \\ \theta_{x1} \\ \theta_{s1} \\ u_2 \\ v_2 \\ w_2 \\ \theta_{x2} \\ \theta_{s2} \end{Bmatrix} \tag{5.1}$$

or in the matrix terminology of Chapter 2 $\{u\}_{12} = [L]_{12} \{q\}_{12}$

The correct representation of all six rigid body motions presents no problems in the case of a straight side. If any combination of displacements describing a rigid body movement is entered into (5.1) then the equations give the correct distributions of displacements along the side.

5.3.2.2 The Curved Sides 13 and 24

Basically, as above, it is possible to allow linear variation of displacements in the tangent plane of the shell and cubic variation of the normal displacement w. However, if the simple interpolation formulae of the previous section were used they would not represent rigid body motions of the curved side correctly. Because of the curvature, displacements are coupled under rigid body movement and it is necessary to modify certain terms to give an exact representation. The relationships of Cantin(54) and Cantin and Clough(45) are used and the assumption is constructed in two stages.

Initially an assumption is made in terms of ten general variables $\{\alpha\}$ which can later be related to the nodal displacements. The first six of these general variables can be considered to represent the six possible rigid body motions of the curved side whilst the last four are used to supply the extra variation of displacements allowed. In this case the angle ϕ shown in Fig.(5.3) is used as a measure of the distance along the curved sides. $\phi=\beta$ and $\phi=-\beta$ determine the two ends of the side.

The initial assumption is:

$$\begin{Bmatrix} u \\ v \\ w \\ \theta_x \\ \theta_s \end{Bmatrix} = \begin{bmatrix} U_x & U_y & U_z & \Theta_x & \Theta_y & \Theta_z \\ 1 & & & & R(\cos\phi-\cos\beta) & -R\sin\phi \\ & \cos\phi & -\sin\phi & -R(1-\cos\phi\cos\beta) & & \\ & \sin\phi & \cos\phi & R\cos\beta\sin\phi & & \\ & & & 1 & & \\ & & & & \cos\phi & -\sin\phi \end{bmatrix} \quad (5.2)$$

$$\cdot \begin{Bmatrix} \alpha_1 \\ \alpha_2 \\ \vdots \\ \alpha_9 \end{Bmatrix}$$

$$\begin{bmatrix} (\phi/\beta) & & \\ (\phi/\beta)^2 & (\phi/\beta)^3 & \\ -\frac{1}{R}(\phi/\beta) & \frac{2}{R\beta}(\phi/\beta) & \frac{3}{R\beta}(\frac{\phi}{\beta})^2 \\ & & (\phi/\beta) \end{bmatrix}$$

The first six columns of this assumption give the distribution of displacements along the side associated with the six rigid body movements of Fig.(5.4).

The ten coefficients $\{\alpha\}$ of (5.2) can then be related to the nodal variables at the ends of the side by substitution of $\phi = \beta$ and $\phi = -\beta$ into (5.2). For example, along side 13

$$\begin{Bmatrix} q_1 \\ q_3 \end{Bmatrix} = \begin{bmatrix} \quad A \quad \end{bmatrix} \cdot \begin{Bmatrix} \alpha_1 \\ \vdots \\ \alpha_{10} \end{Bmatrix} \qquad (5.3)$$

where

$$q_i = \begin{Bmatrix} u_i \\ v_i \\ w_i \\ \theta x_i \\ \theta s_i \end{Bmatrix}$$

The $[A]$ matrix of (5.3) can then be inverted and used to post-multiply (5.2). This will then give the displacement at any point on the curved side in terms of the nodal variables, with rigid body terms included exactly.

5.3.3 Equilibrium Equations

The stress resultants acting on an infinitesimal element of a cylindrical shell are shown in Fig.(5.2). The sign convention is that used by Novozhilov(1). The relationships between these stress resultants and the actual stresses in the shell are given in Appendix 1. The following six equilibrium equations can be shown to hold for no external applied loading.

x direction	$R\partial N_x/\partial x + \partial N\phi x/\partial\phi = 0$	(a)
s direction	$R\partial N x\phi/\partial x + \partial N\phi/\partial\phi + Q\phi = 0$	(b)
perp. direction	$\partial Q\phi/\partial\phi + R\partial Q_x/\partial x - N\phi = 0$	(c)
θx direction	$-\partial M\phi/\partial\phi - R\partial M x\phi/\partial x + RQ\phi = 0$	(d)
θs direction	$R\partial M_x/\partial x + \partial M\phi x/\partial\phi - RQ_x = 0$	(e)
θ perp.	$RN x\phi - RN\phi x - M\phi x = 0$	(f)

(5.4)

If there is an external applied loading, the above equations have to be modified. For example, pressure loading of Plb/in modifies (5.4)(c) to become

$$\partial Q\phi/\partial\phi + R\,\partial Qx/\partial x - N\phi = PR \qquad (5.5)$$

The variable ϕ is related to s, the distance measured on the surface of the element by $s = R\phi$.

5.3.4 The Stress Assumptions

Following the method outlined in Chapter 2, a stress assumption is made in terms of a finite number of parameters which satisfies the homogeneous equilibrium equations (5.4). For the evaluation of a consistent loading vector to represent, for instance, pressure loading an additional particular assumption must be made to satisfy the inhomogeneous equations (5.5) in the manner described by Pian(30) and Tong and Pian(31). The theory for this is also included in Chapter 2.

Many approximate shell theories, for instance that of Love described in Chapter 1, make the assumption in (5.4) that $Nx\phi = N\phi x$ and $Mx\phi = M\phi x$. This, however, introduces inconsistencies - one being that (5.4)(f) cannot be satisfied except by having $M\phi x$ always equal to zero. This is unsatisfactory. More refined shell theories such as that of Novozhilov(1) differentiate between these quantities. However, Novozhilov proves that to the accuracy of his initial thin shell approximations the twisting moments $Mx\phi$ and $M\phi x$ can be considered equal. This is thought to be the reason why the element of Henshell et al.(53), which makes separate assumptions for these stress resultants, gives unsatisfactory answers in this respect. It was decided here to use the same expressions for $Mx\phi$ and $M\phi x$ but to make slightly different assumptions for $Nx\phi$ and $N\phi x$ such that (5.4)(f) is always satisfied.

In this, as in all hybrids, there is a minimum length of the stress assumption to prevent the appearance of spurious rigid body modes (28,29,30,31) but theoretically no maximum. The assumption is composed of both bending and membrane components. In bending there are twelve degrees of freedom with three rigid body modes and the membrane effects are described by eight degrees of freedom (three rigid body modes). Therefore there must be at least nine columns in the bending part of the stress assumption and at least five in the membrane part. The assumption must then involve a total of at least fourteen undetermined coefficients.

Two additional features were also included:

(i) The uniform approximation of all stresses. This meant including at least the variations 1,x,s in all stresses.

(ii) When the element is reduced to a flat plate the assumptions should become uncoupled to produce satisfactory separate bending and membrane assumptions.

Figure (5.5) shows a complete stress assumption involving 29 parameters, having at least quadratic representation of all stresses in both x and s. Each column of the assumption satisfies the homogeneous equilibrium equations (5.4). Tests using both the complete assumption and just the first 16 linear terms were carried out and results will be presented later.

To evaluate a consistent pressure loading vector a particular solution of (5.4) (with (5.5) instead of (5.4)(c)) was chosen to be

N_x	N_ϕ	$N_{x\phi}$	$N_{\phi x}$	M_x	M_ϕ	$M_{x\phi}$	Q_x	Q_ϕ
$\frac{p_x^2}{2R}$	0	$-\frac{p_{xs}}{2R}$	$-\frac{p_{xs}}{R}$	0	0	$\frac{p_{xs}}{2}$	$\frac{p_x}{2}$	$\frac{p_s}{2}$

There are many possibilities for choosing a particular assumption to satisfy the in-homogeneous equations. This particular assumption

was chosen since in the flat case the pressure is carried equally by the two shear stress resultants Q_x and $Q\phi$. Generally, the loading vector obtained will depend upon the particular assumption made. It can be shown, however, (31) that if all the terms of the possible particular solutions are included in the homogeneous stress assumption, then the loading vector obtained will be independent of the particular assumption chosen.

In the present case only this particular assumption was used with both 16 and 29 term homogeneous assumptions and satisfactory loading vectors were obtained in all cases.

5.3.5 The Stress-Strain Relationship

In Appendix 1, Novozhilov's relationships between the stress-resultants and strains of the middle surface are given and their derivation is outlined. The analysis is concerned with a general, doubly curved shell. In the present case, with cylindrical geometry, one of the radii of curvature is infinite and the expressions given in Appendix 1 are somewhat simplified.

If, at this stage, the coordinates x and ϕ are used to replace 1 and 2 of Appendix 1, and the equations for S and H in (A1.9) are expanded taking into account $Rx = \infty$ they become:

$$\begin{aligned} N_{x\phi} - M_{\phi x}/R &= N_{\phi x} = \left[Et/2(1+\nu)\right]\omega \\ M_{x\phi} + M_{\phi x} &= \left[Et^3/6(1+\nu)\right]\tau \end{aligned} \qquad (5.6)$$

Equations (5.6) are insufficient to express $N_{x\phi}$, $N_{\phi x}$, $M_{x\phi}$ and $M_{\phi x}$ uniquely in terms of ω and τ, but it can be shown that

$$\begin{aligned} N_{x\phi} &= \left[Et/2(1+\nu)\right]\left(\omega + t^2\tau/6R\right) - \Phi/R \\ N_{\phi x} &= \left[Et/2(1+\nu)\right]\omega \\ M_{x\phi} &= \left\{Et^3/12(1+\nu)\right\}\tau + \Phi \qquad M_{\phi x} = \left\{Et^3/12(1+\nu)\right\}\tau - \Phi \end{aligned} \qquad (5.7)$$

where Φ may be chosen to suit convenience.

In general, this indeterminacy is not important, since it is not necessary to find separately the forces and moments $N_{x\phi}$, $N_{\phi x}$, $M_{x\phi}$ and $M_{\phi x}$. They only enter into the equilibrium equations and boundary conditions in the combinations denoted by S and H. They are, however, required separately for the determination of the shear stress resultants Q_x and Q_ϕ. These, though, are usually of little practical interest since they are small compared with the other forces. However, for the construction of a hybrid finite element the quantities Q_x and Q_ϕ must be determined for the calculation of the edge work - hence it is necessary to have the equations in the form (5.7).

Novozhilov(1), proves that the magnitude of $\bar{\Phi}$ in (5.7) is in fact insignificant, because it introduces changes which are beyond the limit of the error of the initial thin shell assumptions. It is possible, then, for practical purposes, for $\bar{\Phi}$ to be neglected.

It was decided, in the present element, to use the individual stress resultants $N_{x\phi}$ and $N_{\phi x}$, but only $M_{x\phi}$ (since $M_{x\phi} = M_{\phi x}$ in (5.7)) (see Section 5.3.4). The corresponding strains of the middle surface are $\epsilon_{x\phi}$, $\epsilon_{\phi x}$ and the curvature $\chi_{x\phi}$. These are related to ω and τ by

$$\begin{aligned} \omega &= \epsilon_{x\phi} + \epsilon_{\phi x} \\ \tau &= \chi_{x\phi} = \chi_{\phi x} + \epsilon_{x\phi}/R. \end{aligned} \tag{5.8}$$

Using the relationships in Appendix 1 (equations A1.9) and those in (5.7), the complementary strain energy of the shell expressed in terms of the vector of stress-resultants $\{\sigma\}$ is

$$\text{C.S.E.} = \iint \tfrac{1}{2}\{\sigma\}^T [D]\{\sigma\}\, R\, dx\, d\phi \tag{5.9}$$

where $$\{\sigma\}^T = \{N_x, N_\phi, N_{x\phi}, N_{\phi x}, M_x, M_\phi, M_{x\phi}\}$$

and $[D]$ is the matrix

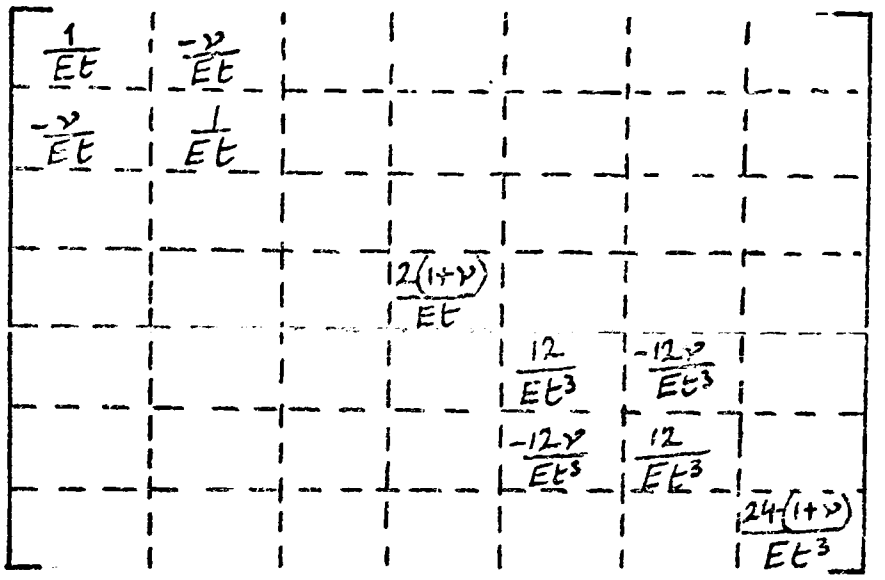

This can be shown to be equivalent to Novozhilov's strain energy expression (equation (A1.4) of Appendix 1).

5.3.6 The Evaluation of the Stiffness Matrix

For the calculation of the stiffness matrix and consistent loading vector, integrals of complementary strain energy and work around the boundary must be evaluated. These integrals are performed numerically using Gauss processes of order 4. Tests with higher order processes were carried out but no change in results was apparent. It was therefore assumed that processes of order 4 performed the integrations with sufficient accuracy.

Each side of the element is considered separately in the evaluation of edge work and it is necessary to construct matrices to transform the edge stresses into forces in the direction of displacements. Along, for instance, edge 1,2 of Fig.(5.3), the forces Fu, Fv, Fw, $F\theta x$, $F\theta s$ (per unit length) in the directions of the u,v,w,θx and θs displacements are given by the following relationships:

$$\begin{Bmatrix} Fu \\ Fv \\ Fw \\ F\theta x \\ F\theta s \end{Bmatrix} = \begin{bmatrix} & & -1 & & & & & & \\ & -1 & & & & & & & \\ & & & & & & & -1 & \\ & & & & 1 & & & & \\ & & & & & -1 & & & \end{bmatrix} \cdot \begin{Bmatrix} Nx \\ N\phi \\ Nx\phi \\ N\phi x \\ Mx \\ M\phi \\ Mx\phi \\ Qx \\ Q\phi \end{Bmatrix} \qquad (5.10)$$

- the relevant stress resultants are shown in Fig.(5.2)

Along the other straight edge, joining nodes 3 and 4 the expression is similar to (5.10) except that the signs in the matrix are reversed.

Along the curved edge 1,3 the relationship is

$$\begin{Bmatrix} Fu \\ Fv \\ Fw \\ F\theta x \\ F\theta s \end{Bmatrix} = \begin{bmatrix} -1 & & & & & & & & \\ & -1 & & & & & & & \\ & & & & & & & -1 & \\ & & & & & & 1 & & \\ & & & & -1 & & & & \end{bmatrix} \cdot \begin{Bmatrix} Nx \\ N\phi \\ Nx\phi \\ N\phi x \\ Mx \\ M\phi \\ Mx\phi \\ Qx \\ Q\phi \end{Bmatrix} \qquad (5.11)$$

with the expression along the other curved edge again having the signs reversed. The calculated work for each side is added into a matrix which then represents the total edge work. This is the $[G]$ matrix of Chapter 2.

The calculation of the complementary strain energy for the element produces the $[H]$ matrix of Chapter 2 and this, together with $[G]$, is used to form the stiffness matrix as indicated. The integrals involving the particular solution are performed simultaneously with those involving the homogeneous stress assumption.

5.3.7 The Calculation of Stresses

When the displacements of individual elements have been

evaluated from the structure displacements it is a relatively simple matter to calculate the stresses. The $[H]^{-1}[G]$ matrix in fact relates displacements directly to the coefficients of the stress assumption

$$\{\beta\} = [H]^{-1}[G].\{q\} \qquad (5.12)$$

The stress assumption is then used to evaluate stresses at any required point within the element.

There is one major organizational problem involved. The $[H]^{-1}[G]$ matrices are calculated in the element routine and must be kept on backing store ready to be used in the stressing routine. In a large structure, with many different sizes of elements, a considerable area of backing store is required.

It is possible using the $[H]^{-1}[G]$ matrix to verify the correct representation of rigid body motions in the boundary displacement assumptions. If nodal displacements $\{q\}$ which define rigid body motions are used in conjunction with the $[H]^{-1}[G]$ matrix, then zero stresses should occur. Six sets of nodal displacements representing the six possible rigid body motions were used and the stress coefficients were found to be zero, or very small, in all cases.

5.4 Problems Analysed

5.4.1 The Pinched Cylindrical Shell

The present element was used to analyse the same pinched cylindrical shell as in Section 4.6.1 of the previous chapter when flat elements were used. The problem is shown in Fig.(4.3) of Chapter 4. In addition to 'exact' displacement distributions,

Lindberg et al.(65) give accurate values for various stress distributions. It was therefore possible to compare with these the values obtained using the present element.

Firstly, a 4 x 4 mesh (Fig.(5.6)) was used to analyse $\frac{1}{8}$ of the shell. Two stress assumptions were used. The first consisted of the first 16 terms of Fig.(5.5) having linear representation of all stresses whilst the second used the full assumption of 29 terms having at least quadratic representation.

Figure (5.6) shows the distribution of normal displacement along the top line of symmetry DC. The 16 term assumption gives slightly better values in the region of the point load and both distributions are seen to be an improvement upon the 4 x 4 mesh of flat triangular elements in Fig.(4.4).

Figures (5.7), (5.8) and (5.9) show stress distributions obtained with both assumptions. The stresses plotted are those given along the sides of elements lying along the respective edges. The extra terms in the 29 term assumption give no consistent improvement in the results over those using the 16 term assumption. In most cases the linear assumption gives stresses lying closer to the exact values.

An 8 x 8 mesh of elements with linear stress assumptions was then used. Fig.(5.6) also shows the normal displacements along DC obtained here. The exact distribution is very closely followed, with the value under the point load being overestimated by about 4%. The stresses are shown in Figs. (5.10), (5.11) and (5.12). The least accurate answers are given in the region of the point load - that for $N\phi$ being the worst.

Also shown are some results quoted by Lindberg et al.(65) which will be discussed later.

5.4.2 The Simply Supported Panel under Pressure Loading

To examine all stress distributions obtained with the element, the simply supported panel of Section 4.6.2 was again considered. The dimensions etc. are given in Fig.(4.5) of Chapter 4.

With the present elements the pressure loading vector for each element was evaluated in a consistent manner, as outlined in Chapter 2, using the particular stress assumption described earlier. However, when the loading vectors for individual elements are combined, it turns out that the loading applied to the structure consists of exactly the same set of point loads used in Section 4.6.2 together with some small bending moments along the edges.

Both 16 and 29 term stress assumptions were used with 4 x 4 and 8 x 8 meshes on $\frac{1}{4}$ of the panel. The linear version again gave marginally better answers and these are shown in Figs. (5.13) to (5.21). It was apparent from these results that not all stress resultants had converged to exact answers (e.g. M_ϕ along CD) so a 16 x 16 mesh was then used to determine if, in fact, accurate convergence took place. The results demonstrated this to be so and are shown in Figs. (5.22) to (5.30). In addition to giving accurate values for non-zero stresses it was thought important that the idealization should also converge to give zero stresses in appropriate places (e.g. $N_{x\phi}$ along CD and BD) (Fig.(4.5)). Some results from these investigations are shown in Figs. (5.31) to (5.32).

5.4.3 The Cylindrical Shell Roof Problem

This well known problem is shown in Fig.(5.33) and has been

used by many workers (65,55,66,57) as a measure of performance of finite elements. The shell is supported on diaphragms at the two curved ends, is free along its two straight edges and is loaded by its own weight. Most authors use the vertical deflection at the centre of a free edge as a measure of convergence and less attention has been paid to stress distributions. The problem provides a good test of finite elements because both bending and stretching modes of deformation are important. The solutions used for comparison purposes are those of Scordelis and Lo(67).

Since all the preceding results had indicated the superiority of the 16 term linear stress assumption, this alone was used in the shell roof problem. Both 4 x 4 and 8 x 8 meshes were used to model $\frac{1}{4}$ of the structure and these involved 92 and 344 degrees of freedom. The loading was applied by approximating the dead weight by a series of point loads. The evaluation of a consistent loading vector would, in principle, have been possible - but complicated. The direction of the load is always vertical and therefore the direction with respect to an element would depend upon the physical position of the element in the structure. Remembering the small difference between consistent and non-consistent loading vectors in the previous problem, it was thought here that the effort involved was not justified.

Figures (5.34) to (5.36) show the displacements and stress distributions obtained. The vertical deflection at the central section and the axial deflection at the support are both predicted with excellent accuracy. The vertical deflection at the centre of the free edge is given as 3.52" compared with the exact of 3.7".

The longitudinal stress and bending moment distributions are

also shown. Generally good agreement with exact values is obtained. In the case of the longitudinal moment at the central section (Fig. (5.36)) fairly large discontinuities between elements are present, especially at the coarse mesh. The reasons for this, and possible methods of improvement will be discussed later.

5.5 Conclusions

5.5.1 The Stress Assumptions

It is apparent from the pinched cylindrical shell and simply supported panel problems that no real improvement is gained by using the 29 term quadratic assumption. It is, perhaps, somewhat surprising that the extra terms do not cause much larger differences in the results.

Also, from the panel and shell roof problems, it can be seen that in most cases the linear variations of stresses allowed in the 16 term assumption are useful in approximating exact distributions. Exceptions are the x variation in Nx and the s variation in $N\phi$, since Nx and $N\phi$ take up virtually constant values in these directions. However, it is these variations which are coupled with $Nx\phi$ and $N\phi x$ (Fig.(5.5)) to give linear variation in these. In the pinched cylinder problem, especially at coarse meshes, the linear terms in $Nx\phi$ and $N\phi x$ are useful - so on balance it was decided to retain these terms in the assumption. However, it is apparent on all problems at fine meshes, that Nx is virtually constant with x, $N\phi$ constant with s and $Nx\phi$ constant with x and s within each element.

5.5.2 The Boundary Displacement Assumptions

It is possible, by examining the form of the boundary displacement

assumptions, to put forward tentative explanations for some of the phenomena outlined above. In Chapter 2 the basis of hybrid elements was described in mathematical terms, but it is also useful to consider what happens qualitatively in an attempt to explain some of the results. This type of approach was used when considering the characteristics of equilibrium stress models, hybrids, and conforming displacement assumption models in Section 2.3.4.7 of Chapter 2.

Basically, the boundary displacement assumptions in each element constitute a constraint on the structure, i.e. the boundaries are only allowed to displace in certain ways. The minimization procedures then arranges for the stress assumptions to be partially compatible with these displacement assumptions. If the form of the displacement assumption imposes restrictions on the stress distribution, the minimization procedure will tend to enforce these. Therefore, variations in the stress assumption not implied by the boundary displacements will tend to be eliminated during the minimization process.

It is thought that the behaviour of the Nx and $N\phi$ stresses outlined in Section 5.5.1 can be explained in this way. The Novozhilov stress-displacement relations for the two in-plane stress resultants are:

$$Nx = \{Et/(1-\nu^2)\}\{\partial u/\partial x + \nu\partial v/\partial s + \nu w/R\}$$

and

$$N\phi = \{Et/(1-\nu^2)\}\{\partial v/\partial s + w/R + \nu\partial u/\partial x\} \qquad (5.21)$$

where u, v and w are the three "natural" displacements in the tangent plane and perpendicular to the shell surface. The terms $\partial u/\partial x$ and $\partial v/\partial s$ dominate the first and second expressions respectively.

Along a straight side of the element (in the x direction) the assumption for u is linear with x and therefore $\partial u/\partial x$ is constant. Similarly for v and $\partial v/\partial s$ in the curved s direction. The dominant terms in Nx and $N\phi$ are therefore constant in the x and s directions respectively. No such restrictions are present in the other directions.

Since, in the minimization procedure some attempt is made to approximately satisfy (5.21), it is understandable why the stresses take up approximately constant values in the directions indicated. However, no such simple arguments can be applied to other (Mx, $M\phi$ etc.) stress distributions since they involve more complicated expressions and the dominant terms are difficult to determine. From the results it can be concluded, however, that linear variations, at least, are implied in the stresses Mx, $M\phi$ and $Mx\phi$ by the displacement assumptions.

5.5.3 The Convergence of Stresses

On all problems, with the possible exception of the region around the point load in the pinched cylindrical shell, 8 x 8 meshes are sufficient to ensure convergence with small discontinuities between adjacent elements. It is therefore possible to comment on the accuracy of these solutions compared with exact values. The simply supported panel will be considered.

An 8 x 8 mesh on $\frac{1}{4}$ of the panel gives excellent values for in-plane stresses lying on or close to the exact curves (Figs. (5.16) to (5.18)). Generally the same can be said for the bending moments except that along CD $M\phi$ has converged to a value much lower than the exact (Fig.(5.20)). Distributions along lines parallel to CD were also examined but these had all converged to correct values. It was therefore assumed that the $M\phi$ stress along

CD was in some way difficult for the elements to model and a 16 x 16 mesh was tried.

These results are very similar to the 8 x 8 set except that M_ϕ has now converged to an acceptable value. It appears, then, that the rate of convergence of all stresses is not the same when the mesh size is successively refined. This is also demonstrated in Figs. (5.31) to (5.32) where the convergence of stresses to zero is examined. Reasonable values are given at the 4 x 4 mesh, but these diverge from zero with the 8 x 8 mesh, only to return to acceptable values at the very finest mesh used.

Solutions for the shell roof problem are generally satisfactory at an 8 x 8 mesh except for some quite large discontinuities in the longitudinal moment (Mx) in the s direction. This will be discussed later (Section 5.5.5).

Stresses in the region of the point load in the pinched cylinder could, it is thought, be improved by a locally refined mesh in the region.

5.5.4 Comparison with other Finite Element Results

The pinched cylindrical shell problem has been used by Lindberg et al.(65) to test their triangular shell element. The Shell Roof has been used by many workers, e.g. Zienkiewicz et al.(66) and Neale(55).

The finest uniform mesh used by Lindberg et al. is a 5 x 5 idealization on $\frac{1}{8}$ of the pinched cylinder. Their element, however, uses 12 degrees of freedom at each node and on a degree of freedom basis their 5 x 5 mesh is roughly equivalent to the 8 x 8 mesh of the present elements. Lindberg et al.'s results are also plotted

in Figs. (5.10) to (5.12) where it can be seen that the results using the present element are of the same order of accuracy.

More comparisons are possible on the shell roof problem. Neale(55) using the hybrid element which was the forerunner of the present one obtains an answer of 3.6776" for the deflection at the centre of the free edge using 393 degrees of freedom. (The correct value is 3.7033".) The present 8 x 8 mesh using 348 degrees of freedom gives a stiffer answer of 3.52". The difference is due, obviously, to a combination of the new conforming edge displacement assumptions and the more complete stress assumption. The reason for the larger number of degrees of freedom used by Neale(55) for nominally the same idealization is the fact that in his case the normal rotation to the shell surface was not eliminated, but six general freedoms in global directions were used at points on the surface. On the basis of experiments carried out by the present author it is thought this has negligible effects.

A reasonable comparison is also possible with the results for the same problem presented by Zienkiewicz et al.(66). The 4 x 4 mesh of the present elements uses 92 degrees of freedom and the 2 x 2 mesh in (66) has 76. The element used by Zienkiewicz et al. is also of rectangular planform and the purpose of the paper is to demonstrate the very significant improvements possible by "under-integrating" or using a Gauss process of insufficient order to evaluate the strain energy.

The results using the present element are superior to those of Zienkiewicz et al. when accurate integrations are used, but the modified form of their element gives excellent results which are marginally better than the present.

5.5.5 Interpretation of Results in Future Problems

It is possible by comparing exact and finite element predictions in the problems considered here to lay down rough guidelines to enable results to be interpreted accurately in future problems. Firstly, a mesh should be used, if possible, such that discontinuities in stresses between elements are small. Answers of similar accuracy to those obtained for the panel can then be expected. However, as an additional check, it would be wise to try a still finer mesh to determine whether any further convergence takes place (in a manner similar to the Mϕ stress in the panel).

If the in-plane and bending stresses are considered separately, it can be said that for the in-plane stresses, predictions are good even at relatively coarse meshes. If discontinuities are fairly large (for instance in the Nx stress when it takes up virtually constant values in the x direction (Fig.(5.16))) it appears that good answers can be obtained by using values given halfway along the side of the element under consideration.

The interpretation of bending moments is more involved. With the exception of the Mx stress in the x direction, all bending moments in the 16 term assumption are allowed to vary linearly within each element and generally take up values lying on, or close to exact curves. The Mx stress, however, can have quadratic variation with x and at coarse meshes, e.g. the 4 x 4 mesh on the simply supported panel (Fig.(5.19)), takes up a marked quadratic shape within the elements.

This has an adverse affect on the distribution of the moment obtained in the ϕ direction - shown in Fig.(5.19) along BD and demonstrated even more clearly (in Fig.(5.36)) in the cylindrical

shell roof where discontinuities using a 4 x 4 mesh are quite large. It is clear, however, by inspection of Fig.(5.19) that in the case of the simply supported panel, good answers close to the exact would be obtained if average "least squares" straight lines were fitted to the quadratic distributions. This method was tried on the cylindrical shell roof (Fig.(5.36)) and the improvement in the longitudinal moment at the central section with a 4 x 4 mesh is quite marked.

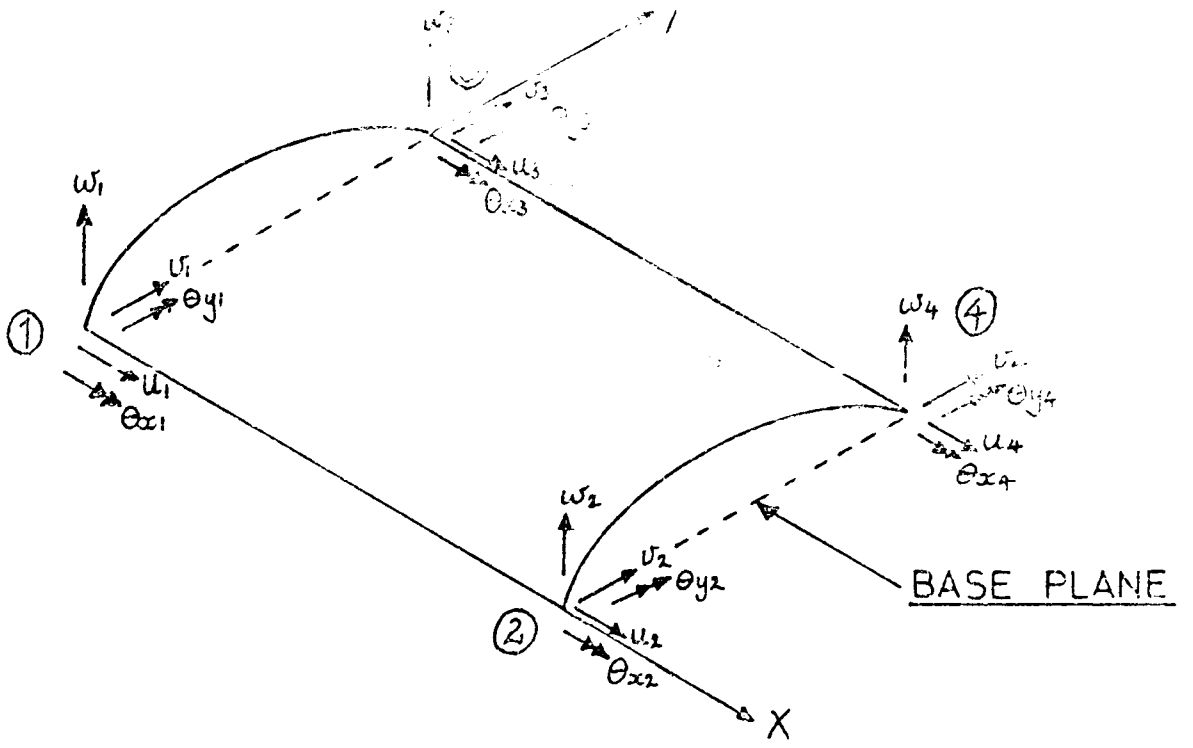

FIG. 5.1 THE EXISTING CYLINDRICAL SHELL ELEMENT

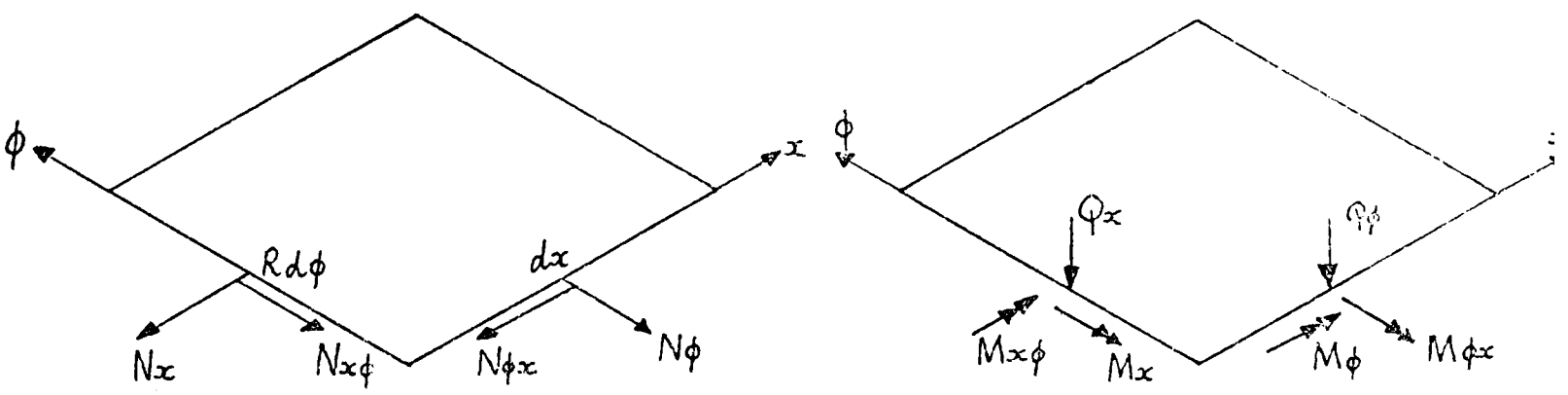

IN PLANE RESULTANTS. BENDING RESULTANTS

FIG. 5.2 STRESS RESULTANTS ON ELEMENTAL PORTION OF SHELL.

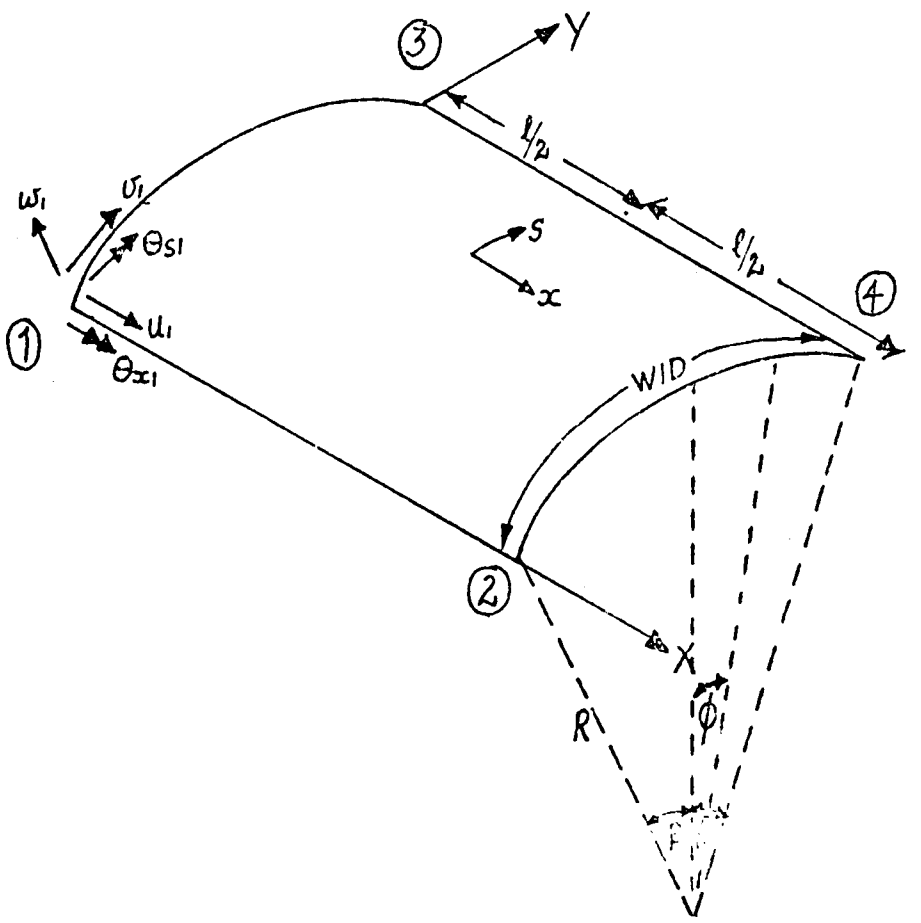

$s = R\phi$

$WID = 2R\beta$

NODAL VARIABLES

$$\begin{Bmatrix} u_i \\ v_i \\ w_i \\ \theta_{xi} \\ \theta_{si} \end{Bmatrix} \quad i = 1,2,3,4$$

FIG. 5.3 THE NEW CYLINDRICAL SHELL ELEMENT.

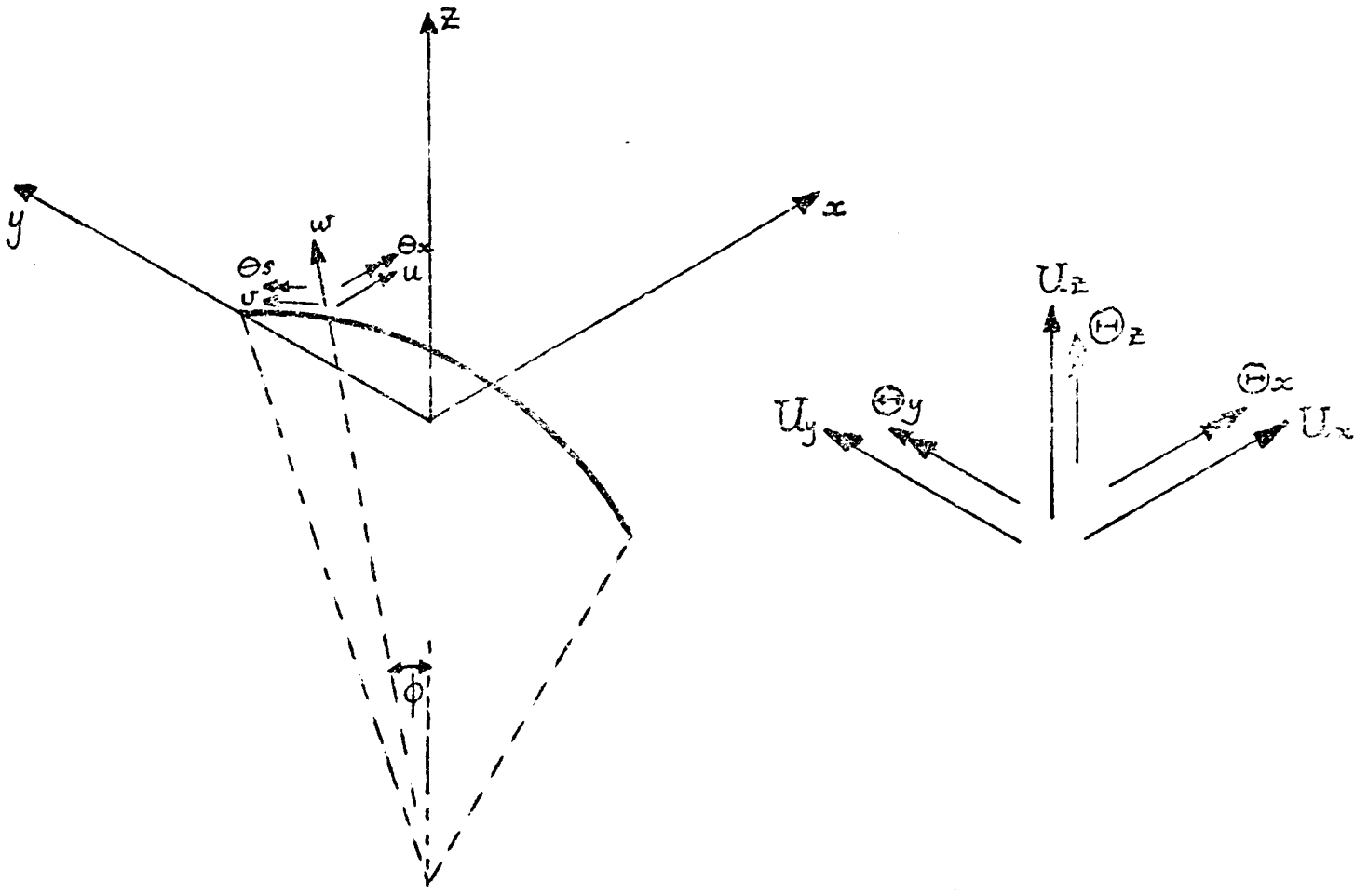

FIG. 5.4 RIGID BODY MOTIONS OF CURVED SIDE.

	1	2	3	4	5	6	7	8	9	10	11	12	13	14	15	16	17	18	19	20	21	22	23	24	25	26	27	28	29
	1	x	s														x^2	xs	s^2			$\frac{-x^2}{R}$							
				1	x	s											s^2			x^2	xs								
ϕ		-s				-x	1						$\frac{-x}{R}$	$\frac{1}{R}$	$\frac{-x}{R}$	$\frac{s}{R}$	-2xs	$\frac{-s^2}{2}$			$\frac{-x^2}{2}$	$\frac{sx}{R}$				$\frac{-x^2}{2R}$	$\frac{-xs}{R}$	$\frac{-x^2}{R}$	$\frac{s^2}{R}$
x		-s				-x	1						$\frac{-x}{R}$		$\frac{-2x}{R}$		-2xs	$\frac{-s^2}{2}$			$\frac{-x^2}{2}$	$\frac{2xs}{R}$				$\frac{-x^2}{2R}$		$\frac{-2x^2}{R}$	
=				$\frac{x^2}{2R}$	$\frac{x^3}{6R}$	$\frac{sx^2}{2R}$		1	x	s							$\frac{s^2x^2}{2R}$			$\frac{x^4}{12R}$	$\frac{sx^3}{6R}$	x^2	xs	s^2						
											1	x	s												x^2	xs	s^2		
														1	x	s						-xs					-xs	x^2	s^2
ϕ				$\frac{x}{R}$	$\frac{x^2}{2R}$	$\frac{sx}{R}$		1								1	$\frac{sx^2}{R}$			$\frac{x^3}{3R}$	$\frac{sx^2}{2R}$	x	s				-x		2s
													1		1							-s				x	s	2x	

β β_2

FIG.5.5 29 TERM QUADRATIC STRESS ASSUMPTION

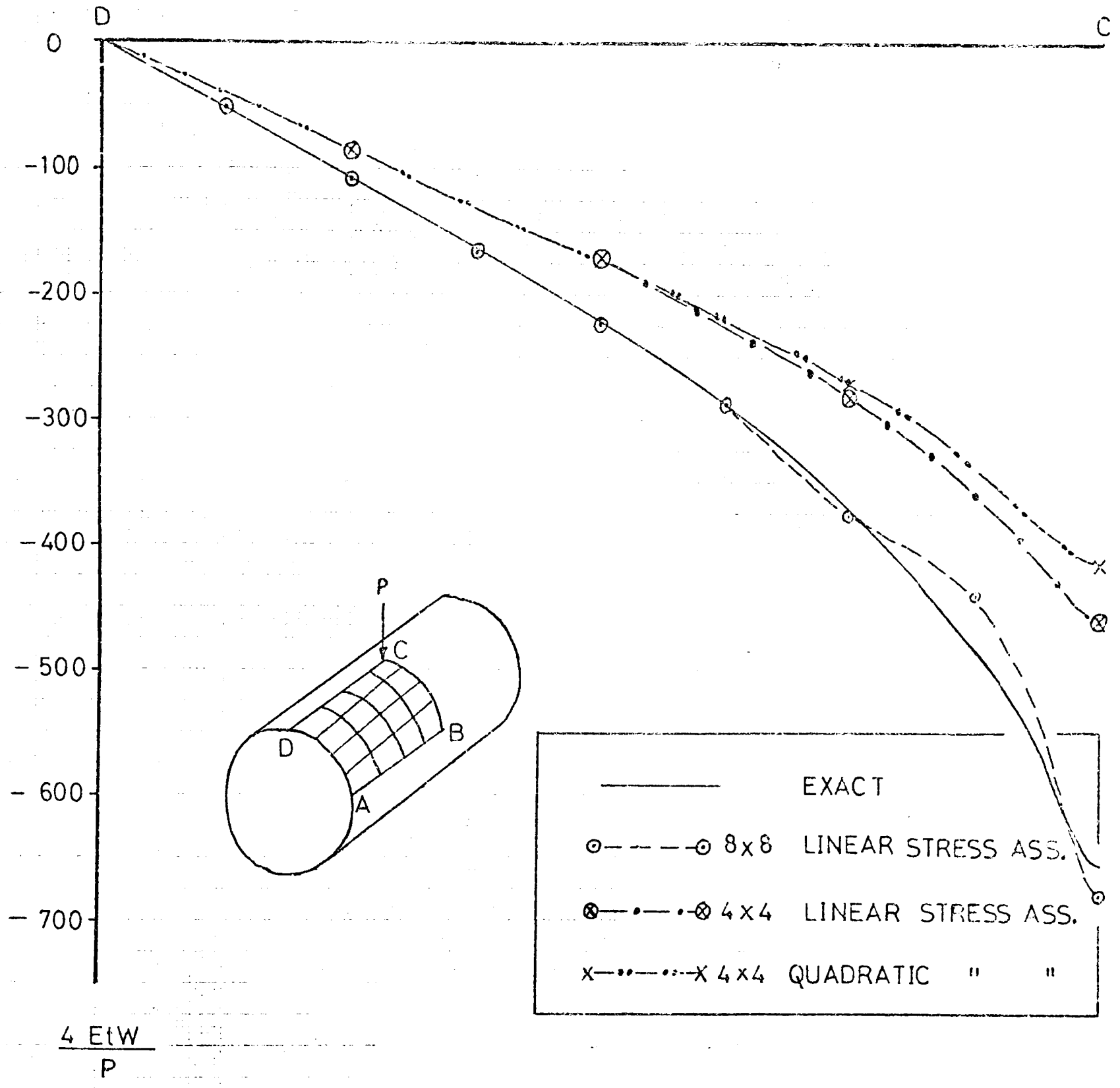

FIG. 5.6 DISPLACEMENTS OF PINCHED CYLINDRICAL SHELL USING HYBRID RECTANGLES.

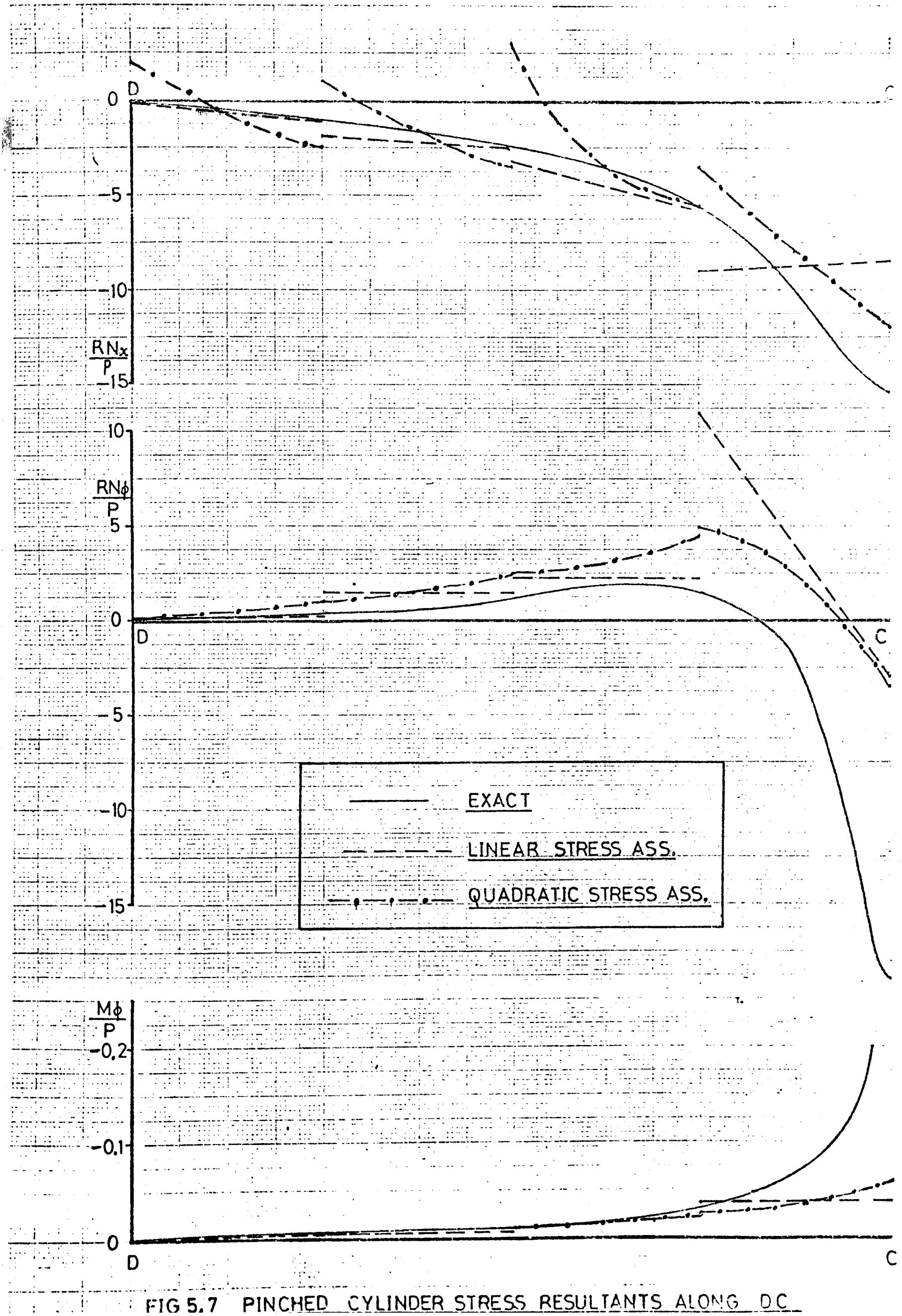

FIG 5.7 PINCHED CYLINDER STRESS RESULTANTS ALONG DC

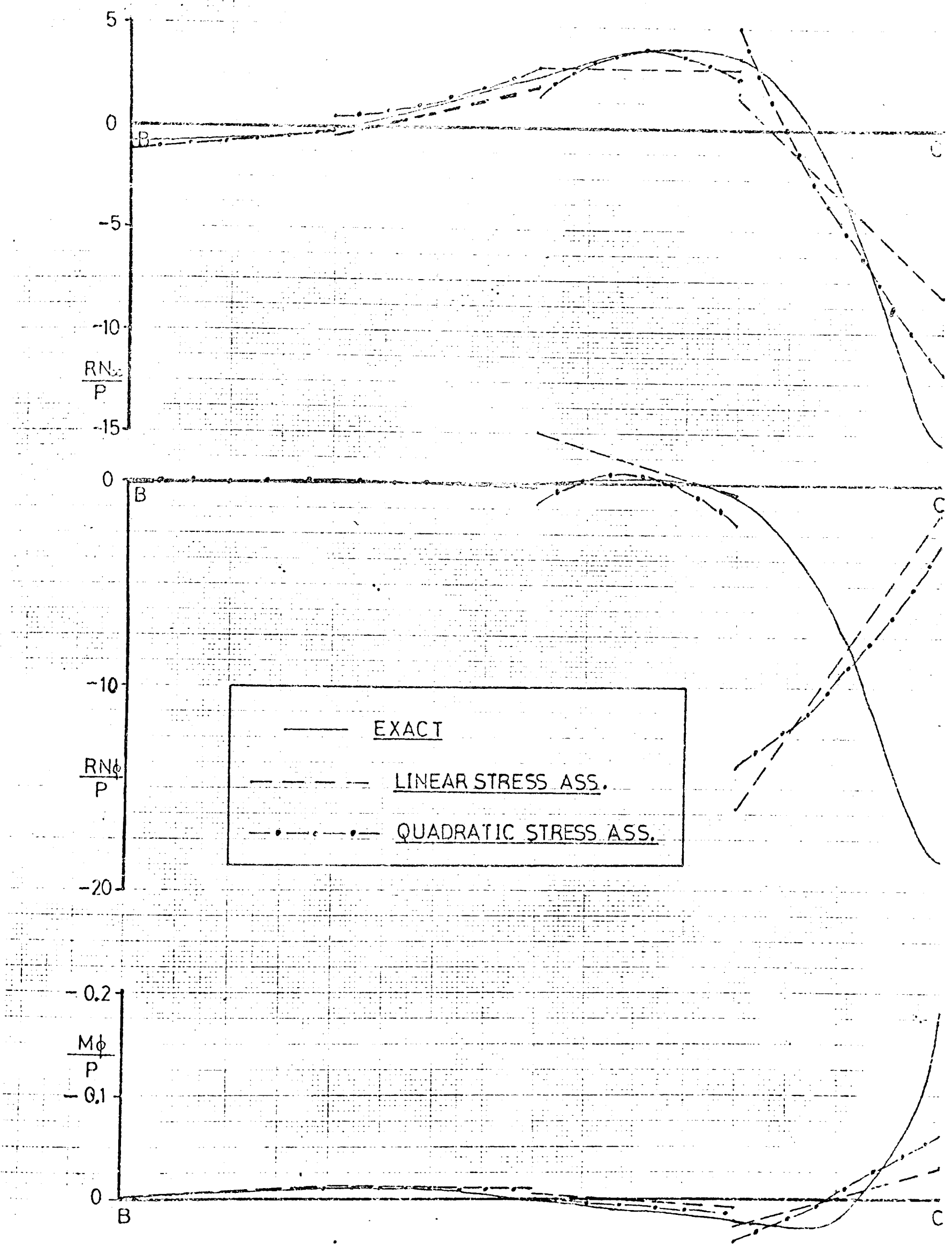

FIG. 5.8 PINCHED CYLINDER STRESS RESULTANTS ALONG BC USING 4X4 MESH OF RECTANGULAR ELEMENTS.

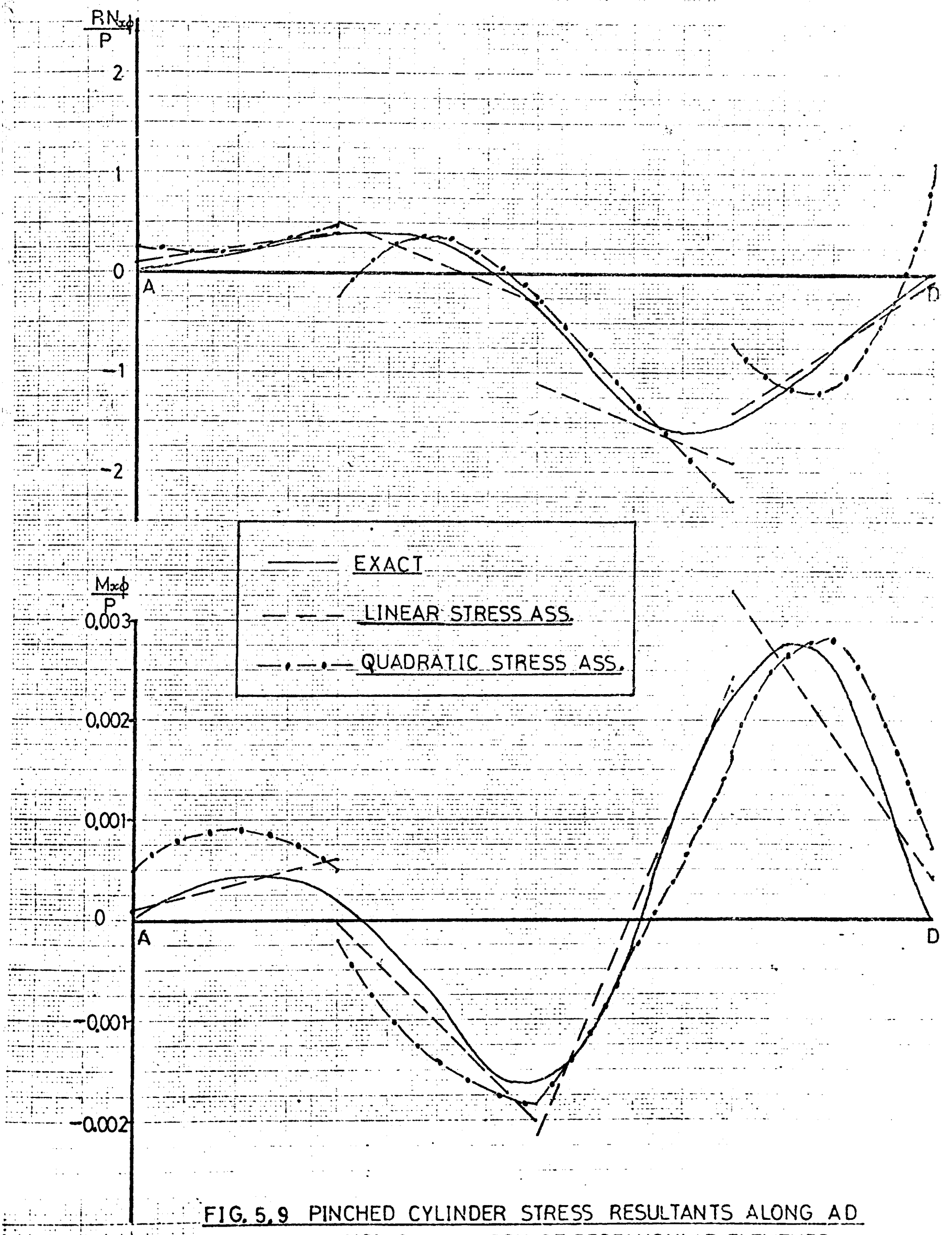

FIG. 5.9 PINCHED CYLINDER STRESS RESULTANTS ALONG AD USING 4x4 MESH OF RECTANGULAR ELEMENTS.

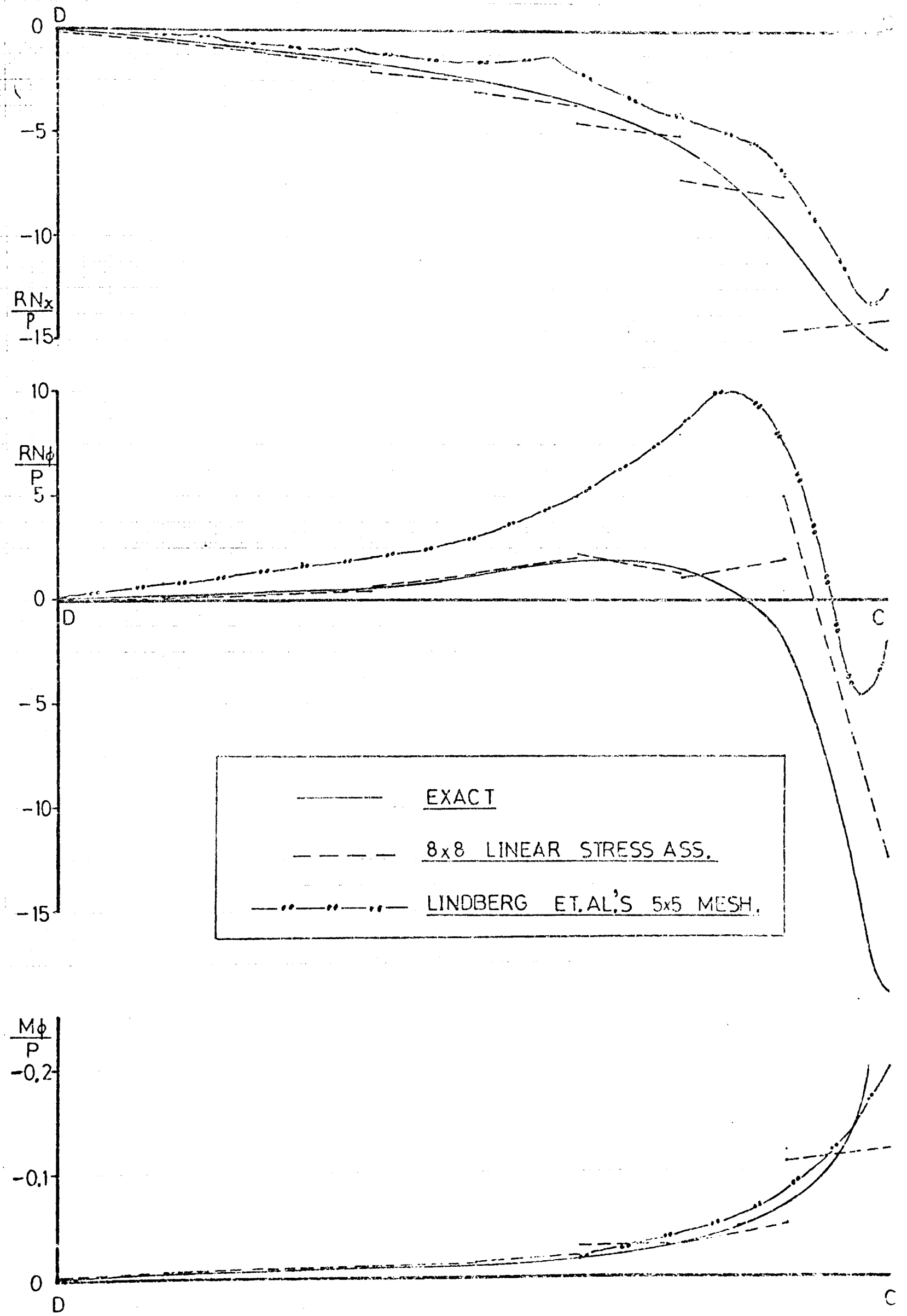

FIG 5.10 PINCHED CYLINDER STRESS RESULTANTS ALONG DC
USING 8x8 MESH OF RECTANGULAR ELEMENTS

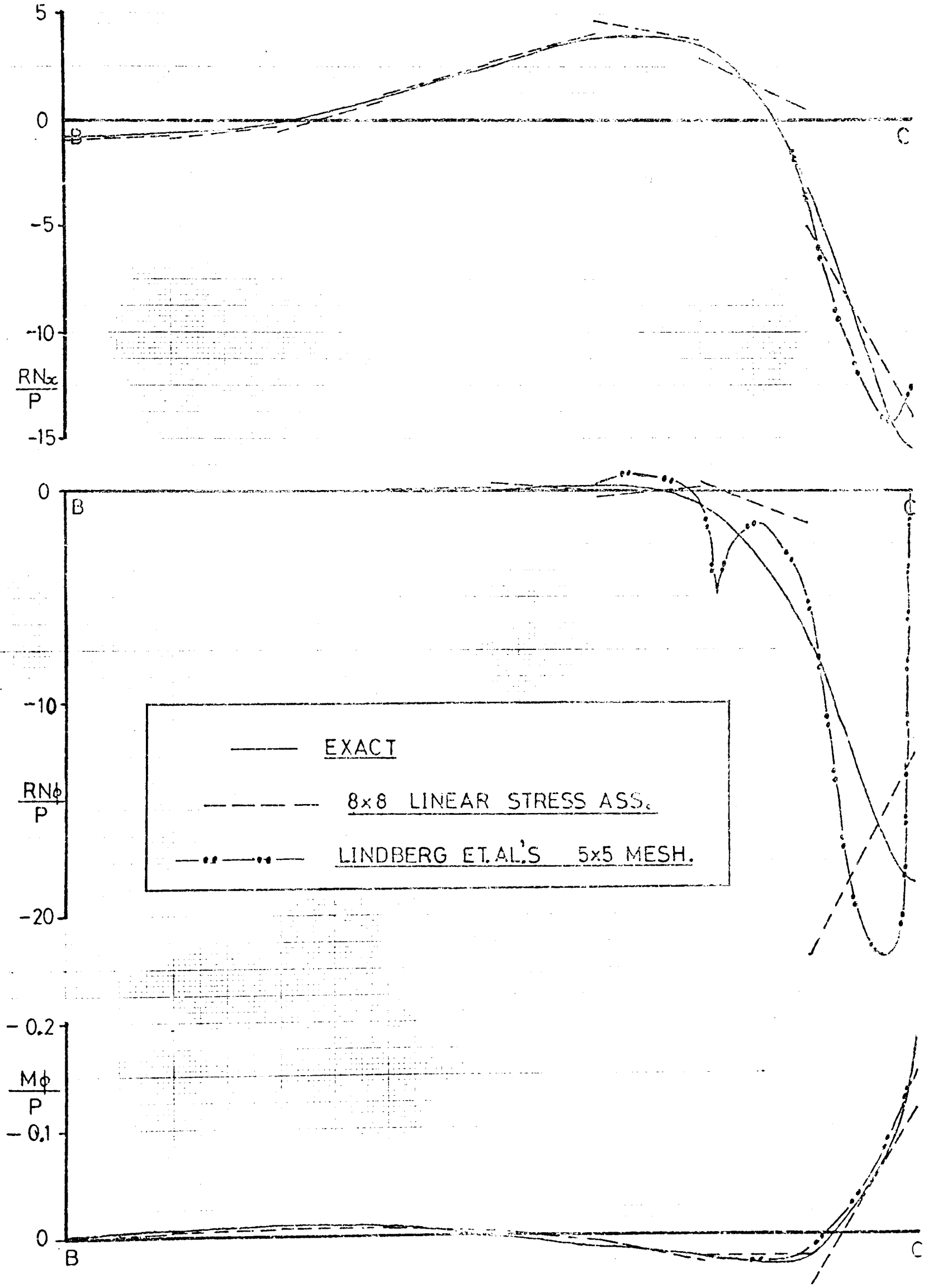

FIG. 5.11 PINCHED CYLINDER STRESS RESULTANTS ALONG BC USING 8x8 MESH OF RECTANGULAR ELEMENTS

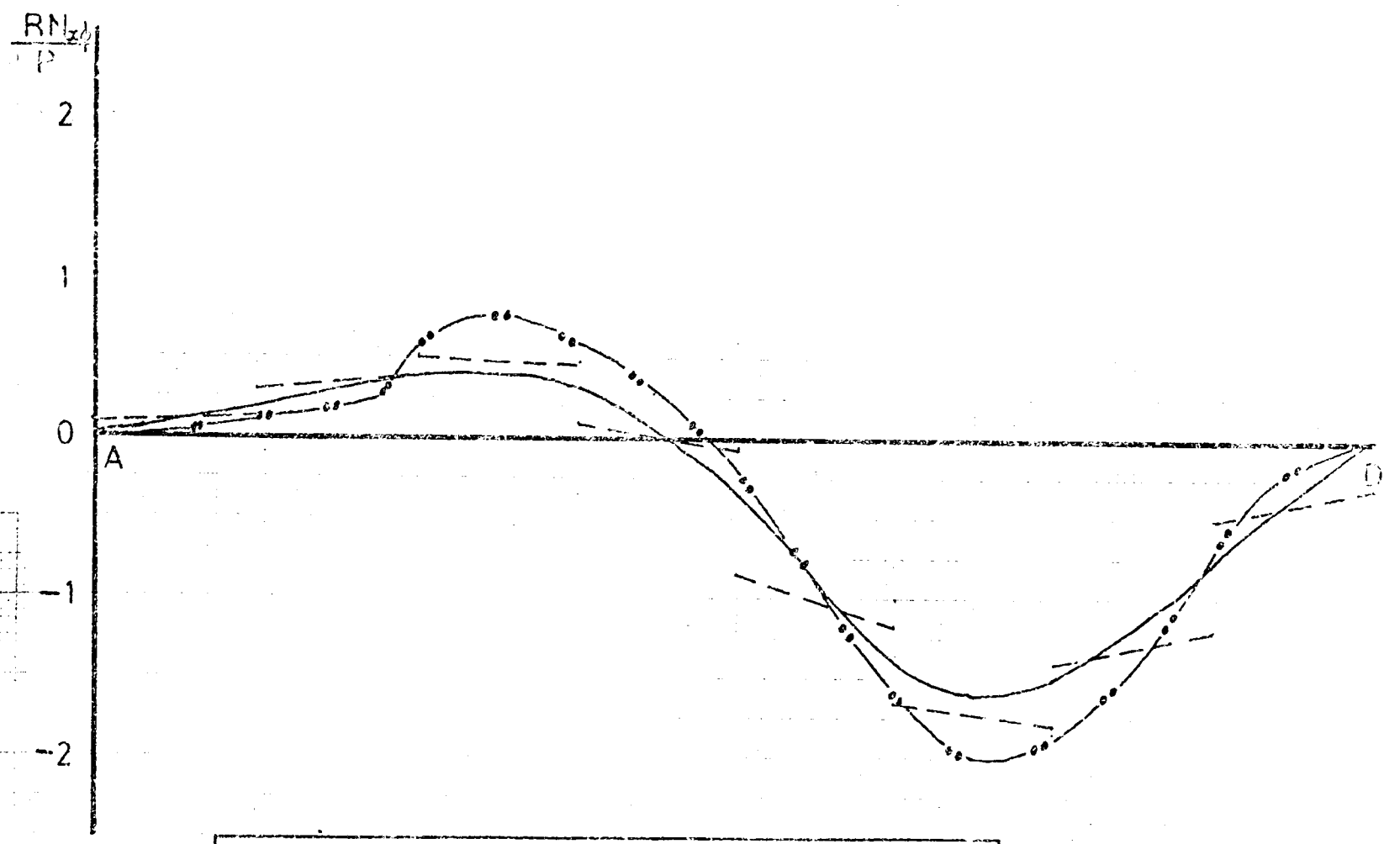

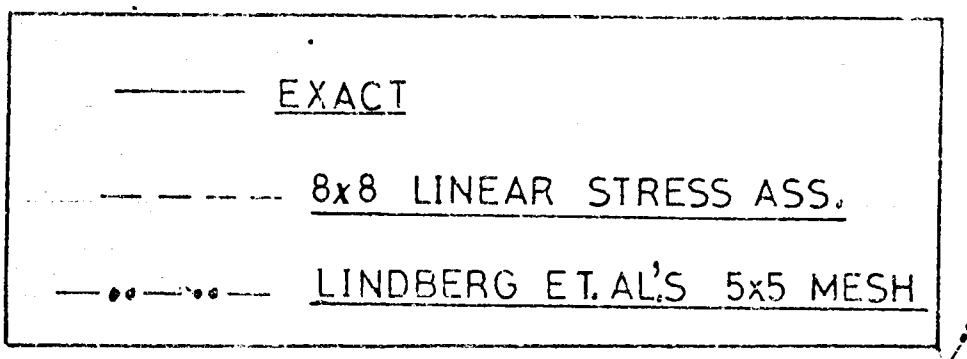

FIG. 5.12 PINCHED CYLINDER STRESS RESULTANTS ALONG AD USING 8 x 8 MESH OF RECTANGULAR ELEMENTS.

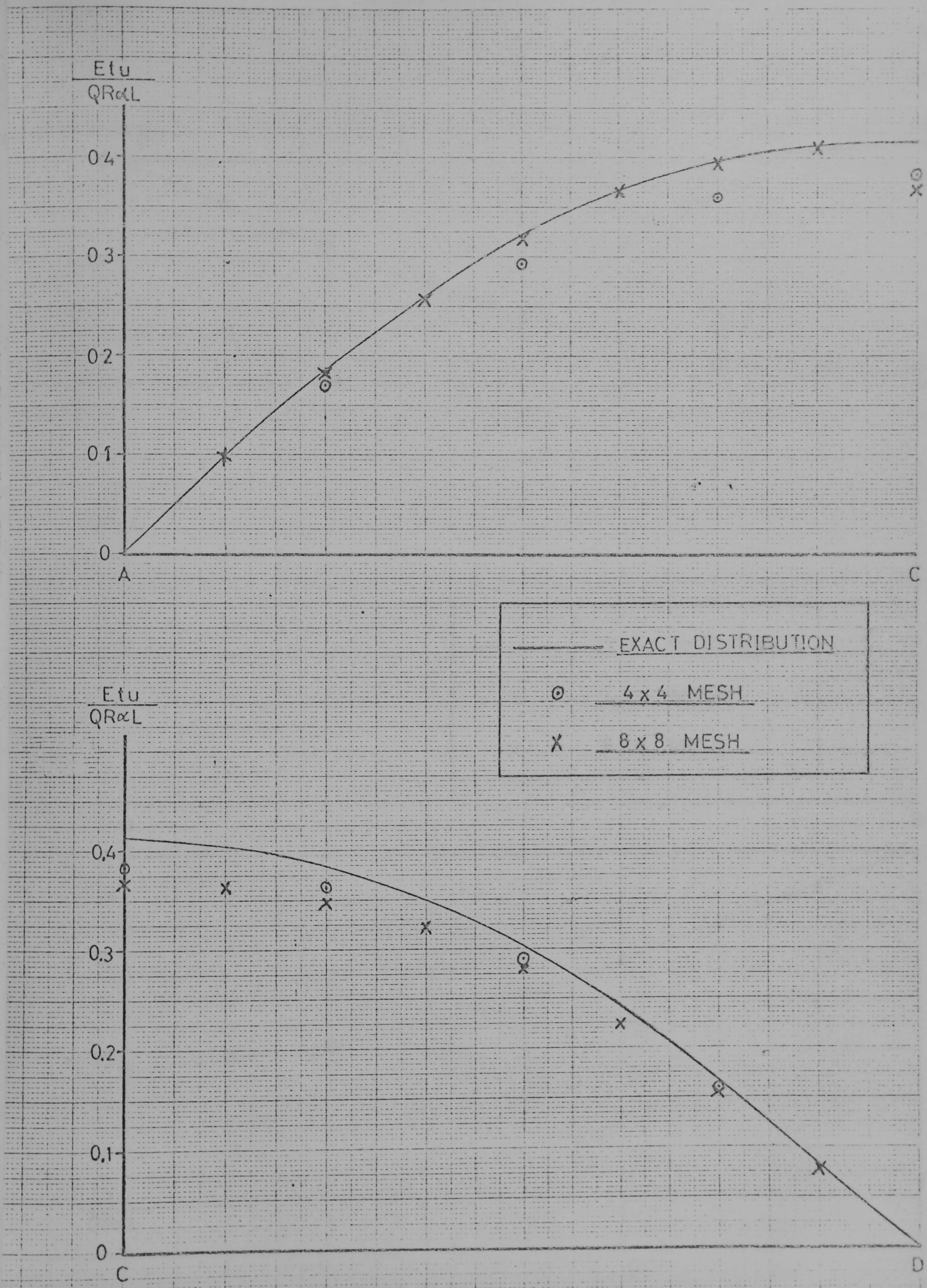

FIG 5.13u DISPLACEMENTS OF PANEL USING $\frac{4 \times 4}{8 \times 8}$ MESH OF RECTANGULAR ELEMENTS

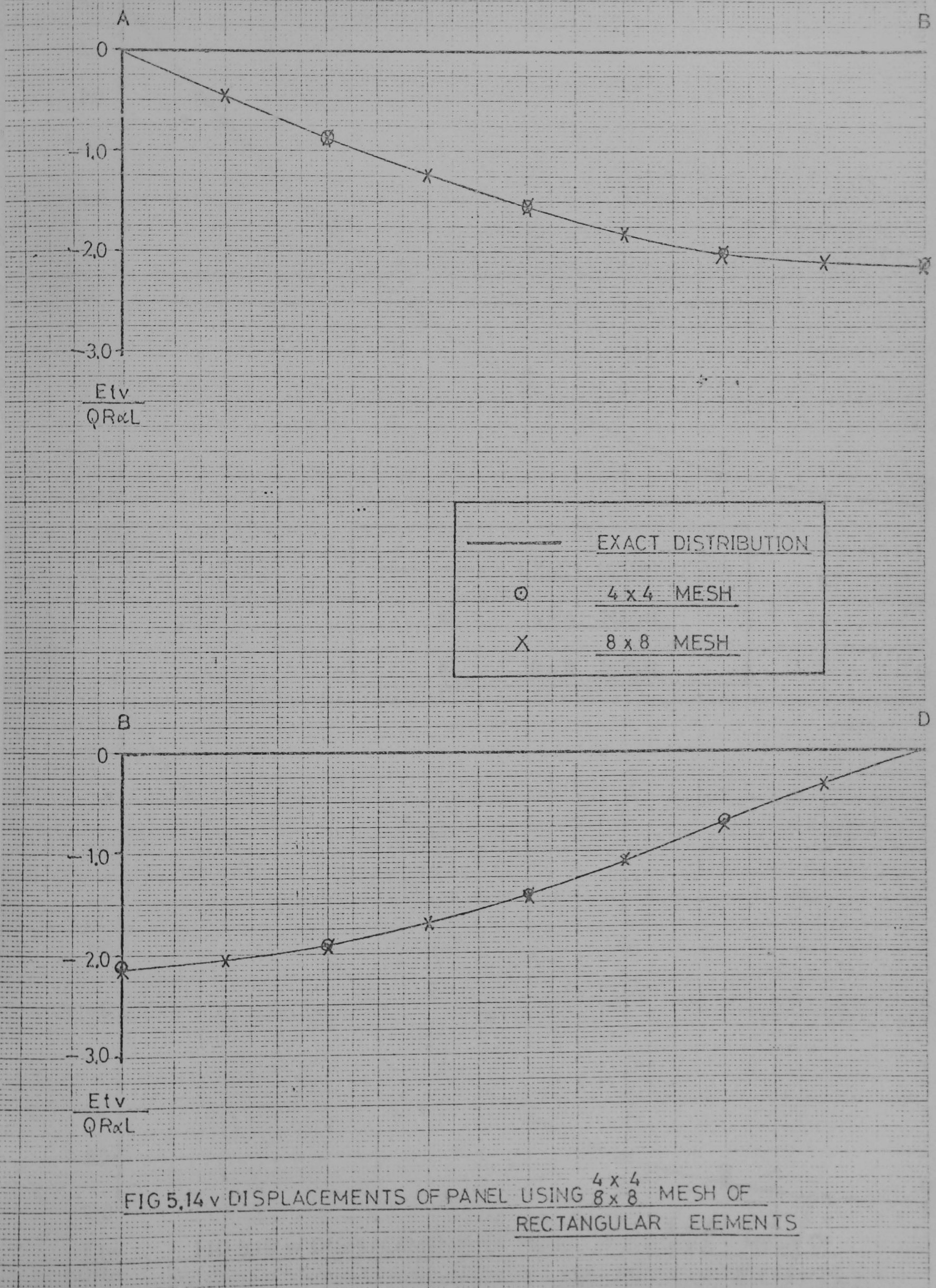

FIG 5.14 v DISPLACEMENTS OF PANEL USING $\frac{4 \times 4}{8 \times 8}$ MESH OF RECTANGULAR ELEMENTS

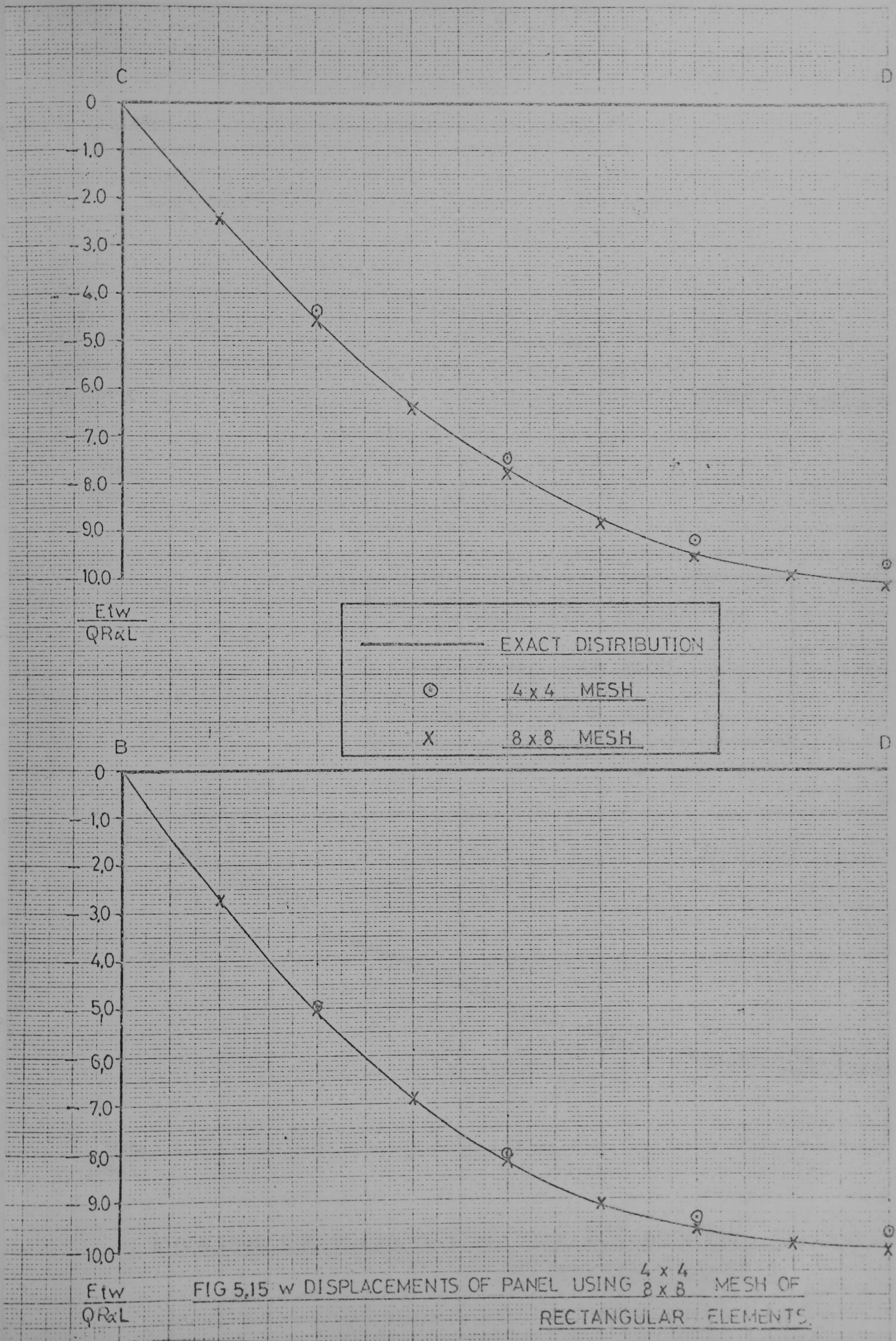

FIG 5.15 w DISPLACEMENTS OF PANEL USING $\frac{4 \times 4}{8 \times 8}$ MESH OF RECTANGULAR ELEMENTS.

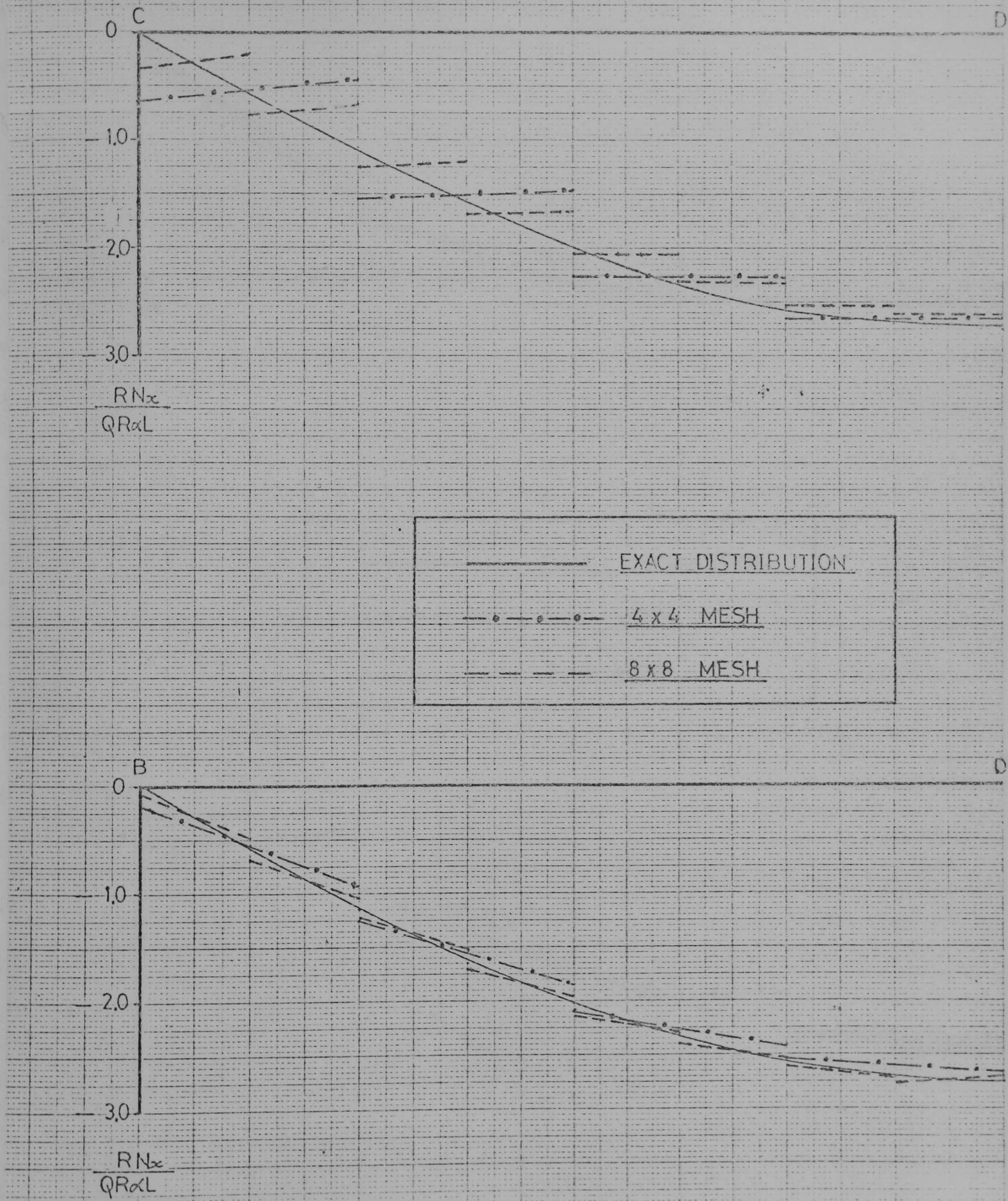

FIG 5.16 N_x STRESS RES. ON PANEL USING $\frac{4 \times 4}{8 \times 8}$ MESH OF RECTANGULAR ELEMENTS.

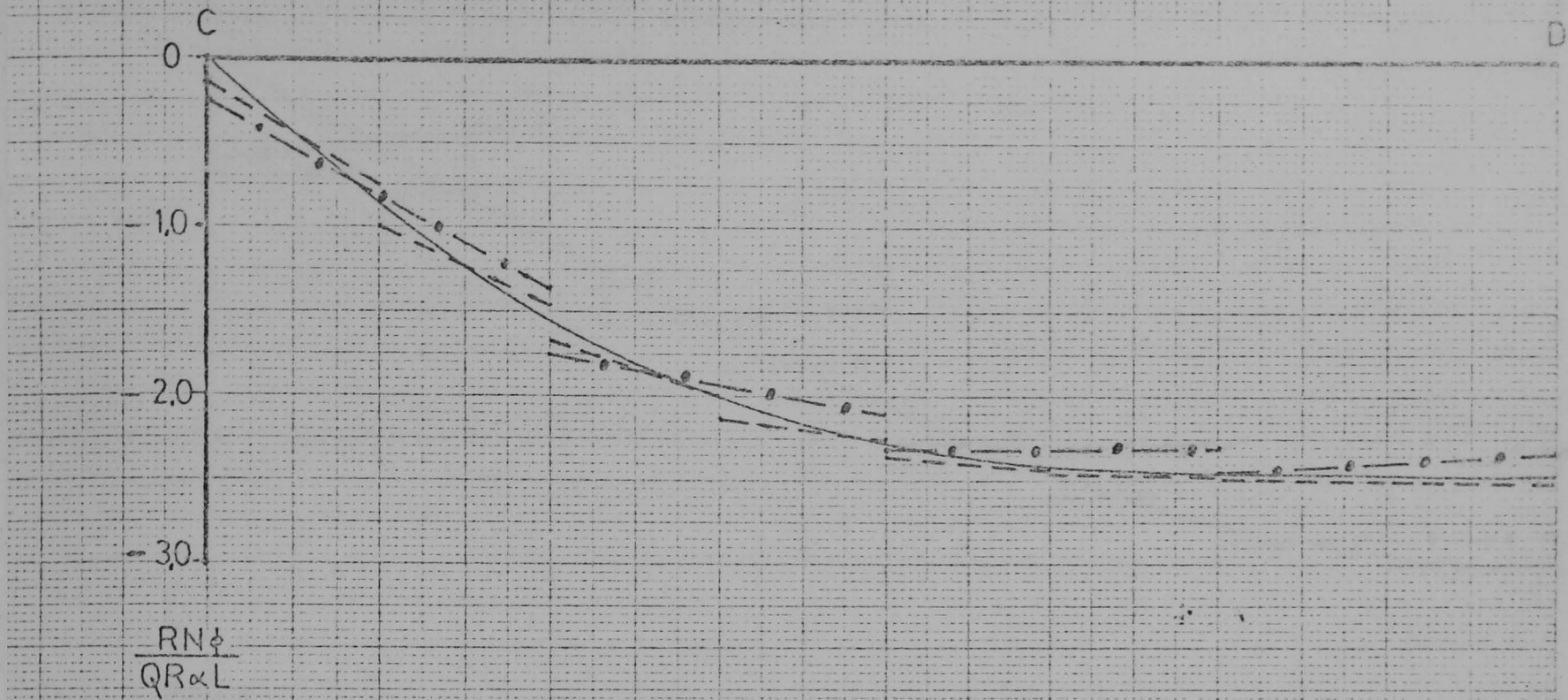

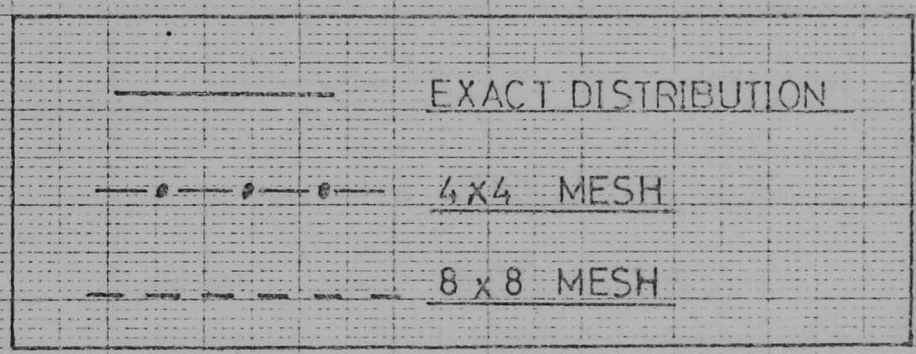

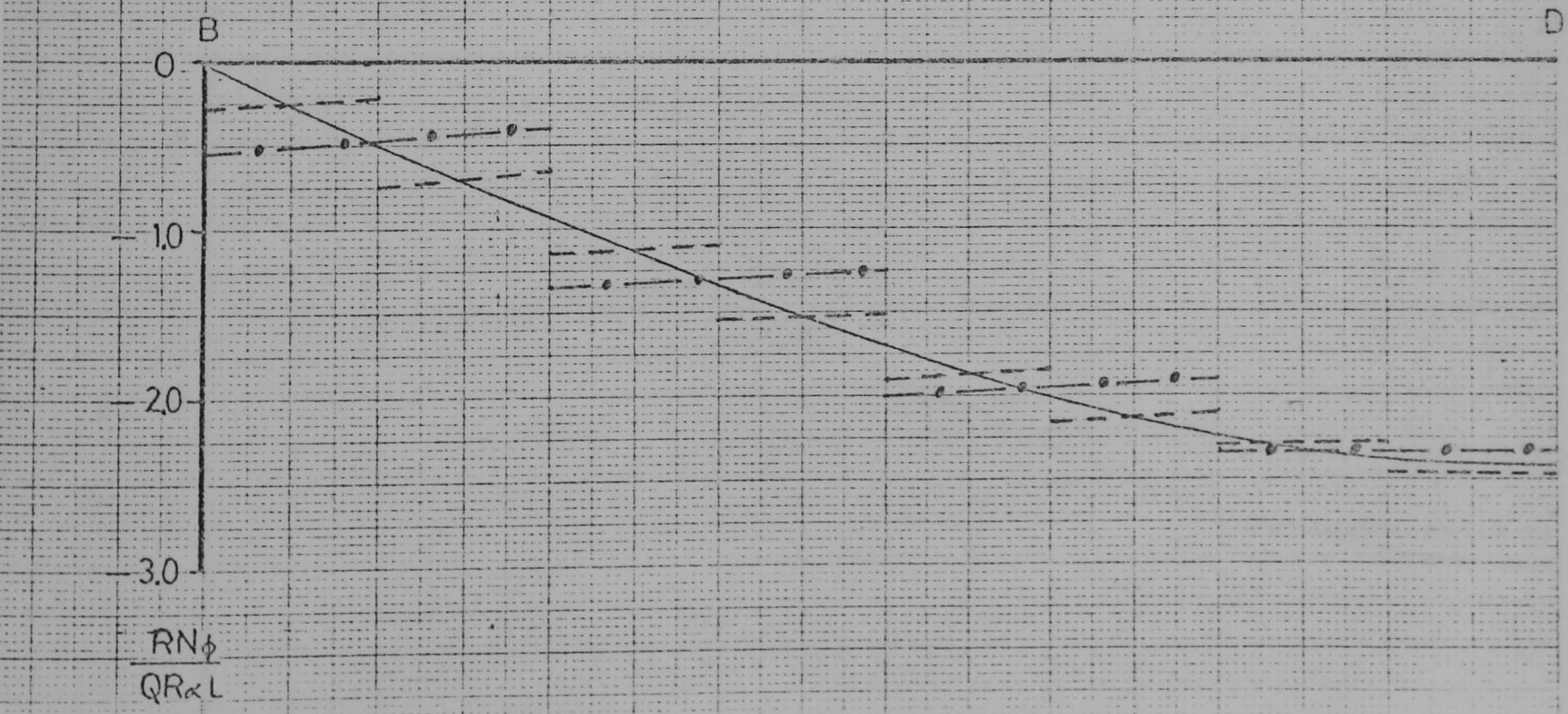

FIG. 5.17 N_ϕ STRESS RES. ON PANEL USING $\frac{4 \times 4}{8 \times 8}$ MESH OF RECTANGULAR ELEMENTS

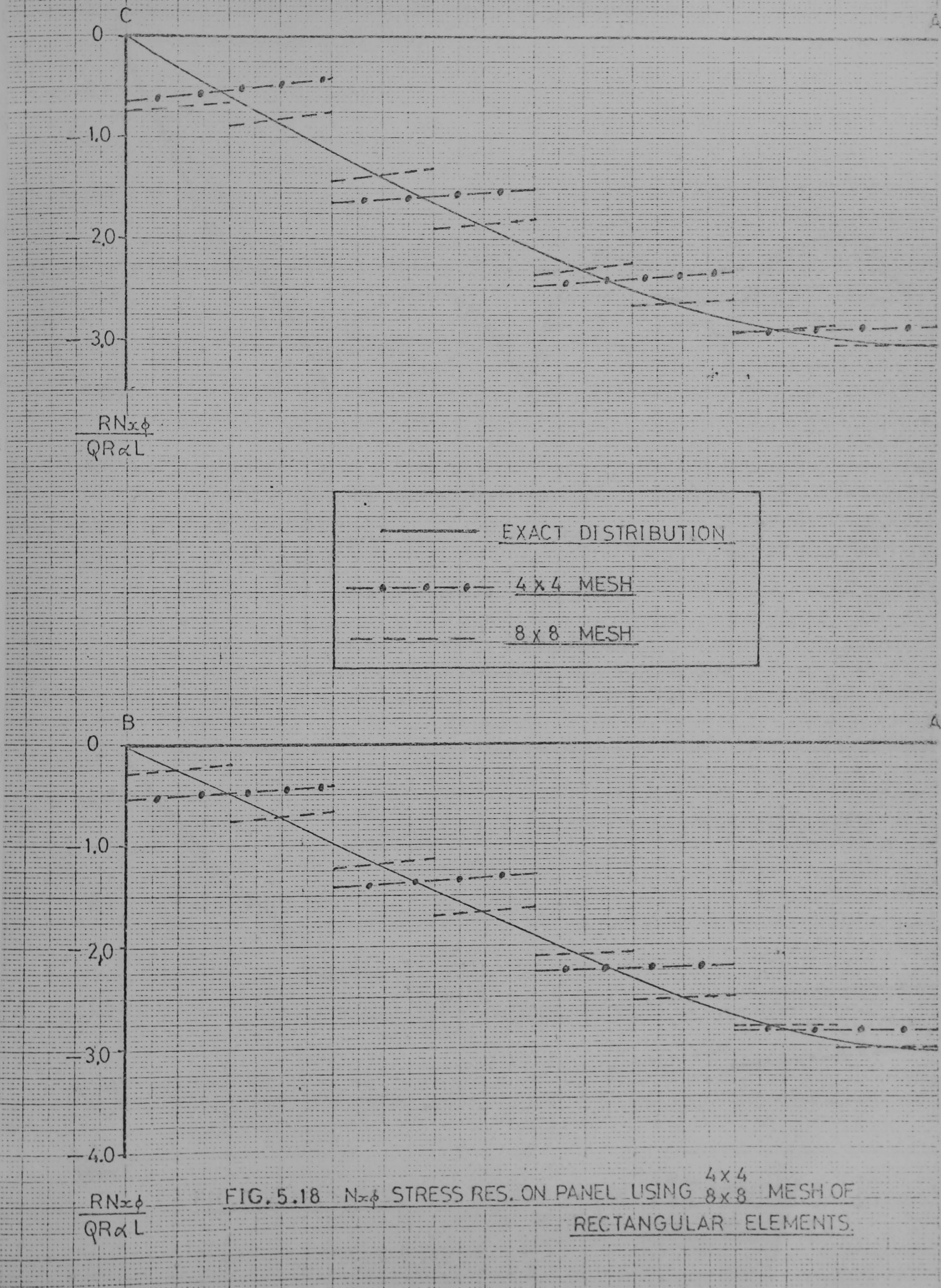

FIG. 5.18 $N_{x\phi}$ STRESS RES. ON PANEL USING $\frac{4\times4}{8\times8}$ MESH OF RECTANGULAR ELEMENTS.

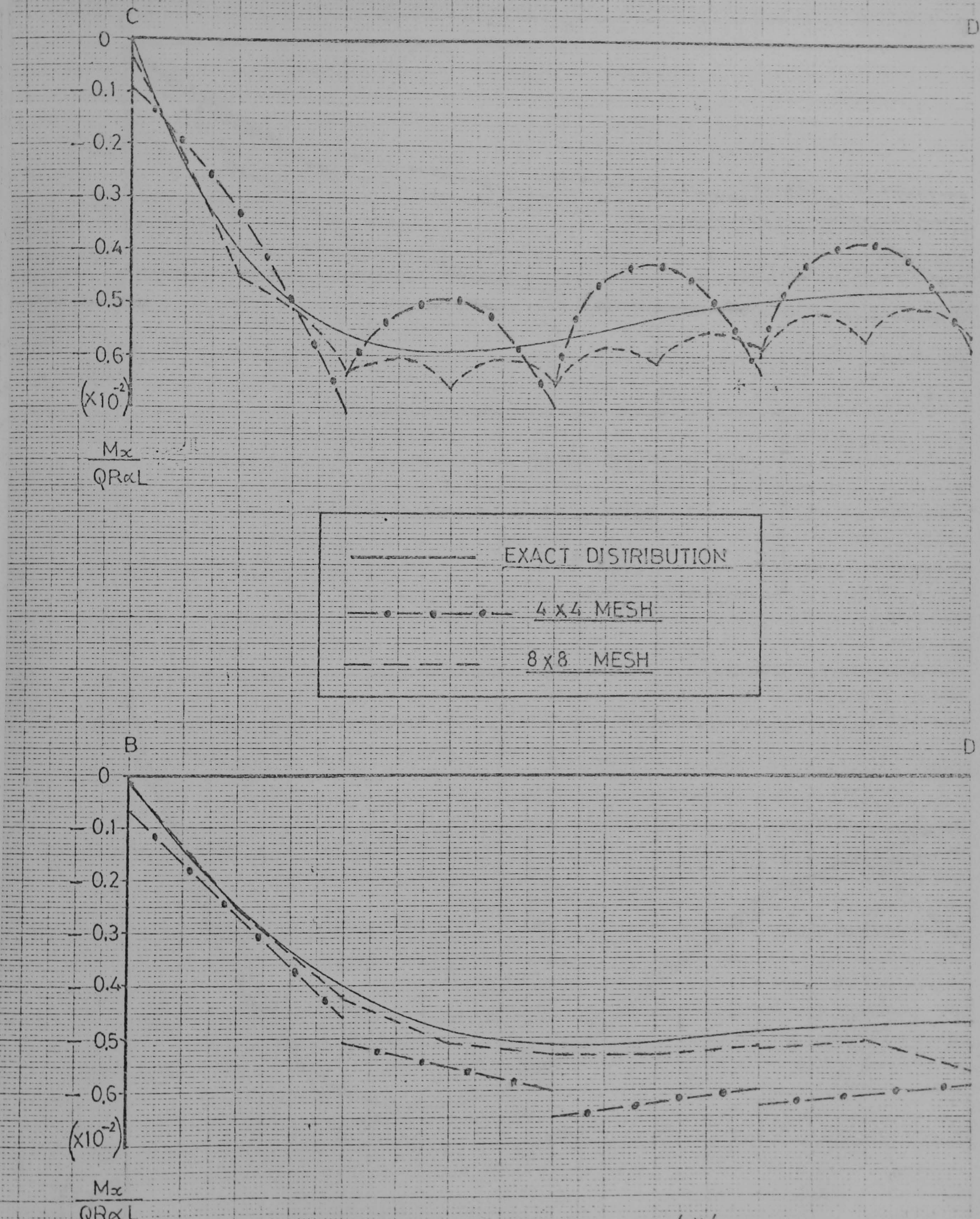

FIG. 5.19 M_x STRESS RES. ON PANEL USING $\overset{4\times4}{8\times8}$ MESH OF RECTANGULAR ELEMENTS

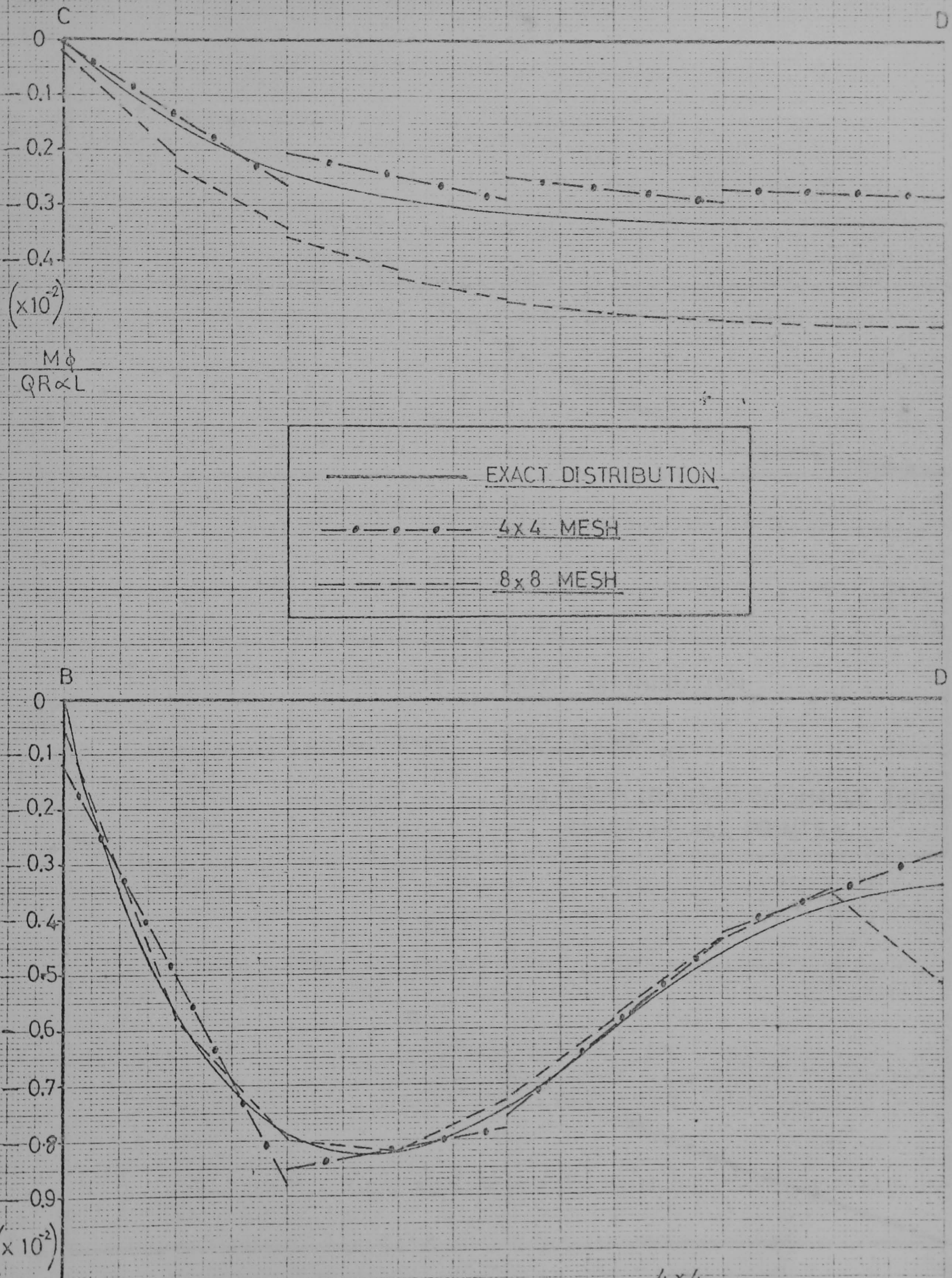

FIG 5.20 Mϕ STRESS RES. ON PANEL USING $\frac{4\times4}{8\times8}$ MESH OF RECTANGULAR ELEMENTS.

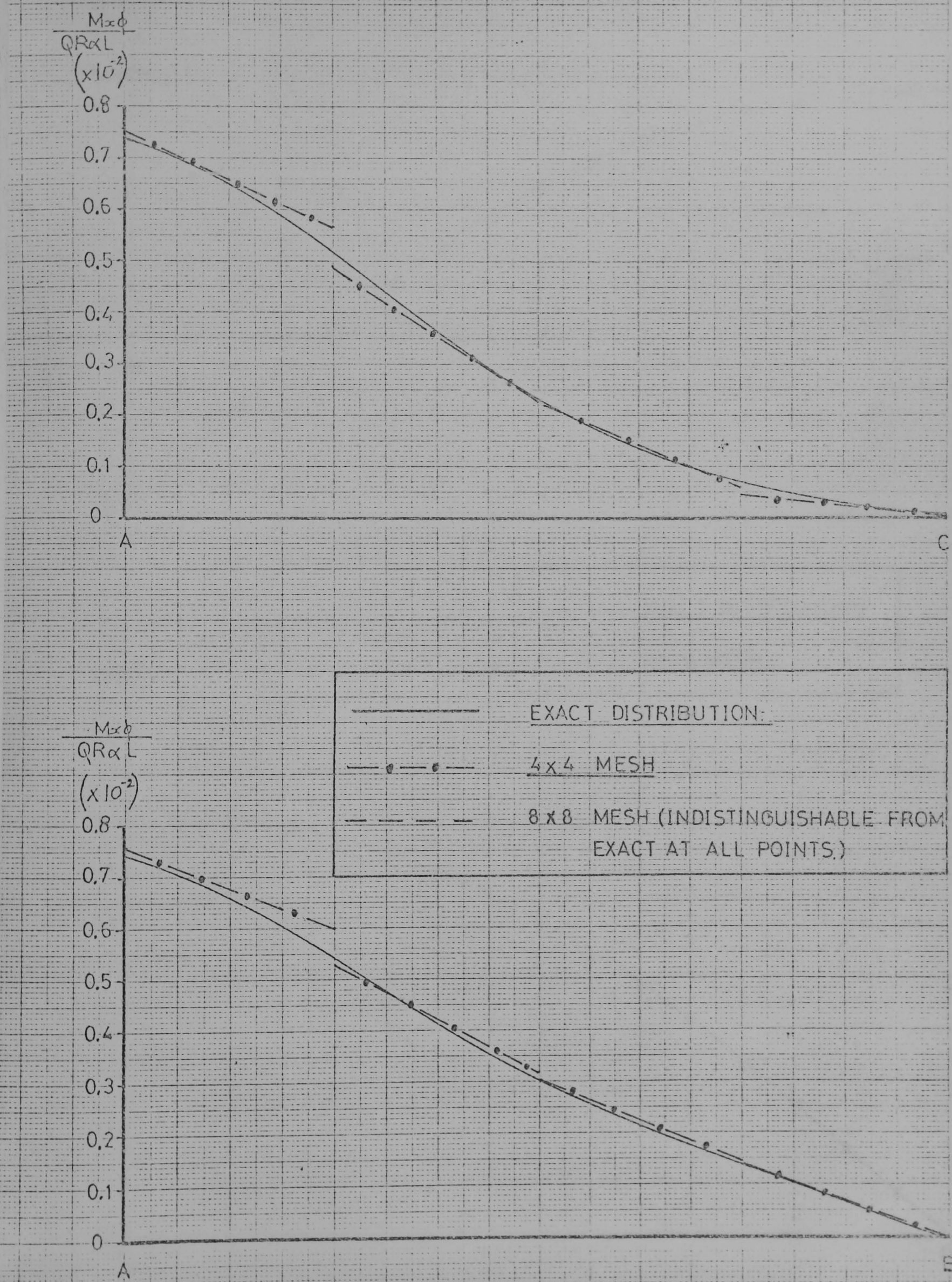

FIG. 5.21 Mxφ STRESS RES. ON PANEL USING $\frac{4 \times 4}{8 \times 8}$ MESH OF RECTANGULAR ELEMENTS.

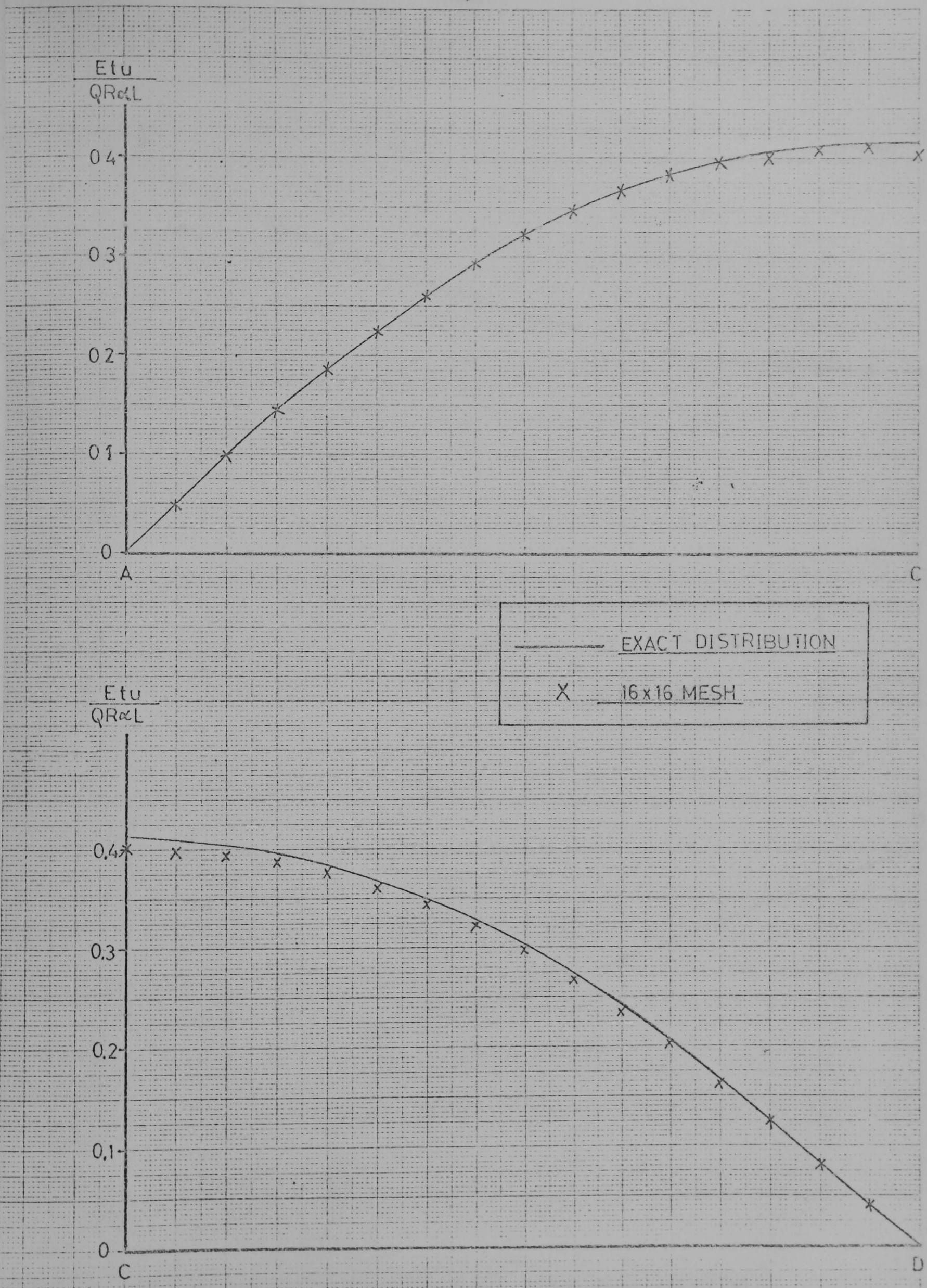

FIG. 5.22u DISPLACEMENTS OF PANEL USING 16 x 16 MESH OF RECTANGULAR ELEMENTS

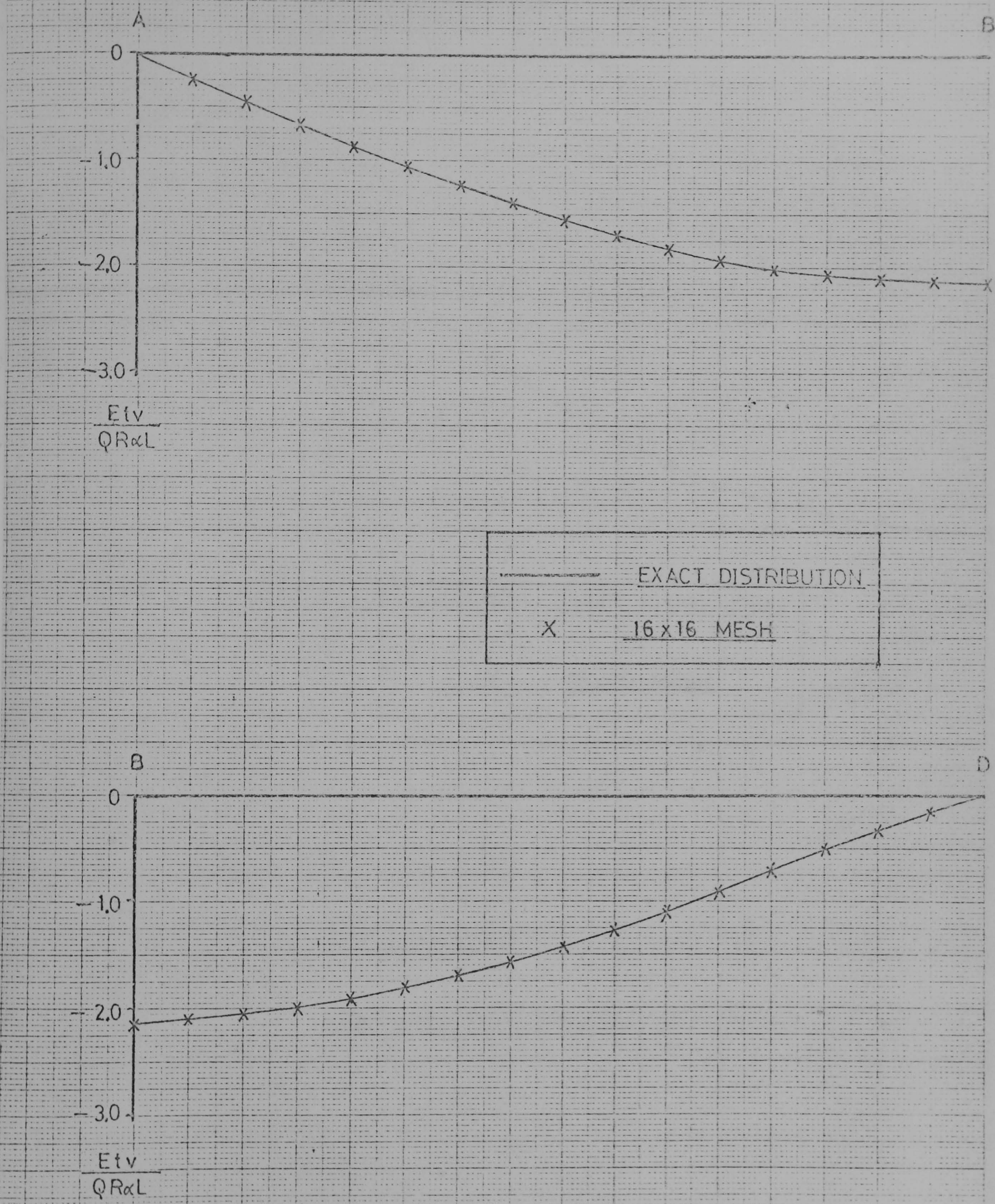

FIG 5.23 v DISPLACEMENTS OF PANEL USING 16 x 16 MESH OF RECTANGULAR ELEMENTS

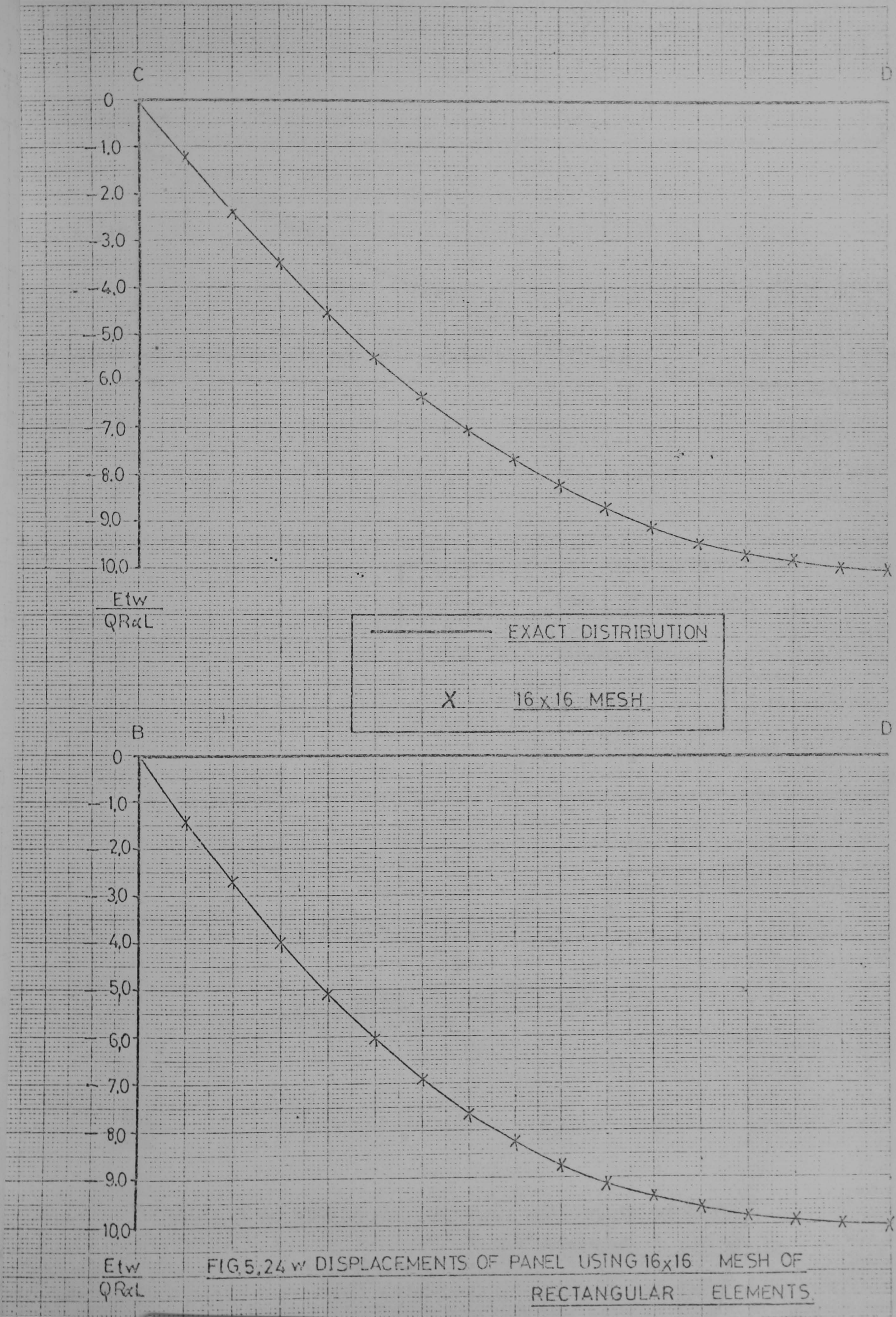

FIG. 5.24 w DISPLACEMENTS OF PANEL USING 16x16 MESH OF RECTANGULAR ELEMENTS.

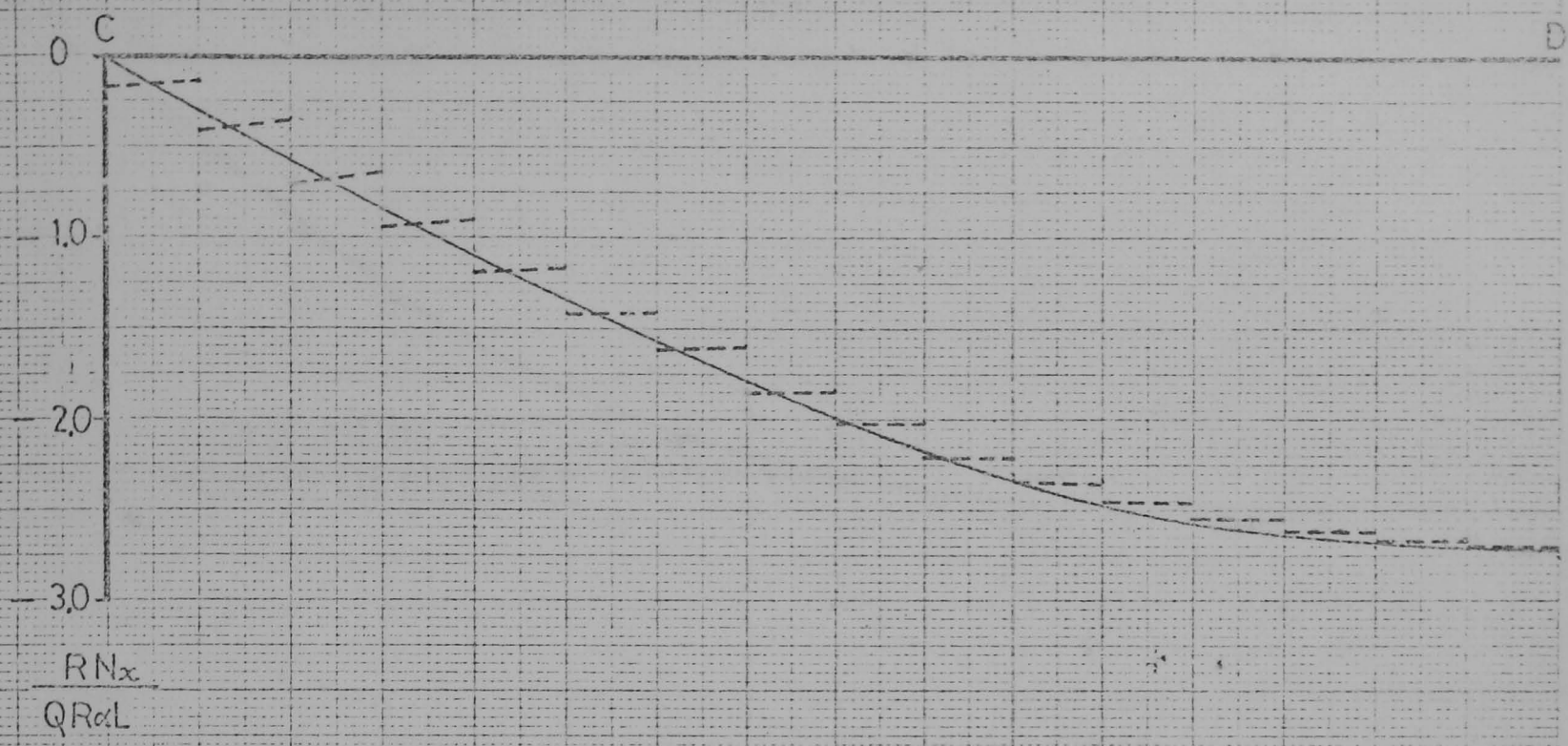

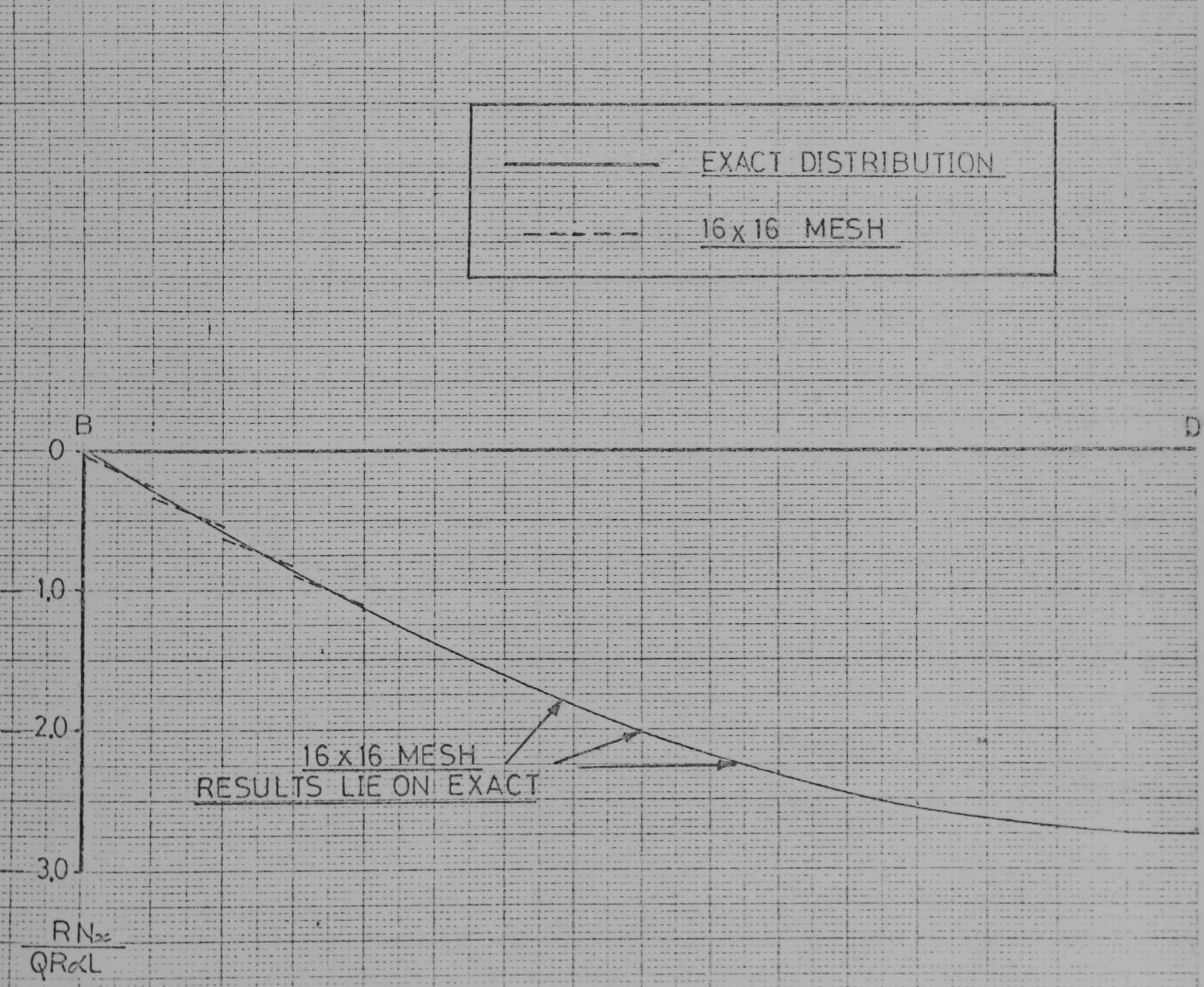

FIG 5.25 N_x STRESS RES. ON PANEL USING 16 x 16 MESH OF RECTANGULAR ELEMENTS.

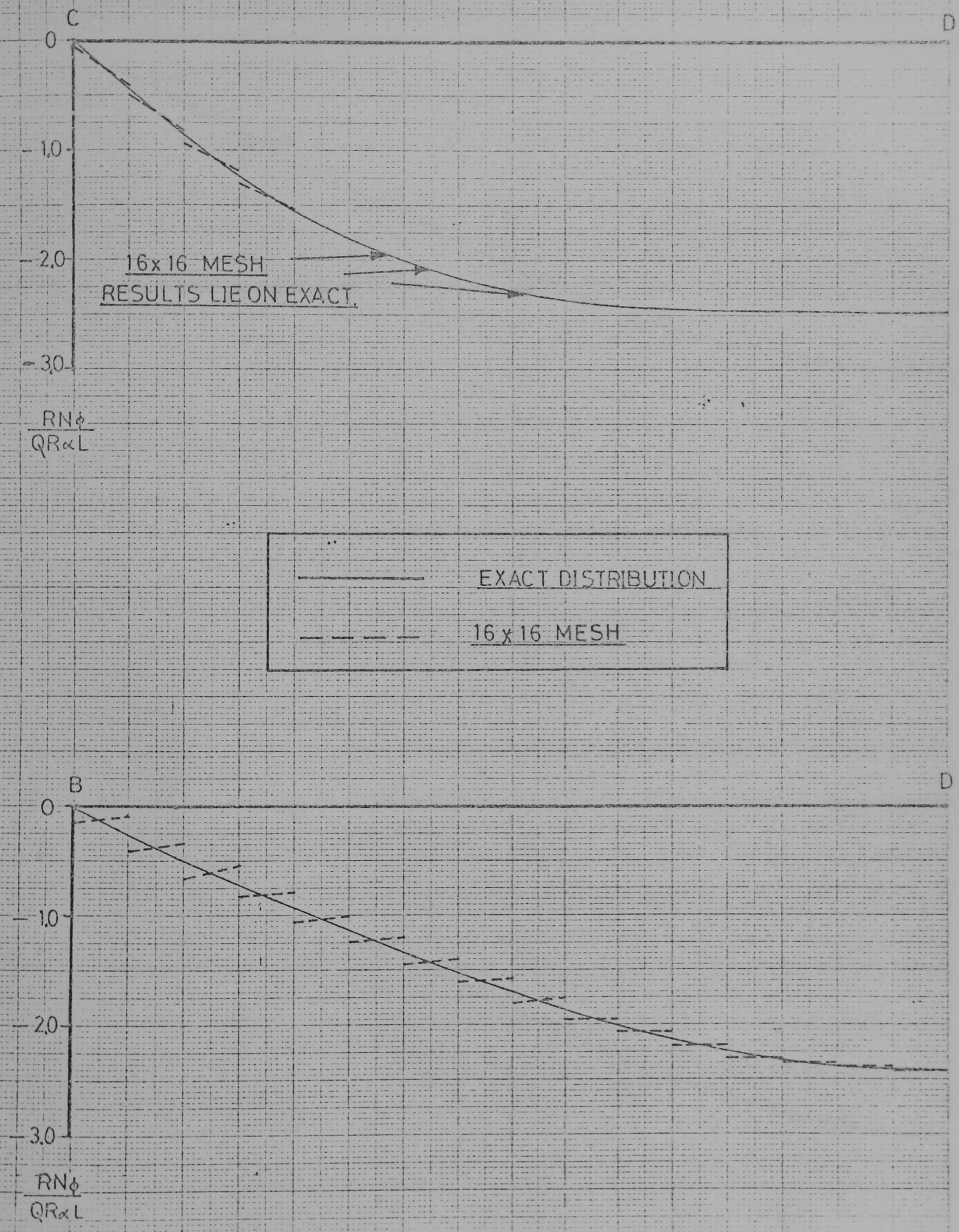

FIG. 5.26 Nφ STRESS RES. ON PANEL USING 16x16 MESH OF RECTANGULAR ELEMENTS

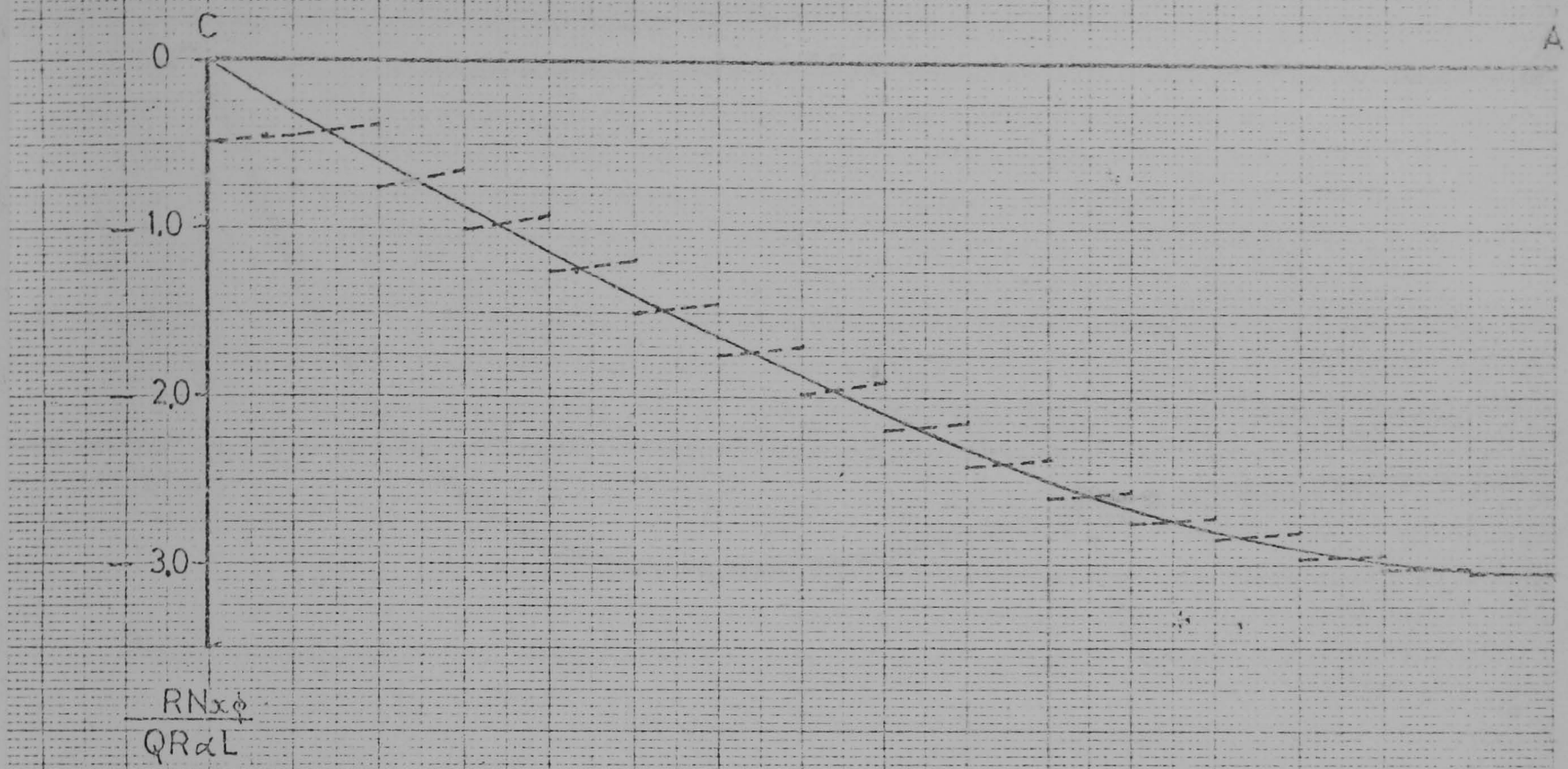

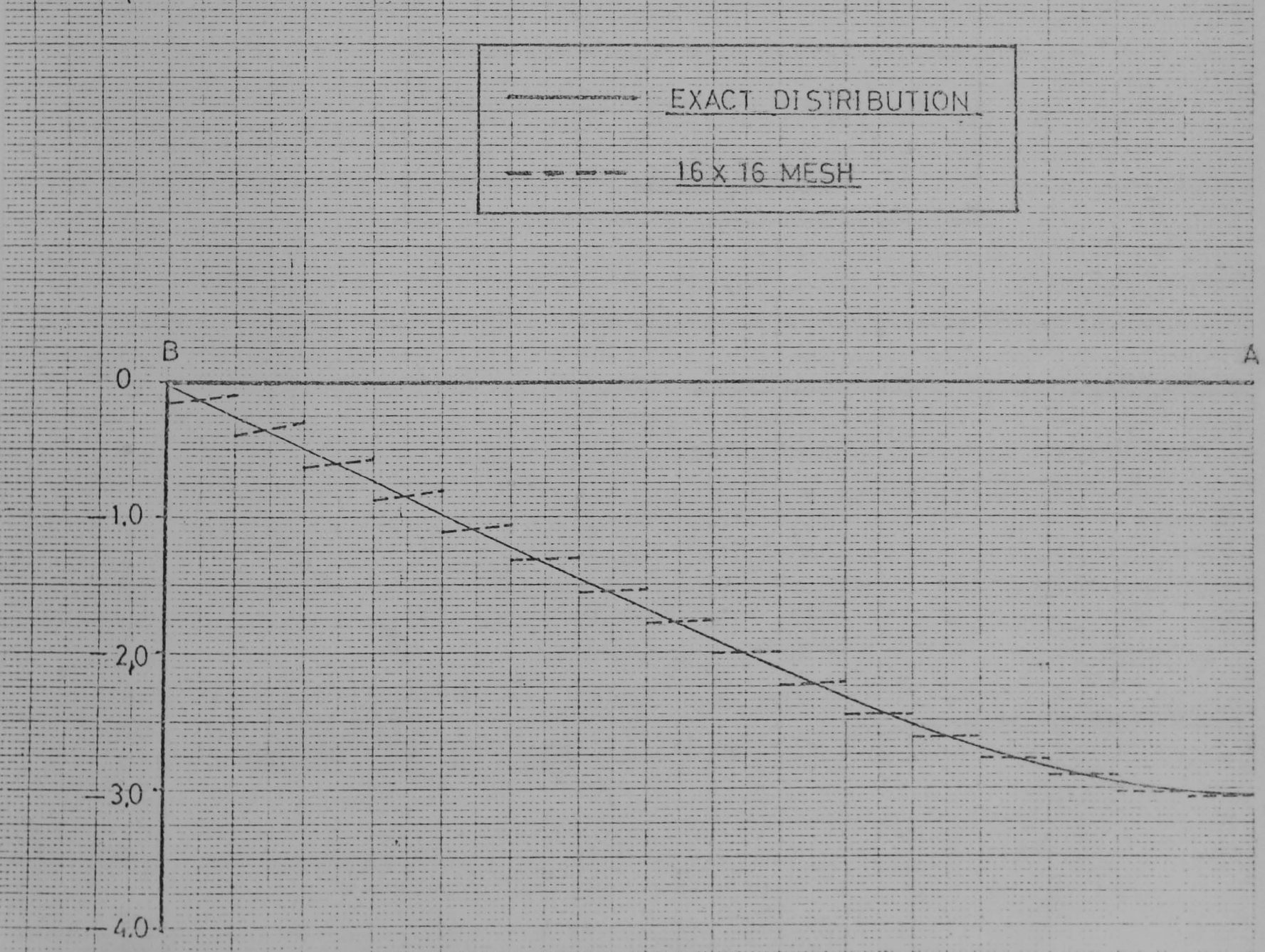

FIG 5.27 $N_{x\phi}$ STRESS RES. ON PANEL USING 16x16 MESH OF RECTANGULAR ELEMENTS.

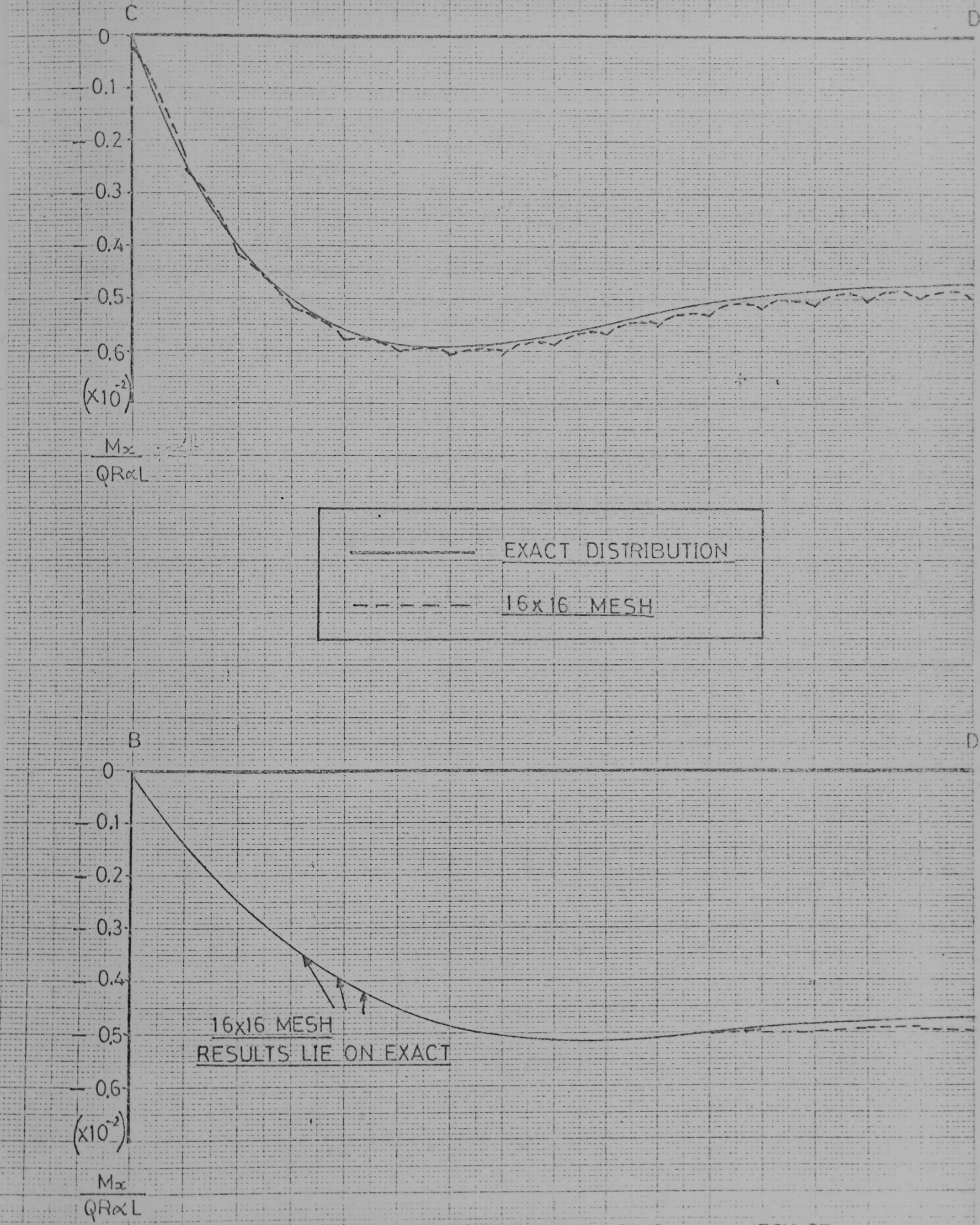

FIG.5.28 M_x STRESS RES. ON PANEL USING 16x16 MESH OF RECTANGULAR ELEMENTS

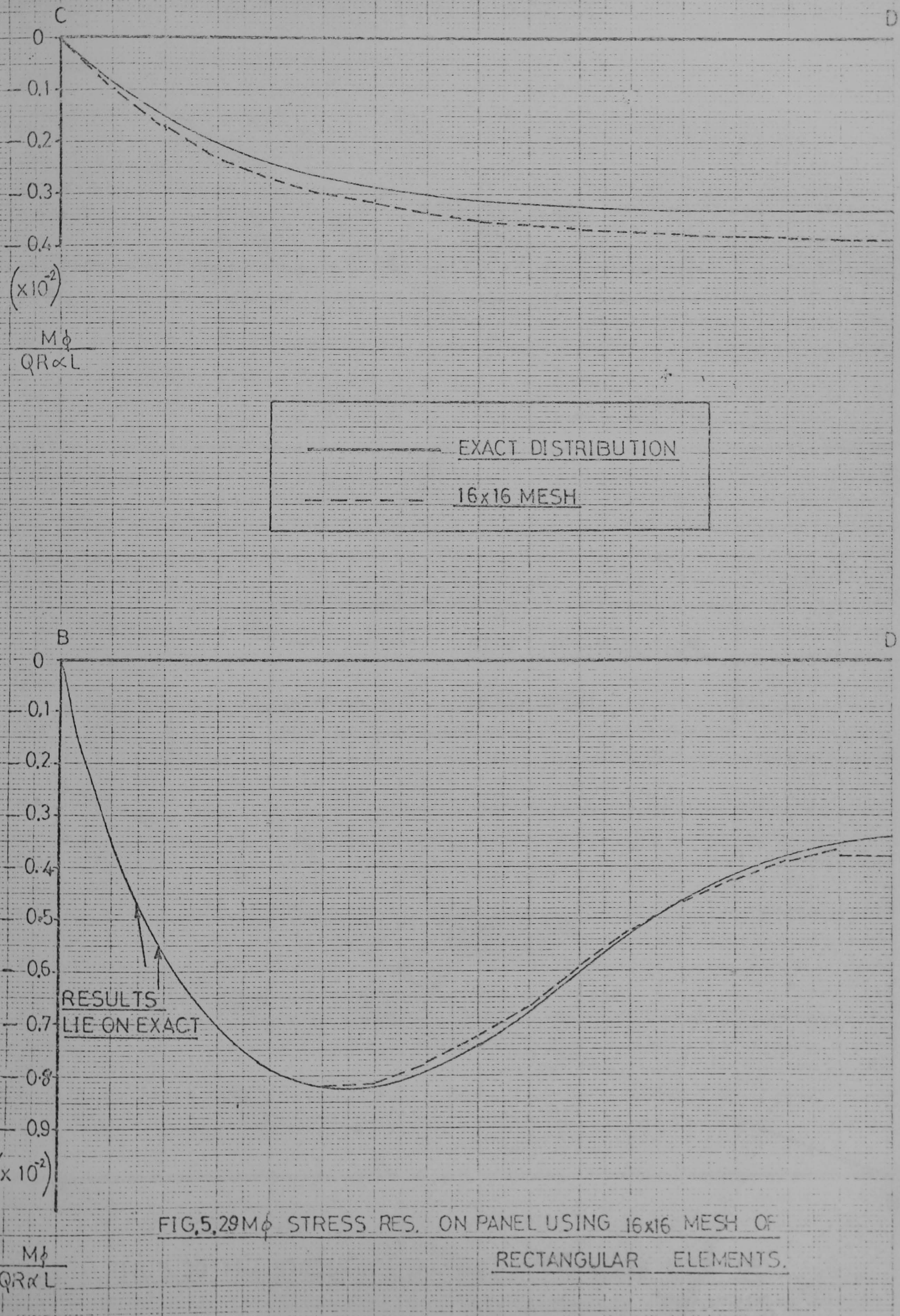

FIG.5.29 Mϕ STRESS RES. ON PANEL USING 16x16 MESH OF RECTANGULAR ELEMENTS.

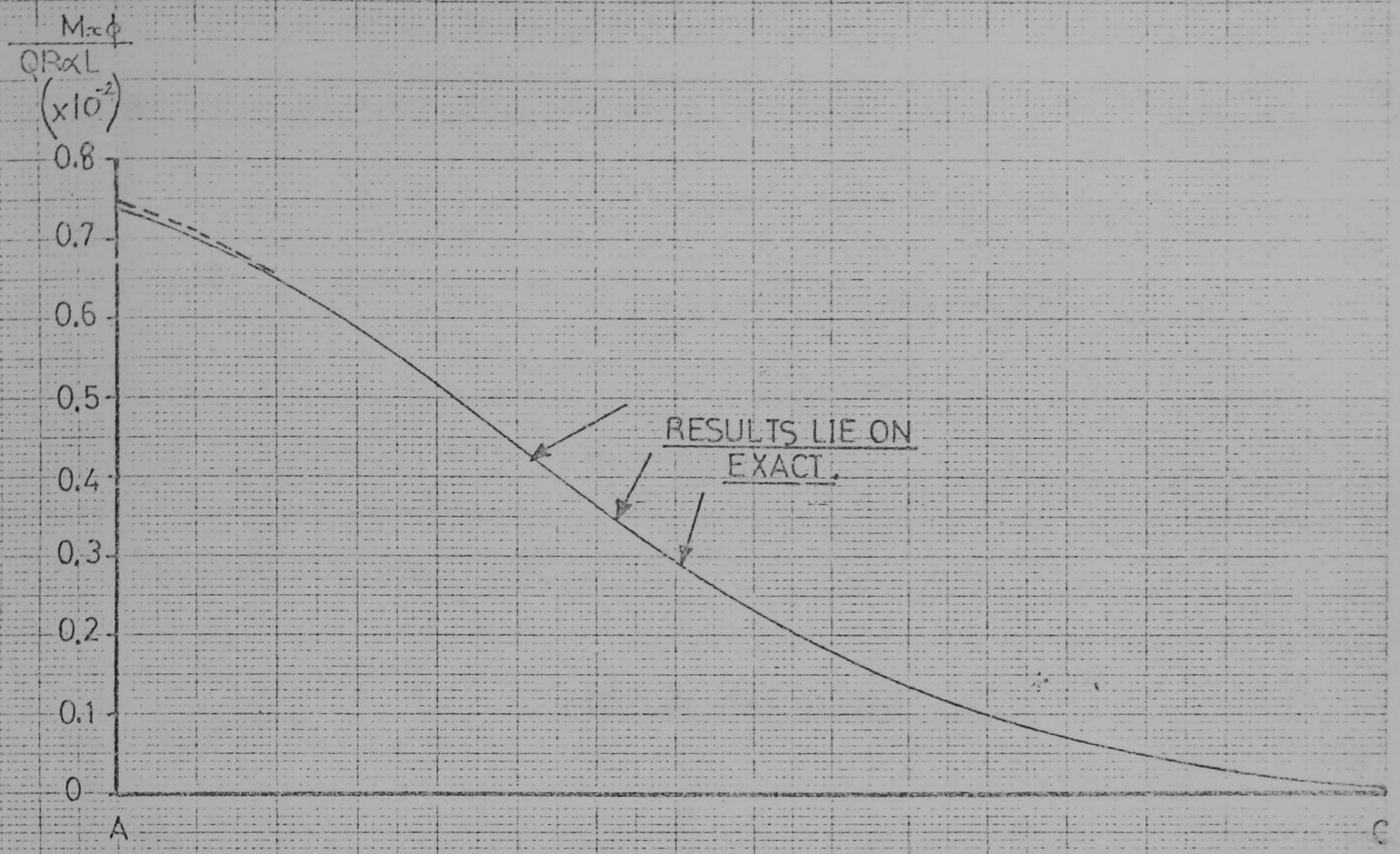

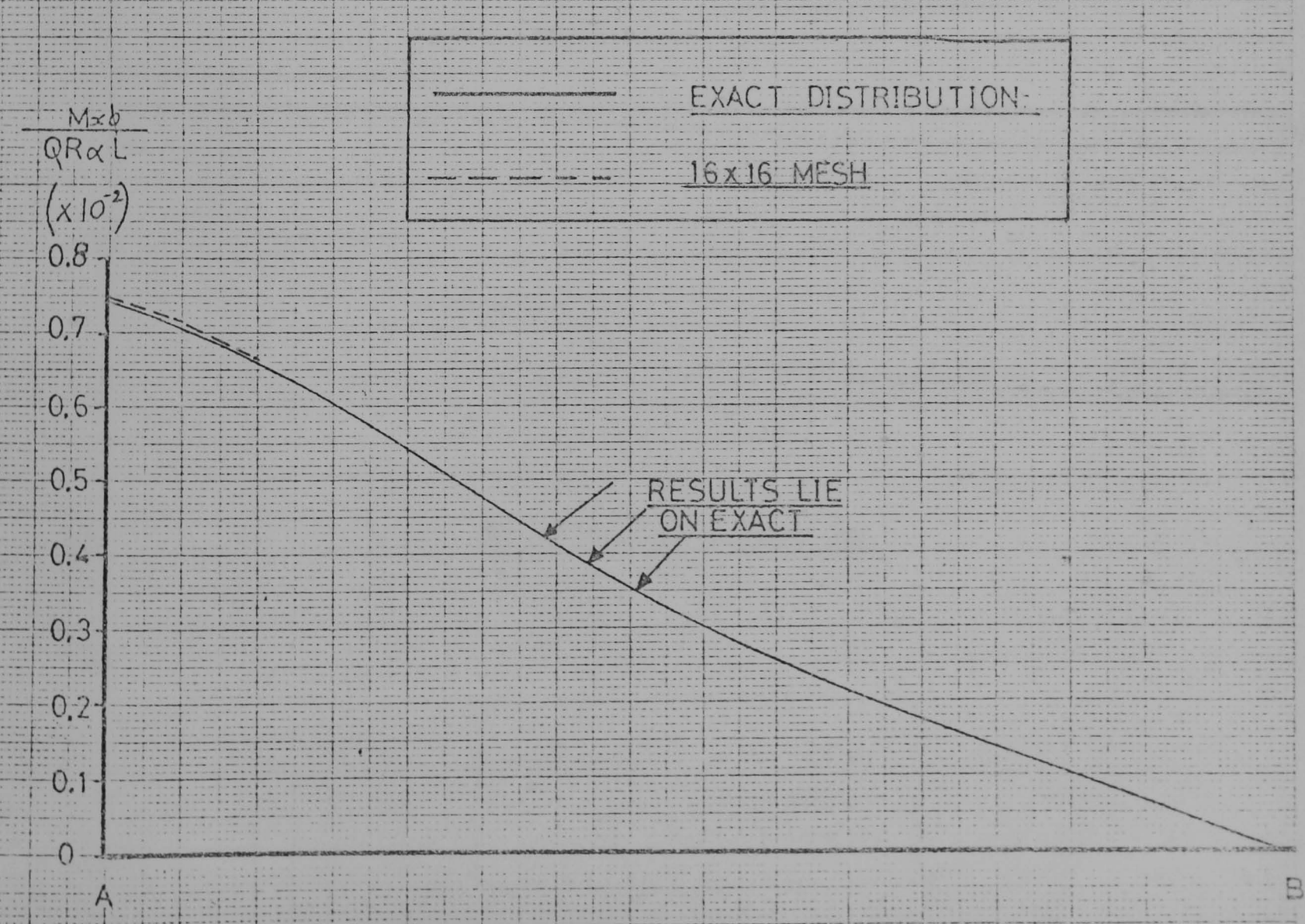

FIG. 5.30 Mxφ STRESS RES. ON PANEL USING 16 x 16 MESH OF RECTANGULAR ELEMENTS.

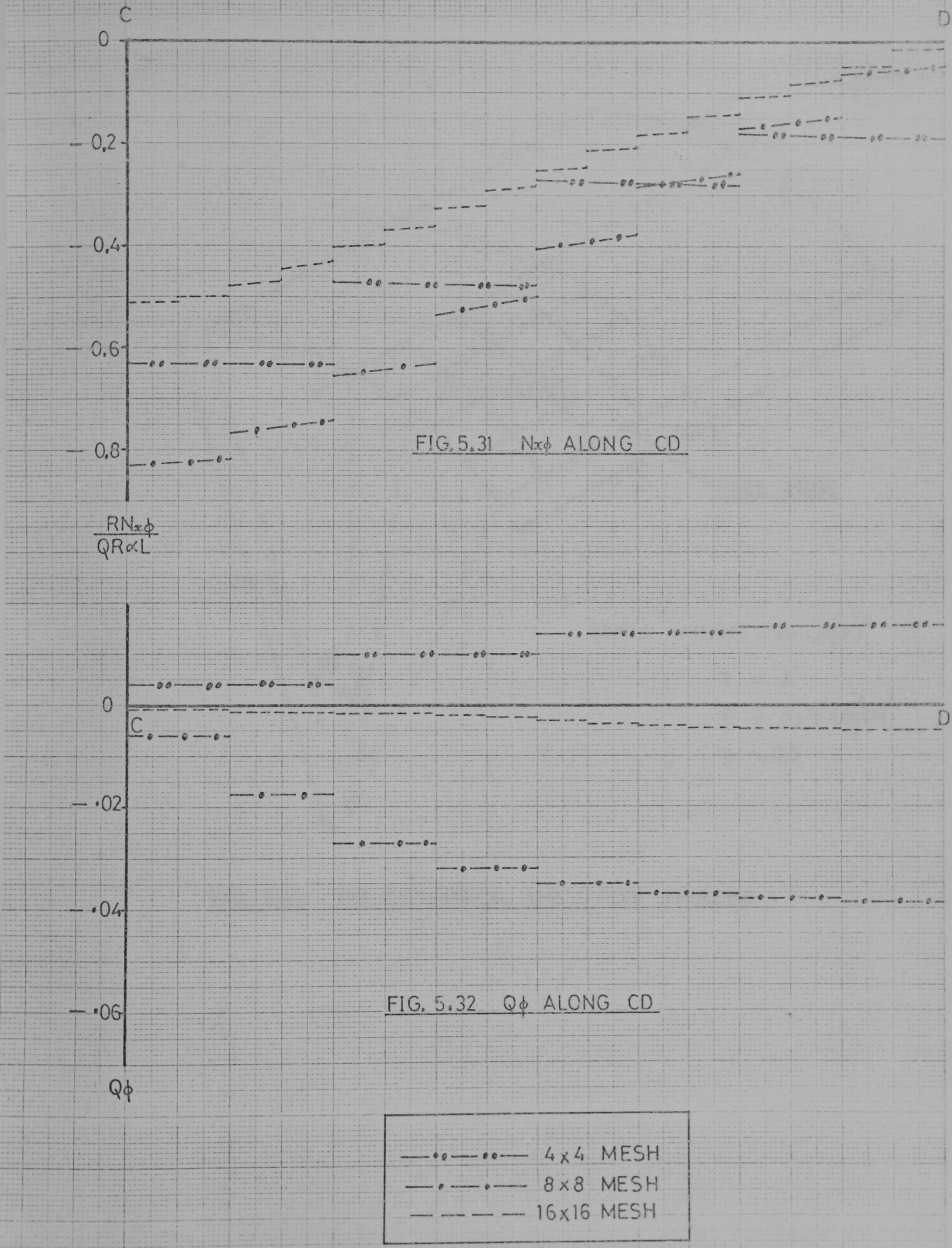

FIG. 5.31 $N_{x\phi}$ ALONG CD

FIG. 5.32 $Q\phi$ ALONG CD

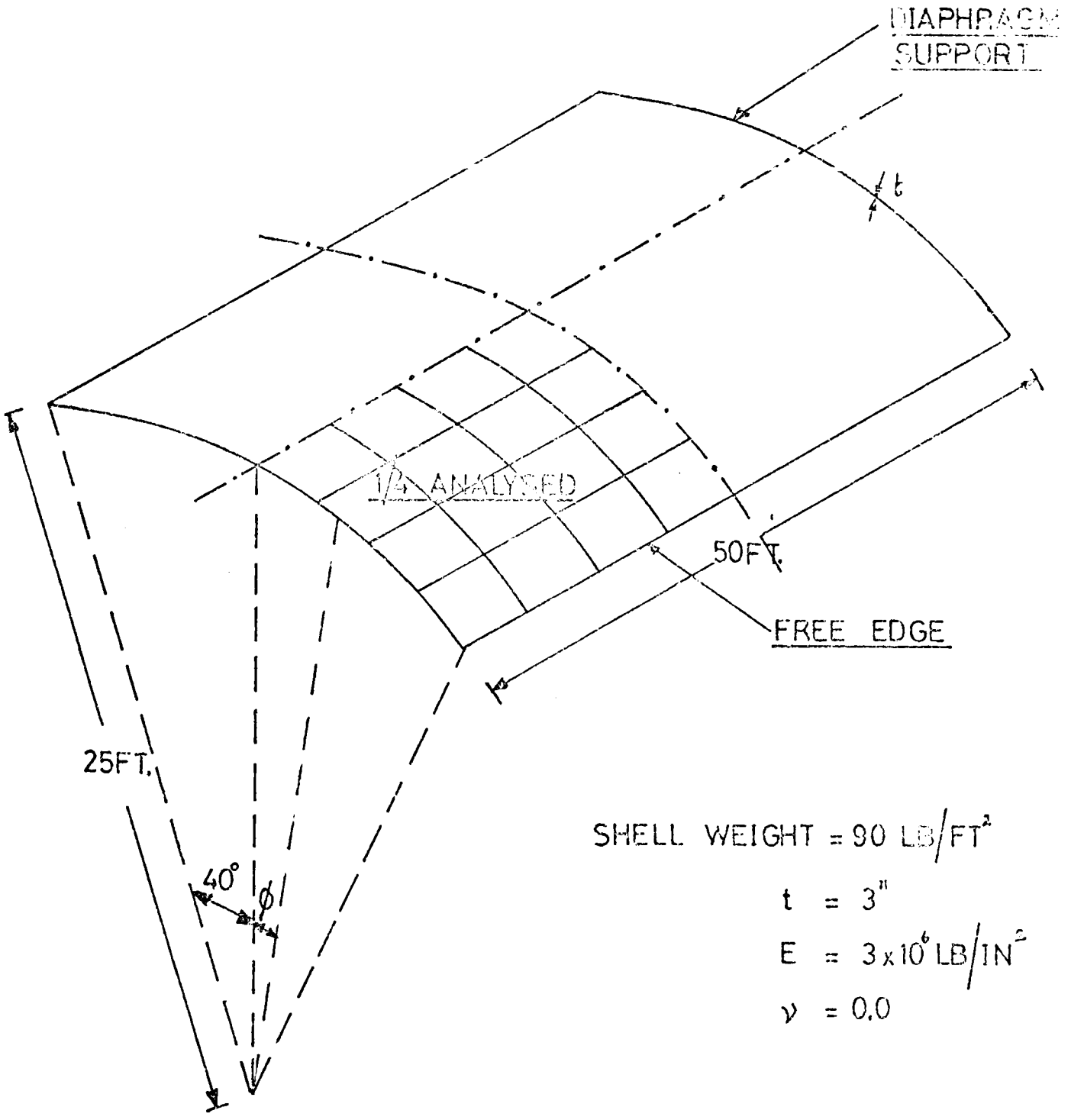

FIG. 5.33 THE CYLINDRICAL SHELL ROOF PROBLEM.

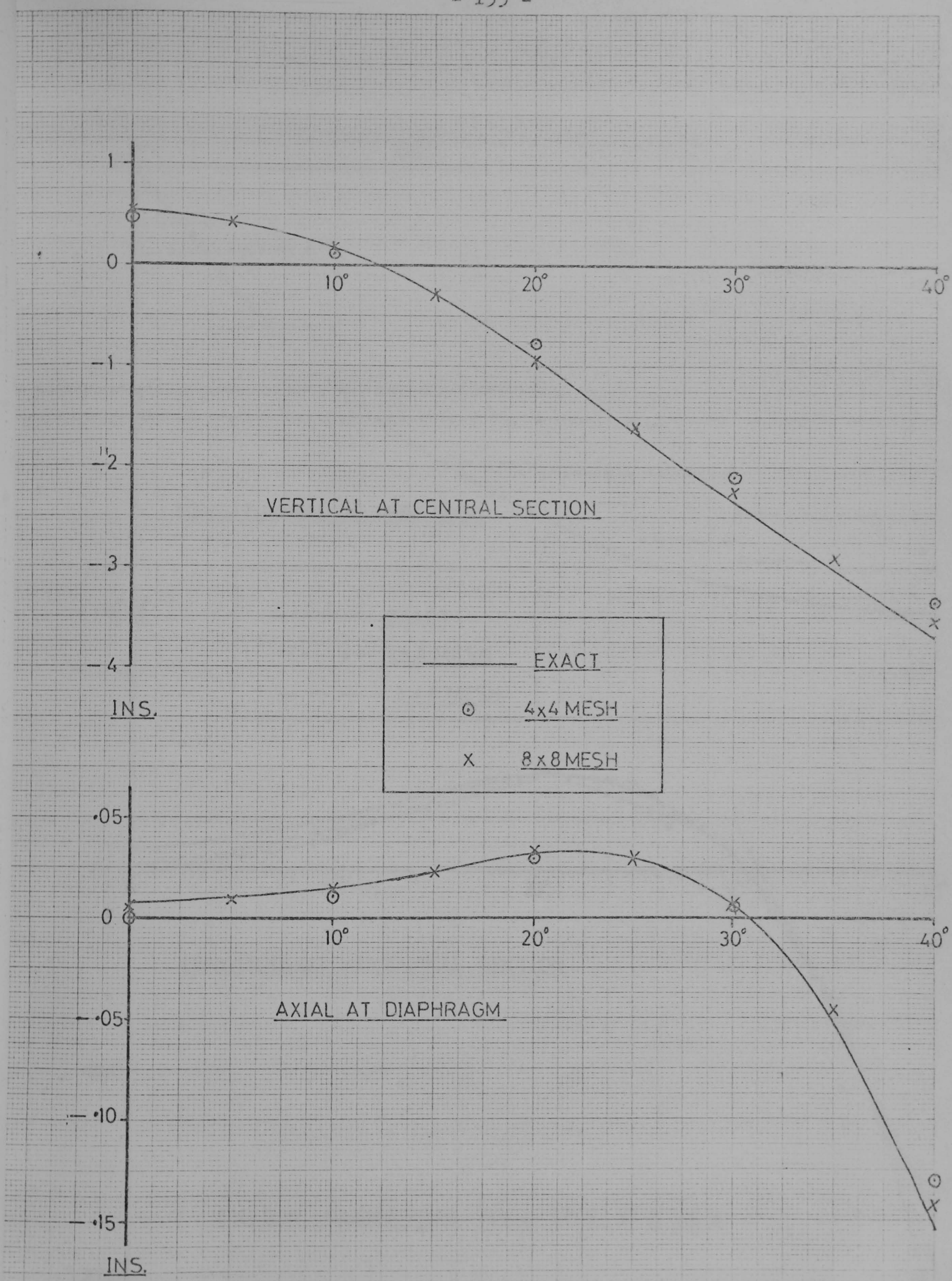

FIG 5.34 CYLINDRICAL SHELL ROOF DISPLACEMENTS USING RECTANGULAR ELEMENTS.

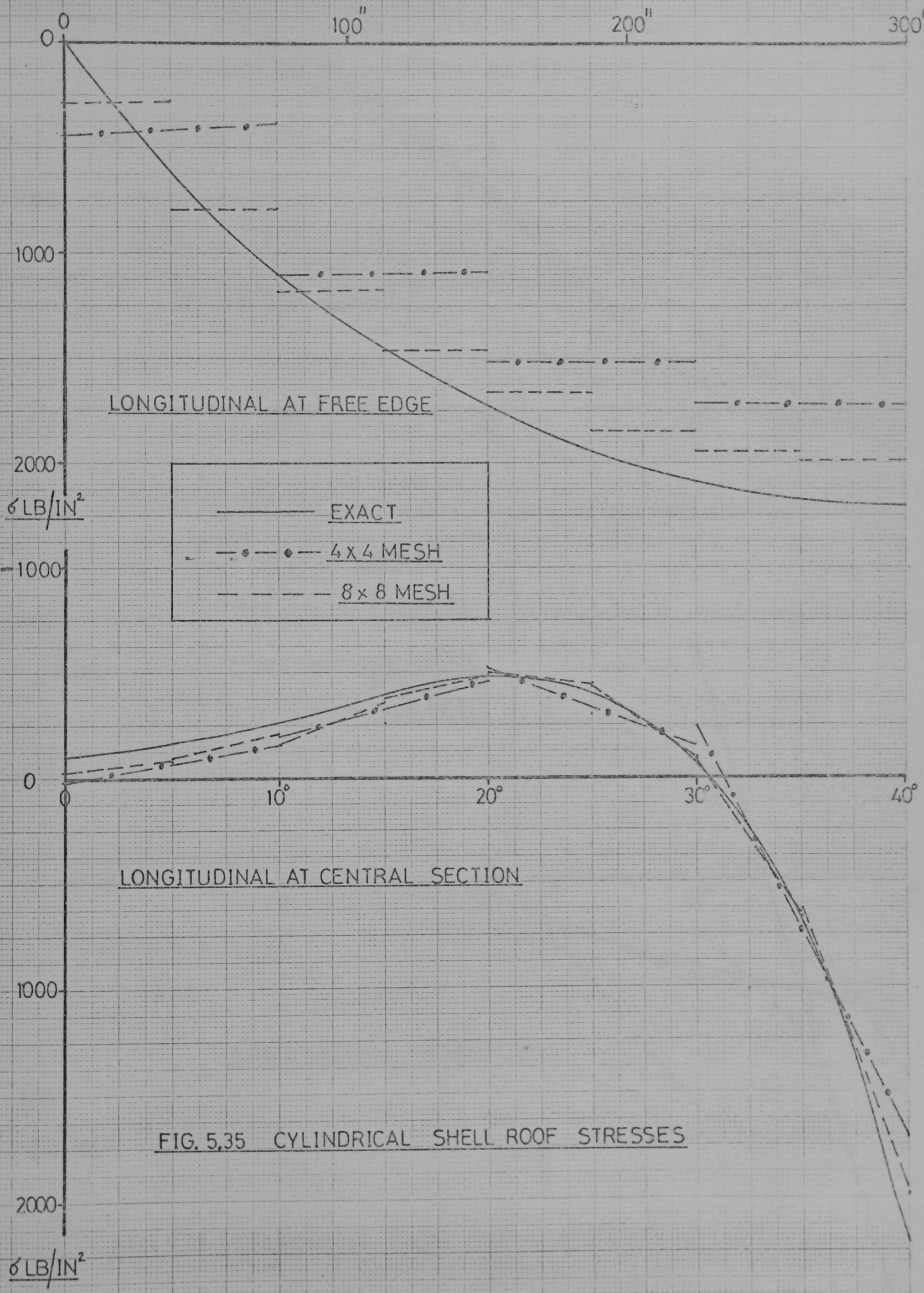

FIG. 5.35 CYLINDRICAL SHELL ROOF STRESSES

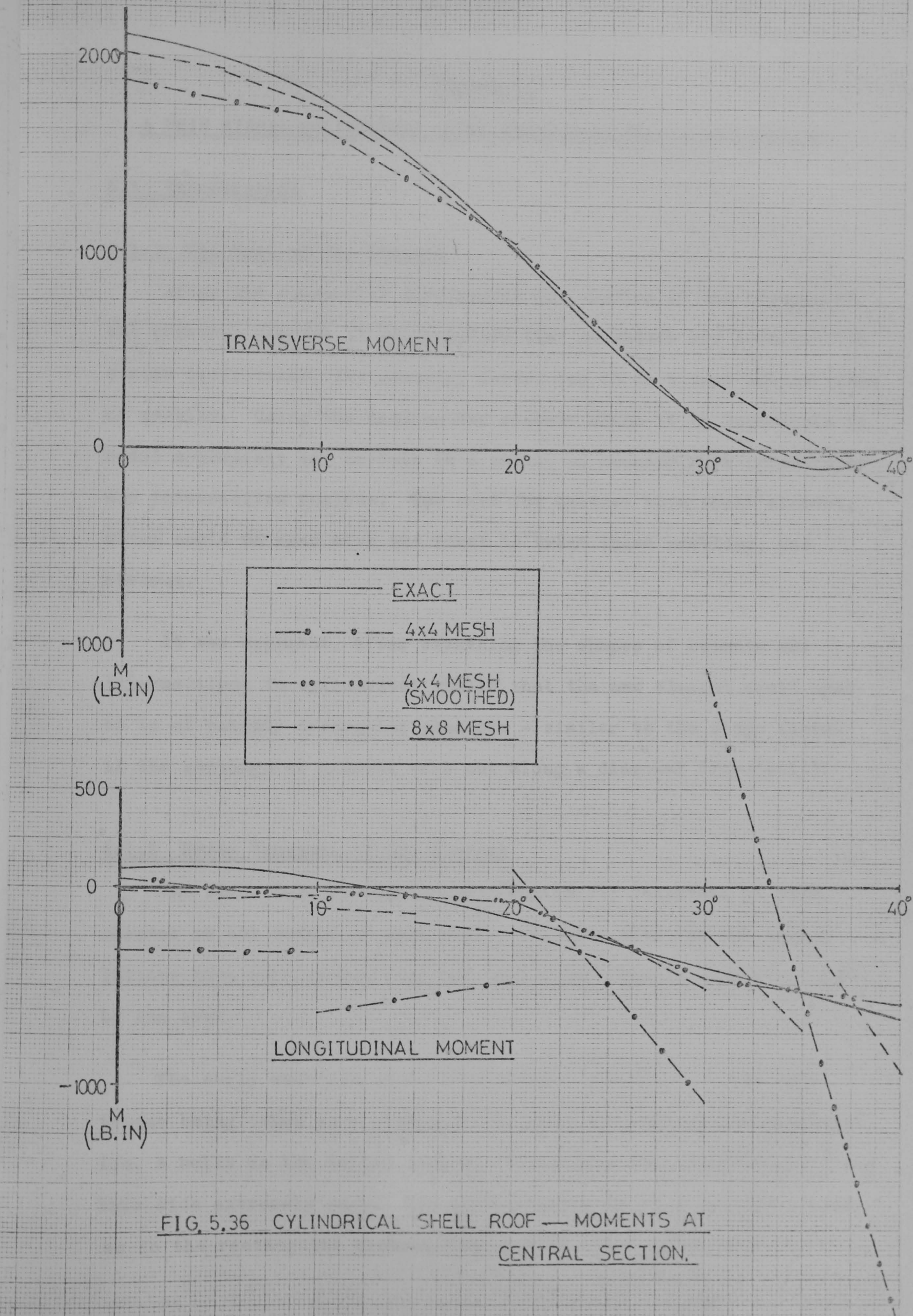

FIG. 5.36 CYLINDRICAL SHELL ROOF — MOMENTS AT CENTRAL SECTION.

Chapter 6

A THIN HYBRID CYLINDRICAL SHELL ELEMENT OF TRIANGULAR PLANFORM

6.1 Introduction

6.1.1 The Uses of the Element

After the successful development and testing of the element of the previous chapter it was realized that no matter how accurate its stress predictions, its geometry restricted it to a very narrow class of problem. Using the rectangular element alone it is impossible to model accurately any cutouts in a shell, or perhaps more importantly any intersection regions. The need for another thin shell element, which could be used with the first to treat these problems, was obvious.

It was apparent, after examining the shapes of cutouts and intersections in cylindrical shells that the new element would need to be of roughly triangular planform - similar to the shape formed if the rectangular element were cut along a diagonal (Fig.(6.1)).

6.1.2 Early Versions of the Element

The final form of the element (Fig.(6.1)) described in this chapter is the result of much work. Elements with various formulations have been constructed and this final form is considered to be the best.

The early versions used three nodes - the shape of the hypotenuse being taken as a straight line when the surface was developed i.e. a helix on the curved surface. This made the integrations along this side extremely easy. The same freedoms at each node were used as in the rectangular element giving this three noded version

15 degrees of freedom. Tests were performed on the length of the stress assumption and virtually the same form was decided upon. However, columns 2 and 6 of Fig.(5.5) were omitted from the 16 term assumption giving 14 terms.

All results using the three noded element tended to be stiff compared with those using rectangular elements. Also the need was seen for having a more generally shaped hypotenuse, since lines of intersection in cylindrical shells would not always be conveniently in the shape of a helix. It was decided, therefore, to introduce a fourth node, on the hypotenuse, (Fig.(6.1)) which, it was thought, would give a double advantage. The shape of the side could be specified more generally - as a quadratic curve in the development; also with the extra freedoms associated with the fourth node, a more flexible displacement assumption could be made.

6.1.3 Later Developments

The effect of the introduction of the fourth node did not improve results significantly and as such was a disappointment. When the element was tested on the simply supported panel, discontinuities in stresses were often very large and the results were in no way comparable with those of the previous chapter, or with those using the flat triangular element in Chapter 4. However, although the fourth node was responsible for extra complications with little gain in the quality of stress predictions, it was decided to retain it purely for geometrical reasons.

A feature of the element up to this point had been the somewhat unusual form of the displacement assumption along the hypotenuse. Rigid body terms, similar to those in the rectangular element, were included in the low order variations. These, as

before, were expressed in terms of ϕ (Fig.(6.1)) and for convenience the high order variations were also expressed in terms of ϕ . Thus ϕ, in effect, was taken as a measure of distance along the hypotenuse. This was found to cause difficulties when the element was distorted and will be explained later. The final form of the displacement assumption still has the rigid body terms included in terms of ϕ , but the other variations explicitly in terms of S , the distance measured along the hypotenuse. (Fig.(6.2))

A major improvement in the results was found, however, when a change was made in the approach adopted in the assumptions for Θ_x and Θ_s along the hypotenuse (Figs.(6.1) and (6.2)). In this, the final form of the element, the results are now of the same order of accuracy as those obtained using the rectangle and flat triangle.

It is necessary to have explicit expressions for Θ_x and Θ_s (rather than for the rotations along and perpendicular to the side) for convenience of integration. In the form of the element giving bad results, however, Θ_x was expressed directly in terms of other quantities $\frac{1}{R}\left(\frac{\partial w}{\partial \phi} - v\right)$, and Θ_s was assumed independently. It was then realized that along all other sides of the element the rotations along and perpendicular to the sides had been assumed independently. Thus along the side 1,4,3 of Fig.(6.2) the displacements Θ_s and Θ_x instead of being completely unrelated should, in fact, be coupled. The independent variables must be the rotations along and perpendicular to the side (Θ_t and Θ_n) and then Θ_x and Θ_s can be expressed in terms of these. Details will be given later.

6.2 The Formulation of the Element

6.2.1 Geometry and Degrees of Freedom

The element is shown in Fig.(6.1) and has been described in

general terms already. There are twenty degrees of freedom in all - five at each node. As in the rectangle the three displacements and two rotations in "natural" coordinates of the shell surface are used. This results in a (24 x 24) stiffness matrix in base-plane coordinates.

The development of the curved surface is shown in Figs.(6.1) and (6.2). The angle at node 2 is a right angle and the side 1,4,3 (the hypotenuse) is defined as a curve of the form $Y = AX + BX^2$. The tangent to the curve at any point is defined by the angle ψ. In practice the element will join with rectangular elements along sides 1,2 and 2,3 but only with the corresponding sides of other triangles along side 1,4,3.

6.2.2 Edge Displacement Assumptions

6.2.2.1 Rigid Body Terms

The displacements at any point along a side are again expressed in terms of the nodal values. The straight side 1,2 and the curved side 2,3 are the same as in the rectangular element and the displacement assumptions described previously are used. Rigid body movements are exactly represented.

The side 1,4,3, however, has fifteen degrees of freedom associated with it. A similar approach is used as for the other curved side, but a longer displacement assumption in terms of fifteen general parameters can now be made. The first six of these parameters are again taken to be exact representations of the six rigid body movements. If rigid body motions of the side about point RBM (Fig.(6.1)) are considered the displacements are given by

$$\begin{Bmatrix} u \\ v \\ w \\ \Theta x \\ \Theta s \end{Bmatrix} = \begin{bmatrix} Sx & Sy & Sz & \Theta x & \Theta y & \Theta z \\ 1 & & & & R(\cos\phi - \cos\beta) & -R\sin\phi \\ & \cos\phi & -\sin\phi & -R(1-\frac{\cos\phi}{\cos\beta}) & x\sin\phi & x\cos\phi \\ & \sin\phi & \cos\phi & R\cos\beta\sin\phi & -x\cos\phi & x\sin\phi \\ & & & 1 & & \\ & & & & \cos\phi & -\sin\phi \end{bmatrix} \cdot \begin{Bmatrix} \alpha_1 \\ \alpha_2 \\ \alpha_3 \\ \alpha_4 \\ \alpha_5 \\ \alpha_6 \end{Bmatrix} \quad (6.1)$$

$\alpha_1 \rightarrow \alpha_6$ represent the rigid body displacements (Sx,Sy,Sz) along axes parallel to X,Y,Z and the rotations ($\Theta_x, \Theta_y, \Theta_z$) about the same three axes. The only difference between this set of rigid body modes and the set used for the other curved side is the presence of the terms involving x in the rotations about the Y and Z axes. These are needed because the side is at an acute angle to the x axis which introduces components of v and w when subjected to these rigid body motions.

6.2.2.2 Extra Variations

Because of the freedoms associated with the side it is possible to have quintic variations of w with S (S being the distance measured along the side (Fig.(6.2)) from node 1) and quadratic variation of surface displacements u_n and u_t and normal slope Θt.

For a curved line in space, such as the side under consideration, the displacements which can be varied independently are u_n, u_t w and Θt (Fig.(6.2)). The rotation Θ_n is dependent upon w and the in-plane displacements. Therefore in the present case basic assumptions must be made for the above four displacements and the required quantities (u, v, w, Θx and Θs) must be derived from them.

It can be shown from Fig.(6.2) that the relationships needed are

$$\begin{aligned} u &= u_t \cos\psi - u_n \sin\psi \\ v &= u_t \sin\psi + u_n \cos\psi \\ \theta_x &= -\theta_n \sin\psi + \theta_t \cos\psi \\ \theta_s &= \theta_n \cos\psi + \theta_t \sin\psi \end{aligned} \tag{6.2}$$

The assumption for w is to be made in terms of S so the expression for θ_n is

$$\theta_n = -\partial w/\partial S + \frac{v}{R}\sin\psi \tag{6.3}$$

Before including the extra variations it must first be decided which terms are included approximately in the rigid body motions of Equation (6.1). If the in-plane rigid body motions (Sx, Sy and Θ_z of Equation (6.1)) are considered to act on the side in Fig.(6.2) it can be seen that these give approximately constant variation of u_n and u_t and also linear variation of u_n along the edge. Therefore the following extra terms involving three additional parameters should be added

$$\begin{aligned} u_n &= \alpha_7 S^2 \\ u_t &= \alpha_8 S + \alpha_9 S^2 \end{aligned} \tag{6.4}$$

If the remaining three rigid body motions of (6.1) are considered (Sz, Θx and Θy) these can be seen to give approximately constant and linear variation of w and constant variation of θ_t.

Therefore the extra terms allowed are

$$\begin{aligned} w &= \alpha_{10} S^2 + \alpha_{11} S^3 + \alpha_{12} S^4 + \alpha_{13} S^5 \\ \theta_t &= \alpha_{14} S + \alpha_{15} S^2 \end{aligned} \tag{6.5}$$

thus using the fifteen possible parameters.

If, now, equations (6.2) and (6.3) are applied to the assumptions (6.4) and (6.5), the boundary displacement assumption can be

transformed into the required form involving u, v, w, Θx and Θs. The extra variations to be added on to Equation (6.1) can then be summarized in matrix form as:

$$\begin{Bmatrix} u \\ v \\ w \\ \theta_x \\ \theta_s \end{Bmatrix} = \left[\begin{array}{c|c|c|c} -S^2\sin\psi & S\cos\psi & S^2\cos\psi & \\ \hline S^2\cos\psi & S\sin\psi & S^2\sin\psi & \\ \hline & & & S^2 \\ \hline -\frac{1}{R}S^2\cos\psi & -\frac{1}{R}S\sin\psi & -\frac{1}{R}S^2\sin\psi & 2S\sin\psi \\ \hline & & & -2S\cos\psi \end{array}\right.$$

$$\left.\begin{array}{c|c|c|c|c} & & & & \\ \hline & & & & \\ \hline S^3 & S^4 & S^5 & & \\ \hline 3S^2\sin\psi & 4S^3\sin\psi & 5S^4\sin\psi & S\cos\psi & S^2\cos\psi \\ \hline -3S^2\cos\psi & -4S^3\cos\psi & -5S^4\cos\psi & S\sin\psi & S^2\sin\psi \end{array}\right] \cdot \begin{Bmatrix} \alpha_7 \\ \alpha_8 \\ \alpha_9 \\ \alpha_{10} \\ \alpha_{11} \\ \alpha_{12} \\ \alpha_{13} \\ \alpha_{14} \\ \alpha_{15} \end{Bmatrix} \qquad (6.6)$$

6.2.2.3 The Assumption in Terms of Nodal Variables

It is now possible with the combined assumption of (6.1) and (6.6) to express the fifteen general α's in terms of the displacements at the nodes 1, 4 and 3. Each node has unique x, ϕ, S and ψ values associated with it and if these are in turn substituted into the combined (6.1) and (6.6) a matrix equation of the following form is obtained.

$$\begin{Bmatrix} q_1 \\ q_3 \\ q_4 \end{Bmatrix} = \left[\ \text{DISPL}\ \right] \cdot \begin{Bmatrix} \alpha_1 \\ \vdots \\ \alpha_{15} \end{Bmatrix} \qquad \text{where } q_i = \begin{Bmatrix} u_i \\ v_i \\ w_i \\ \theta x_i \\ \theta s_i \end{Bmatrix} \qquad (6.7)$$

and $\left[\text{DISPL}\right]$ is a (15 x 15) matrix.

By inverting [DISPL] in (6.7) the α's can be expressed in terms of the nodal variables along the edge. This, then, enables the assumption (6.1)+(6.6) to be made in terms of the nodal variables by postmultiplying by $[DISPL]^{-1}$.

A feature of earlier forms of the element was that the assumption of Equation (6.6) was made in terms of ϕ - the angle measured around the other curved side. However, when the position of the fourth node was defined such that the side became tangent to the horizontal at point 3 (Fig.(6.2)), it was found that the [DISPL] matrix became singular. The problem was resolved by including the variations in terms of S as in (6.6).

6.2.2.4 The Expression for the Distance along the Side

The equation of the hypotenuse joining nodes 1,4,3 (Fig.(6.1)) when developed into a flat surface with coordinates X and Y centred at node 1 is of the form $Y = AX + BX^2$. The constants A and B can be expressed in terms of the nodal coordinates X_4, Y_4 and dimensions of the element WID and L as:

$$B = \left\{Y_4 - (WID/L).\ X_4\right\} \Big/ \left\{X_4^2 - L.X_4\right\}$$
$$A = (WID - B.L^2)/L \qquad (6.8)$$

It is necessary, for the purpose of setting up the displacement assumption of the previous section to have an explicit expression for S (Fig.(6.2)) in terms of X, the distance along the straight side measured from node 1.

The distance S is given by the integral calculus as:

$$S = \int_0^{X_S} \sqrt{1 + (dY/dX)^2}\ dX$$
$$= \int_0^{X_S} \sqrt{1 + (A + 2BX)^2}\ dX \qquad (6.9)$$

where the limits are from 0 to X_S, the value of X for which S is required.

If $(1 + A^2) = A'$, $4.B.A = B'$ and $4B^2 = C'$ and then $Q' = 4A'C' - (B')^2$ $K' = 4C'/Q'$ $X' = A' + B'X + C'X^2$ then it can be shown that the integral is a standard form having the result

$$S = \left[\frac{(2C'X + B')\sqrt{X'}}{4C'} + \frac{1}{2K'\sqrt{C'}} \log_e \left(2\sqrt{C'X'} + 2C'X + B'\right) \right]_0^{X_s} \quad (6.10)$$

6.2.3 The Stress Assumption

The same approach as in the rectangular element was used. The full quadratic assumption of Fig.(5.5) was tried initially on both 3 and 4 noded versions of the element and was found to give unsatisfactory stresses. The first 16 terms were then used and finally the assumption was reduced to its absolute minimum length by elimination of columns 2 and 6 of Fig.(5.5). It will be recalled that these variations proved marginally useful in the rectangular element but they proved to be of no advantage in any of the problems tested here. The final form of the assumption is shown in Fig.(6.3).

To evaluate a consistent loading vector for pressure loading the particular assumption used for the rectangular element was again used.

6.2.4 The Evaluation of the Complementary Strain Energy

To evaluate the integral of Complementary Strain Energy over the area of the element it was decided to construct a transformation between the natural coordinates of the element surface (X,Y) and a (ξ,η) plane (Fig.(6.4)). The transformation is such that the element in the (X,Y) plane is mapped into a triangle with coordinates (0,0), (2,0) and (2,2) in the (ξ,η) plane. The transformation

was also constructed such that the reverse mapping of the line $\eta = \xi$ in the (ξ, η) plane always gives the line $Y = AX + BX^2$.

The relationship which carries out the transformation can be shown to be

$$\begin{Bmatrix} X \\ Y \end{Bmatrix} = \left[\begin{array}{c|c|c} \xi & 1 & \\ \hline \eta & & \xi\eta \end{array}\right] \begin{Bmatrix} \alpha_1 \\ \alpha_2 \\ \alpha_3 \end{Bmatrix} \tag{6.11}$$

where the constants $\alpha_1, \alpha_2, \alpha_3$ are expressed in terms of the element coordinates

$$\alpha_1 = X_2/2 \qquad \alpha_2 = (Y_3 - 4\alpha_3)/2$$
$$\alpha_3 = \left(\frac{L}{2}\right)^2 \left\{ Y_4 - \left(\frac{W1D}{L}\right) X_4 \right\} \Big/ \left(X_4^2 - L.X_4\right) \tag{6.12}$$

The integral, as for the rectangular element, is evaluated numerically. Gauss points are chosen in the (ξ, η) plane and transformed into values in the (X,Y) plane using (6.11). The stress assumption is then evaluated at the point (X,Y) (after expressing (X,Y) in terms of the coordinates (x,s) in which the stress assumption is made).

The integral is then carried out in the (ξ, η) plane using the Jacobian of the transformation $|J|$

$$|J| = \begin{vmatrix} \frac{\partial x}{\partial \xi} & \frac{dx}{d\eta} \\ \frac{dy}{d\xi} & \frac{dy}{d\eta} \end{vmatrix} = \alpha_1(\alpha_2 + \alpha_3 \xi) \tag{6.13}$$

In the terminology used in the previous chapter

$$C.S.E. = \iint_{area} \frac{1}{2} \{\sigma\}^T [D] \{\sigma\} |J| \, d\xi \, d\eta \tag{6.14}$$

where the $[D]$ matrix relating stresses and strains is the same as that used in the rectangular element.

6.2.5 The Evaluation of Edge Work

The work done by the assumed stresses around the boundary of the element must also be evaluated. The work along sides 1,2 and 2,3 is carried out in exactly the same way as in the rectangular element. However along the hypotenuse 1,4,3 a different approach is now adopted to enable the integration to be carried out more easily.

The equation of this side in (X,Y) coordinates (Fig.(6.4)) is $Y = AX + BX^2$ where A and B are given by (6.8). The required integral is of the form

$$\text{Work} = \int_S (\text{stress}^T \times \text{boundary force matrix}) \times (\text{displacements})\, dS \qquad (6.15)$$

where S is the distance measured along the side from node 1. Equation (6.15) can be transformed into an integral along the X axis

$$\text{Work} = \int (\text{stress}^T \times \text{boundary force matrix}) \times (\text{displacements}) \times \left(\frac{dS}{dX}\right) . dX \qquad (6.16)$$

where dS/dX along the side is given by standard calculus as

$$\frac{dS}{dX} = \sqrt{1 + (dY/dX)^2} = \sqrt{1 + (A+2BX)^2} \qquad (6.17)$$

Gauss points can now be chosen along the X axis and stresses and displacements evaluated at corresponding points on the curved side. The integration is thus carried out along the X axis in the same part of the program as that along side 1,2.

The boundary force matrix in (6.16) performs the same function as along the other sides, i.e. it transforms the stress resultants into forces in the directions of the displacements. At any point on the side the tangent makes an angle ψ with the X axis and the following matrix gives the forces Fu, Fv, Fw and the moments $F\partial x$

and $F_{\theta s}$ in terms of the stress resultants

$$\begin{Bmatrix} F_u \\ F_v \\ F_w \\ F_{\theta x} \\ F_{\theta s} \end{Bmatrix} = \begin{bmatrix} -\sin\psi & & & \cos\psi & & & & & \\ & \cos\psi & -\sin\psi & & & & & & \\ & & & & & & -\sin\psi & \cos\psi & \\ & & & & -\cos\psi & \sin\psi & & & \\ & & & -\sin\psi & & \cos\psi & & & \end{bmatrix} \cdot \begin{Bmatrix} N_x \\ N_\phi \\ N_{x\phi} \\ N_{\phi x} \\ M_x \\ M_\phi \\ M_{x\phi} \\ Q_x \\ Q_\phi \end{Bmatrix} \qquad (6.18)$$

The angle ψ however, is a function of position along the side. Its value can be obtained from

$$\tan\psi = dY/dX \qquad = A + 2BX \qquad (6.19)$$

6.2.6 Calculation of Results

The stiffness matrix and consistent loading vector for the element are calculated following the theory in Chapter 2 in a similar manner as for the rectangle. The $[H]^{-1}[G]$ matrix relating stress coefficients to displacements for each element must again be kept on backing store for use in the stressing routine.

It was explained in the previous chapter how this matrix can be used to test the correct representation of rigid body motions in the displacement assumptions. Similar tests were carried out here and satisfactory results were obtained.

6.3 Test Problems

6.3.1 Introduction

The element was designed to be used in conjunction with the rectangle of the previous chapter to model edge and intersection regions. It has not, therefore, been tested in its own right on such a wide variety of problems but a series of basically simple tests have been carried out to verify that it behaves in a

reasonable manner. Also, the simply supported panel has been analysed to gain an idea of the accuracy of stress predictions possible. Interesting comparisons can therefore be made with the results using the flat hybrid triangle of Chapter 4.

The simple tests mentioned above were designed to gain information on the following points:

(i) Can the radius of curvature of the element be declared negative without producing any anomalies? The work of the next chapter on intersection problems was anticipated here. It proves necessary when analysing an intersection to have, not only an element such as that in Fig.(6.1) which is convex upwards, but also one whose shape is concave upwards. Geometrically this is defined by declaring the radius of curvature negative and altering the z value of node 4 (Fig.(6.1)).

(ii) What is the effect of changing the position of the fourth node on the hypotenuse? If node 4 is placed in several different positions, each, however, defining geometrically similar hypotenuses, will different results be obtained? It was thought, before tests were carried out, that exactly the same results should be obtained irrespective of the position of the fourth node.

(iii) What is the effect on stress predictions when the hypotenuse is distorted? The simply supported panel was analysed with various shapes of hypotenuse.

6.3.2 Tests Involving Negative Curvature

Three elements, all of the same size were considered separately as in Fig.(6.5). Elements 1 and 3 were declared 2 1 8 7 and 3 4 10 5, both with negative curvature. Element 2 was declared 2 3 9 6 with positive curvature. The elements were considered to be fixed along

the x axis as shown and various loads were applied at points 8, 9 and 10. These had components both in the plane of and perpendicular to the element surfaces. In all cases, where the loadings with respect to the elements were equivalent, identical stress systems were set up. This indicated that the element was behaving in a consistent manner when negative curvature was defined.

6.3.3 Tests on Changing the Position of the Fourth Node

A series of individual elements were again tested. In Fig.(6.6) elements 1 and 2 are of exactly the same geometrical shape as are elements 3 and 4. The position of the nodes defining the shapes of the hypotenuses were different, however, as indicated. Elements 1 and 2 were fixed along the X axis and elements 3 and 4 were fixed along their shortest curved sides. Identical point loads were applied to nodes 3 and 6 of elements 1 and 2 and nodes 10 and 14 of elements 3 and 4. The deflections and stresses in the pairs of elements 1 and 2, and 3 and 4 were identical. It is obvious, therefore, that for individual geometrically similar elements results are unaffected by the position of the fourth node.

6.3.4 The Simply Supported Panel under Pressure Loading

To compare predictions obtained with exact distributions, the simply supported panel considered in earlier chapters was again analysed (Fig.(4.5)). Consistent pressure loading vectors were used and (4 x 4) and (8 x 8) meshes of the present elements were considered on $\frac{1}{4}$ of the panel. Fig.(6.7) shows (4 x 4) meshes. The first (4 x 4) mesh consisted of elements having undistorted hypotenuses, i.e. the hypotenuse is a straight line in the development. Two "distorted" meshes were also considered. The nodes were (a) moved along the axis of the panel and (b) moved around the

circumference to form two geometrically identical meshes having the maximum possible distortion (such that the hypotenuses formed tangents with the horizontal) as shown. These meshes will be referred to as "x distortion" and "ϕ distortion" respectively. On the basis of the results of Section 6.3.3, it was thought that the two distorted meshes should give identical answers.

The displacements and stresses on the panel given by the three (4 x 4) meshes are shown in Figs.(6.8) to (6.16) where it is seen that: (a) the undistorted mesh gives generally the best answers for stresses and deflections and (b) the two undistorted meshes both give reasonable (but not identical) answers. These results will be discussed later. To investigate convergence of the elements an 8 x 8 undistorted mesh was then used. These results are shown in Figs.(6.17) to (6.25).

6.4 Discussion of Results

6.4.1 Tests Involving Negative Curvature

The results of these tests were as expected and really only provided a test of the correctness of the formulation.

6.4.2 Changing the Position of the Fourth Node

For the geometrically similar elements the displacements along the hypotenuses are defined as continuous functions of the element coordinates in terms of fifteen general coefficients. Three points are chosen and these coefficients are expressed in terms of displacements at the points. The two end points of the side are always chosen, but the position of the third node can be varied. However, no matter where it lies on the side, the same displacement distribution can be defined.

Therefore, in the tests of Section 6.3.3 when similar loads are placed on nodes 3 and 6 of elements 1 and 2 (Fig.(6.6)), the displacement distributions along the hypotenuses are identical because the values at nodes 4 and 7 are not constrained in any way. Since the two elements are also the same in all other respects, identical stresses and displacements are obtained. The same arguments can be applied to elements 3 and 4.

6.4.3 The Simply Supported Panel

6.4.3.1 Comparisons with the Previous Elements

The results of the undistorted 4 x 4 mesh on the panel (Figs. (6.8) to (6.16)) are comparable with those using a 4 x 4 mesh of rectangular elements in Chapter 5 (Figs.(5.13) to (5.21)). However, because of the extra nodes on the hypotenuses the present idealization uses twice as many degrees of freedom (160 compared with 80).

The general accuracy of these results is also very similar to those using the flat triangular hybrids in Chapter 4. (For both 4 x 4 and 8 x 8 meshes.) The present curved elements give slightly better values for the lateral displacements and in-plane stress resultants, but there is no consistent improvement in the bending and twisting moments.

On the basis of this simple problem, then, it would seem that the flat hybrid is more efficient, since it uses fewer freedoms to give comparable results. However, the purpose of the present curved hybrid is to model the geometry of intersection regions accurately - a job which the flat element is incapable of doing. The purpose of analysing the panel was to verify that answers of acceptable accuracy are obtained on a simple problem.

6.4.3.2 The Effects of Distortion

The differences in the results using the two distorted meshes were at first very difficult to understand (having regard for the results of Section 6.3.3) since the two idealizations used nominally the same shaped elements.

It was eventually realized that the only explanation fitting all the facts was that displacement incompatibilities existed along hypotenuses of adjoining elements. For example, in Fig.(6.6), displacements along the hypotenuse of element 3 must be incompatible with those in element 1 when the two hypotenuses are of the same geometrical shape. Similarly for elements 2 and 4.

If this is true the different results given by the ϕ and x-distorted meshes can be explained. The nodes on the hypotenuses constrain the two incompatible displacement assumptions to be the same at different points. The net result is then different displacement distributions in the two distorted meshes.

The above hypothesis was proved numerically. Elements such as those in Fig.(6.6) and others subtending larger (e.g. 90°) angles were considered in matching pairs. Identical, arbitrary, displacements were imposed at the nodes and the displacement distributions along the hypotenuses were plotted. In all cases significant incompatibilities were present in the in-plane displacements u and v, slight incompatibilities in θ_x and θ_s and smaller ones in w (the lateral deflection). Elements whose hypotenuses were straight in the development (i.e. undistorted elements) were also tested in this way and no incompatibilities were found.

The reasons for these incompatibilities is not immediately obvious since they are only present in distorted elements. The

facts are, that when S (the distance along the side) is measured from node 1 towards 4 (element 1 in Fig. (6.6)) a different displacement distribution is obtained from that when S is measured in the opposite direction from node 3 towards 4 (as it is in a matching element such as 3).

After some thought it has been concluded that the part of the assumption in Equation (6.6) is not invariant under a change of axes for a distorted side. When S is measured from the opposite end of the hypotenuse as described above, a change of axes must take place. If S and ψ are values measured in one set of axes (such as those for element 1 in Fig.(6.6)), the values for the same point in the axes of the matching element are $(ST-S)$ and ψ (where ST is the total length of the side. If $(ST-S)$ is used in (6.6) instead of S additional variations are introduced (because ψ is variable along a distorted side) which, it is thought, account for the incompatibilities.

The original reason for undertaking these tests with distorted meshes was to gain information on the changes introduced in the stress predictions. It is apparent, generally, that the changes are relatively small. In practical terms the above displacement incompatibilities are unimportant. In the analysis of a real structure (see next chapter), two triangular elements would never be joined as in the meshes of Fig.(6.7), since it would be more efficient to use a rectangle. Triangular elements would only be joined along their hypotenuses where a physical discontinuity in the shell surface was present. This would introduce displacement incompatibilities similar to those in the flat elements of Chapter 4 which, it is thought, would be more significant than those present for the reasons discussed here.

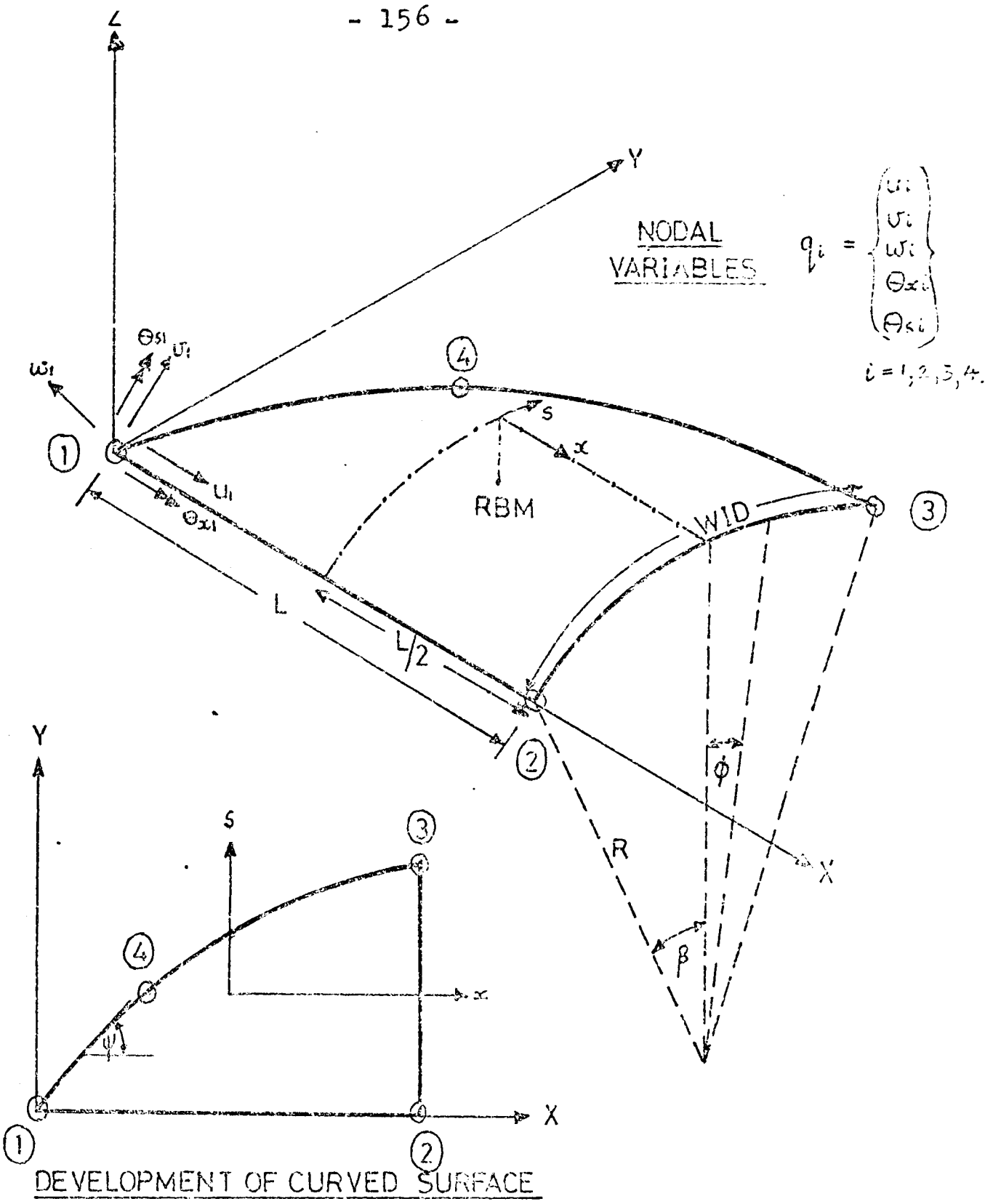

FIG. 6.1 THE TRIANGULAR HYBRID SHELL ELEMENT.

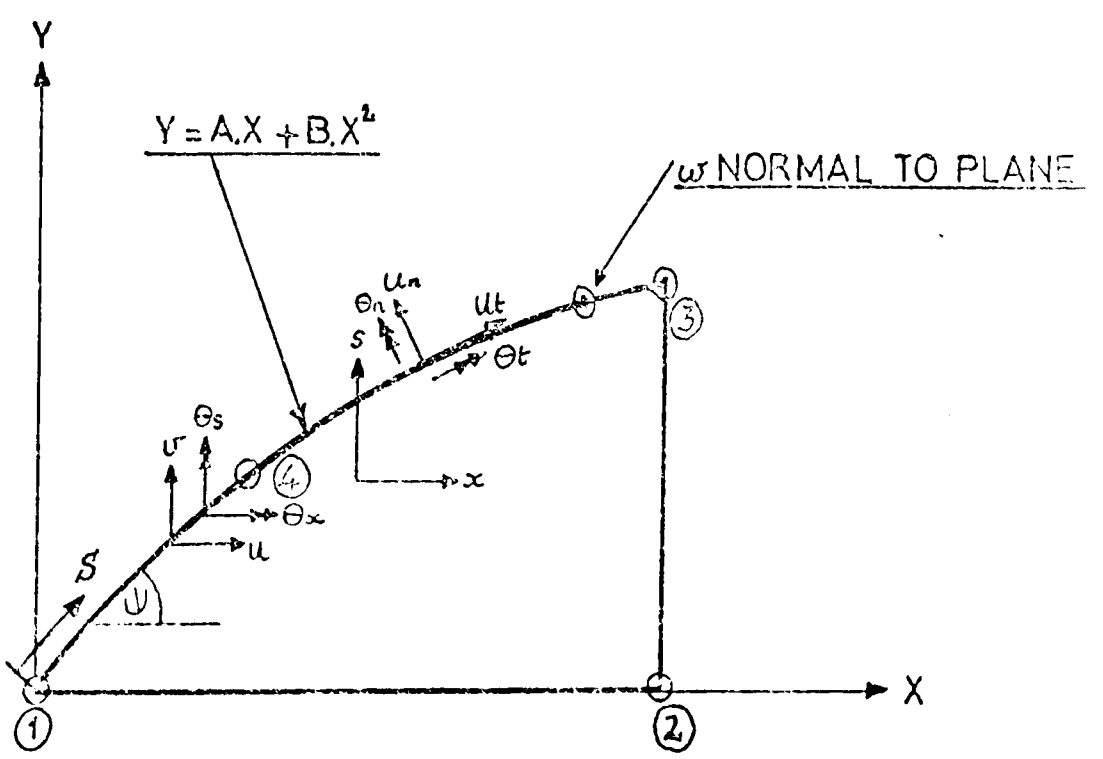

FIG. 6.2 DISPLACEMENTS ALONG CURVED SIDE 1 4 3

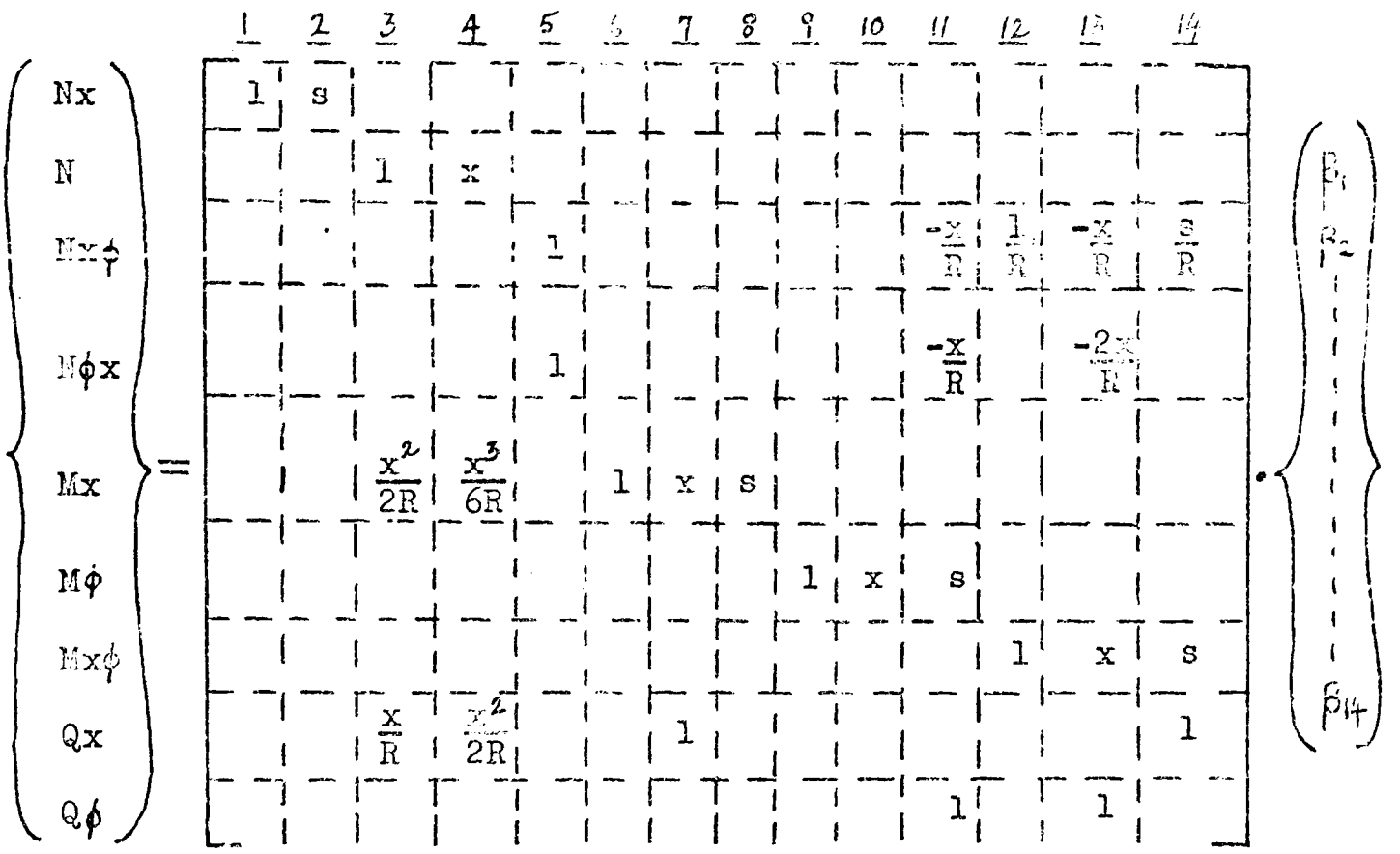

FIG.6.3 STRESS ASSUMPTION FOR TRIANGULAR HYBRID ELEMENT

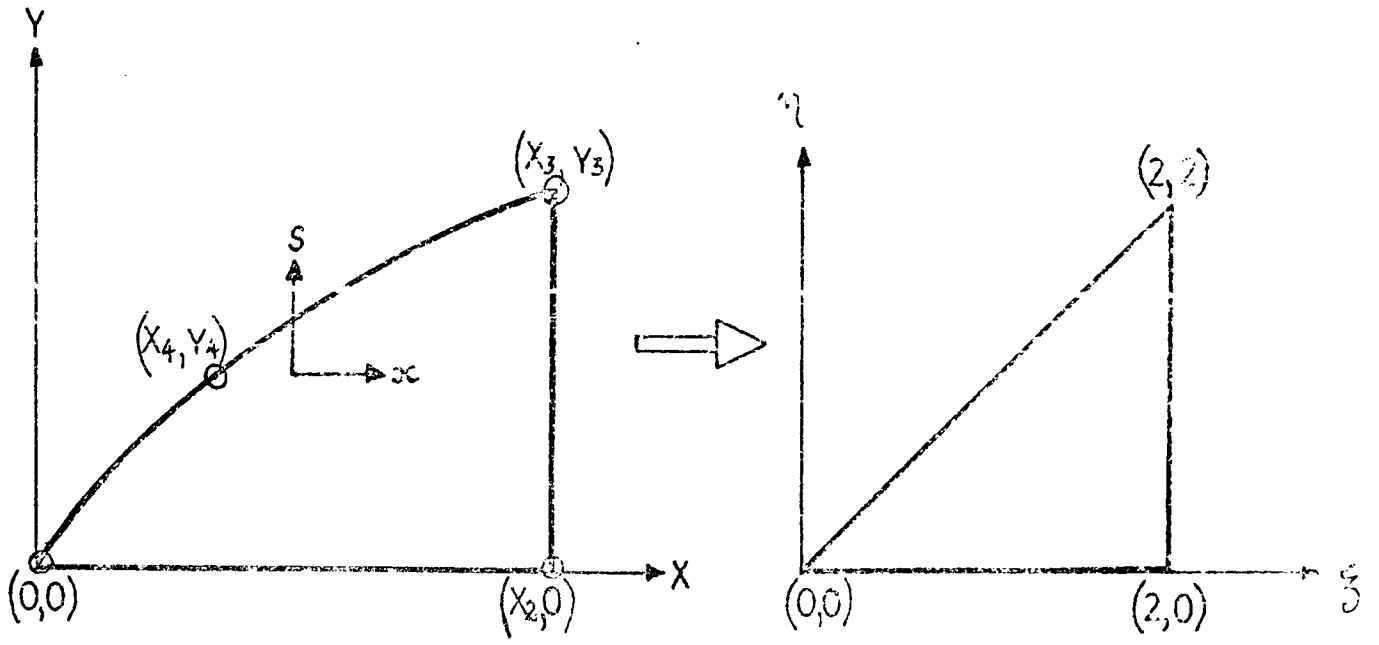

FIG. 6.4 THE TRANSFORMATION

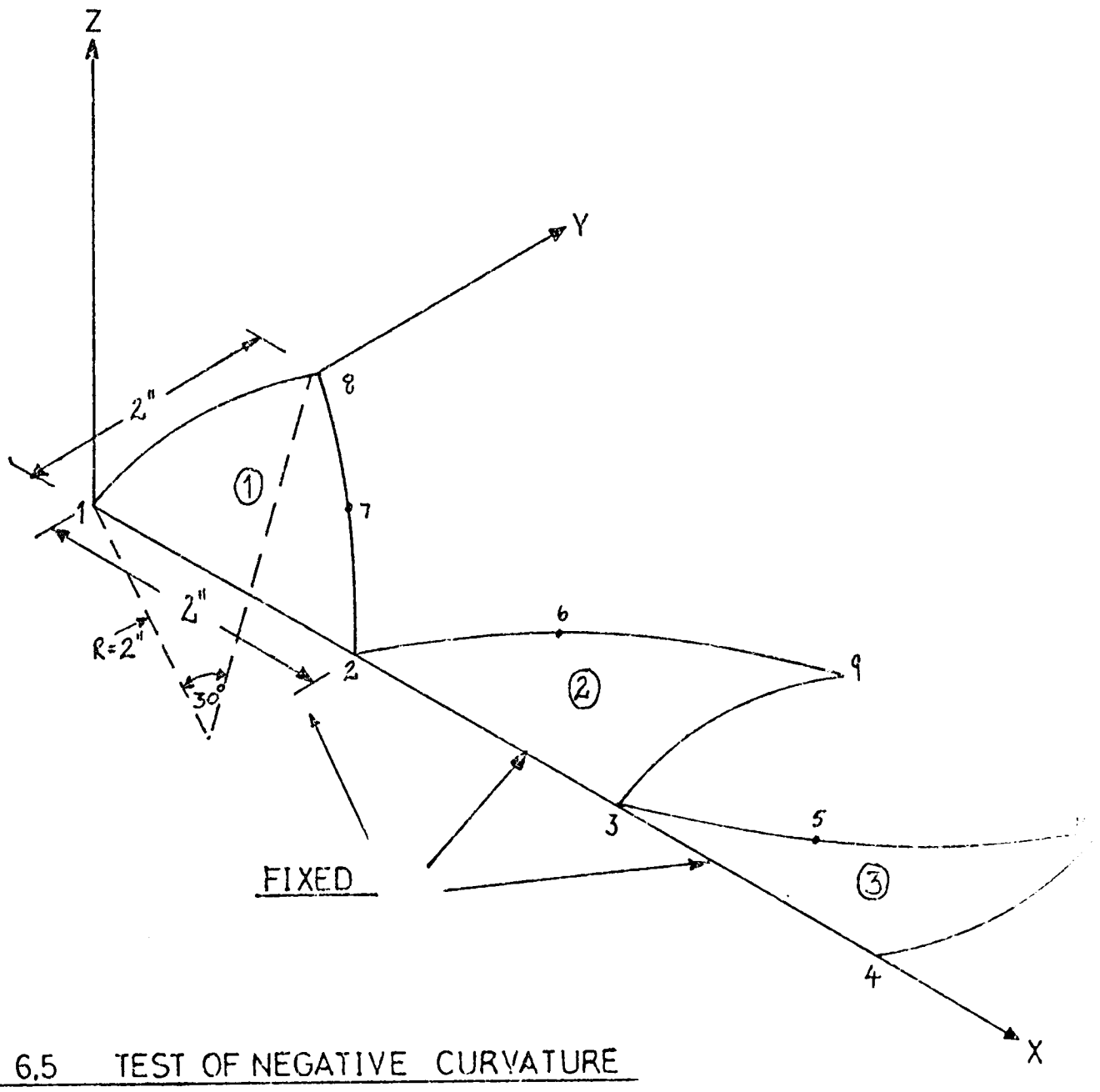

FIG. 6.5 TEST OF NEGATIVE CURVATURE

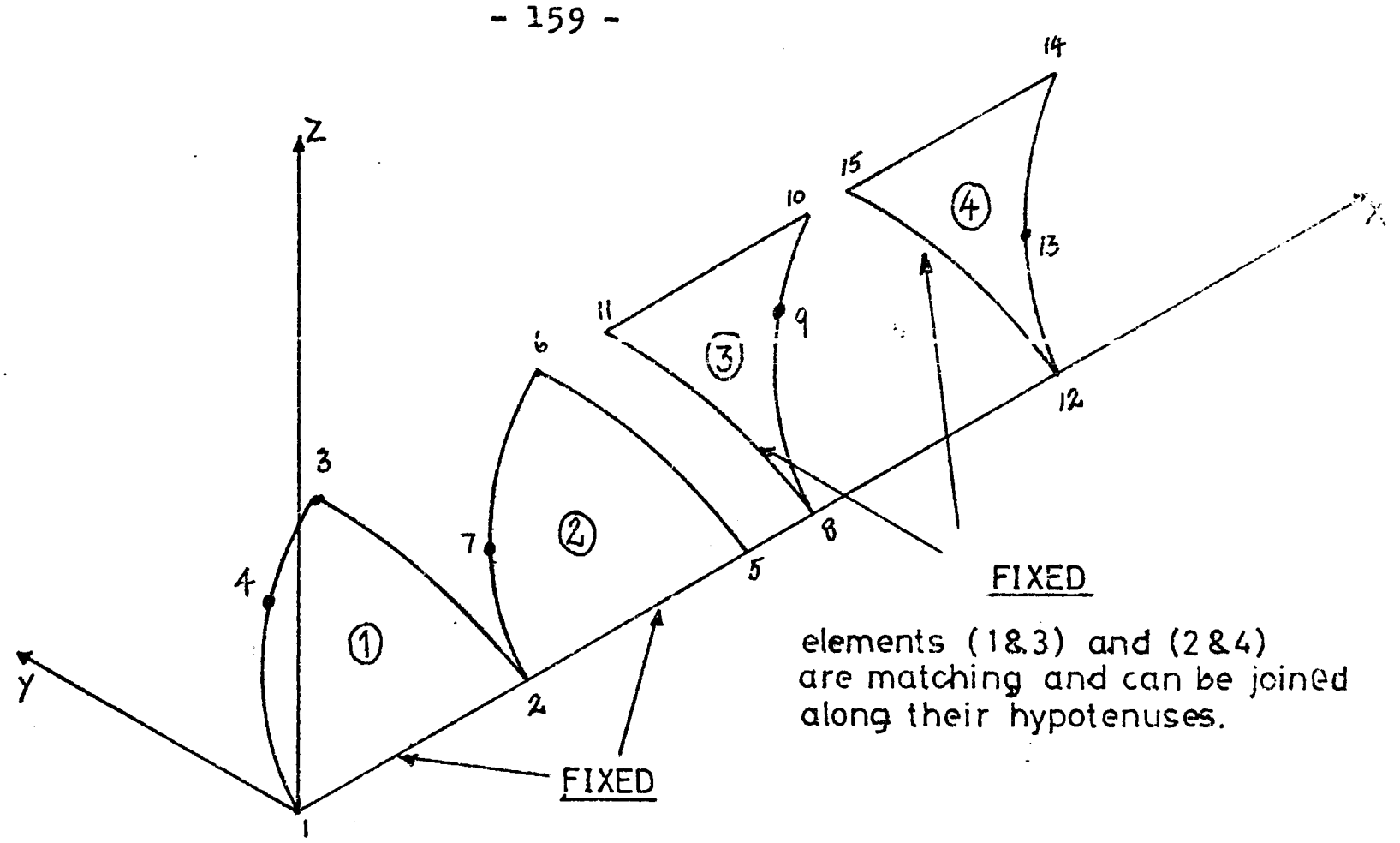

FIG. 6.6 CHANGING THE POSITION OF THE FOURTH NODE.

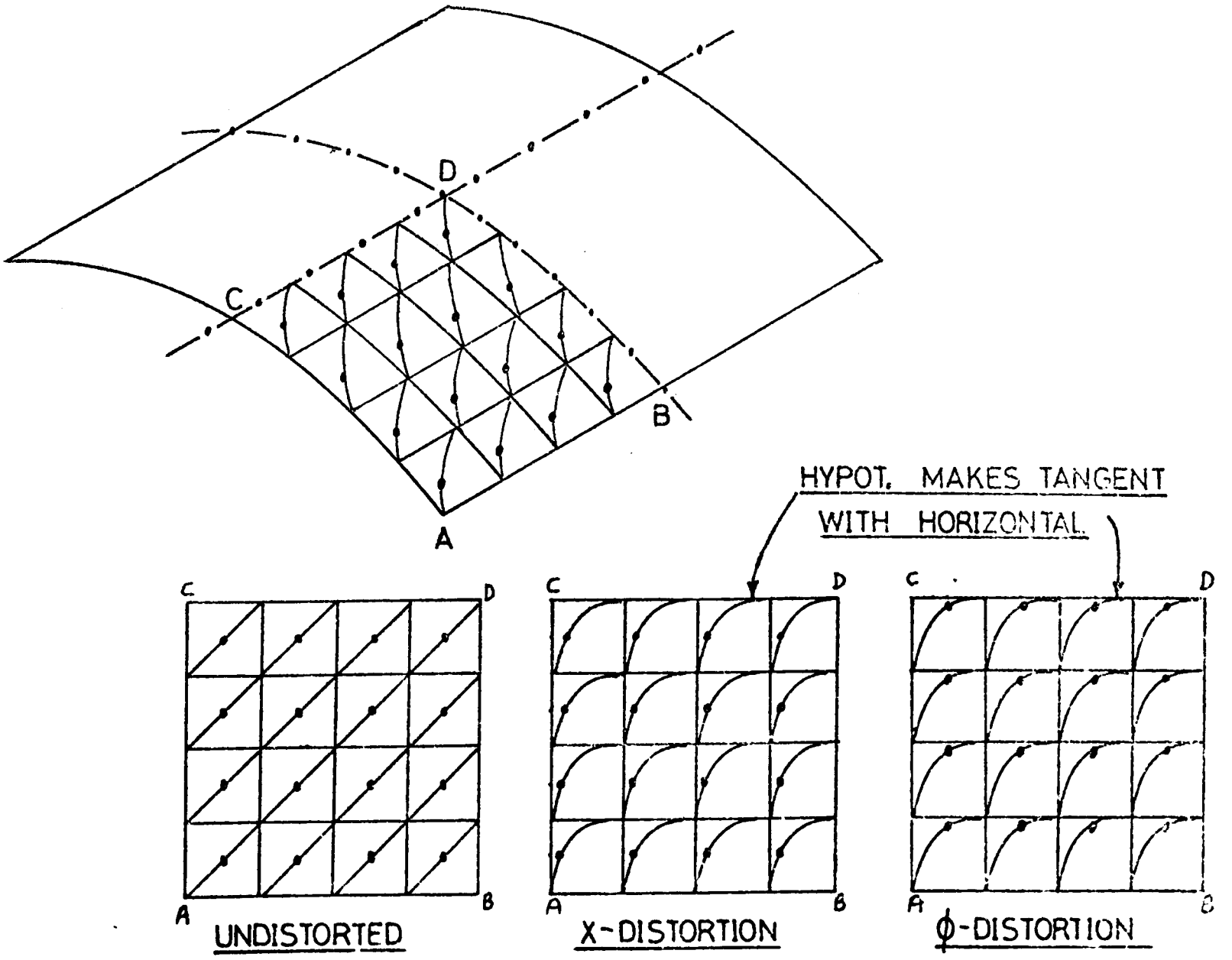

FIG. 6.7 SIMPLY SUPPORTED PANEL USING CURVED HYBRID TRIANGLES

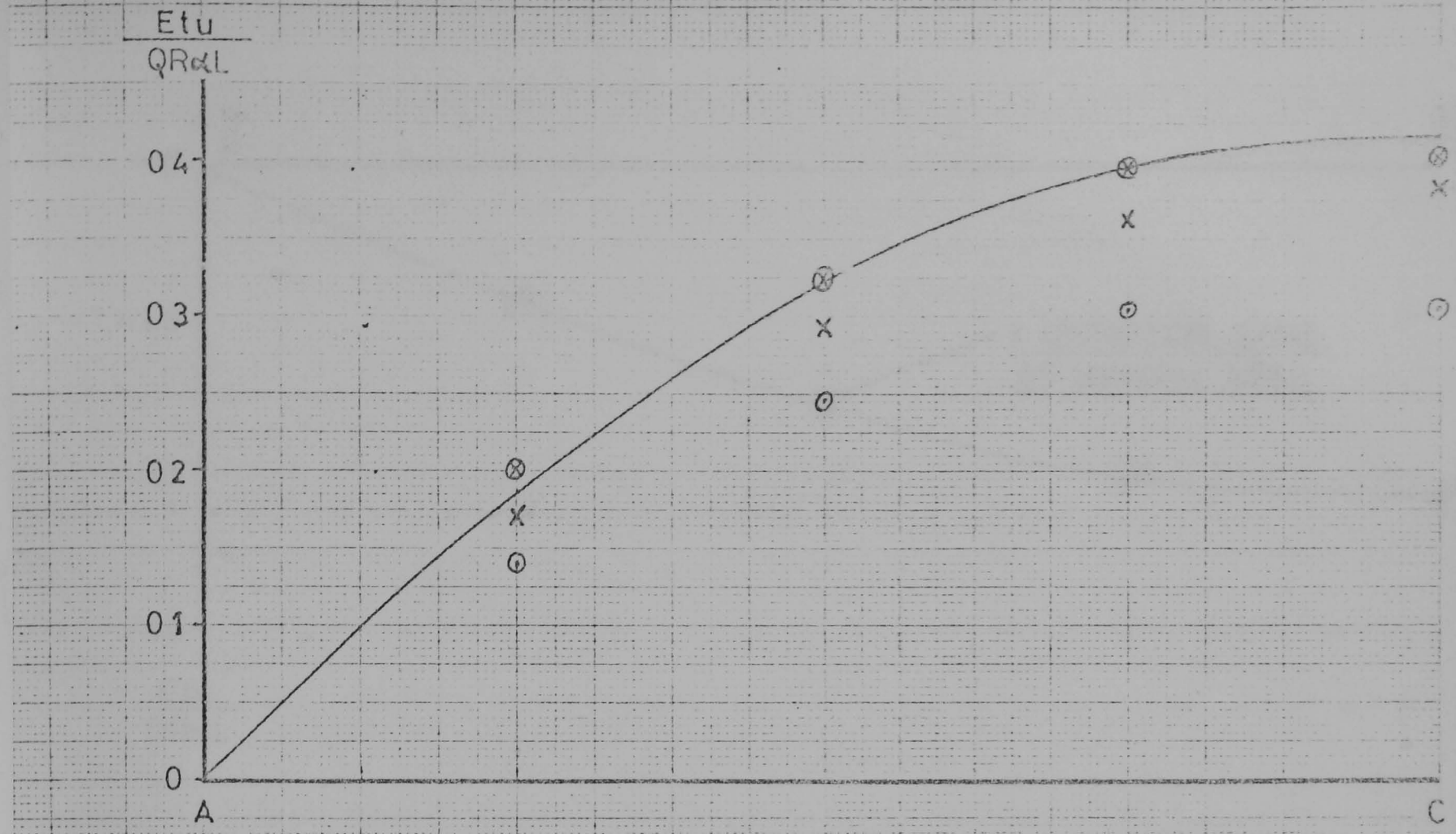

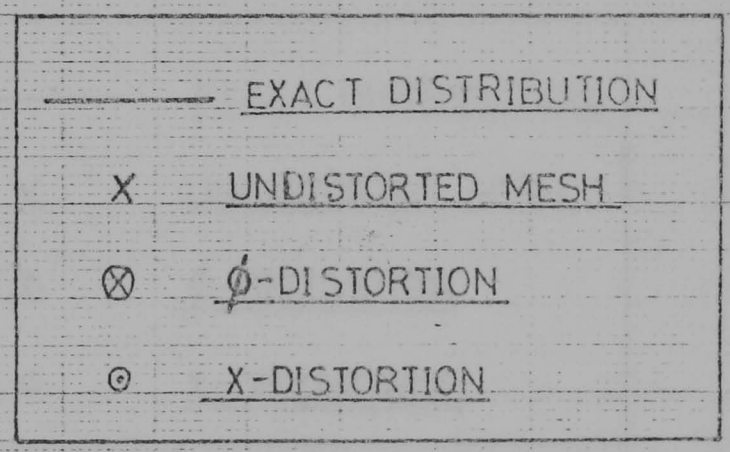

FIG.6.8 u DISPLACEMENTS OF PANEL USING 4 x 4 MESH OF CURVED TRIANGULAR ELEMENTS

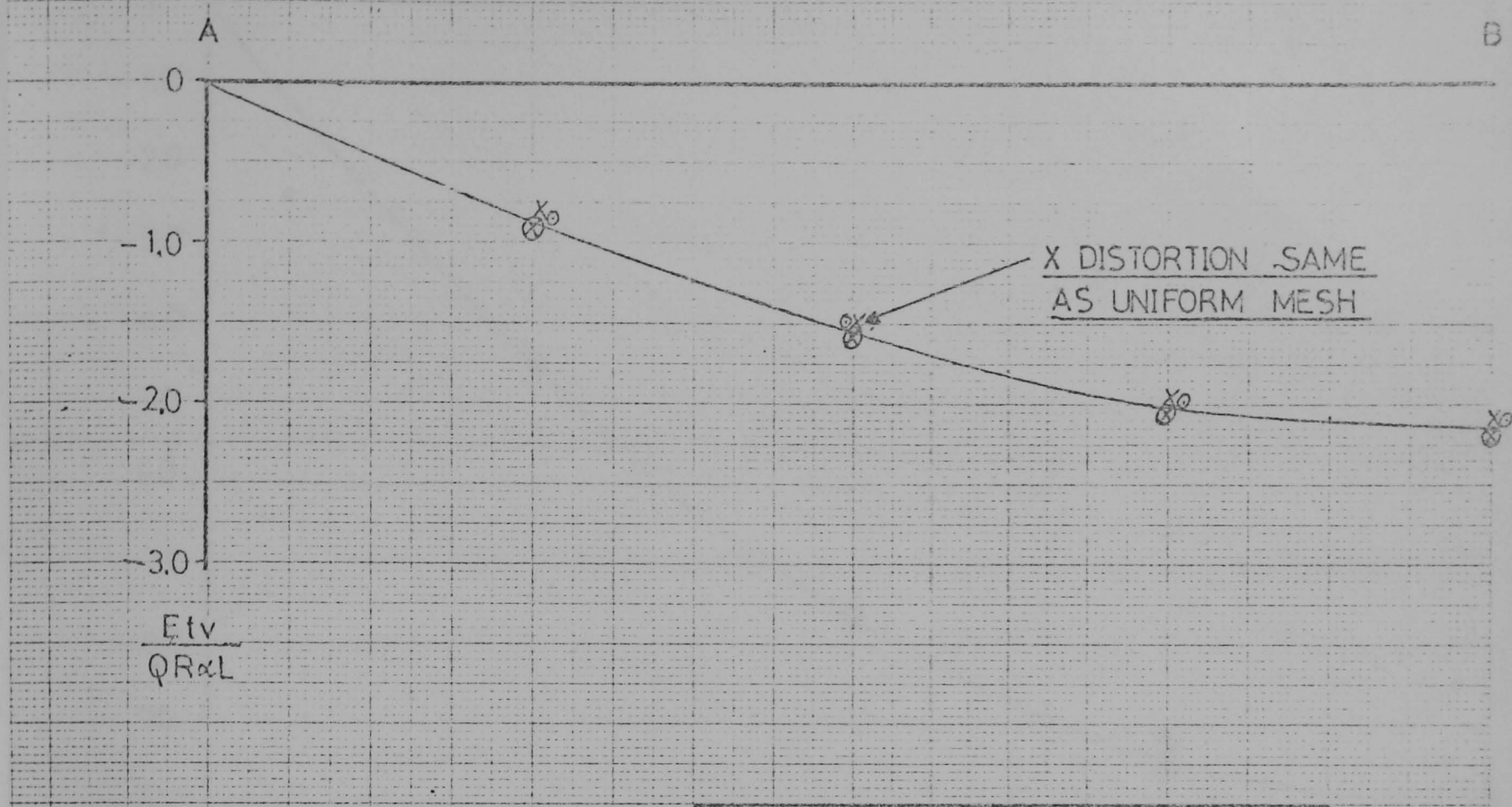

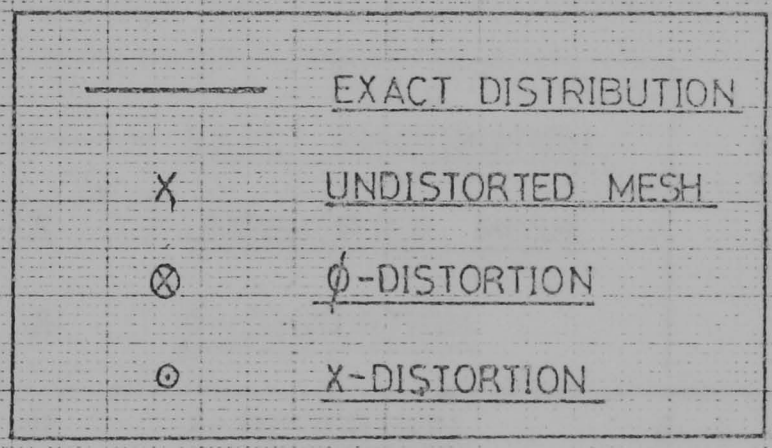

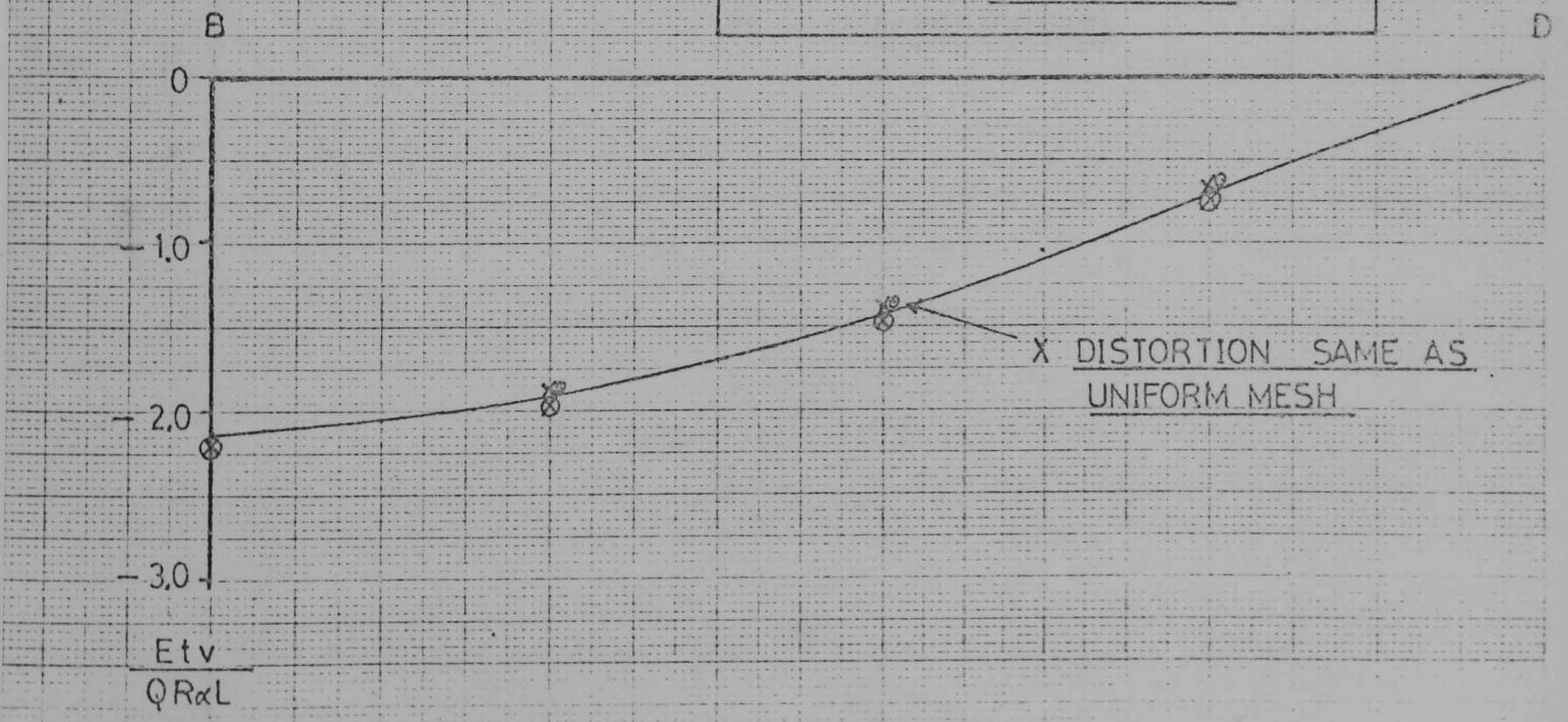

FIG.6.9 v DISPLACEMENTS OF PANEL USING 4 x 4 MESH OF CURVED TRIANGULAR ELEMENTS

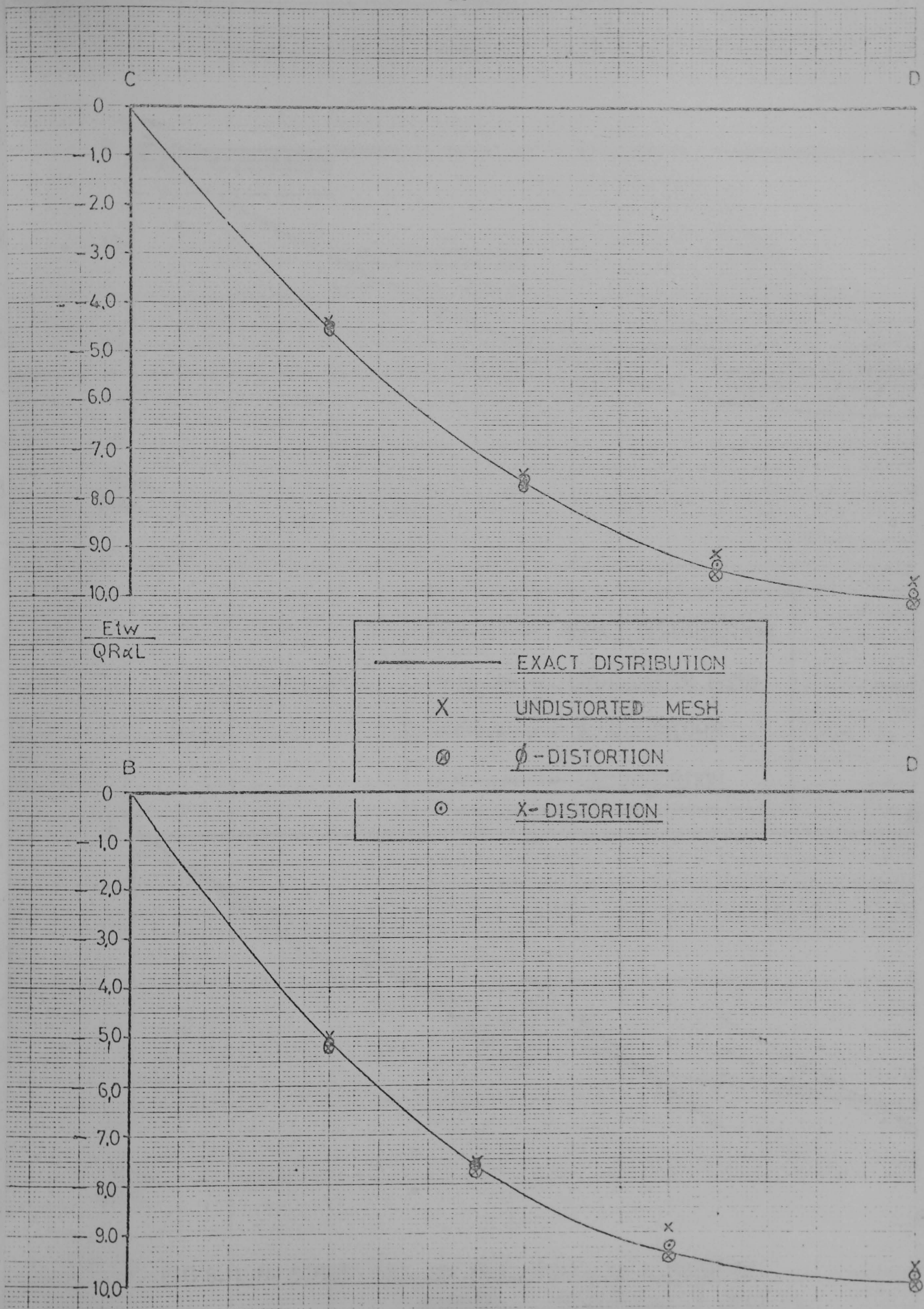

FIG.6.10 w DISPLACEMENTS OF PANEL USING 4 X 4 MESH OF CURVED TRIANGULAR ELEMENTS

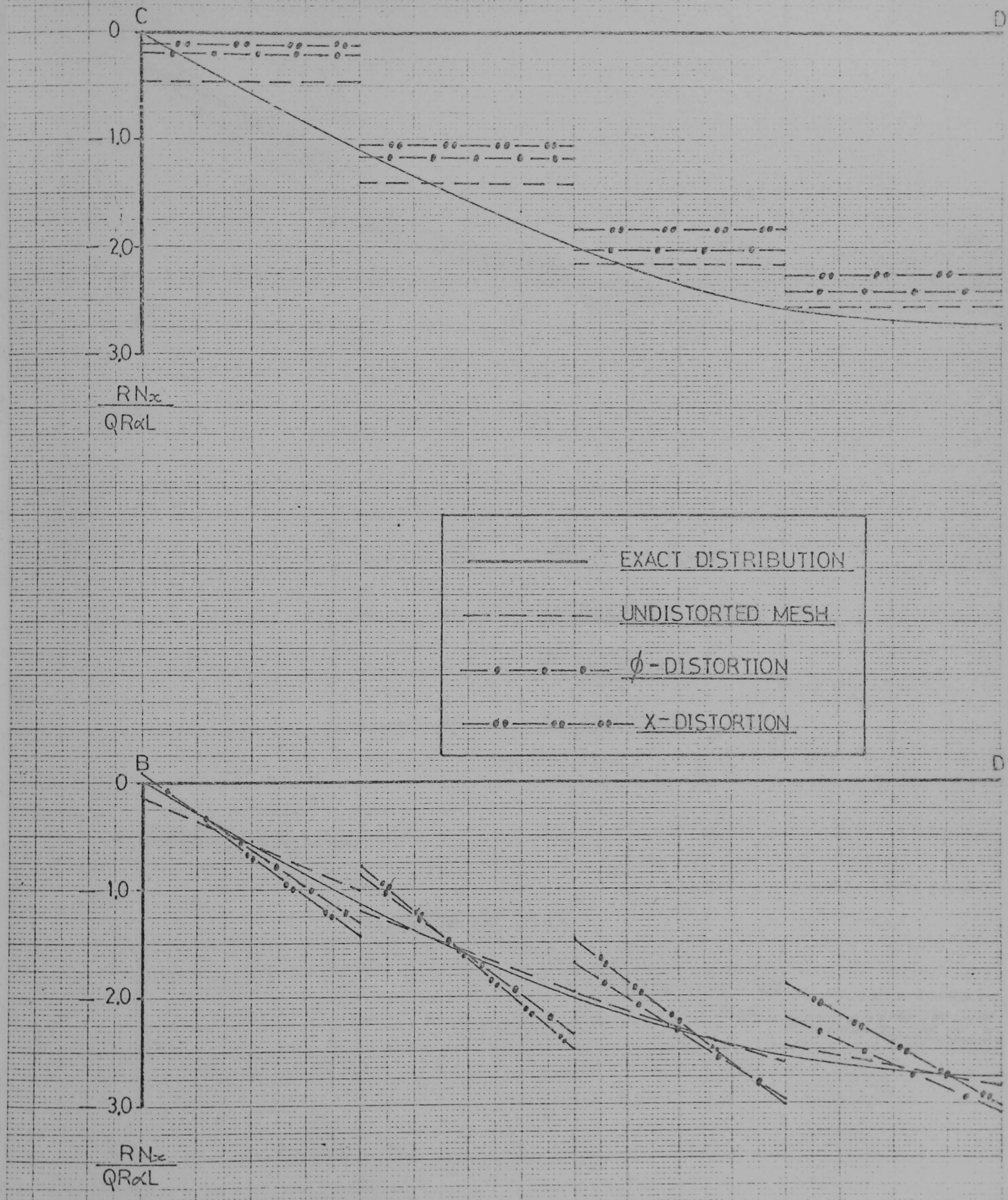

FIG 6.11 N_x STRESS RES. ON PANEL USING 4 x 4 MESH OF CURVED TRIANGULAR ELEMENTS.

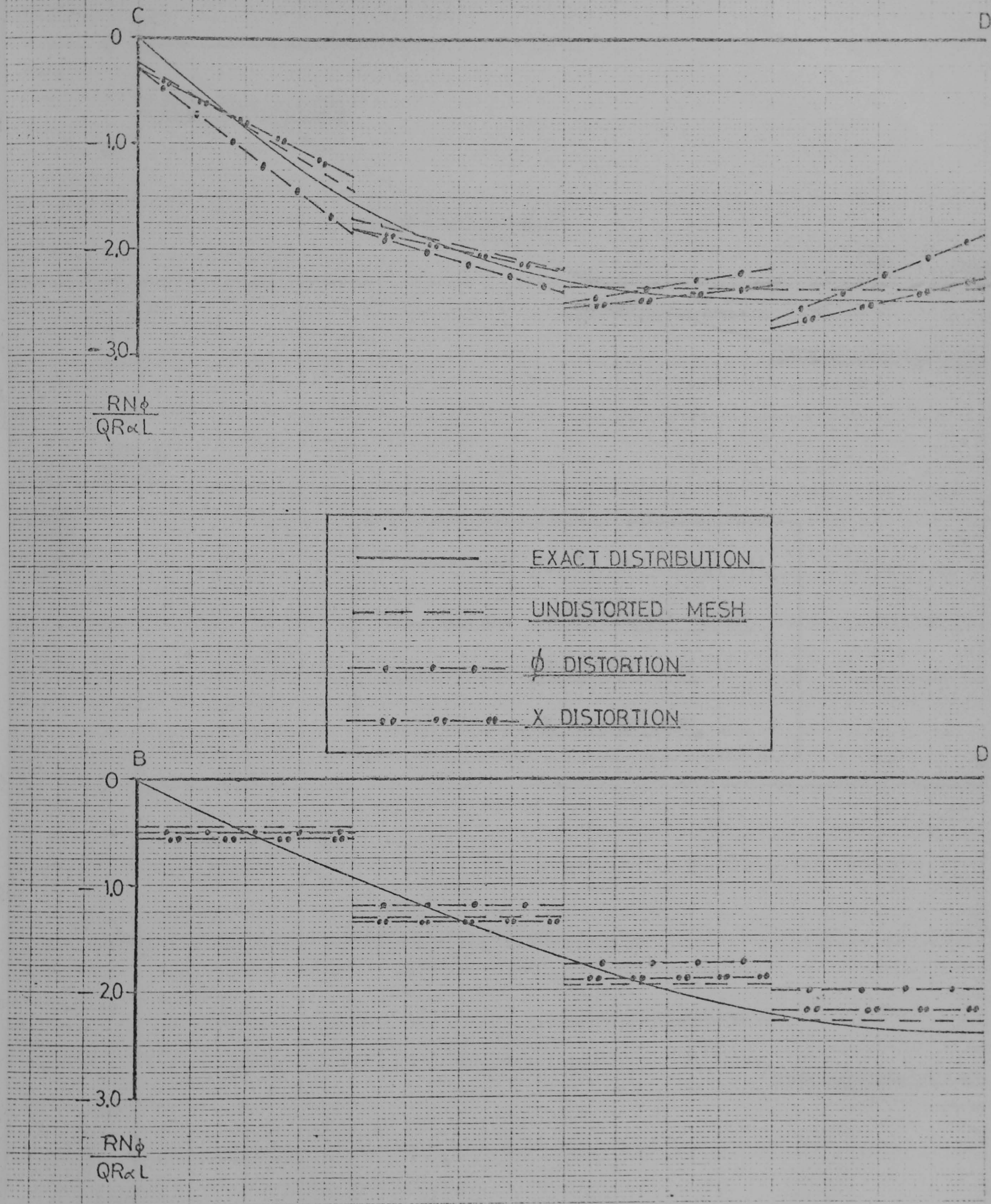

FIG 6.12 Nφ STRESS RES. ON PANEL USING 4 x 4 MESH OF CURVED TRIANGULAR ELEMENTS

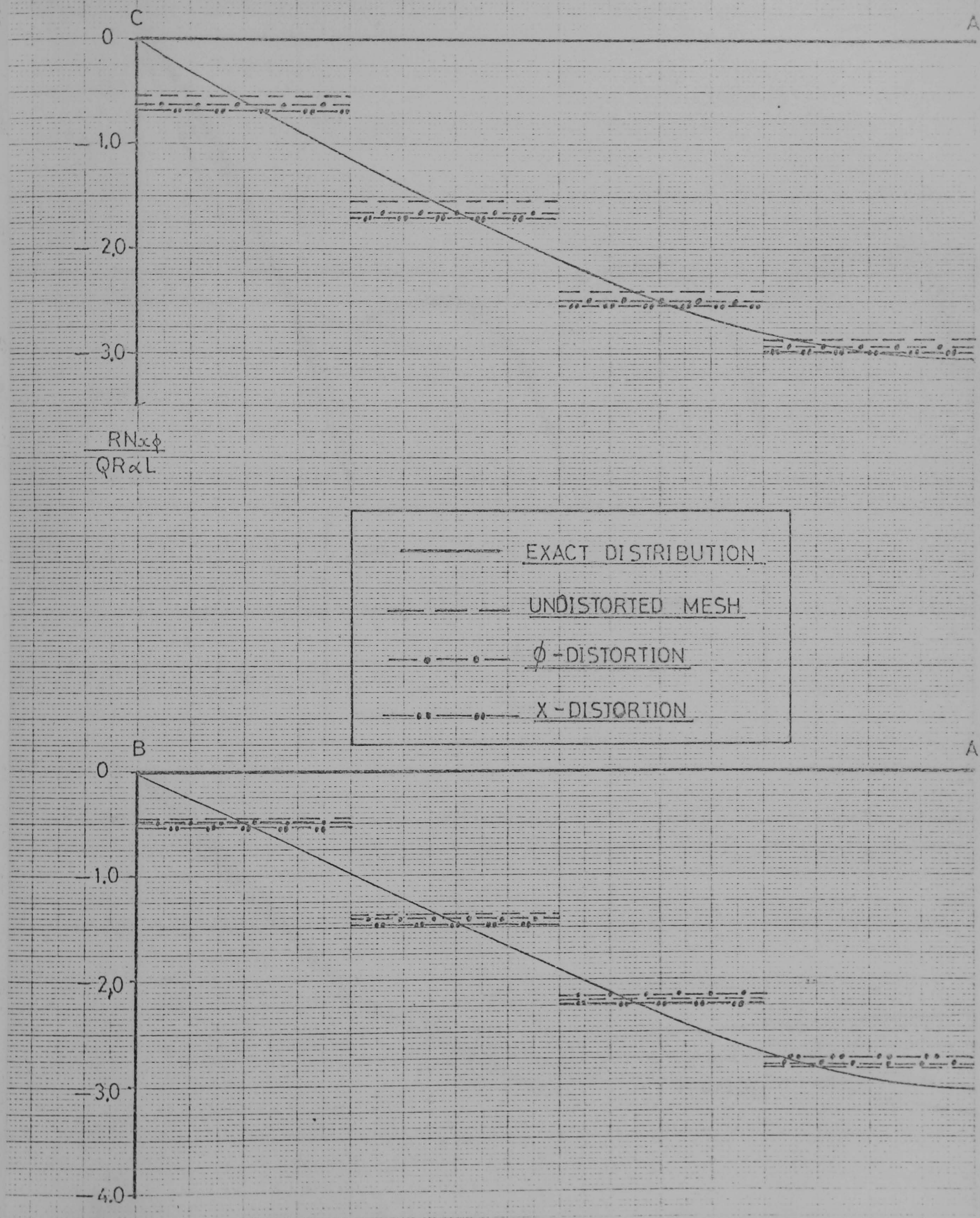

FIG. 6.13 $N_{x\phi}$ STRESS RES. ON PANEL USING 4 X 4 MESH OF CURVED TRIANGULAR ELEMENTS.

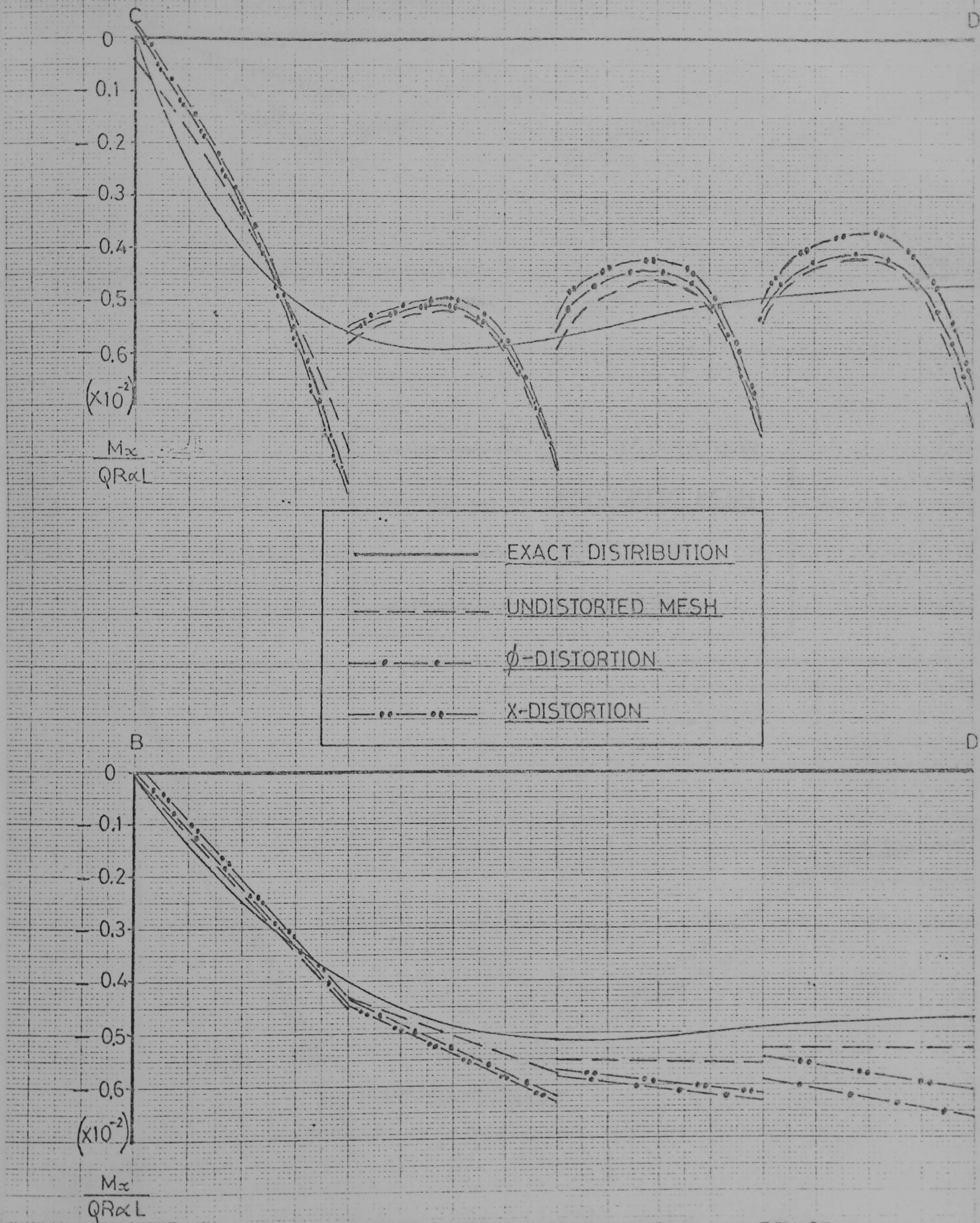

FIG.6.14 M_x STRESS RES. ON PANEL USING 4 x 4 MESH OF CURVED TRIANGULAR ELEMENTS

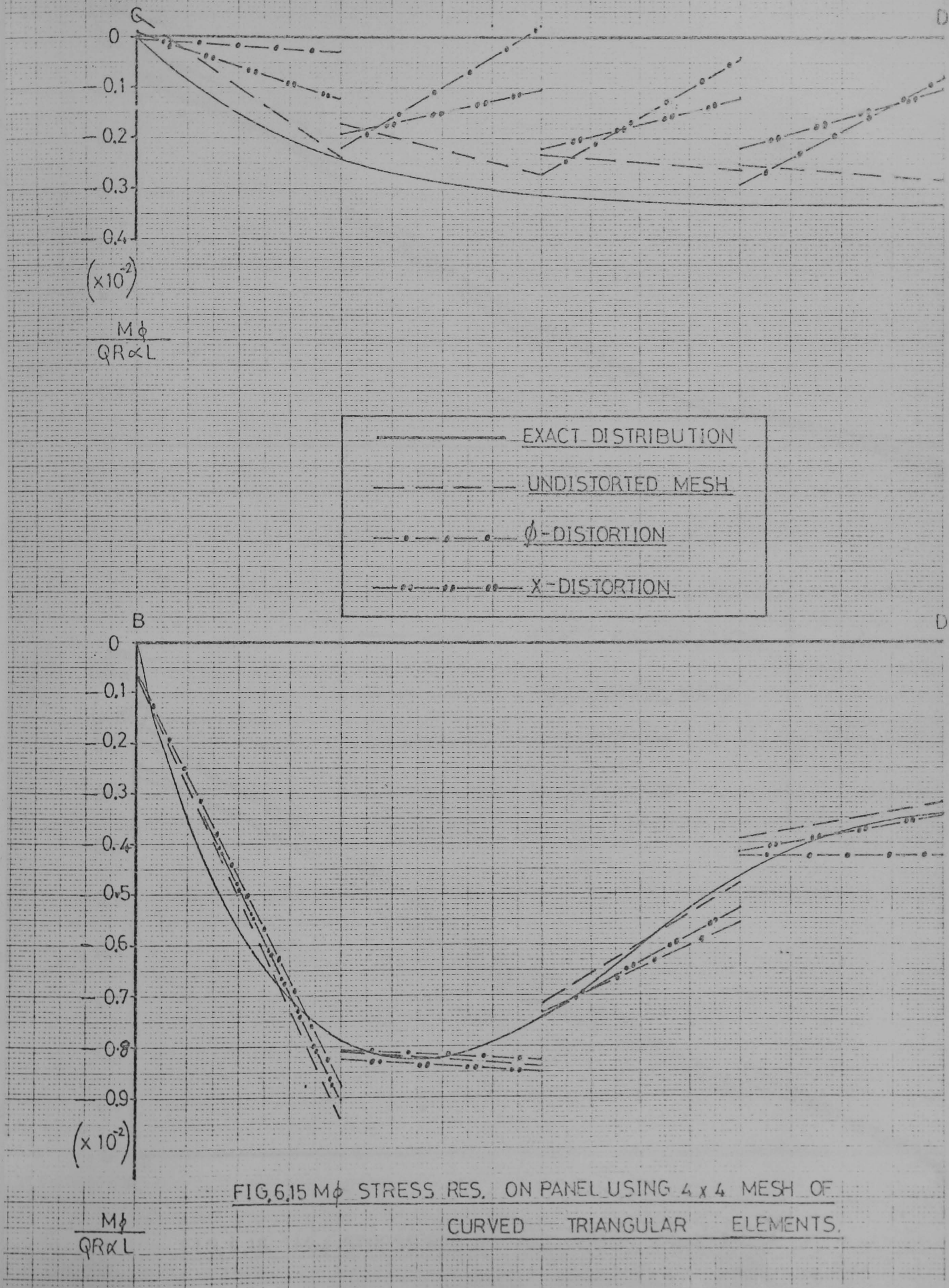

FIG.6.15 Mφ STRESS RES. ON PANEL USING 4 x 4 MESH OF CURVED TRIANGULAR ELEMENTS.

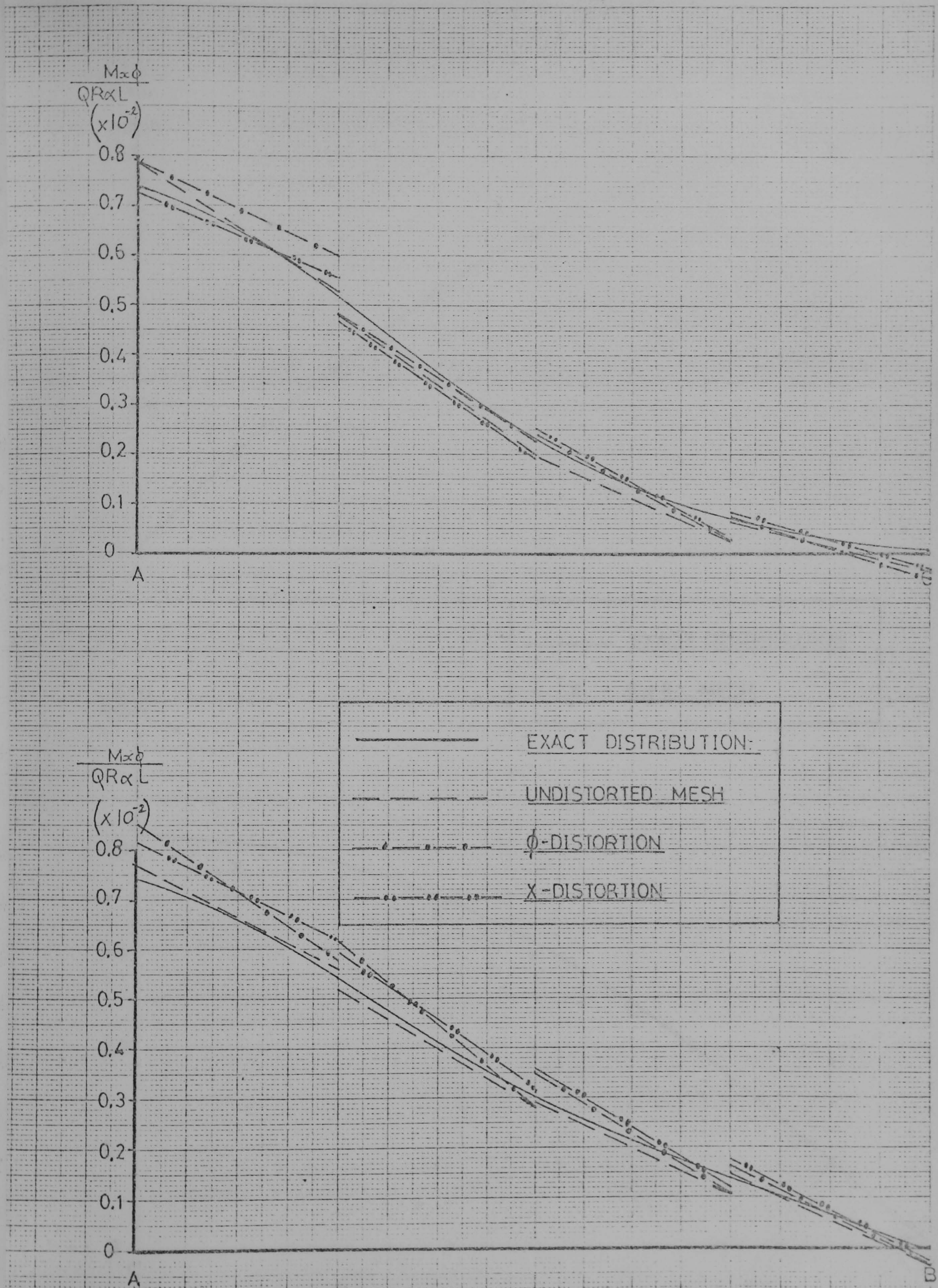

FIG. 6.16 $M_x\phi$ STRESS RES. ON PANEL USING 4 x 4 MESH OF CURVED TRIANGULAR ELEMENTS

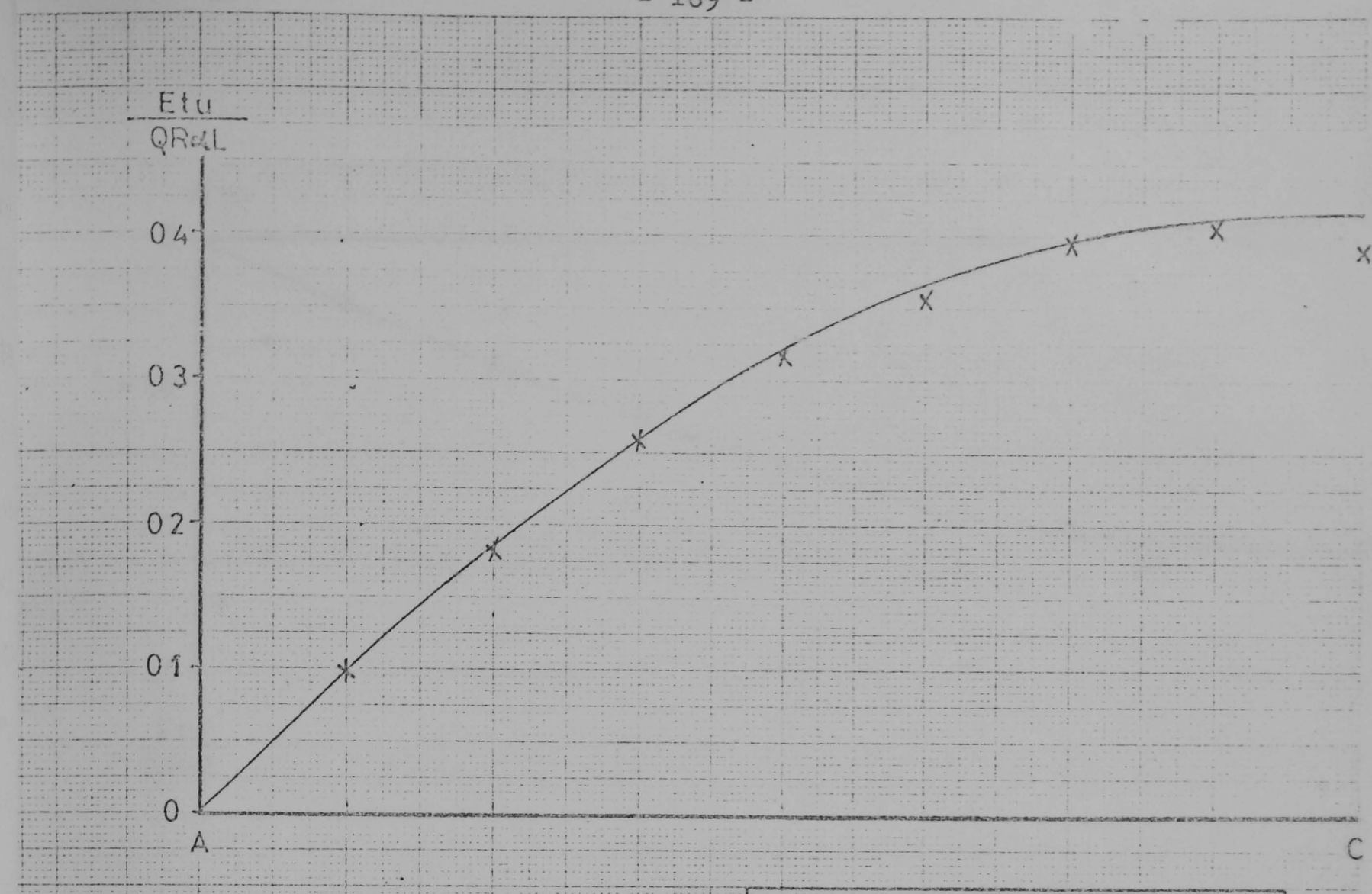

FIG. 6.17 u DISPLACEMENTS OF PANEL USING 8 x 8 MESH OF CURVED TRIANGULAR ELEMENTS

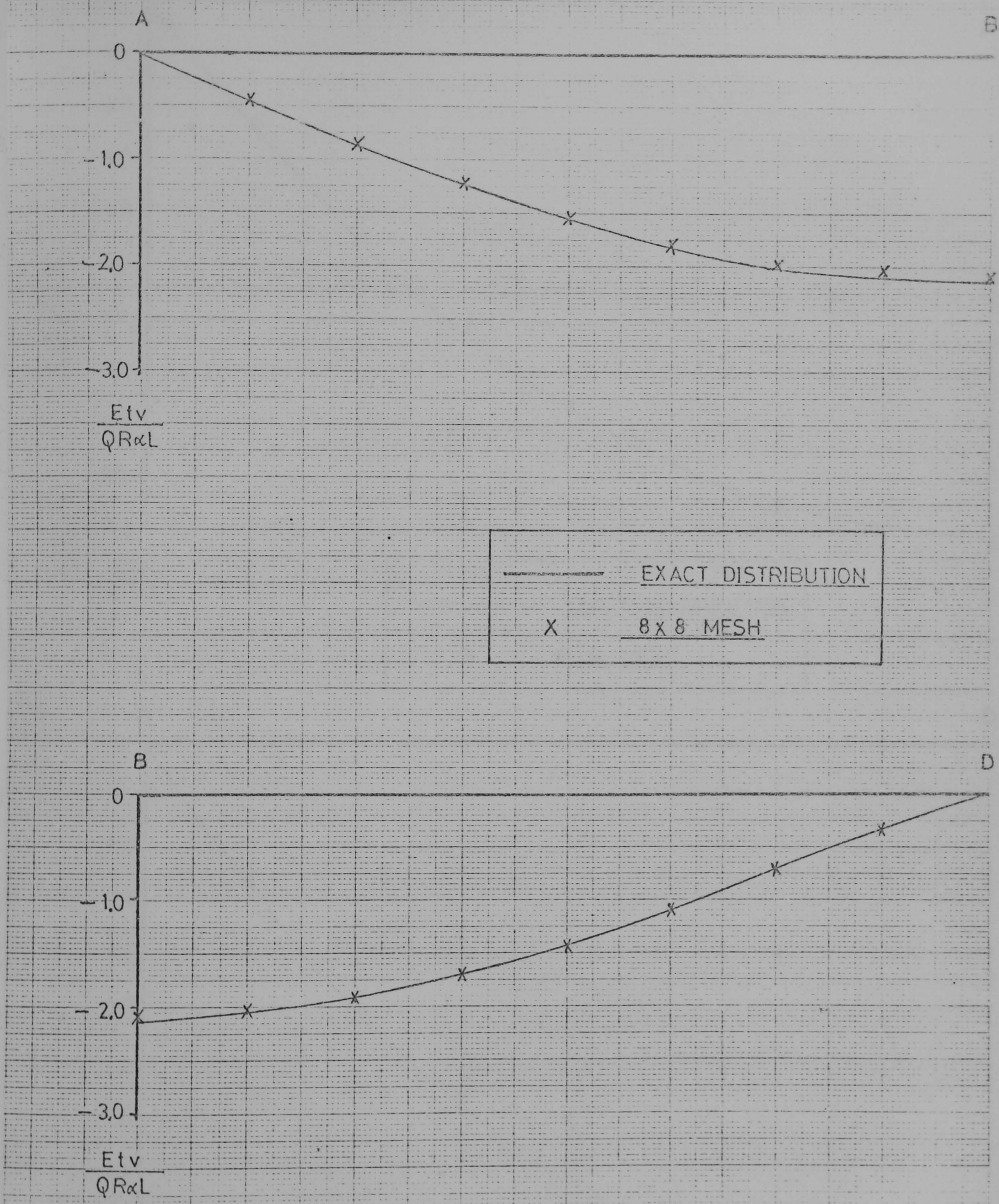

FIG.6.18 v DISPLACEMENTS OF PANEL USING 8 x 8 MESH OF CURVED TRIANGULAR ELEMENTS

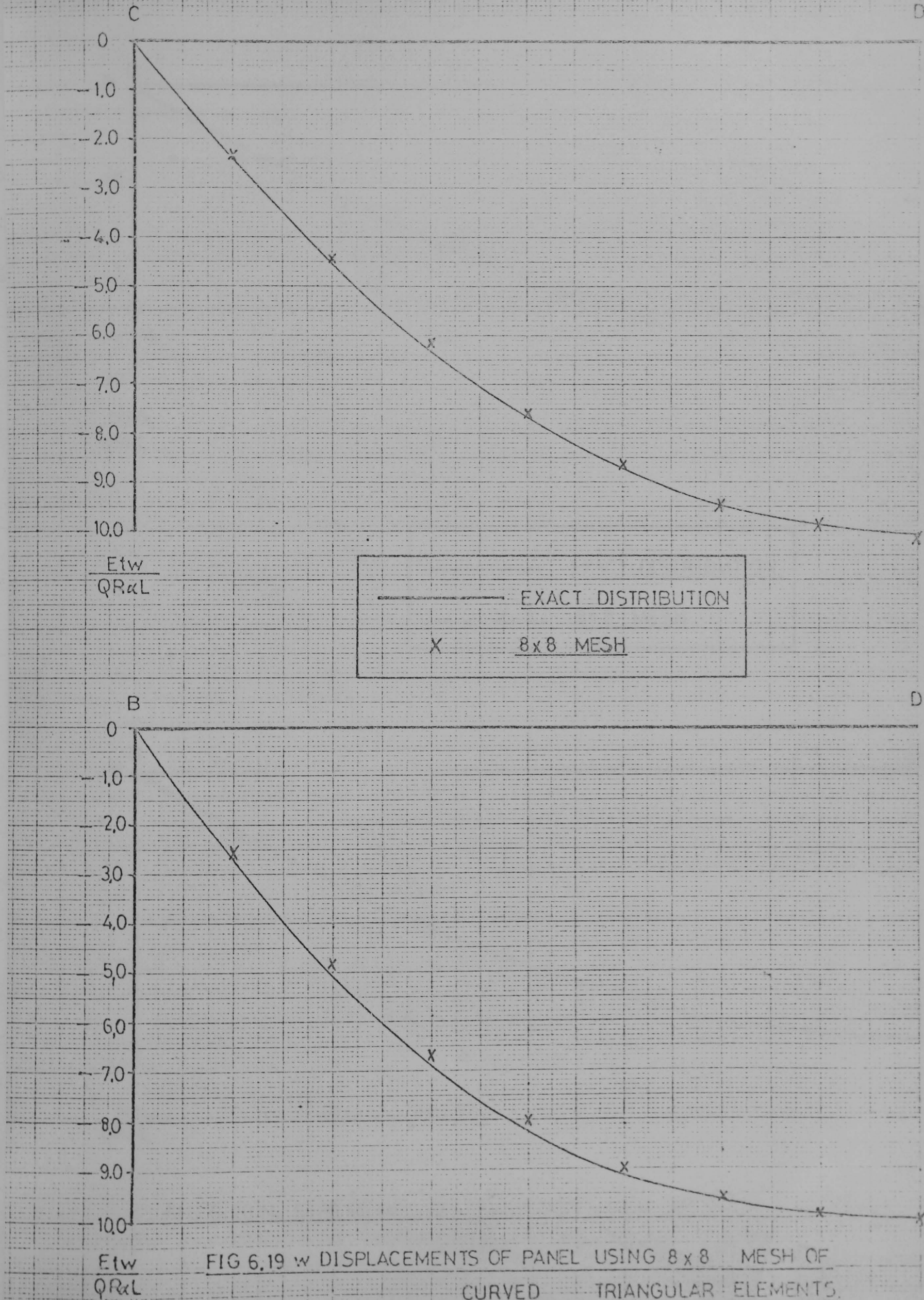

FIG 6.19 w DISPLACEMENTS OF PANEL USING 8 x 8 MESH OF CURVED TRIANGULAR ELEMENTS

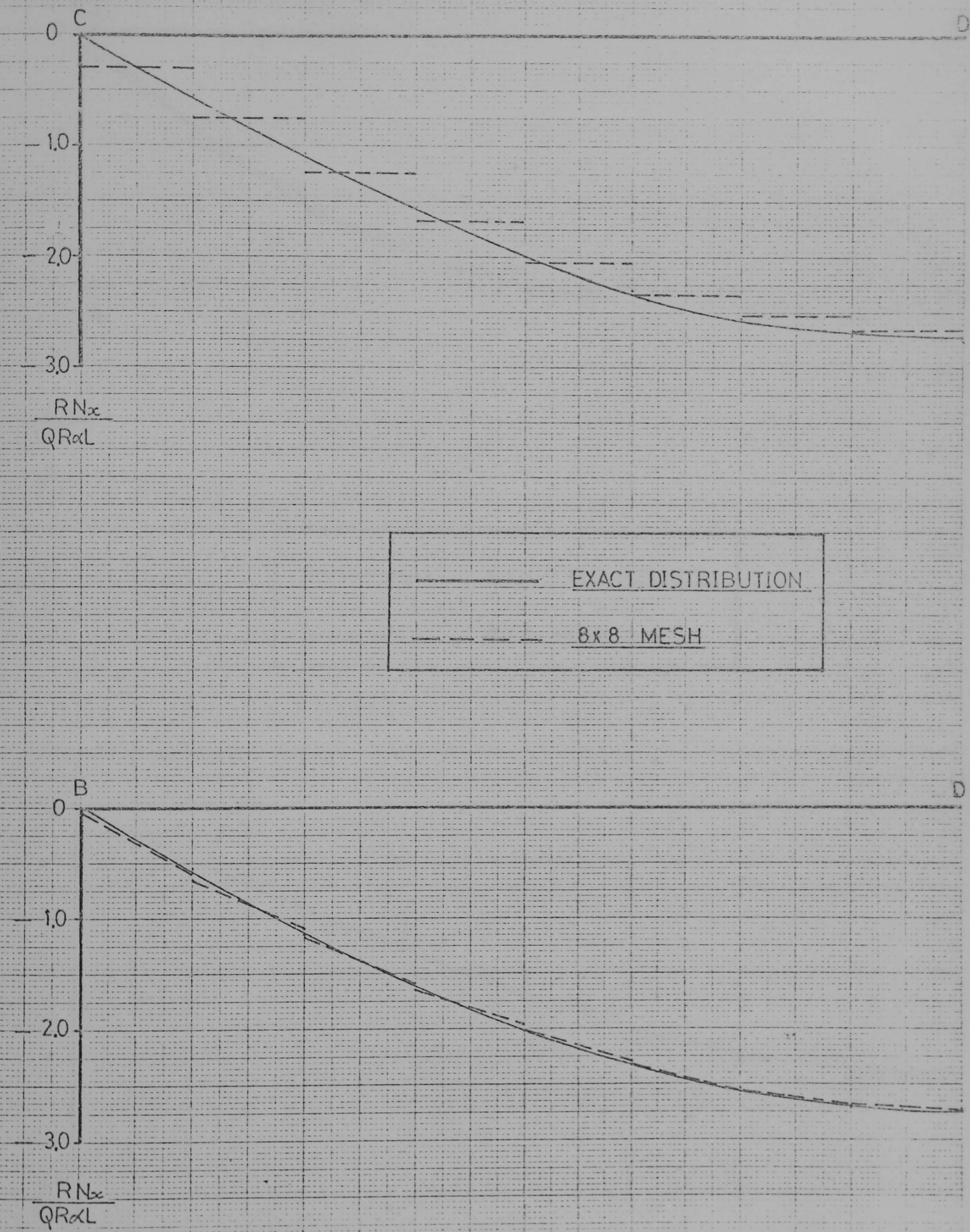

FIG 6.20 N_x STRESS RES. ON PANEL USING 8x8 MESH OF CURVED TRIANGULAR ELEMENTS.

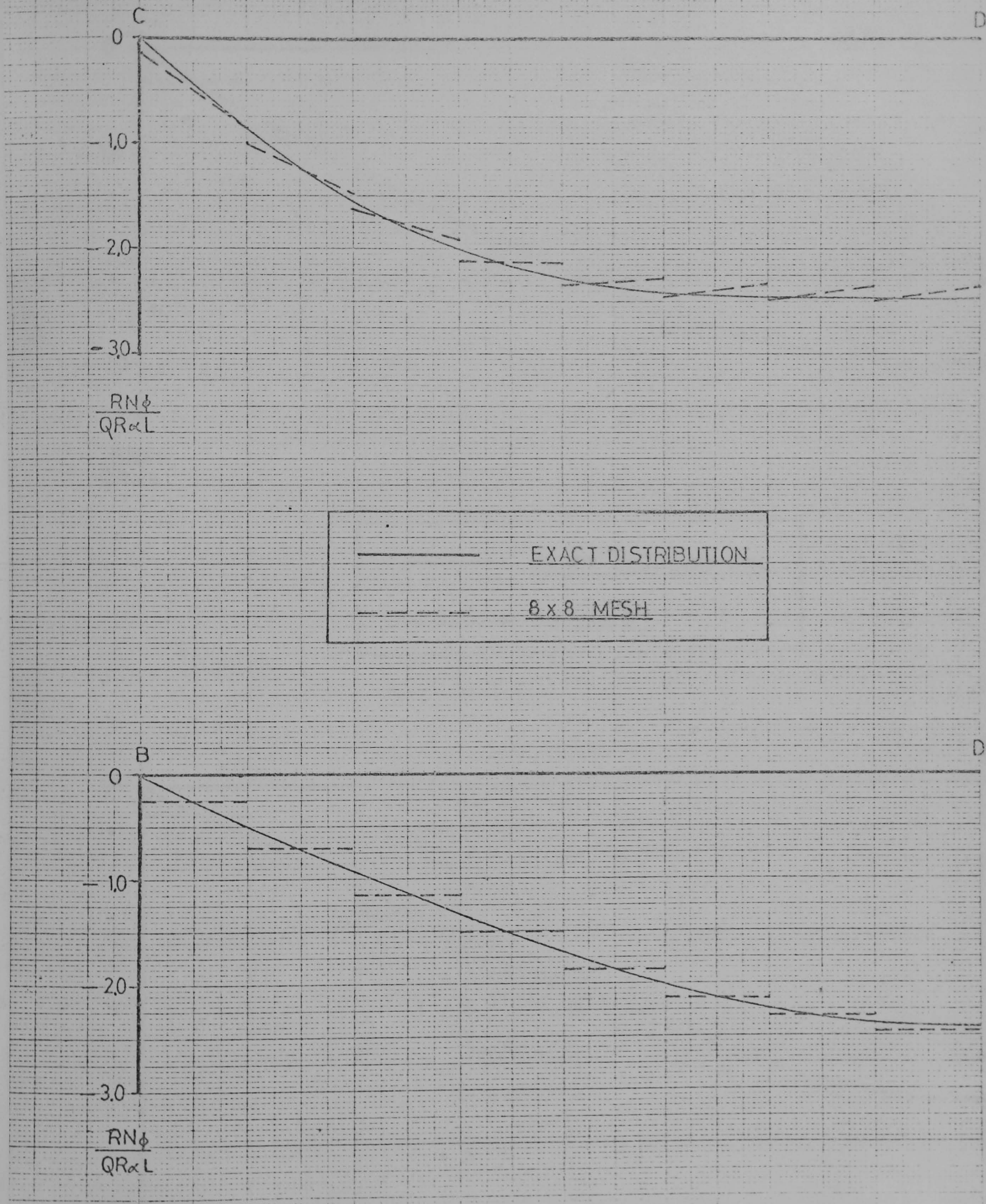

FIG. 6.21 N_ϕ STRESS RES. ON PANEL USING 8 x 8 MESH OF CURVED TRIANGULAR ELEMENTS

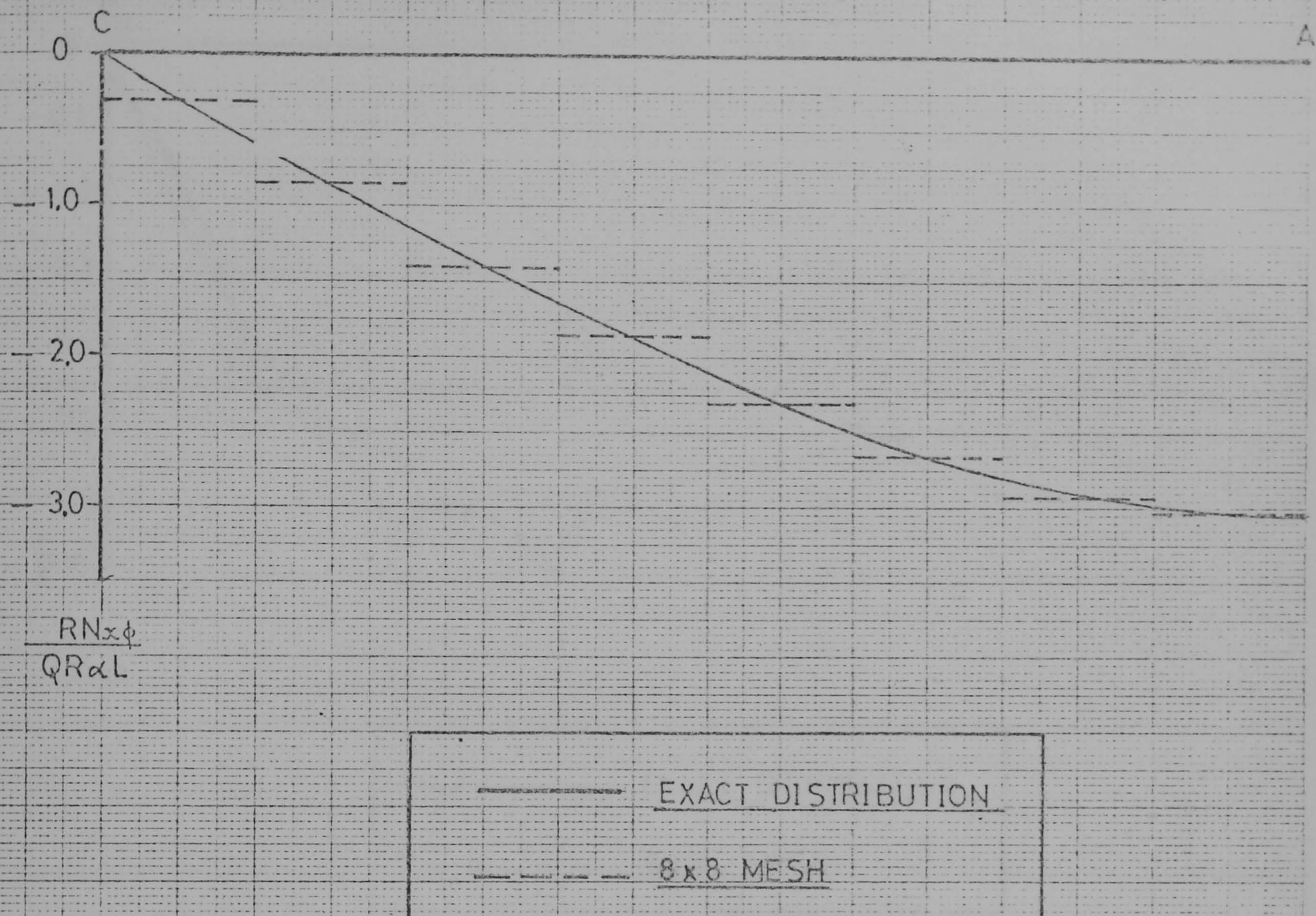

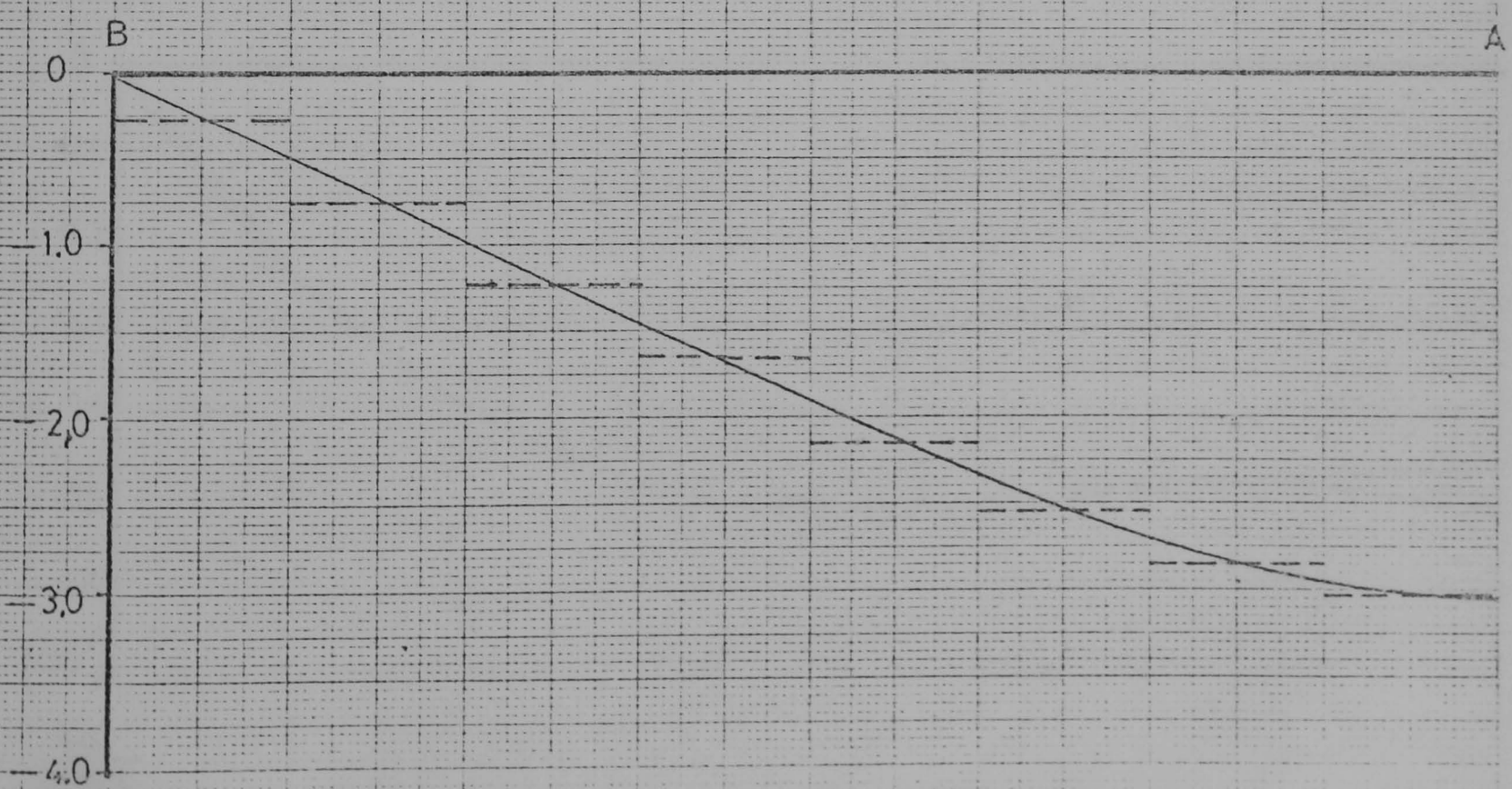

FIG. 6.22 $N_x\phi$ STRESS RES. ON PANEL USING 8x8 MESH OF CURVED TRIANGULAR ELEMENTS.

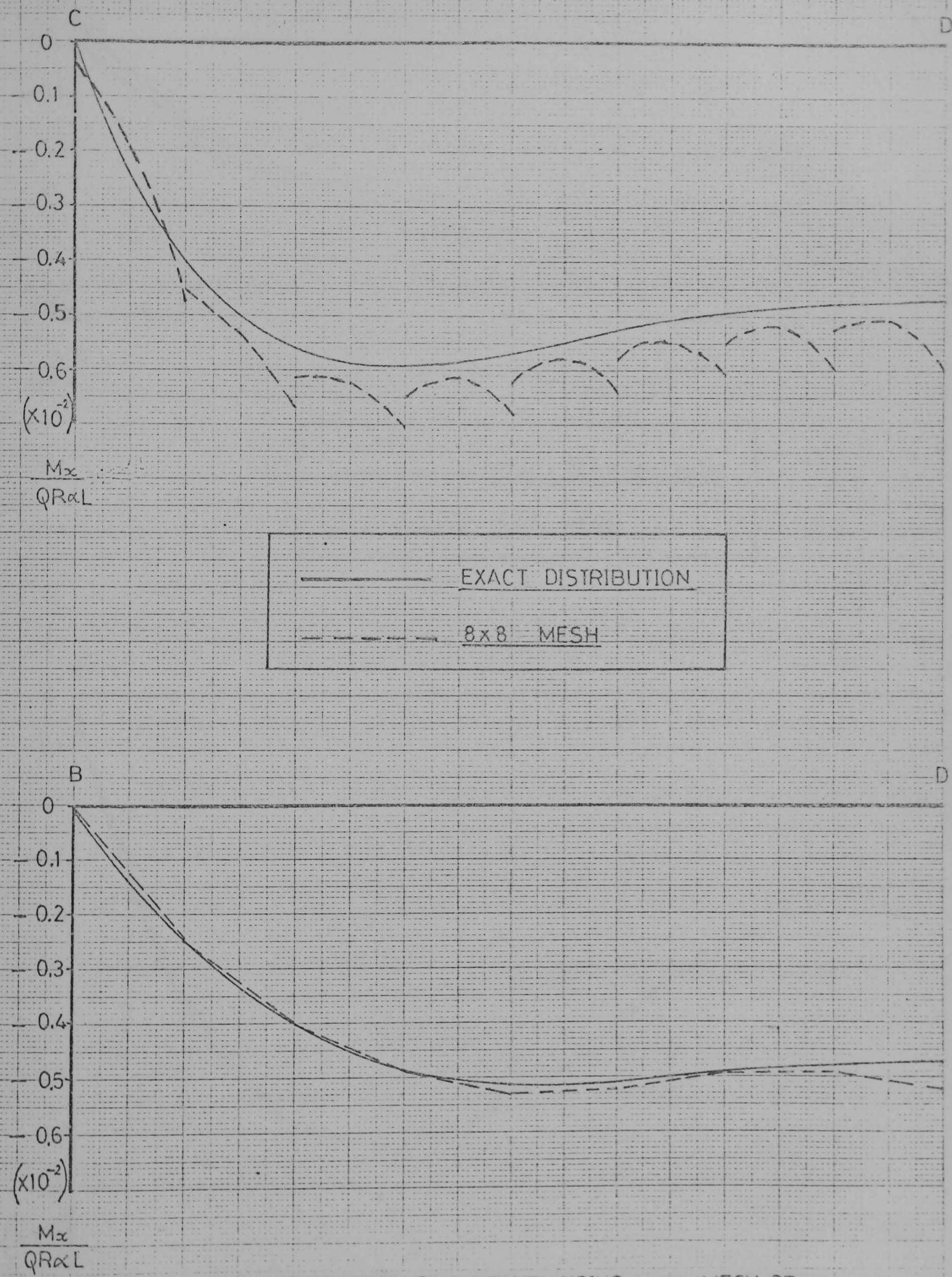

FIG. 6.23 M_x STRESS RES. ON PANEL USING 8 x 8 MESH OF CURVED TRIANGULAR ELEMENTS

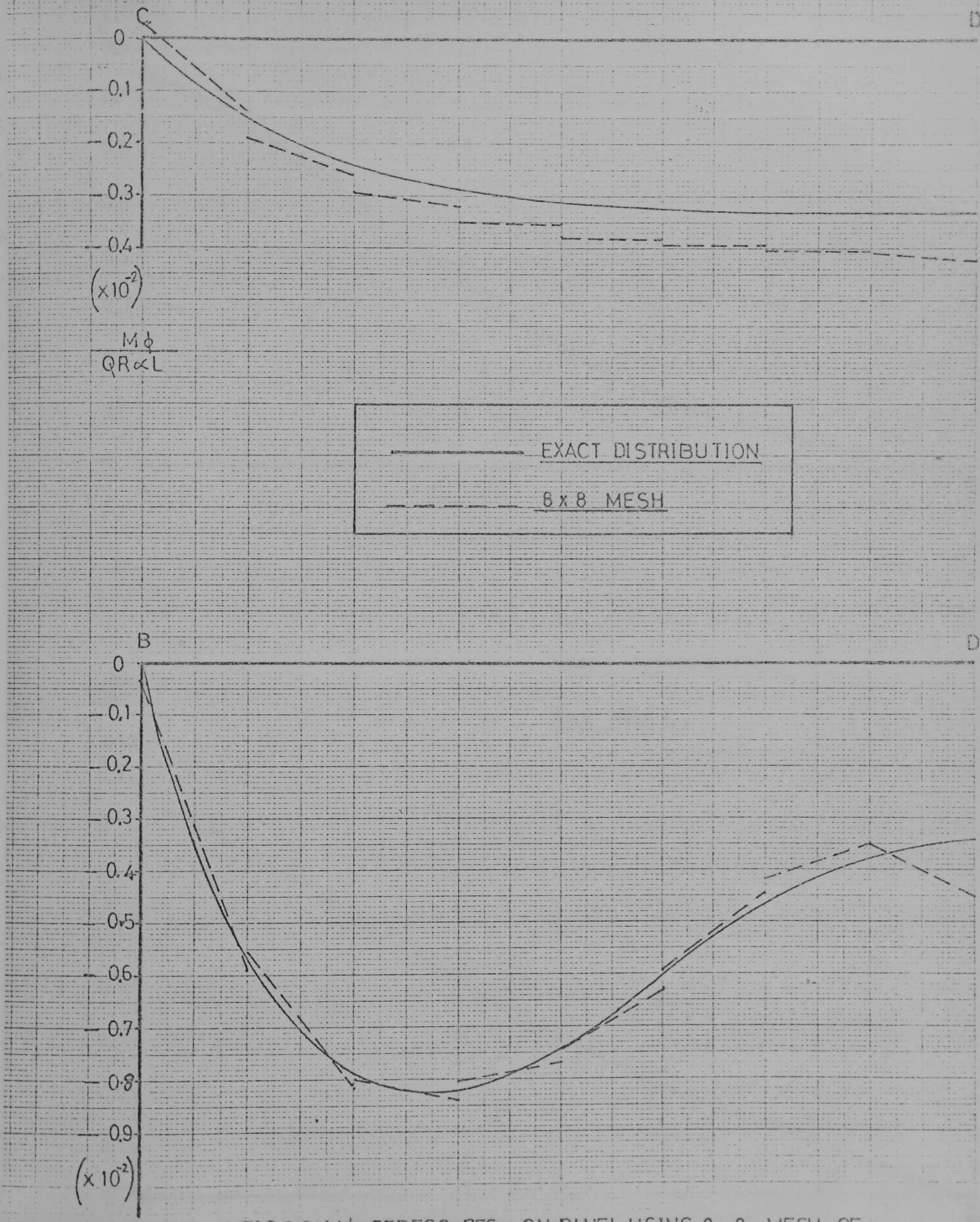

FIG.6.24 Mϕ STRESS RES. ON PANEL USING 8 x 8 MESH OF CURVED TRIANGULAR ELEMENTS.

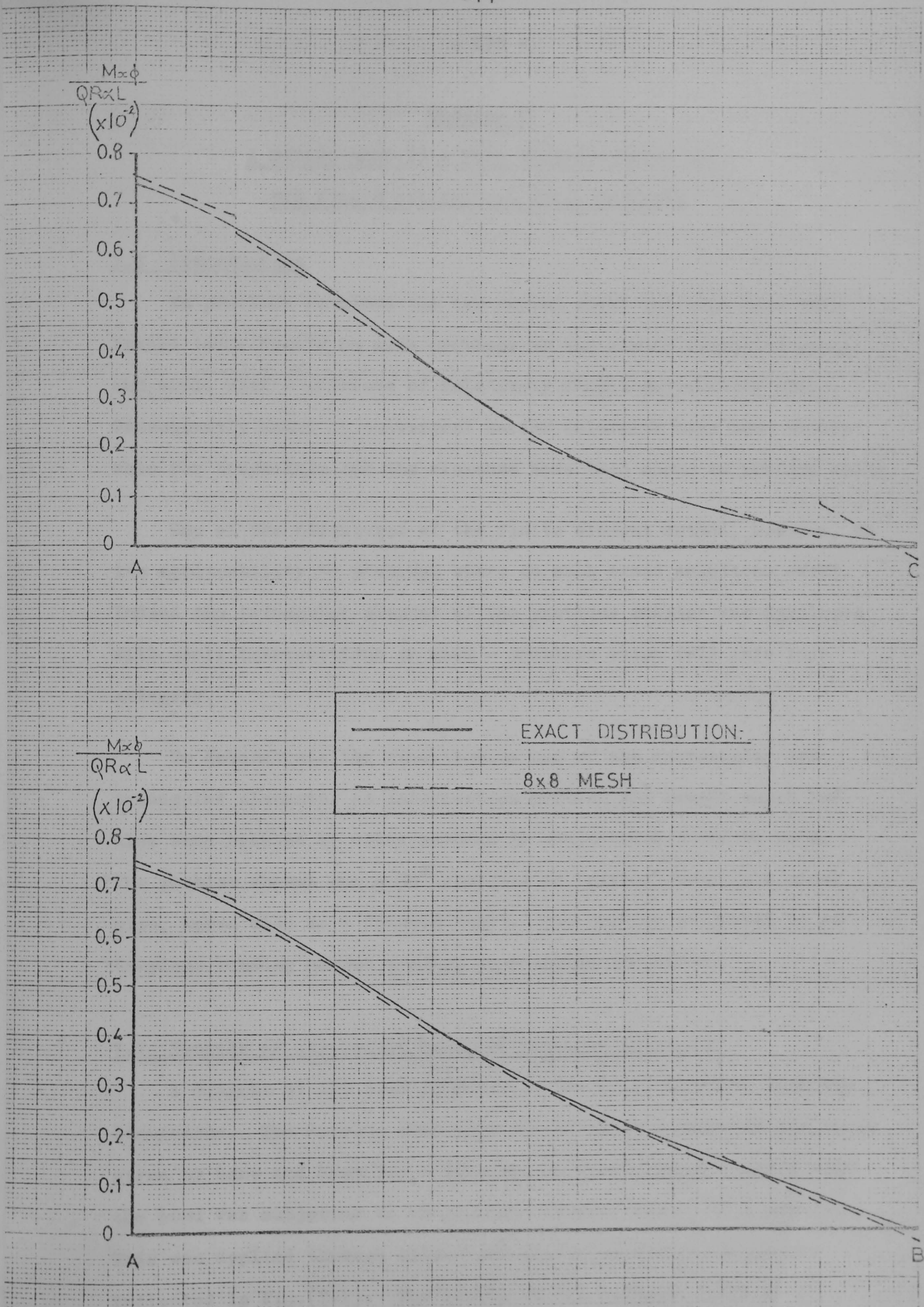

FIG.6.25 Mxφ STRESS RES. ON PANEL USING 8 x 8 MESH OF CURVED TRIANGULAR ELEMENTS.

Chapter 7

A MITRED BEND IN A PIPE ANALYSED USING THE TWO HYBRID CYLINDRICAL SHELL ELEMENTS

7.1 Introduction

In previous sections the two curved shell elements have been tested individually on such problems as the simply supported panel and shell roof - problems of relatively simple geometrical shape. Consequently exact or convergent series solutions have been available for comparison and the elements have been shown to perform well.

One of the advantages of the finite element method, however, is its applicability to problems where no such exact solutions exist. Indeed the triangular element of the previous chapter was developed with shell intersections in mind - problems which fall into this category.

To demonstrate the simultaneous use of the rectangular and triangular elements, an intersection problem was sought which had also been treated by other methods so comparisons could be made. The problem chosen was a 90^{o} gusseted or "mitred" bend in a steel pipe, known also as a "3-weld bend". The bend is subjected to an in-plane bending moment tending to decrease its radius.

7.2 Details of the Mitred Bend and Previous Solutions

A diagram of the bend is given in Fig.(7.1) together with the dimensions. The results used here for comparison purposes are those given by Lane and Rose(74) - obtained by strain gauge methods when the bend was subjected to an in-plane bending moment of 1 ton-inch. This was applied through welded end-plates on tangent pipes as indicated in Fig.(7.1). The length of the tangent pipes was

approximately two diameters - considered sufficient to prevent any interference with the stress system of the bend due to the method of application of the loads. Also the stresses due to thrusts are a negligible proportion of the bending stresses present.

The change in diameter of the bend was measured at section BB using a large micrometer with a pointed anvil fitting into small conical depressions in the pipe. The distribution of strain gauges used at sections BB and AA is also shown in Fig.(7.1). Section BB is halfway along a segment of the bend whilst AA is $\frac{3}{8}$" away from the intersection. This was the closest point to the intersection at which results could be obtained due to the physical size of the gauges. In (74) Lane and Rose were attempting to measure the stresses at the actual intersection and they conclude that in all probability the stresses measured at AA are underestimates of these. It was expected at the outset of the present work to be able to obtain values at the intersection in addition to those at sections AA and BB.

Several practical points relating to the strain gauge tests are worth noting at this stage. Firstly, the pipe was made of good quality mild steel and the joints were welded. The weld reinforcements were dressed off to give sharp intersections between the segments and a gamma-radiographic examination was made of the welds. Only infrequent evidence of minor porosity was found. However, in the finite element analysis no allowance can be made for possible differences between the material of the weld and the pipe - nor for any heat-treatment effects during or after welding. Also, typical values for Young's modulus and Poisson's ratio for mild steel have to be assumed.

The strain gauge results quoted are, in fact, averages of

three tests on three different mitred bends, nominally of the same size and characteristics in every respect. Lane and Rose(74) found that the stresses differed by, at the most, 5% between bends. The arrangement of the strain gauges in Fig.(7.1) shows a greater concentration in the $0^{o} \rightarrow +90^{o}$ region than in that from $0^{o} \rightarrow -90^{o}$. The stress distributions in the region where more gauges are present are obviously more reliable. The relevance of this will become apparent later.

7.3 The Finite Element Idealization

Because of the symmetry conditions of both the structure and the loading about OC (Fig.(7.1)) it was sufficient to analyse only one half of the bend. Also, it was only necessary to model 180^{o} of the circumference. The idealization used is shown in Fig.(7.2). In the body of each segment eight rectangular elements are used around 180^{o} - each therefore subtending $22\frac{1}{2}^{o}$ at the centre of the pipe. The triangular elements are used only in the intersection regions, e.g. near sections AA and FK.

Symmetrical displacement conditions were imposed along the edges EFG and LKJ of Fig.(7.2). These involved allowing no displacement perpendicular to the plane of the figure and also no rotation about the edges. Around the curved line LME the symmetry condition is one of zero displacement in the x direction. These symmetry conditions constrain the portion of the bend in Fig.(7.2) as a rigid body in all except the global z direction. It was therefore necessary to fix one point in the z direction and the point M was chosen for this purpose.

The length of the tangent pipe NGJK was chosen in the experiments to be of about two diameters - for reasons explained earlier.

In the finite element idealization this length was reproduced approximately and the bending moment applied by three equal horizontal forces as shown, such that the total bending moment about M was $\frac{1}{2}$ ton-inch, (since half of the total bending moment is carried by the 180° of the pipe under consideration). The forces were chosen to be equal since this, it was thought, would give the best approximation to the actual loading condition applied through a welded end-plate.

The complete idealization involved 204 elements and 1070 degrees of freedom.

7.4 Conversion of the Finite Element Stresses into the Form Necessary for Comparisons

The results quoted in (74) give (a) the change in diameter of the pipe at section BB and (b) the hoop and longitudinal stresses at the inner and outer surfaces of the pipe at sections BB and AA. The stresses quoted are strictly parallel and normal to the sections under consideration, so they are truly hoop and longitudinal only at section BB. Here the element axes are coincident with the section so evaluation of stresses is straightforward. At section AA and at the intersection, however, the element axes are at 15° to the section so the evaluation of stresses parallel and perpendicular to AA is more complicated.

If Nx and Mx are the longitudinal stress resultant and bending moment (in lb/inch and lb.inch/inch respectively) given by the finite element idealization at BB, then the longitudinal stress σ_L at a distance z from the middle surface is given by

$$\sigma_L = \frac{N_x}{t} + \frac{12\, M_x}{t^3} z \qquad lb/in^2 \qquad (7.1)$$

where t is the thickness of the pipe and the outer and inner surfaces are given by Z = $\pm$ t/2.

A similar relation involving N_ϕ and M_ϕ gives the hoop stress at section BB (σ_H)

$$\sigma_H = \frac{N_\phi}{t} + \frac{12 M_\phi Z}{t^3} \quad lb/in^2 \qquad (7.2)$$

Relations (7.1) and (7.2) can be obtained from the definitions of the stress-resultants given in Appendix 1 by assuming linear variation of stress across the thickness (a distribution implied by the initial thin shell assumptions).

Equations (7.1) and (7.2) can also be applied to the finite element stress resultants along AA and at the intersection. However, they will give true hoop and longitudinal stresses and not those parallel and perpendicular to the sections. In order to calculate these it is also necessary to obtain values for the shears from the finite element idealization. An equation similar to (7.1) and (7.2) gives the shears acting at the outer and inner surfaces as:

$$\tau_{x\phi} = \frac{N_{x\phi}}{t} + \frac{12 M_{x\phi} Z}{t^3} \; lb/in^2 \left(Z = \pm \frac{t}{2}\right) \qquad (7.3)$$

With the stresses acting along and perpendicular to the axis of the pipe (from (7.1) and (7.2)) and with the shears from (7.3), standard theory using the Mohr's circle approach gives equivalent stresses acting along AA and the intersection. In the following discussions, when "hoop" and "longitudinal" stresses at AA and the intersection are referred to, it should be understood that they are not strictly hoop and longitudinal - but parallel and perpendicular to the particular section.

7.5 Results Obtained

7.5.1 Change of Diameter at Section BB

Comparisons are possible between the finite element and experimental displacements at section BB. Changes of diameter are considered. The results are shown in Fig.(7.3) where it can be seen that good correlation is obtained at all positions.

7.5.2 Stresses at Section BB

To evaluate the longitudinal and hoop stresses around BB (via equations (7.1) and (7.2)) it is first necessary to plot separately the distributions of Nx, $N\phi$, Mx and $M\phi$ given in the finite elements around this section. At each position around BB (Fig.(7.2)) values can be obtained from the elements each side of BB, thus providing a check on the continuity of the predictions. The stress resultants around BB are plotted in Figs.(7.4) to (7.7). Generally good continuity is obtained between adjacent elements in both the longitudinal and hoop directions. Smooth curves are drawn through the predicted values in the elements.

The values given by these smooth curves are then combined as in equations (7.1) and (7.2) to give the inside and outside longitudinal and hoop stresses. These are shown plotted in Figs.(7.8) and (7.9) compared with the strain gauge values quoted by Lane and Rose. Good agreement is shown - the largest errors being in the 0^{o} to -90^{o} region.

7.5.3 Stresses at Section AA and the Intersection

Initially stress resultants in the region of the section AA were plotted around the circumference of the cylinder in the manner of the previous section. This approach was abandoned because the

predictions, generally in the triangular elements, showed discontinuities such that accurate interpretations were impossible. This, however, was seen to be a localized effect, confined to the immediate region of the intersection.

A rather more laborious approach was adopted in order to obtain the best possible predictions in this region. All stress resultants were plotted along all lines around the circumference parallel to the axis of the pipe, e.g. lines K'L' and K"L" of Fig.(7.2). In this way the distribution of stresses throughout the segment was obtained and it was possible to extrapolate with reasonable accuracy in the intersection region.

As examples of the quality if predictions obtained, the distribution of the stress resultants Nx, Nϕ, Mx and Mϕ along the line at 0^{o} leading to point M (Fig.(7.2)) are plotted in Figs.(7.10) to (7.13). It can be seen, in general, that reasonable correlation is obtained between the stresses in the elements above and below this line - but the correlation becomes worse as the intersection region is approached. Smooth lines were fitted to the finite element stresses in all cases and in this way values at the section AA and at the intersection were obtained. The stress resultants in Figs.(7.10) to (7.13) are typical of the general quality of the predictions obtained along all lines. It was noticeable, as shown in Fig.(7.11), that in all cases the Nϕ stress resultant showed the largest discontinuities in the intersection region.

Figs.(7.14) and (7.15) show the "hoop" and "longitudinal" stresses at the outside and inside surfaces at section AA - compared with the strain gauge values. Figs.(7.16) and (7.17) show the predicted stresses at the actual intersection. These are seen to be generally larger than those at AA by, in some cases, 100%.

7.6 Discussion of Results

7.6.1 Deflections

It is clear from these results that the stresses and deflections predicted by the finite element idealization are very close to those measured on the actual pipe. Fig.(7.3) shows the marked flattening effect at section BB. In the region $+45^{\circ}$ to -45° the diameter increases whilst from -90° to -45° and from $+90^{\circ}$ to $+45^{\circ}$ it decreases. The difference between the finite element and measured deflections at 0° is of the order of 5%.

7.6.2 Stresses at BB

The stresses around BB are predicted with excellent accuracy. The distributions given in the finite elements (Figs.(7.4) to (7.7)) show good continuity defining smooth curves very accurately. The hoop stresses due to bending dominate the direct hoop stress - the result being that the inside and outside hoop stresses are virtually mirror images of one another (Fig.(7.8)). This is consistent with the hoop and radial deflections at BB which amount to squashing of the pipe.

The longitudinal direct stresses around BB (Fig.(7.5)), however, are at least as important as those due to the longitudinal moment Mx (Fig.(7.4)). In Fig.(7.5) it is seen that Nx is of similar value (but of opposite sign) in the 0° to 90° and 0° to -90° regions. This represents tension in the upper part of the pipe and compression in the lower half.

It is of interest to note that in Figs.(7.8) and (7.9) the largest differences between the measured and predicted stresses are in the 0° to -90° region. In Fig.(7.1) the distribution of

strain gauges in this region is seen to be very sparse - with gauges only at 0°, -45° and -90°. The actual shape of the strain-gauge curves, therefore, in this region of Figs.(7.8) and (7.9) must be a little speculative. This, it is thought, could be one of the reasons for the differences. Also, results between the three pipes tested varied by 5%. This difference is small, but not negligible, on the graphs.

7.6.3 Stresses at Section AA

The correlation between finite element and measured stresses is slightly less satisfactory at section AA (Figs.(7.14) and (7.15)). Here the strain gauges were more evenly distributed and greater weight can be placed on the actual shape of the curves. The obvious new source of error, compared with section BB, is that involved in interpreting the finite element stresses because of the discontinuities in the intersection region, (Figs.(7.10) to (7.13)). Nevertheless, the agreement is generally good.

The hoop stress distributions at this section are the same shape as those at BB - but rise to higher values (-0.12 tons/in.^{2} as opposed to -0.08 tons/in.^{2}). There is a major change, however, in the form of the longitudinal stress, compared with section BB. A large component of longitudinal bending stress has arisen in the 0° to -90° segment (compressive at the outer surface) which radically changes the distribution here. (Compare Figs.(7.15) and (7.9))

7.6.4 Stresses Predicted at the Intersection

Rose and Lane(74) state that stress gradients measured at section AA were very high and in all probability the stresses at the actual intersection considerably exceeded those at AA. This is

confirmed by the finite element predictions. Interpretation of the results is again subject to the same inaccuracies as at section AA but certain features are apparent.

Firstly, (Fig.(7.16)) the hoop stresses are not significantly greater than those at AA and have the same general distribution. However, the effect noticed at AA - the appearance of a longitudinal bending moment has become even more apparent (Fig.(7.17)), giving extremely large longitudinal stresses at outside (-0.24 tons/in.^{2}) and inside(0.14 tons/in.^{2}) surfaces. Also a component of longitudinal bending stress has appeared in the $+45^\circ$ to $+90^\circ$ region leading to significant changes here also.

7.6.5 The General Performance of the Elements

This problem has demonstrated the accuracy of results which can be obtained using the two hybrid elements on a real problem. The mesh used seems perfectly adequate in the region of section BB as shown by the quality of stress predictions there. However, near the intersection, the discontinuities in the stress predictions (particularly in the triangular elements) become relatively large.

The obvious explanation for the discontinuities lies in the physical characteristics of the intersection region. The sharp discontinuity in the shell surface means that triangular elements must meet at an angle such that there is a discontinuity in their surfaces. Although along the intersection, the physical shapes of the hypotenuses are defined by three nodes for each pair of elements - between these nodes there will not be geometrical compatibility because of the discontinuity of surface. The discontinuity of surface also leads to an incompatibility in the edge displacement assumptions in two elements on each side of the intersection

(similar to that introduced when flat elements are used to model a shell in Chapter 4) which is superimposed on any incompatibility present for the reasons of the previous chapter. These features must adversely affect the quality of stress predictions in this region.

It would be interesting to see the results using a finer mesh - perhaps using 16 elements around the circumference. This, it is thought, would lead to better predictions in the intersection region. It is impossible, however, using these two elements, to refine the mesh in the region of the intersection without refining it throughout the structure.

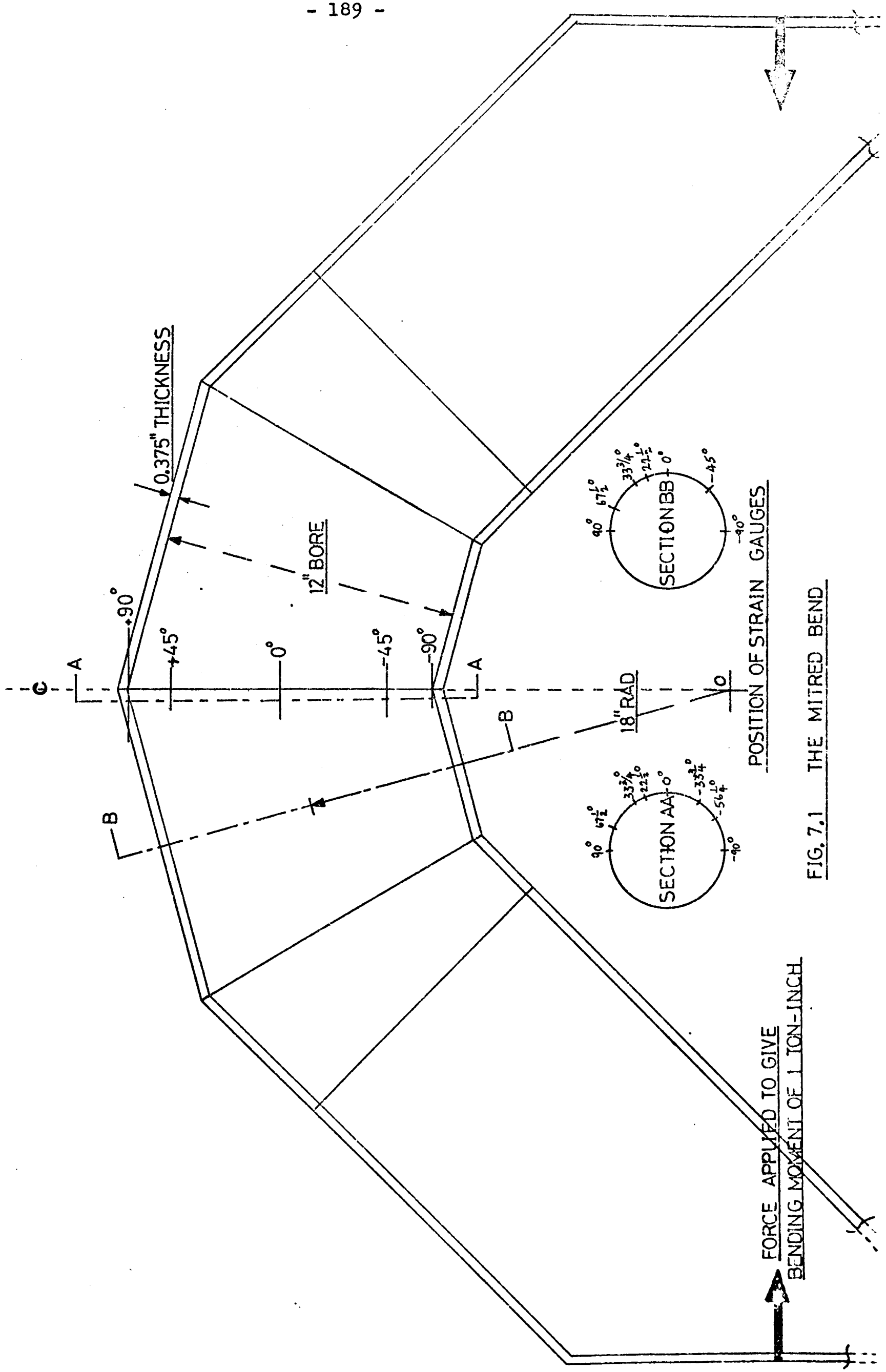

FIG. 7.1 THE MITRED BEND

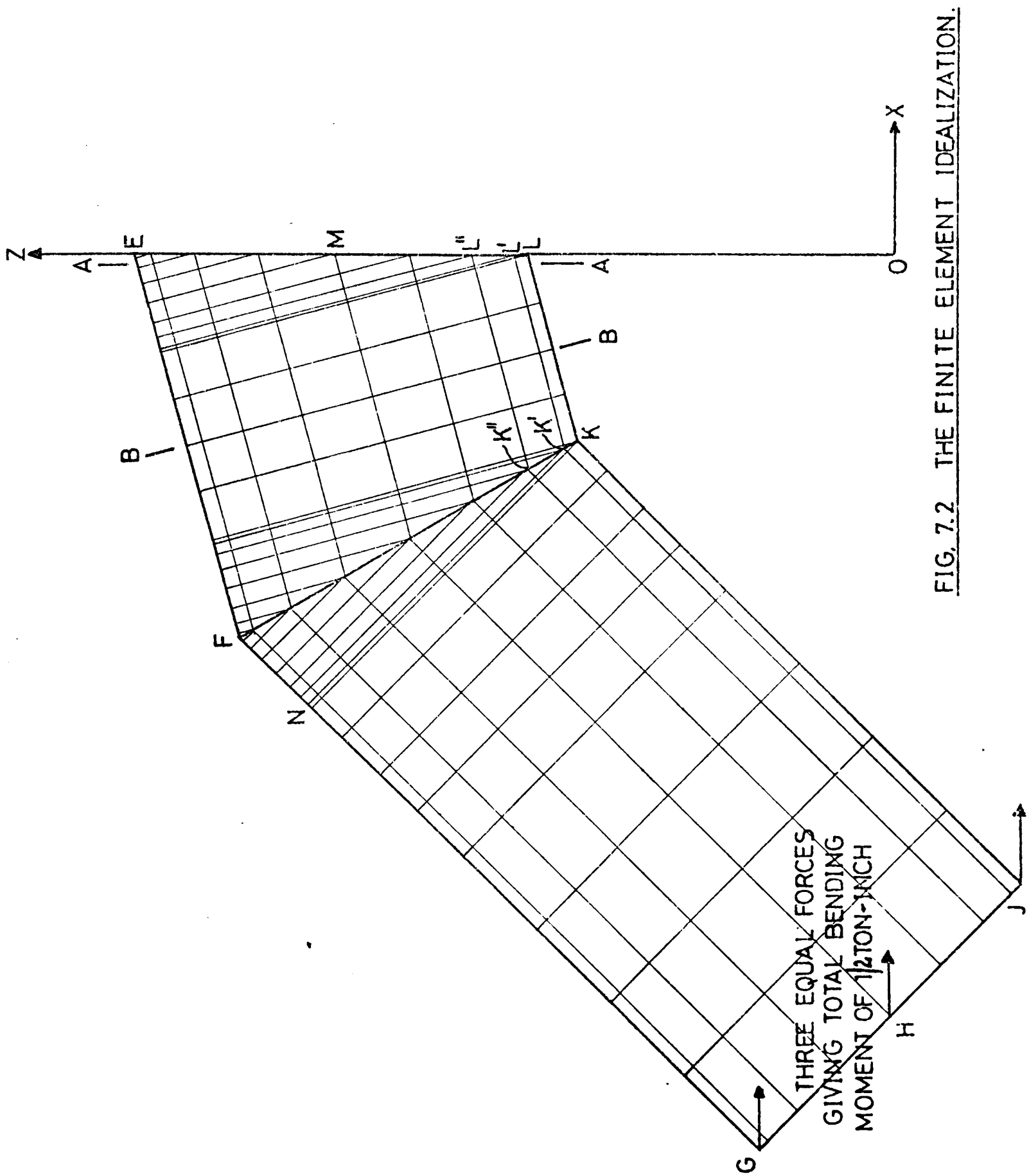

FIG. 7.2 THE FINITE ELEMENT IDEALIZATION.

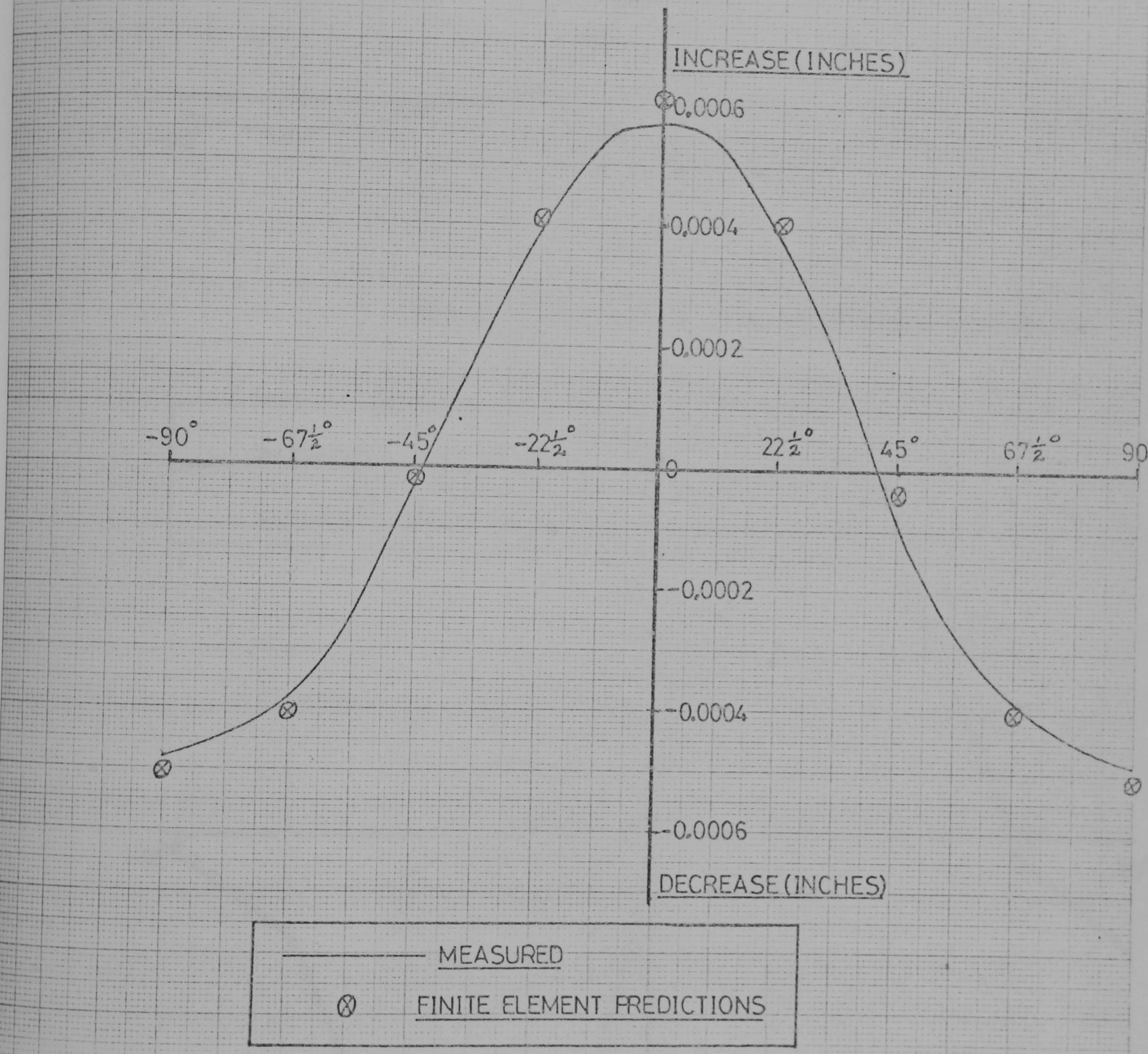

FIG. 7.3 CHANGE OF DIAMETER AT SECTION BB

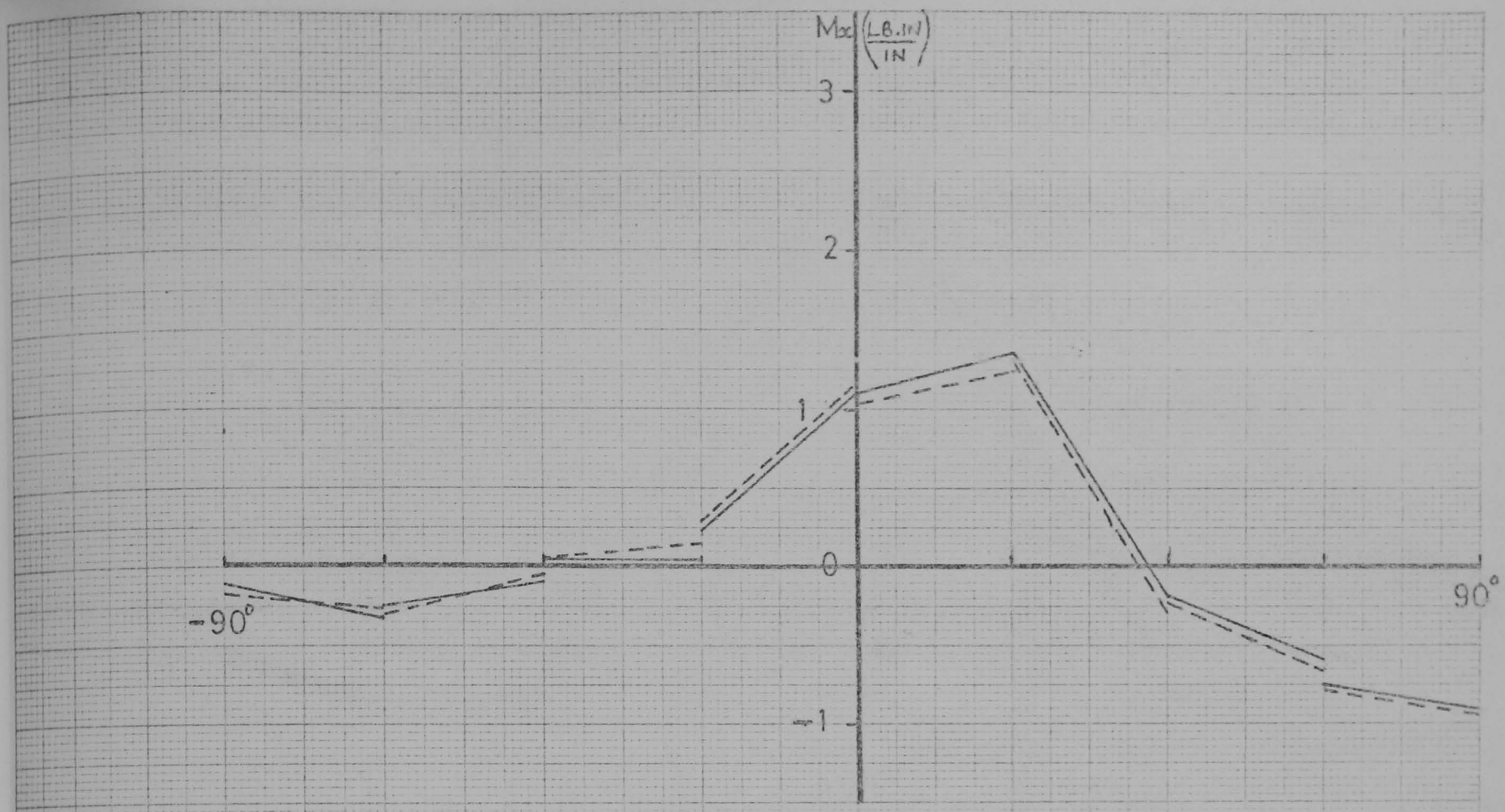

FIG. 7.4 LONGITUDINAL(M_x) BENDING MOMENT AT BB

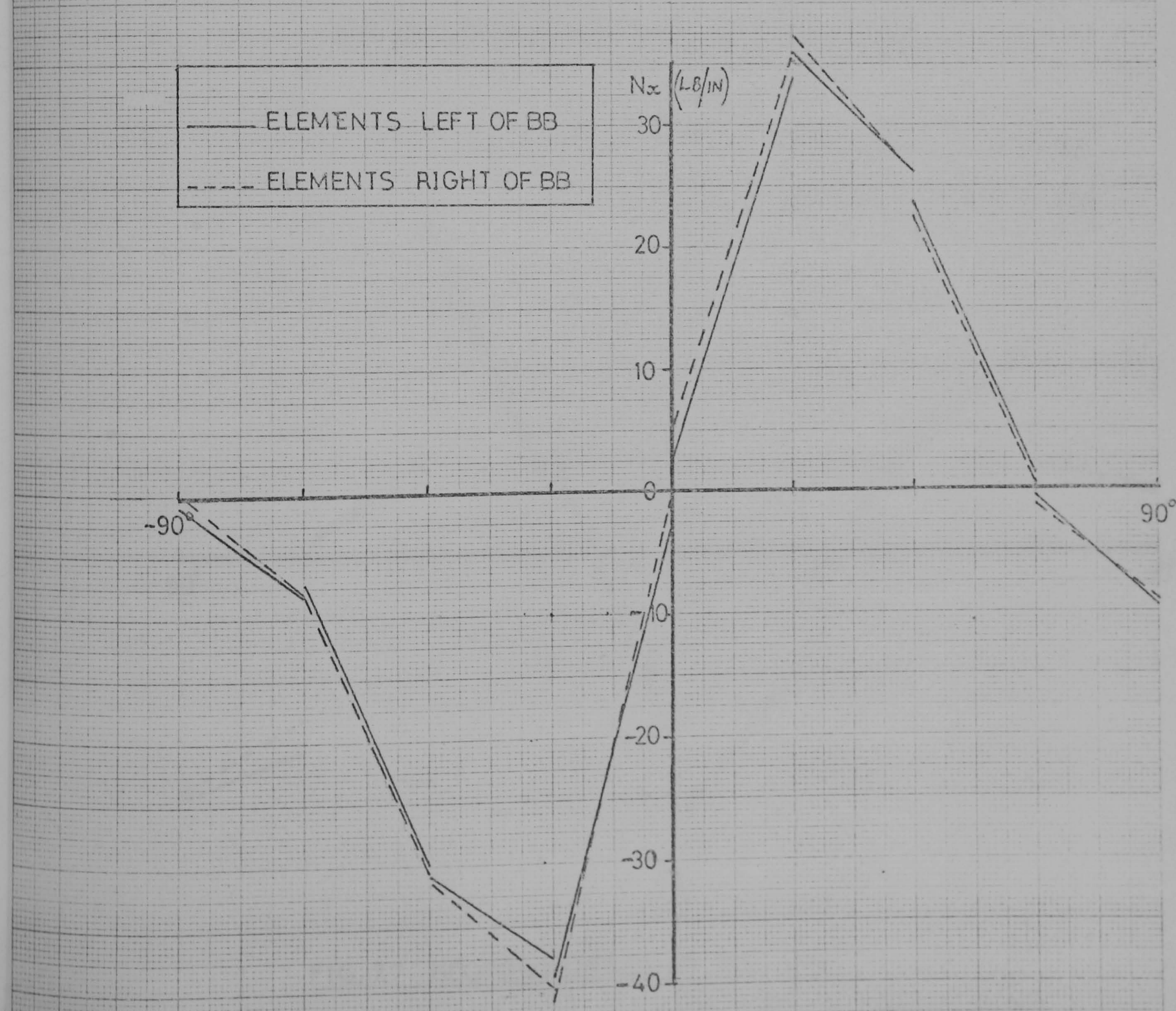

FIG. 7.5 LONITUDINAL (N_x) STRESS AT BB

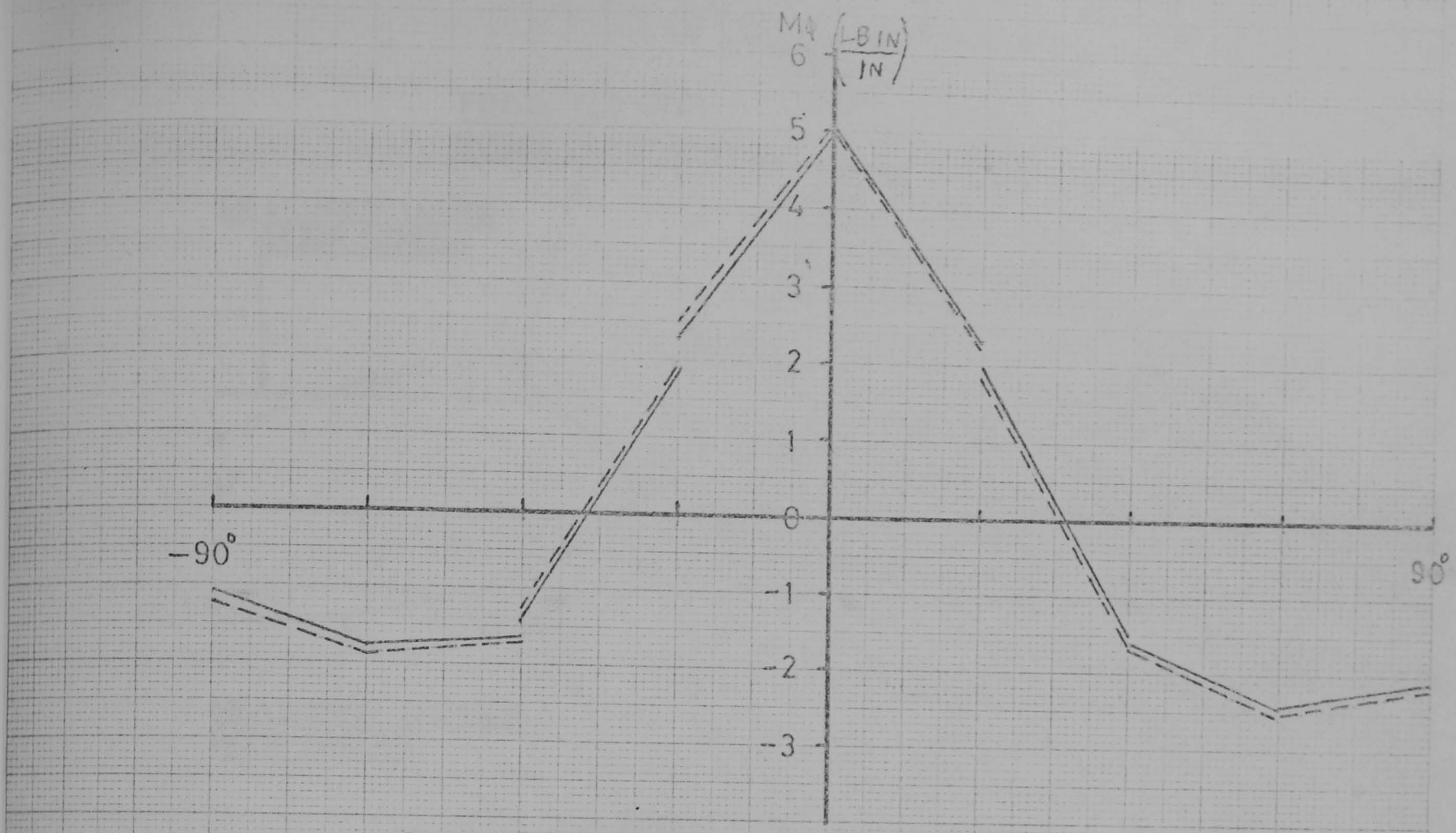

FIG. 7.6 HOOP (Mϕ) BENDING MOMENT AT BB

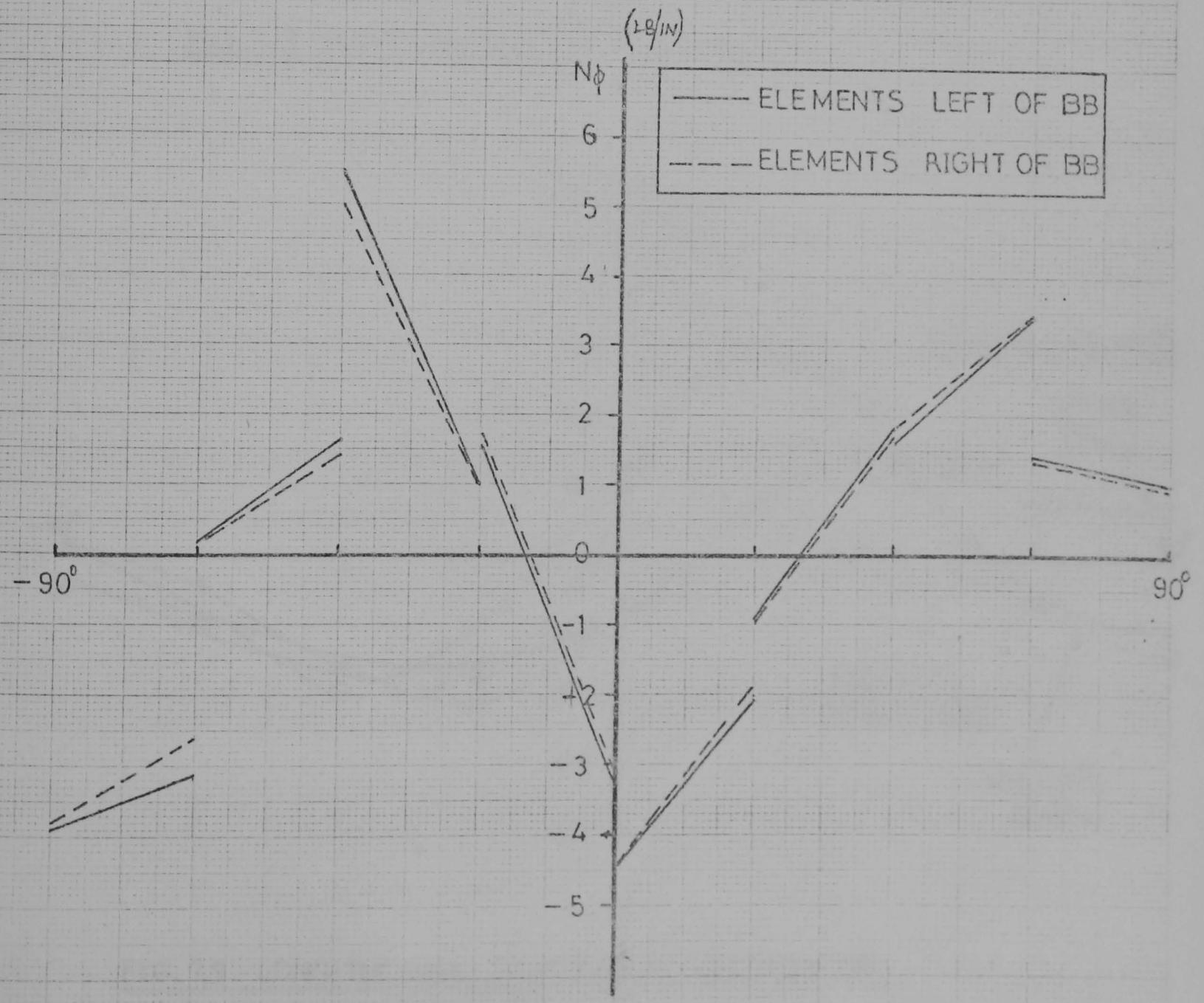

FIG. 7.7 HOOP (Nϕ) STRESS AT BB

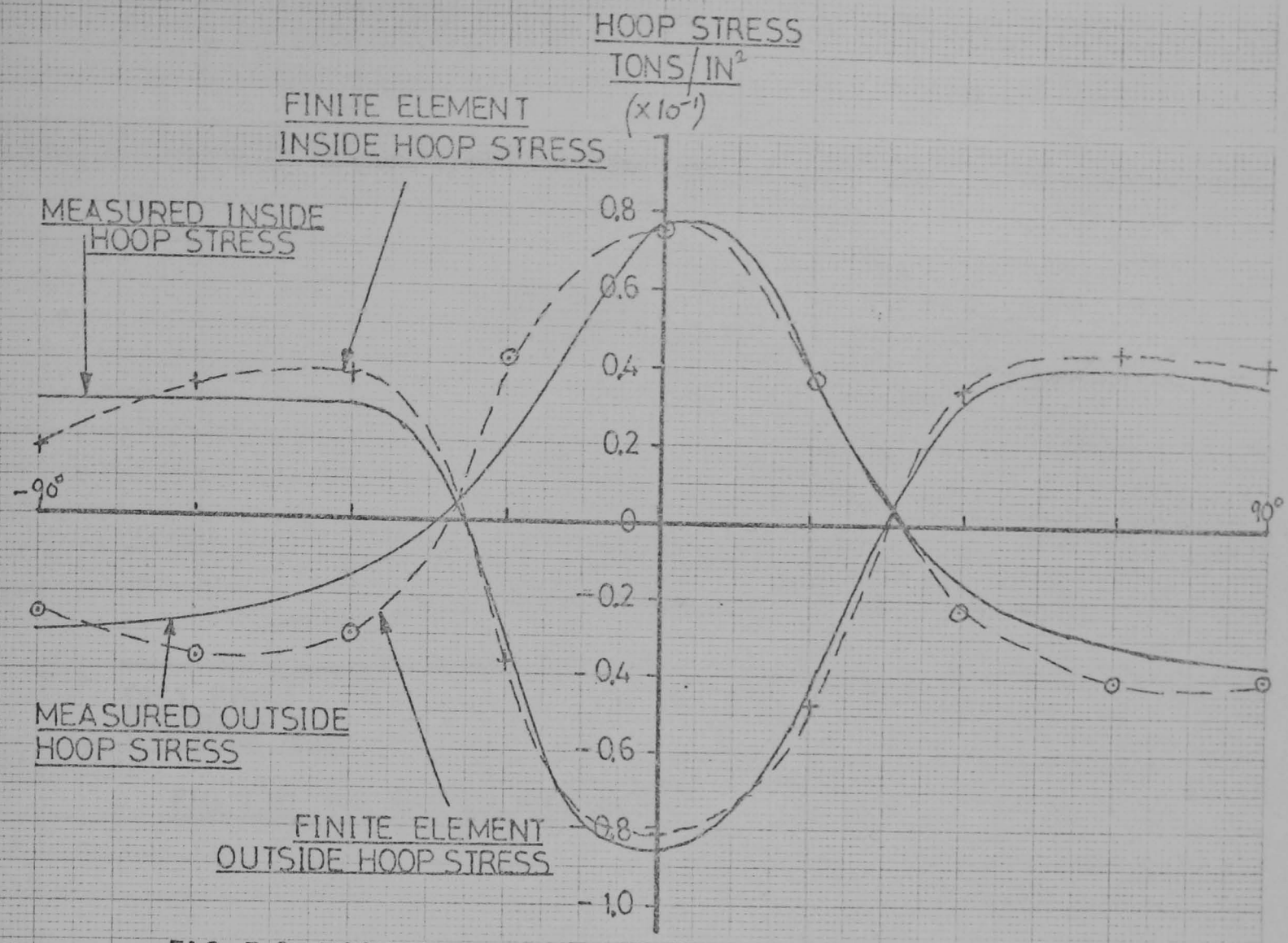

FIG. 7.8 HOOP STRESSES AT SECTION BB

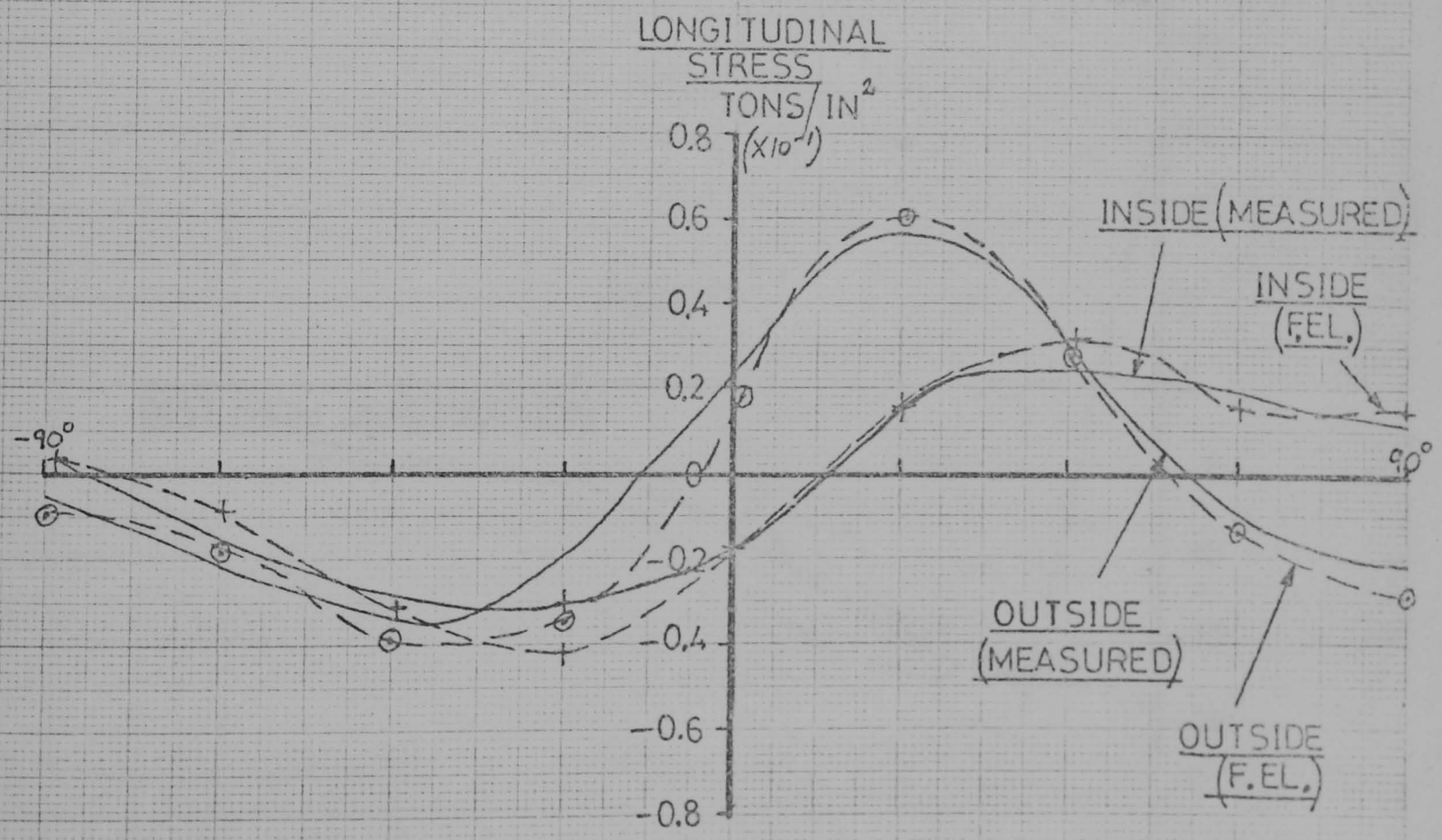

FIG. 7.9 LONGITUDINAL STRESSES AT SECTION BB.

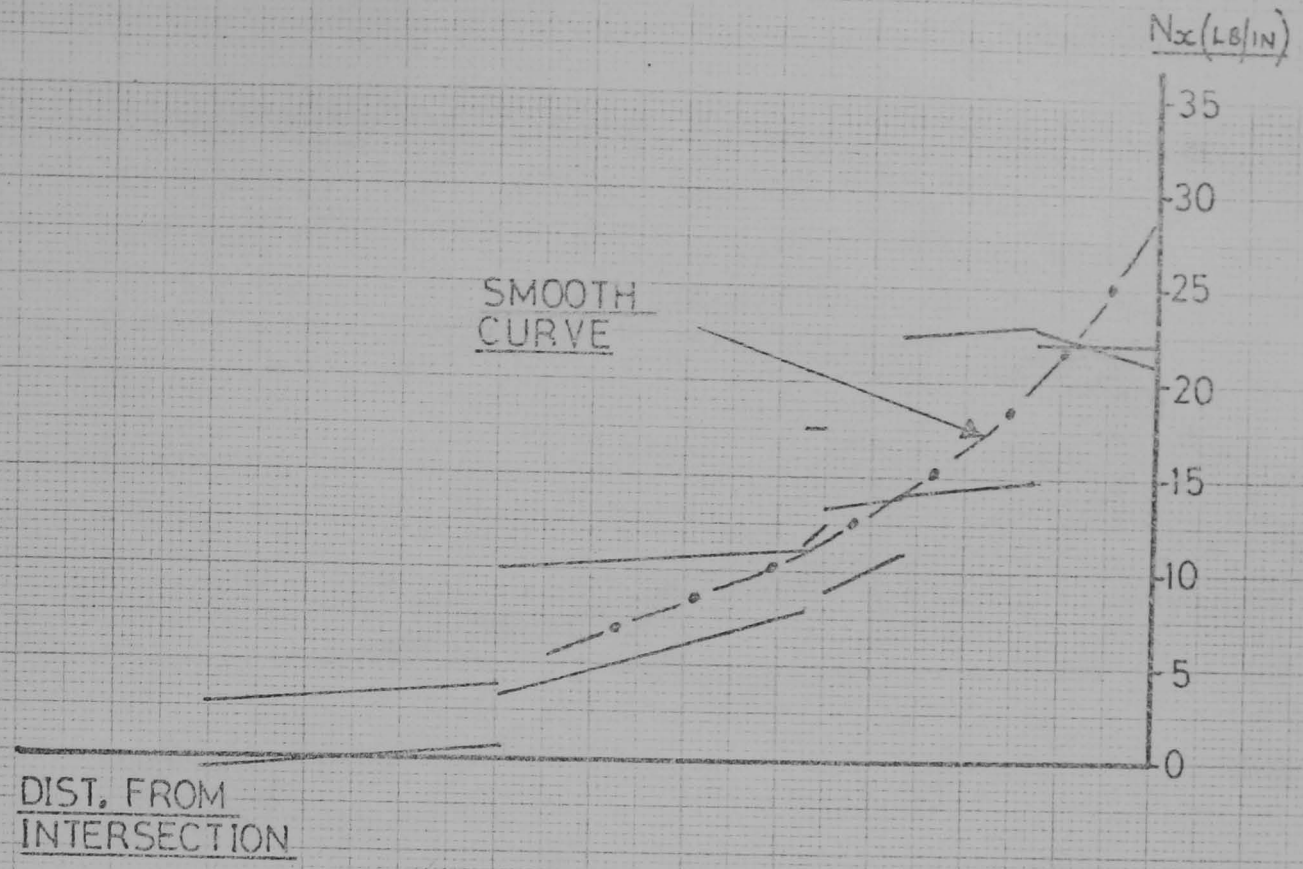

FIG. 7.10 N_x STRESS RES. AT 0°

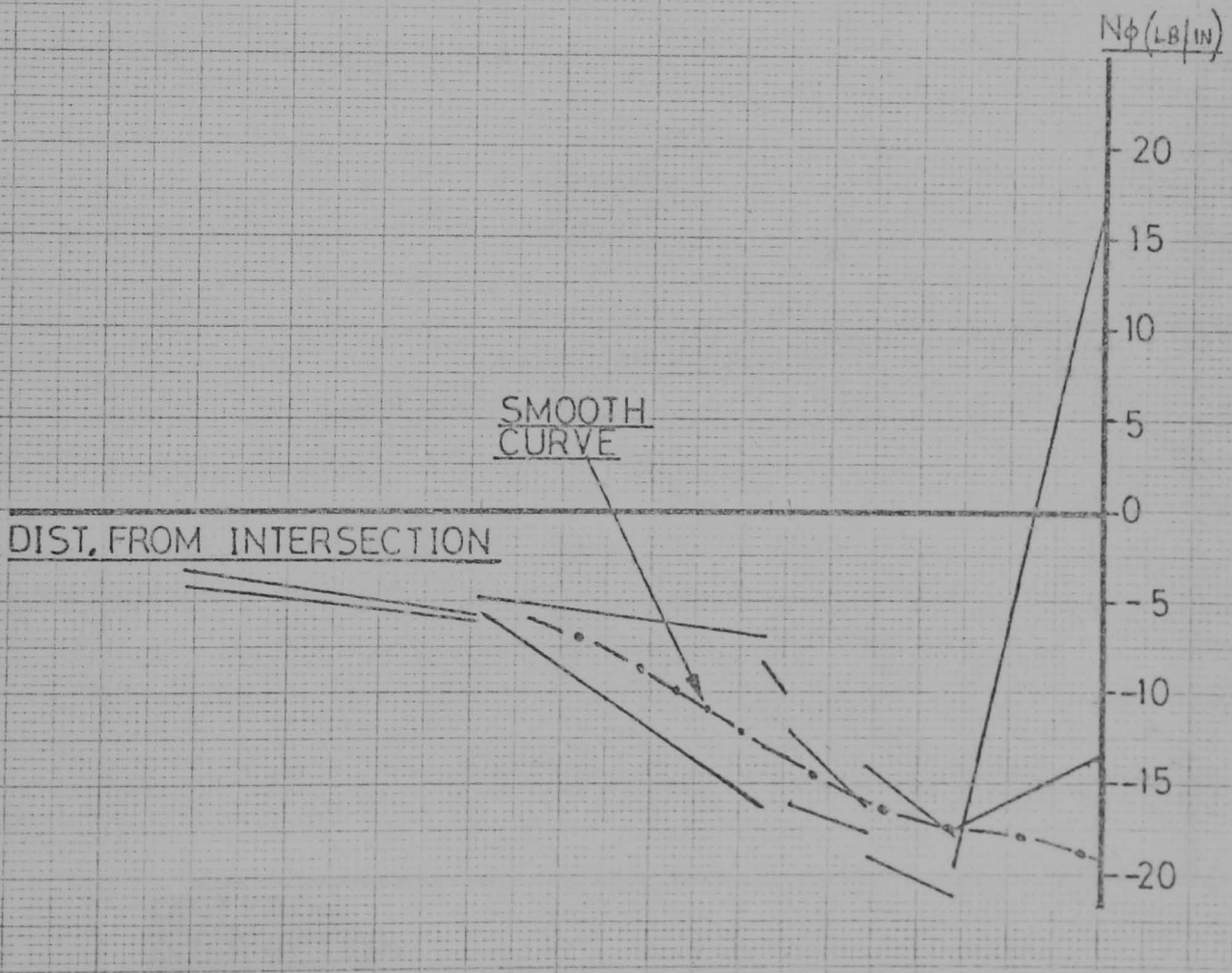

FIG. 7.11 N_ϕ STRESS RES. AT 0°

FIG. 7.12 Mx STRESS RES. AT 0°

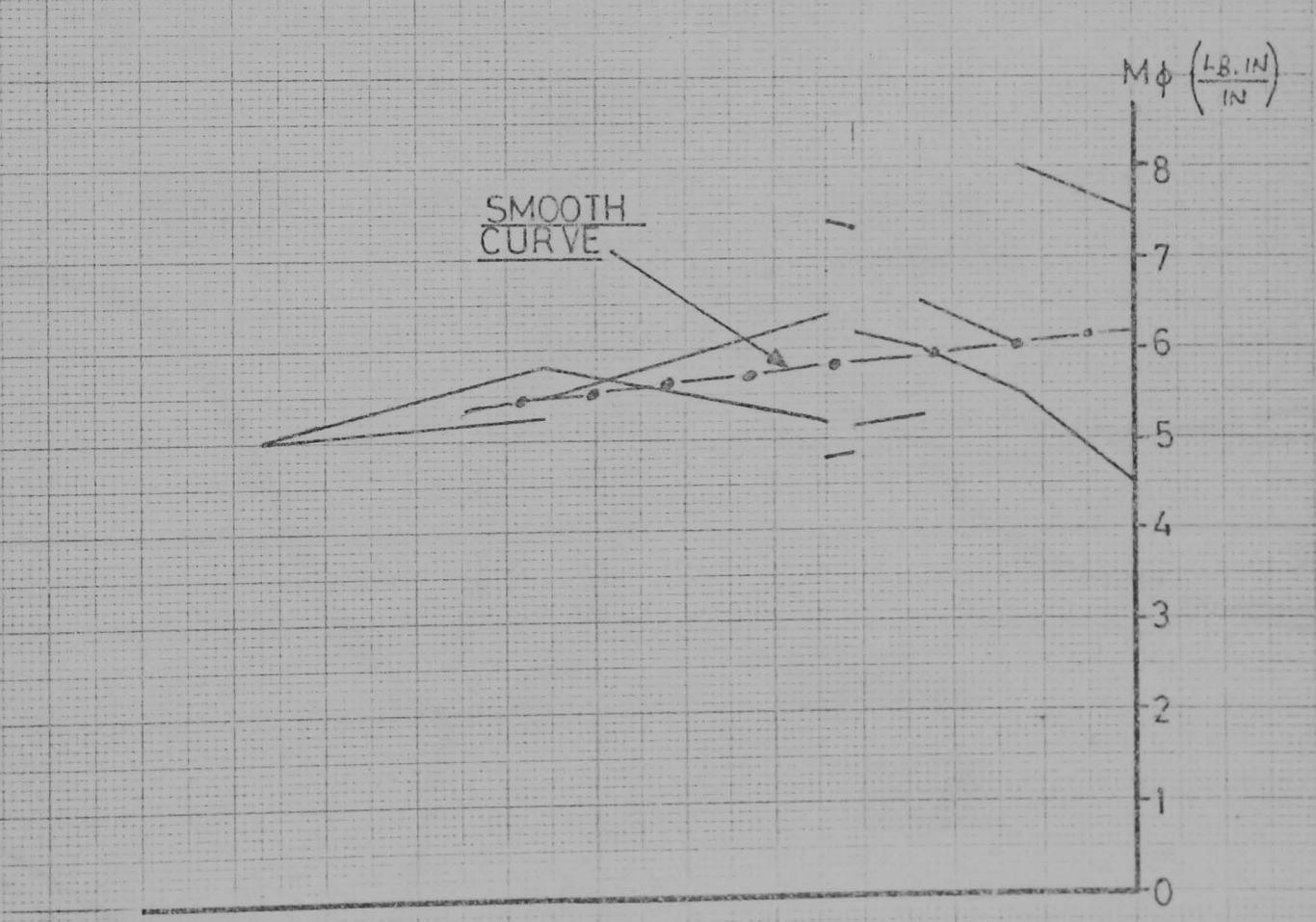

FIG. 7.13 Mφ STRESS RES AT 0°

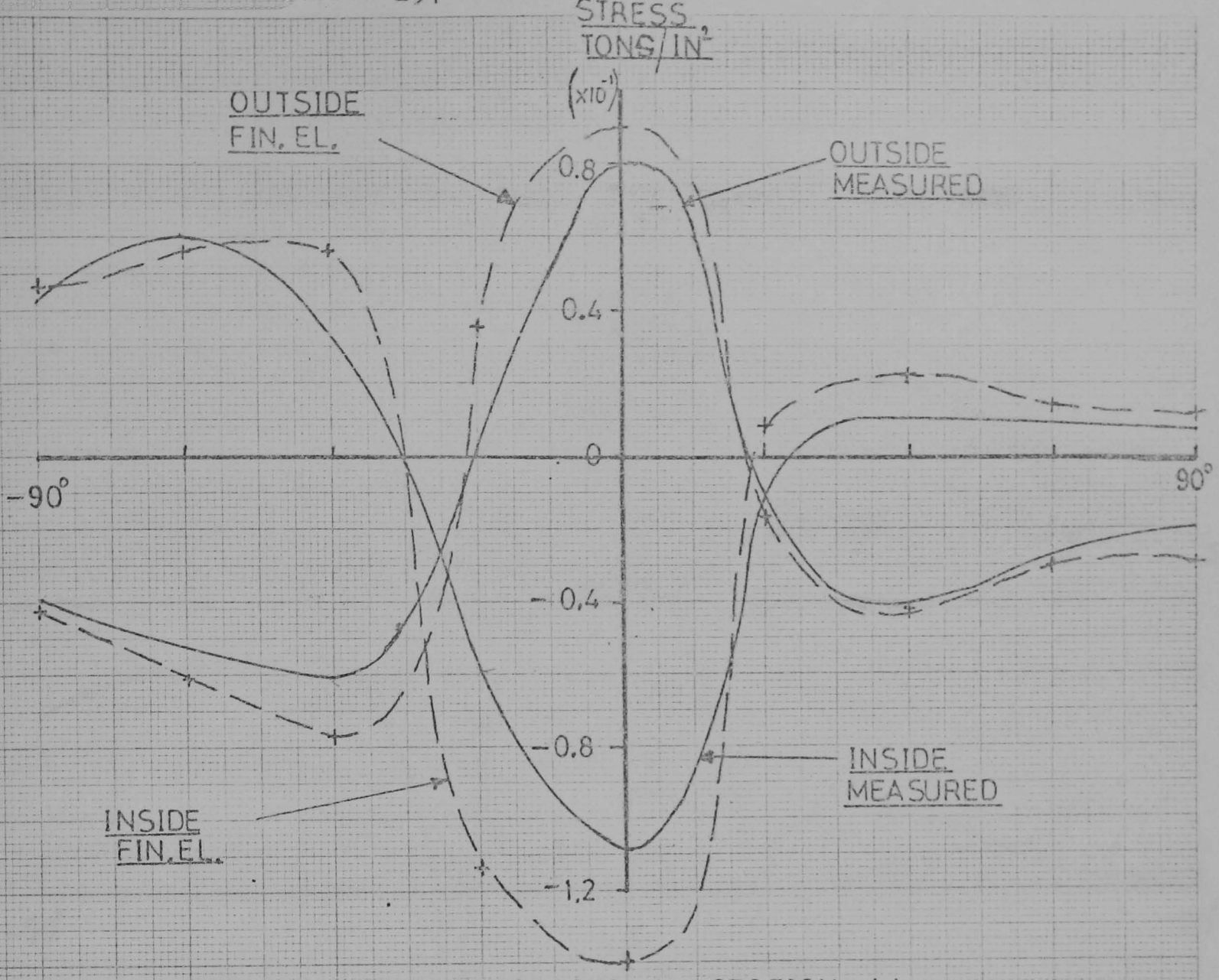

FIG. 7.14 HOOP STRESSES AT SECTION AA

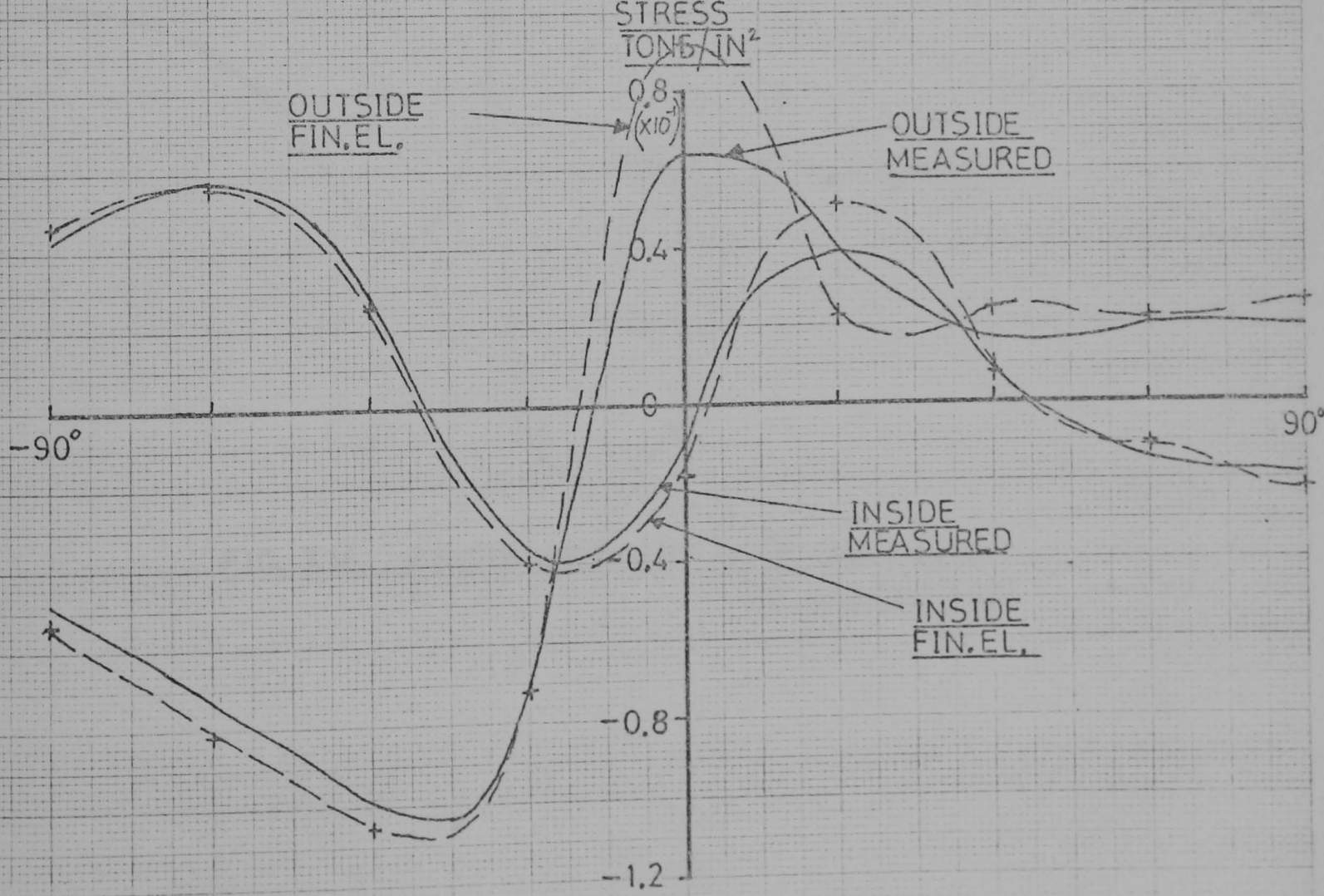

FIG. 7.15 LONGITUDINAL STRESSES AT SECTION AA

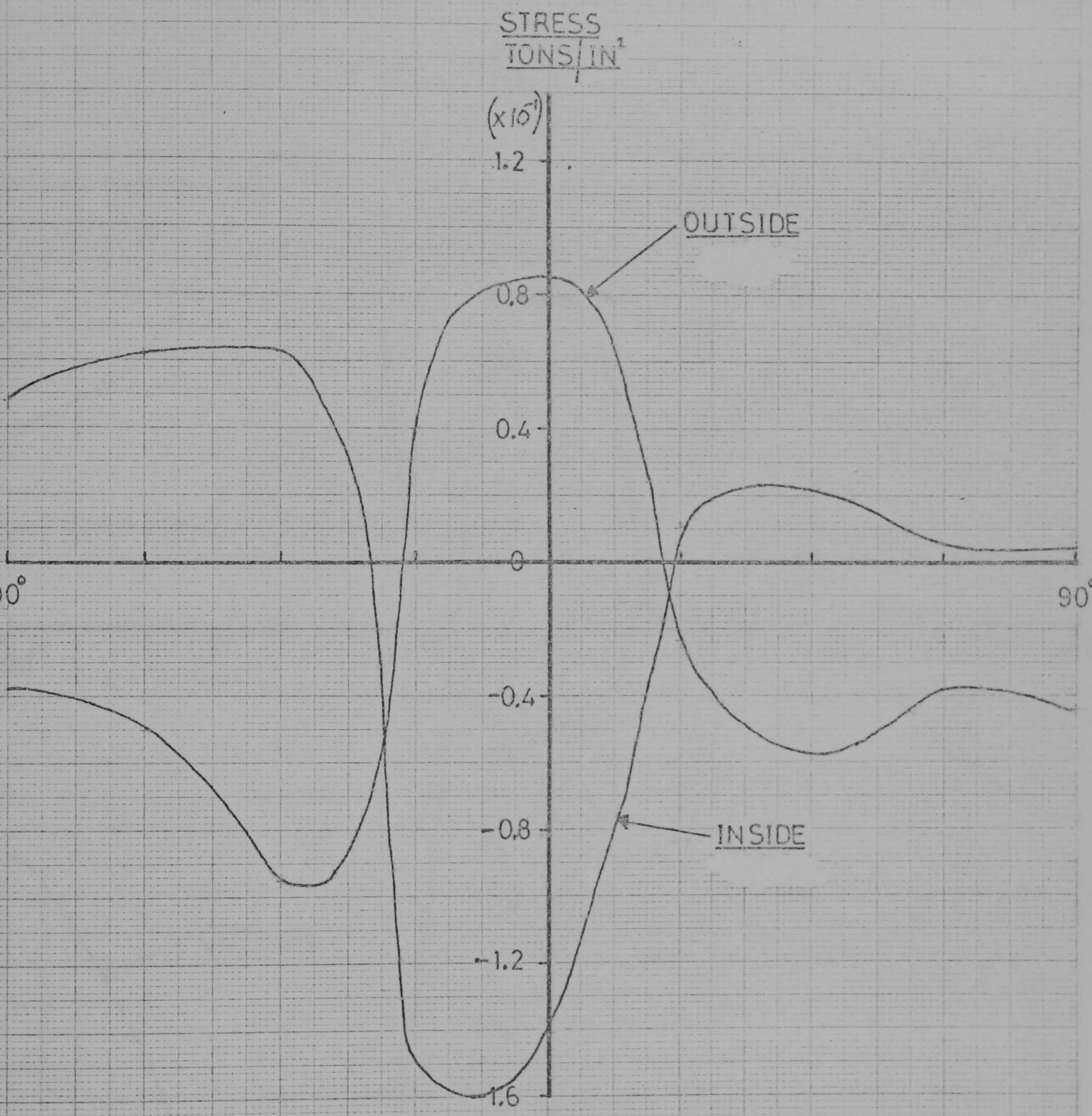

FIG. 7.16 FINITE ELEMENT HOOP STRESSES AT INTERSECTION

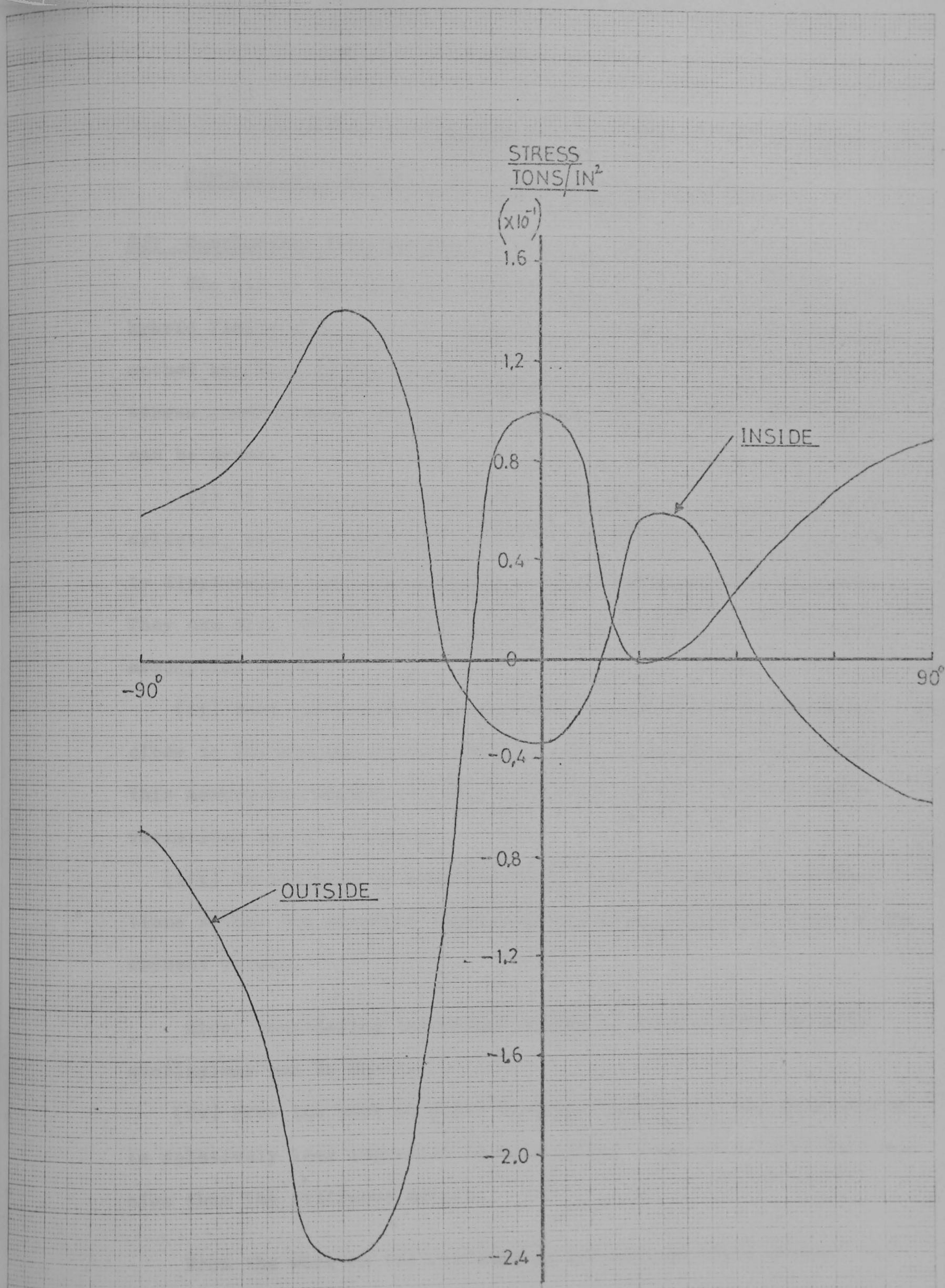

FIG. 7.17 FINITE ELEMENT LONGITUDINAL STRESSES AT INTERSECTION

Chapter 8

CONCLUSIONS, THOUGHTS AND SUGGESTIONS FOR FURTHER WORK

8.1 Conclusions from the Work

The aim of the work has been to systematically investigate the hybrid finite element method when applied to shell structures. The method has been demonstrated to work and to give generally good stress predictions. From all the results some general conclusions can be drawn.

(i) If stress and edge displacement assumptions are carefully selected, elements produced by the hybrid method are often superior to displacement assumption elements using the same nodal freedoms. They can also compare favourably with more complicated displacement assumption forms.

(ii) Best results are usually obtained if a stress assumption close to the minimum length is used. For good stress predictions this assumption should include, as far as possible, the low order variations in all stresses.

(iii) In addition to stresses given at nodal points, distributions within the elements themselves are generally quite close to the correct values.

Also, considering individual elements, several more specific conclusions can be drawn.

(iv) From the work on plate bending (Chapter 3), the mass matrix is relatively less important in determining accurate natural frequencies than the stiffness matrix.

From the work on the rectangular cylindrical shell element the following points are apparent:

(v) To satisfy the equilibrium equations for a thin cylindrical

shell it is correct to make separate assumptions for the shear stress resultants $N_{x\phi}$ and $N_{\phi x}$ but not to distinguish between the twisting moments $M_{x\phi}$ and $M_{\phi x}$.

(vi) It is possible to include exact rigid body terms in the edge displacement assumptions and still have displacement compatibility between elements.

(vii) The rate of convergence of all stresses is not the same. Some may appear to diverge before converging to acceptable values on refining the mesh.

(viii) Certain stresses, whose distribution is not linear within the elements, may be improved by a "least squares" straight line fit to the distributions obtained.

Finally, from the work on the curved triangle:

(ix) Reasonable results can be obtained when incompatible displacement assumptions are used (a fact also evident from the analysis of shells using flat elements in Chapter 4).

8.2 Thoughts on the Hybrid Method in General

Some of the advantages and difficulties of programming and using hybrid elements are worth noting at this stage.

The physical amount of coding involved in an element routine is usually quite large because of the complicated nature of the formulation. Also relatively large amounts of storage are used because of the size of some of the matrices which have dimensions (length of stress assumption) x (number of degrees of freedom).

This is partly compensated by the simple nature of the stressing routine. It consists mainly of coding designed to transform global displacements into values relating to a particular

element. However, a complication from the organizational point of view is that the $[H]^{-1}[G]$ matrices of Chapter 2 must be kept on backing store and brought into the stressing routine. For a large structure a considerable amount of backing store is required.

The fact that there is no bound to the total strain energy when using hybrid elements is considered a disadvantage by some theoreticians. If a structure is subjected only to a point load it is useful to have a bound (such as provided by conforming displacement and equilibrium models) since the deflection under this load is a measure of the strain energy. However, in most practical situations point loads are not present and deflections may not, indeed, be as important as stresses. The fact that no bound is present is not usually, then, particularly important in practice.

In one of Pian's earliest papers on the hybrid method (29) it is suggested that results can be improved if, in addition to boundary displacement constraints, boundary stress conditions are also imposed. This, according to the theory outlined in Chapter 2, is not necessary for convergence but Pian concludes that better results can often be obtained. To apply the method it is necessary to construct special elements to deal with the edges of the structure.

This is difficult to implement in a general finite element scheme but the approach is also advocated by Wolf(63) who states that in certain difficult problems the stress boundary condition must be imposed to give adequate convergence. This situation has not arisen in any of the work reported here, but it would seem worthwhile to attempt to establish just in which cases, and why, this occurs.

In the limited amount of vibration work undertaken here conventional mass matrices are derived from a displacement assumption and used with hybrid elements. Pian(71) comes to the conclusion (see Chapter 2) that the method can be justified on the basis of a modified form of the Hellinger-Reissner variational principle - but he admits that there are inconsistencies. In fact, the only consistent hybrid method for vibration analysis is that due to Tabarrok(73). Here inertia properties for the element are obtained from the assumed stresses which are chosen to satisfy the dynamic equilibrium equations.

The formulation, explained fully in (73), leads to a frequency dependent mass matrix and it proves necessary to solve a determinantal equation rather than the more usual eigenvalue one. Pian(71) points out that the approach cannot be used for general dynamic problems such as transient response analysis whilst Henshell et al. (62) outline the practical difficulties involved in implementing the procedure on real systems. The approach, then, is mathematically justifiable but of restricted practical use.

8.3 Suggestions for Further Work

8.3.1 Work on Elements Developed in this Thesis

When new elements are developed it is difficult to be certain when the stage is reached at which they can be said to be fully tested and proven. Also, in the present case, since one aspect of the performance of the elements has been concentrated upon, there is room for more work to be done. The following lines of investigation could be pursued.

(i) Investigation of the performance of the flat triangular shell element of Chapter 4 on a variety of doubly curved shell problems. For vibration analysis transverse and in-plane mass

matrices could be added.

(ii) The addition of mass matrices to the rectangular and triangular curved shell elements to enable cylinder-cylinder vibration problems to be analysed.

(iii) Further investigations of the four-noded curved triangle as an element in its own right. It has not been tested on a wide range of problems so far.

(iv) Investigation of the possibility of improving the existing elements by increasing the complexity of both the boundary displacement and stress assumptions. This, perhaps, would mean using mid-side nodes. The obvious restriction on this would be the excessive amount of storage needed in the element routine for reasons explained earlier.

8.3.2 Further Applications of the Hybrid Method

8.3.2.1 A Doubly Curved Element

A logical extension of the present work would be the development of a thin hybrid element capable of modelling doubly curved shells exactly. On the basis of the present results the most efficient formulation would seem to be a quadrilateral with mid-side nodes to enable the shapes of the sides to be defined.

Numerical integration would, no doubt, be used and the two principal curvatures and the thickness could then be varied over the surface of the element. Because of the use of the two radii of curvature the equilibrium equations would be more involved and the stress assumption correspondingly more difficult to choose. However, an element such as this would be capable of dealing with problems such as the cylinder-cylinder intersection of Chapter 7.

8.3.2.2 Thick Shell Elements

All shell elements in this thesis are based on "thin" assumptions which consider transverse shear stresses and shear deformations as negligible. Also, in the plate vibration problems, rotary inertia was not considered.

Severn and Taylor(32) point out the convenience of taking transverse shear effects into account using the hybrid method. However, Pian(30) draws attention to the fact that the displacement assumptions used in (32) are not sufficient to model thick behaviour and he suggests that it is necessary to distinguish between rotations and derivatives of transverse displacements. Separate assumptions should be made for transverse displacements and rotations.

It would seem possible, then, using the hybrid method and the above approach to construct thick shell elements. The quality of results possible is worthy of investigation.

Appendix 1 - NOVOZHILOV'S STRAIN ENERGY EXPRESSION FOR THIN SHELLS AND THE STRESS-STRAIN RELATIONSHIP

A1.1 Introduction

Thin shell theory deals with the stresses and displacements of the middle surface of the shell. The underlying assumptions in thin shell theory can be stated as:

(i) straight fibres perpendicular to the middle surface before deformation remain so after deformation and do not change their length;

(ii) normal stresses acting on planes parallel to the middle surface may be neglected in comparison with the other stresses.

These basic assumptions define completely the variations of deformation and hence stresses through the thickness. It is therefore convenient to express deformations in terms of those of the middle surface and to express the stresses as statically equivalent stress resultants acting also at the middle surface.

A1.2 The Strain Energy Expression of Novozhilov

The strain energy for a complete shell can be expressed in the nomenclature of Fig.(A1.1) as

$$V = \frac{1}{2}\iiint \left(\sigma_{11}e_{11} + \sigma_{22}e_{22} + \sigma_{12}e_{12}\right) A_1 A_2 \left(1 + z/R_1\right)\left(1 + z/R_2\right) d\alpha_1 d\alpha_2 dz \quad \text{(A1.1)}$$

where α_1, α_2 = Curvilinear coordinates in surface

R_1, R_2 = Two principal radii of curvature

A_1, A_2 = Lamé parameters relating arc length to α_1, α_2

$\sigma_{11} e_{11}$ etc. = stresses and strains

and the first integral extends through the thickness from z = -t/2 to z = +t/2 (t = thickness of shell).

If the stress normal to the surface is neglected, Hooke's Law

can be stated in the form

$$\sigma_{11} = \left\{E/(1-\nu^2)\right\}\left\{\epsilon_1^{(z)} + \nu\epsilon_2^{(z)}\right\}$$
$$\sigma_{22} = \left\{E/(1-\nu^2)\right\}\left\{\epsilon_2^{(z)} + \nu\epsilon_1^{(z)}\right\} \qquad \text{(A1.2)}$$
$$\sigma_{12} = \left\{E/2(1+\nu)\right\}\omega^{(z)}$$

where E is Young's Modulus, ν = Poissons Ratio and $\epsilon_1^{(z)}$, $\epsilon_2^{(z)}$ and $\omega^{(z)}$ are strains at any point a distance z from the middle surface and determine the change in length and change in shear at this point.

If ϵ_1, ϵ_2 and ω are the corresponding strains of the middle surface and K_1, K_2 and τ are the changes in curvature and torsion of the middle surface, then Novozhilov(1) shows that the quantities $\epsilon_1^{(z)}$, $\epsilon_2^{(z)}$ and $\omega^{(z)}$ of equation (A1.2) can be expressed as

$$\epsilon_1^{(z)} = \epsilon_1 + z\left(K_1 - \epsilon_1/R_1\right)$$
$$\epsilon_2^{(z)} = \epsilon_2 + z\left(K_2 - \epsilon_2/R_2\right) \qquad \text{(A1.3)}$$
$$\omega^{(z)} = \omega + 2z\left(\tau - \left(\tfrac{1}{R_1}+\tfrac{1}{R_2}\right)\tfrac{\omega}{2}\right)$$

The approximations above are due to simplifications such as neglecting small terms of the order (z/R).

If (A1.3) and (A1.2) are substituted into (A1.1) the integration with respect to z can be carried out. By neglecting powers of z higher than the second and also by eliminating certain other small terms, Novozhilov obtains the following strain energy expression in terms of the deformations of the middle surface.

$$V = \left\{Et/2(1-\nu^2)\right\}\iint\left[(\epsilon_1+\epsilon_2)^2 - 2(1-\nu)\left(\epsilon_1\epsilon_2 - \omega^2/4\right)\right]A_1A_2\,d\alpha_1\,d\alpha_2$$
$$+\left\{Et^3/24(1-\nu^2)\right\}\iint\left[(K_1+K_2)^2 - 2(1-\nu)\left(K_1K_2 - \tau^2\right)\right]A_1A_2\,d\alpha_1\,d\alpha_2 \qquad \text{(A1.4)}$$

where the integrals extend over the entire middle surface. The first term in (A1.4) represents the strain energy of extension and shear and the second that of bending and torsion.

A1.3 The Forces at the Middle Surface

Since the deformations of the middle surface only are involved in (A1.4) it is convenient to introduce statically equivalent forces and bending moments also considered to act at the middle surface. Consider the face of the element of Fig.(A1.1) which is perpendicular to the line α_1 (Fig.(A1.2)).

On the shaded area of this face the stresses σ_{11} , σ_{12} and σ_{13} act. If unit length of middle surface is considered, the length of the shaded portion is $(1+z/R_2)$ and the forces/unit length acting at the middle surface are

$$\begin{aligned} N_1 &= \int_{-t/2}^{t/2} \sigma_{11}\left(1+z/R_2\right) dz \\ N_{12} &= \int_{-t/2}^{t/2} \sigma_{12}\left(1+z/R_2\right) dz \\ Q_1 &= \int_{-t/2}^{t/2} \sigma_{13}\left(1+z/R_2\right) dz \end{aligned} \qquad \text{(A1.5)}$$

Similar expressions hold for the forces N_2, N_{21} and Q_2 acting on the face perpendicular to α_2.

Considering next the moments of the stresses σ_{11} , σ_{12} acting on one of the faces, the two quantities

$$\begin{aligned} M_1 &= \int_{-t/2}^{t/2} z\left(1+z/R_2\right)\sigma_{11}\, dz \\ M_{12} &= \int_{-t/2}^{t/2} z\left(1+z/R_2\right)\sigma_{12}\, dz. \end{aligned} \qquad \text{(A1.6)}$$

can be formed which are the bending and twisting moments per unit length of α_2. Similar expressions for M_2 and M_{21} can be formed for the other face.

The six forces N_1 , N_{12} , Q_1 , N_2 , N_{21} , Q_2 and the four moments M_1 , M_{12} , M_2, M_{21} completely characterize the state of stress of the shell. Using the basic assumptions, knowledge of these quantities permits the calculation of the stresses σ_{11} , σ_{12} and σ_{22} at any point of the shell.

A1.4 The Relation between Forces, Moments and Strains

The expression for the variational change of strain energy of a thin shell, given from the theory of elasticity, is of the form

$$\delta(V) = \iiint \left[\sigma_{11}\,\delta(e_{11}) + \sigma_{22}\,\delta(e_{22}) + \sigma_{12}\,\delta(e_{12})\right]\left(1+z/R_1\right)\left(1+z/R_2\right) A_1 A_2 \times d\alpha_1\, d\alpha_2\, dz \qquad \text{(A1.7)}$$

If $\delta(\epsilon_1^{(z)})$ is used for $\delta(e_{11})$ etc. from (A1.3) and equations (A1.2) are used in (A1.7) above, then using the definitions of the stress resultants given in the previous section, equation (A1.7) becomes

$$\delta(V) = \iint \left[N_1\,\delta(\epsilon_1) + N_2\,\delta(\epsilon_2) + S\,\delta(\omega) + M_1\,\delta(K_1) + M_2\,\delta(K_2) + 2H\,\delta(\tau)\right] A_1 A_2\, d\alpha_1\, d\alpha_2 \qquad \text{(A1.8)}$$

where

$$S = N_{12} - M_{21}/R_2 = N_{21} - M_{12}/R_1$$

$$H = \tfrac{1}{2}\left(M_{12} + M_{21}\right)$$

If, now, the variational increment of strain energy is obtained from (A1.4) and the coefficients of terms are compared with those in (A1.8), the following relationships are found between the stress-resultants and strains of the middle surface.

$$N_1 = \left[Et/(1-\nu^2)\right]\left(\epsilon_1 + \nu\epsilon_2\right) \qquad N_2 = \left[Et/(1-\nu^2)\right]\left(\epsilon_2 + \nu\epsilon_1\right) \qquad \text{(A1.9)}$$

$$M_1 = \left[Et^3/12(1-\nu^2)\right]\left(K_1 + \nu K_2\right) \qquad M_2 = \left[Et^3/12(1-\nu^2)\right]\left(K_2 + \nu K_1\right)$$

$$S = \left[Et/2(1+\nu)\right]\omega \qquad H = \left[Et^3/12(1+\nu)\right]\tau.$$

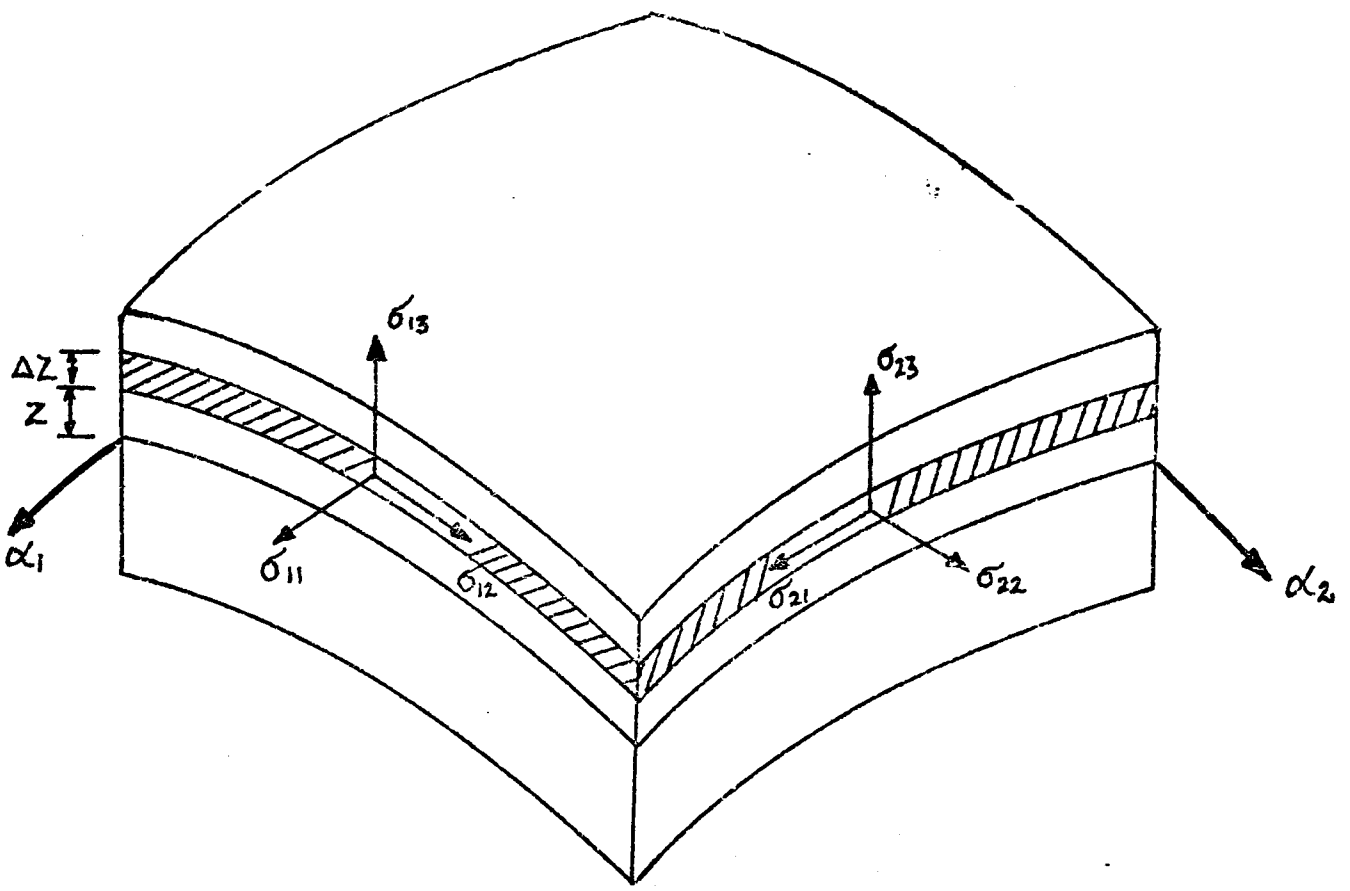

FIG. A1.1 STRESSES ON SHELL

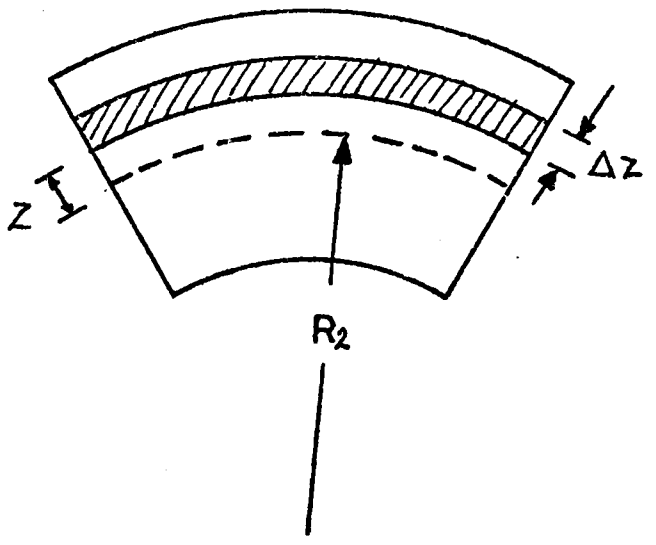

FIG. A. 1.2 FACE PERPENDICULAR TO α_1

Appendix 2 - THE EXACT SOLUTION FOR THE RECTANGULAR SIMPLY SUPPORTED PANEL UNDER PRESSURE LOADING

A2.1 The Panel

The particular dimensions of the simply supported rectangular panel considered in several sections of this thesis are shown in Fig.(A2.1) but the following analysis is valid for a panel with any dimensions. Timoshenko et al.(3) present a similar analysis but the following is a modification of this using Novozhilov's(1) shell theory.

A2.2 Novozhilov's Shell Theory

The stress resultants acting on an infinitesimal element of the panel are shown in Fig.(A2.2). The sign convention is that used by Novozhilov and double headed arrows represent moments whose positive directions are given by a right-hand corkscrew convention.

From considerations of equilibrium the following three equations can be shown to relate the forces and bending moments with a pressure loading q.

$$R\,\partial N_x/\partial x + \partial N_{\phi x}/\partial \phi = 0$$

$$\partial N_\phi/\partial \phi + R\,\partial N_{x\phi}/\partial x + (1/R)\,\partial M_\phi/\partial \phi + \partial M_{x\phi}/\partial x = 0 \qquad \text{(A2.1)}$$

$$(1/R)\,\partial^2 M_\phi/\partial \phi^2 + \partial^2 M_{x\phi}/\partial x \partial \phi + R\,\partial^2 M_x/\partial x^2 + \partial^2 M_{\phi x}/\partial x \partial \phi - N_\phi = q_z R$$

Novozhilov's relationships between the stresses and strains can then be stated in the following form (simplified from those in Appendix 1 as explained in Chapter 5 (Section 5.3.5).

$$N_x = \{Et/(1-\nu^2)\}\{\epsilon_x + \nu\epsilon_\phi\} \qquad M_x = \{Et^3/12(1-\nu^2)\}\{\kappa_x + \nu\kappa_\phi\}$$

$$N_\phi = \{Et/(1-\nu^2)\}\{\epsilon_\phi + \nu\epsilon_x\} \qquad M_\phi = \{Et^3/12(1-\nu^2)\}\{\kappa_\phi + \nu\kappa_x\} \qquad \text{(A2.2)}$$

$$N_{x\phi} = \{Et/2(1+\nu)\}\{\omega + \tfrac{t^2}{6R}\tau\} \qquad M_{x\phi} = M_{\phi x} = \{Et^3/12(1+\nu)\}\tau.$$

$$N_{\phi x} = \{Et/2(1+\nu)\}\,\omega$$

where the vector of strains and curvatures of the middle surface $\{\epsilon_x, \epsilon_\phi, \omega, \kappa_x, \kappa_\phi, \tau\}^T$ can be defined in terms of the displacements u, v and w of the middle surface (Fig.(A2.1)) by:

$$\epsilon_x = \partial u/\partial x \qquad \epsilon_\phi = \frac{1}{R}\partial v/\partial\phi + w/R \qquad \omega = \partial v/\partial x + \frac{1}{R}\partial u/\partial\phi \tag{A2.3}$$

$$\kappa_x = -\partial^2 w/\partial x^2 \qquad \kappa_\phi = -\frac{1}{R^2}\left(\partial^2 w/\partial\phi^2 - \partial v/\partial\phi\right) \qquad \tau = \frac{1}{R}\left(-\partial^2 w/\partial x\partial\phi + \partial v/\partial x\right)$$

If equations (A2.3) are substituted into (A2.2) and these in turn into (A2.1), the three equilibrium equations can be expressed in terms of the displacements u, v and w of the middle surface.

A2.3 Displacement Assumptions

To solve the three differential equations for u, v and w it is necessary to make assumptions concerning the form of these displacements. They are taken to be the sums of infinite trigonometric series in both directions

$$u = \sum_{m=1,3,5\cdots}\sum_{n=1,3,5,\cdots} A_{mn} \sin\left(\frac{n\pi\phi}{\alpha}\right) \cos\left(\frac{m\pi x}{l}\right)$$

$$v = \sum_{m=1,3,5\cdots}\sum_{n=1,3,5\cdots} B_{mn} \cos\left(\frac{n\pi\phi}{\alpha}\right) \sin\left(\frac{m\pi x}{l}\right) \tag{A2.4}$$

$$w = \sum_{m=1,3,5\cdots}\sum_{n=1,3,5\cdots} C_{mn} \sin\left(\frac{n\pi\phi}{\alpha}\right) \sin\left(\frac{m\pi x}{l}\right)$$

These particular forms are chosen because they represent the edge conditions of zero displacement and bending moment accurately.

It is also necessary to represent the uniform pressure loading acting towards the centre of curvature in the form of an infinite series. Timoshenko(3) shows that the following series does this.

$$q = \sum_{m=1,3,5\cdots}\sum_{n=1,3,5\cdots} D_{mn} \sin\left(\frac{m\pi x}{l}\right) \sin\left(\frac{n\pi\phi}{\alpha}\right) \tag{A2.5}$$

where the value of Dmn is given by $(16q/\pi^2 mn)$.

A2.4 Calculation of Results

It is now possible, using (A2.5) and (A2.4) to substitute into the three equilibrium equations (expressed in terms of displacements) and after much algebra the following set of equations is obtained.

$$A_{mn}\pi\left[\left(\frac{Rm}{\ell}\right)^2+\frac{(1-\nu)n^2}{2\alpha^2}\right]+\frac{B_{mn}\pi(1+\nu)Rmn}{2\alpha\ell}-\frac{C_{mn}\nu Rm}{\ell}=0 \qquad \text{(A2.6)}$$

$$\frac{A_{mn}\pi(1+\nu)Rmn}{2\alpha\ell}+B_{mn}\pi\left[\frac{(1-\nu)R^2m^2}{2\ell^2}+\frac{t^2(1-\nu)m^2}{6\ell^2}+\frac{n^2}{\alpha^2}\left(1+t^2/12R^2\right)\right]-C_{mn}\left(\frac{n}{\alpha}\right)\left[1+\left(\frac{\pi^2t^2}{12R^2}\right)\left\{\frac{n^2}{\alpha^2}+(2-\nu)\frac{R^2m^2}{\ell^2}\right\}\right]=0 \qquad \text{(A2.7)}$$

$$A_{mn}\left(\frac{\nu\pi Rm}{\ell}\right)+B_{mn}(\pi n/\alpha)\left[1+\left(\frac{\pi^2t^2}{12R^2}\right)\left\{\frac{R^2(2-\nu)m^2}{\ell^2}+\frac{n^2}{\alpha^2}\right\}\right]-C_{mn}\left[1+\left(\frac{\pi^4t^2}{12R^2}\right)\left(\frac{R^2m^2}{\ell^2}+\frac{n^2}{\alpha^2}\right)^2\right]=\frac{16q}{\pi^2mn}\cdot\frac{R^2(1-\nu^2)}{Et} \qquad \text{(A2.8)}$$

Equations (A2.6), (A2.7) and (A2.8) constitute three equations in the three unknown coefficients Amn, Bmn and Cmn for every value of m and n in the infinite series. For each value of m and n the three equations can be solved and the exact displacements built up using (A2.4). Simultaneously it is possible to build up values for the stress resultants using (A2.3) and (A2.2). The process can be terminated when convergence to the required accuracy is achieved.

For the panel shown in Fig.(A2.1) convergence to three significant figures had taken place when m and n had reached 21.

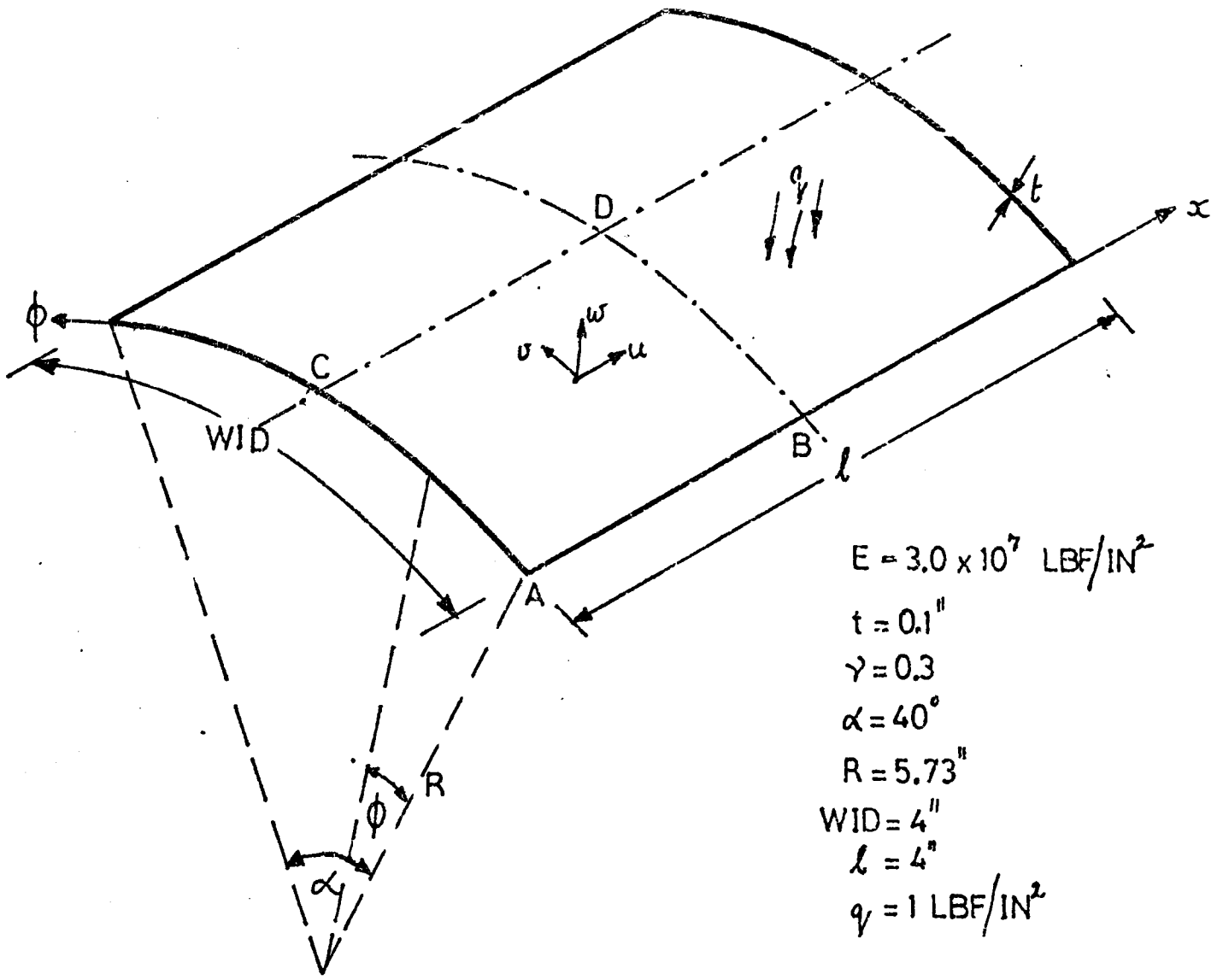

FIG. A 2.1 THE SIMPLY SUPPORTED PANEL

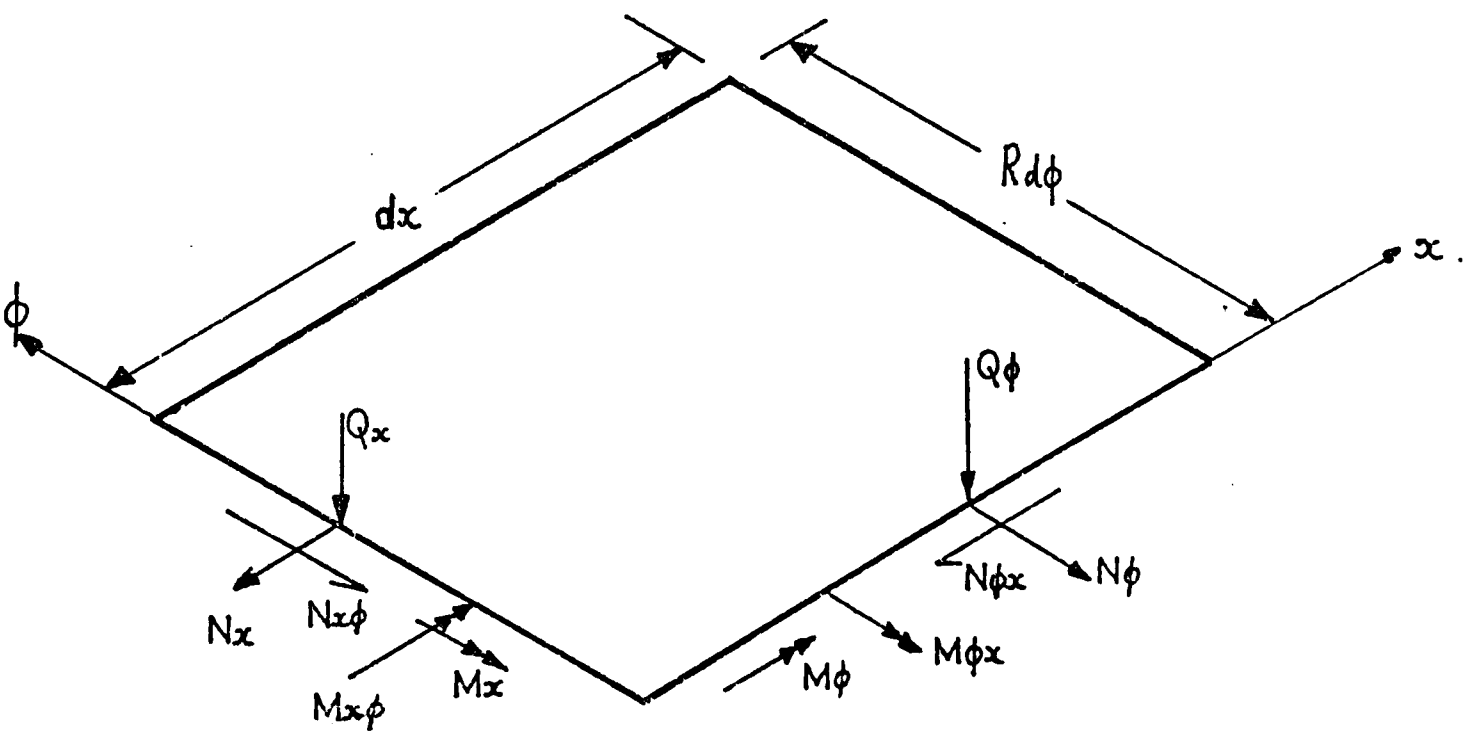

FIG. A.2.2 STRESS RESULTANTS.

Appendix 3 - BIBLIOGRAPHY

1. V. V. Novozhilov - The Theory of Thin Shells. P. Noordhoff-Groningen. 1959.

2. W. Flügge - Stresses in Shells. Springer-Verlag. Berlin. 1962.

3. S. Timoshenko and S. Wionowski-Krieger - Theory of Plates and Shells. 2nd Edition. McGraw-Hill. 1959.

4. A. Cauchy - Sur l'équilibre et le mouvement d'une plaque solid. Exercise de Mathématique. 1828.

5. S. D. Poisson - Mémoire sur l'équilibre et le mouvement des corps solides. Mem. de l'Acad. Sci., Paris. 1829.

6. G. Kirchoff - Vorlesungen über Mathematische Physik, Vol.1, Mechanic. 1876.

7. H. Aron - Das Gleichgewicht und die Bewegung einer unendlich dünnen beliebig gekrümmten, elastischen Schale. Jnl. für reine und ang. Math. 1874.

8. A. E. H. Love - On the Small Free Vibrations and Deformations of Thin Elastic Shells. Phil. Trans. Royal. Soc. 1888.

9. A. E. H. Love - Mathematical Theory of Elasticity. 4th Edition. 1927.

10. B. G. Galerkin - On the Theory of Elastic, Cylindrical Shells. D.A.N. (S.S.S.R.) 1934.

11. B.G. Galerkin - The Equilibrium of Elastic Cylindrical Shells. Trudy - Leningrad Institute of Structures. 1935.

12. A. I. Luré - A Study in the Theory of Thin Shells. Trudy L.P.I. 1937.

13. A. I. Luré - The General Theory of Thin Elastic Shells. Prikl. Mat. Mekh., Akademiyn. Nauk. S.S.S.R. 1940.

14. O. C. Zienkiewicz and Y. C. Cheung - The Finite Element Method in Structural and Continuum Mechanics. McGraw-Hill. New York. 1967.

15. O. C. Zienkiewicz - The Finite Element Method in Engineering Science. (2nd revised, expanded version of the above) McGraw-Hill. 1971.

16. D. J. Dawe - A Finite Element Approach to Plate Vibration Problems. Jnl. Mech. Eng. Sci., 7, pp.28-32. 1965.

17. R. J. Melosh - A Stiffness Matrix for the Analysis of Thin Plates in Bending. Jnl. of the Aerospace Sciences. Vol.28, pp.34-42. 1961.

18. R. W. Clough and C. A. Felippa - A Refined Quadrilateral Element for the Analysis of Plate Bending. Proc. Conf. Mat. Methods in Struc. Mech. W.P.A.B. Ohio. 1968.

19. R. W. Clough and J. L. Tocher - Finite Element Stiffness Matrices for Analysis of Plate Bending. Proc. Conf. Mat. Methods in Struc. Mech. W.P.A.B. Ohio. 1966.

20. A. Adini - Analysis of Shell Structures by the Finite Element Method. Ph.D. dissertation. Dept. Civ. Eng., Univ. Calif., Berkeley. 1961.

21. J. L. Tocher - Analysis of Plate Bending using Triangular Elements. Ph.D. dissertation. Univ. Calif., Berkeley. 1962.

22. F. K. Bogner, R. L. Fox and L. A. Schmit - The Generation of Inter-Element Compatible Stiffness and Mass Matrices by the use of Interpolation Formulae. Proc. Conf. Mat. Methods in Struc. Mech. W.P.A.B. Ohio. 1966.

23. G. A. Butlin and F. A. Leckie - A Study of Finite Elements Applied to Plate Flexure. Symp. Paper. Num. Meths. for Vib. Problems. Vol.3, Univ. of Southampton, July 1966.

24. V. Mason - Rectangular Finite Elements for Analysis of Plate Vibrations. Jnl. Sound and Vib. Vol.7, pp.437-448. 1968.

25. G. P. Bazeley, Y. Cheung, B. M. Irons and O. C. Zienkiewicz - Triangular Elements in Plate Bending - Conforming and Non-Conforming Solutions. Proc. Conf. Mat. Meths. Struc. Mech. W.P.A.B. Ohio. 1966.

26. G. A. Butlin and R. Ford - A Compatible Triangular Plate Bending Finite Element. Int. Jnl. Solids and Structures. Vol.6. 1970.

27. G. R. Cowper, E. Kosko, G. M. Lindberg and M. D. Olsen - Static and Dynamic Applications of a High Precision Triangular Plate Bending Element. A.I.A.A. Jnl. Vol.7. No.10. Oct. 1969.

28. T. H. H. Pian - Derivation of Element Stiffness Matrices by Assumed Stress Distributions. Jnl. A.I.A.A. Vol.2, pp.1333-1336. 1964.

29. T. H. H. Pian - Element Stiffness Matrices for Boundary Compatibility and Prescribed Boundary Stresses. Proc. Conf. Mat. Meths. Struc. Mech. W.P.A.B. Ohio. 1966.

30. T. H. H. Pian and Pin Tong - Rationalization in Deriving Element Stiffness Matrix by Assumed Stress Approach. Proc. Conf. Mat. Meths. Struc. Mech. W.P.A.B. Ohio. 1968.

31. Pin Tong and T. H. H. Pian - A Variational Principle and the Convergence of a Finite Element Method based on Assumed Stress Distribution. Int. Jnl. Solids and Structures. Vol.5, pp.463-472. 1969.

32. R. T. Severn and P. R. Taylor - The Finite Element Method for the Flexure of Slabs when Stress Distributions are Assumed. Proc. Inst. Civ. Eng. 34, pp.153-170. 1966.

33. R. Dungar, R. T. Severn and P. R. Taylor - Vibration of Plate and Shell Structures using Triangular Finite Elements. Jnl. Strain Anal., 2, pp.73-83. 1967.

34. R. J. Allwood and G. M. M. Cornes - A Polygonal Finite Element for Plate Bending Problems using the Assumed Stress Approach. Int. Jnl. Num. Meths. Eng. 1, pp.135-150. 1969.

35. B. K. Neale, R. D. Henshell and G. Edwards - Hybrid Plate Bending Elements. Jnl. Sound and Vib. 23(1), pp.101-112. 1972.

36. B. Fraeijs de Veubeke - Displacement and Equilibrium Models in the Finite Element Method. Stress Analysis. (Eds. O. C. Zienkiewicz and G. S. Hollister) Ch.9, Wiley. 1965.

37. B. Fraeijs de Veubeke and G. Sander - An Equilibrium Model for Plate Bending. Int. Jnl. Solids and Structures. Vol.4, pp.447-468. 1968.

38. L. S. D. Morley - A Triangular Equilibrium Element with Linearly Varying Bending Moments for Plate Bending Problems. Jnl. of the Royal Aeronautical Soc. Vol.71, p.715. Oct. 1967.

39. L. S. D. Morley - The Triangular Equilibrium Element in the Solution of Plate Bending Problems. The Aeronautical Quarterly. May 1968.

40. R. E. Jones and D. R. Strome - A Survey of the Analysis of Shells by the Displacement Method. Proc. Conf. Mat. Meths. Struc. Mech. W.P.A.B. Ohio. 1966.

41. A. Hrennikoff and S. S. Tezcan - Analysis of Cylindrical Shells by the Finite Element Method. Symp. on Problems of Interdependence of Design and Construction of Large Span Shells for Industrial and Civic Buildings. Leningrad. 1966.

42. R. W. Clough and R. J. Johnson - A Finite Element Approximation for the Analysis of Thin Shells. Int. Jnl. Solids and Structures, 4, pp.43-60. 1968.

43. A. J. Carr - A Refined Finite Element Analysis of Thin Shell Structures including Dynamic Loadings. Ph.D. thesis. Univ. Calif., Berkeley. 1967.

44. F. K. Bogner, R. L. Fox and L. A. Schmit - A Cylindrical Shell Discrete Element. A.I.A.A. Jnl. 5, pp.745-750. 1967.

45. G. Cantin and R. W. Clough - A Curved, Cylindrical Shell Finite Element. A.I.A.A. Jnl. 6, pp.1057-1062. 1968.

46. M. D. Olsen and G. M. Lindberg - Vibration Analysis of Cantilevered Curved Plates using a New Cylindrical Shell Finite Element. Proc. Conf. Mat. Meths. Struc. Mech. W.P.A.B. Ohio. 1968.

47. J. J. Connor and C. Brebbia - Stiffness Matrix for Shallow Rectangular Shell Element. Jnl. Eng. Mech. Div. A.S.C.E. 93. 1967.

48. R. H. Gallagher - The Development and Evaluation of Matrix Methods of Thin Shell Structural Analysis. Ph.D. thesis. State Univ. of New York. 1966.

49. S. Utku and R. J. Melosh - Behaviour of Triangular Shell Element Stiffness Matrices Associated with Polyhedral Deflection Distributions. A.I.A.A. Jnl. 6, pp.374-376. 1968.

50. G. E. Strickland and W. A. Loden - A Doubly Curved Triangular Shell Element. Proc. Conf. Mat. Meths. Struc. Mech. W.P.A.B. Ohio. 1968.

51. G. Bonnes, G. Dhatt, Y. M. Giroux and L. P. A. Robichaud - Curved Triangular Elements for the Analysis of Shells. Proc. Conf. Mat. Meths. Struc. Mech. W.P.A.B. Ohio. 1968.

52. G. R. Cowper, G. M. Lindberg and M. D. Olsen - A Shallow Shell Finite Element of Triangular Shape. Int. Jnl. Solids and Structures.

53. R. D. Henshell, B. K. Neale and G. B. Warburton - A New Hybrid Cylindrical Shell Finite Element. Jnl. Sound and Vib. 16 (4), pp.519-531. 1971.

54. G. Cantin - Rigid Body Motions in Curved Finite Elements. A.I.A.A. Jnl. 8, p.1252. 1970.

55. B. K. Neale - Vibration of Shell Structures. Ph.D. thesis. Univ. of Nottingham. 1971.

56. G. B. Warburton - Dynamics of Shells. Proc. Conf. Structural Dynamics. Loughborough Univ. 1969.

57. D. G. Ashwell and A. B. Sabir - A New Cylindrical Shell Finite Element based on Simple Independent Strain Functions. Int. Jnl. Mech. Sci., Vol.14, pp.171-183. 1972.

58. A. Adini and R. W. Clough - Analysis of Plate Bending by the Finite Element Method. Rept. Nat. Sci. Foundation. 1960.

59. R. J. Melosh - Basis for Derivation of Matrices for the Direct Stiffness Method. Jnl. A.I.A.A. 1, p.1631. 1963.

60. PAFEC 70+ Users Manual - Dept. of Mech. Eng., Univ. of Nottingham.

61. B. Tabarrok and N. Gass - Comments on "A New Hybrid Cylindrical Shell Finite Element". Jnl. Sound and Vib. 21 (3). 1972.

62. R. D. Henshell, B. K. Neale and G. B. Warburton - Reply to Ref.61. Jnl. Sound and Vib. 21 (3). 1972.

63. J. P. Wolf - Systematic Enforcement of Stress Boundary Conditions in the Assumed Stress Hybrid Model based on the Deformation Method. Proc. 1st. Int. Conf. Struc. Mech. in Reactor Tech. Berlin. 1971.

64. A. Bengtsson and J. P. Wolf - STRIP (Structural Integrated Programs) Step S. User Manual, Digital Ltd., Zurich, and Nordisk. ADB. Stockholm, August 1969.

65. G. M. Lindberg, M. D. Olsen and G. R. Cowper - New Developments in the Finite Element Analysis of Shells. DME/NAE Quarterly Bulletin, (4), 1969.

66. O. C. Zienkiewicz, P. R. Taylor and J. M. Too - Reduced Integration Technique in General Analysis of Plates and Shells. Int. Jnl. Num. Meths. Eng. Vol.3, pp.275-290. 1971.

67. A. C. Scordelis and K. S. Lo - Computer Analysis of Cylindrical Shells. A.C.I. Jnl. 61, pp.539-561. 1964.

68. G. Cantin - A.I.A.A. Jnl. Vol.6, p.1787. 1968.

69. P. M. Naghdi - Proc. Symp. on Theory of Shells to Honour L. H. Donnell, Univ. of Houston, Texas, p.34. 1967.

70. J. L. Sanders, Jnr. - N.A.S.A. Report No.24. 1959.

71. T. H. H. Pian - Finite Element Methods by Variational Principles with Relaxed Continuity Requirement. Variational Methods in Engineering. Vol.1. Proc. Int. Conf. Southampton. Sept. 1972.

72. R. W. Claassen and C. J. Thorne - Transverse Vibrations of Thin Rectangular Isotropic Plates. NAVWEPS Report 7016. 1960.

73. B. Tabarrok - A Variation Principle for the Vibration Analysis of Continua by the Hybrid Finite Element Method. Int. Jnl. Solids and Structures, 7, pp.251-268. 1971.

74. P. H. R. Lane and R. T. Rose - Experiments on Fabricated Pipe Bends. British Welding Research Association Report. September 1960.

75. D. G. Ashwell and A. B. Sabir - Limitations of Certain Curved Finite Elements when Applied to Arches. Int. Jnl. Mech. Sci. Vol.13, pp.133-139. 1971.

76. D. G. Ashwell, A.B. Sabir and T. M. Roberts - Further Studies in the Application of Curved Finite Elements to Circular Arches. Int. Jnl. Mech. Sci., Vol.13, pp.507-517. 1971.

ACKNOWLEDGEMENTS

This work would not have been possible without both the direct and indirect help of many people.

My supervisor, Dr. J. J. Webster, has been a constant source of ideas and encouragement throughout the three-and-a-half years. I would like to take this opportunity of thanking him.

I am also indebted to past and present members of the Pafec group at Nottingham for the use of the various subroutines in the PAFEC 70+ finite element scheme and for much help and advice.

I was supported financially by the Science Research Council and for this, also, I am duly grateful.

Finally, I extend my thanks to Miss Judith Barton, who typed the manuscript.

Gordon Edwards.
Bramcote.
March 7. 1974.